Caspase interaction of anti-apoptotic Livin as well as the Vacuolar ATPase (V-ATPase) and structural insights into the subunit d and a of the yeast V-ATPase
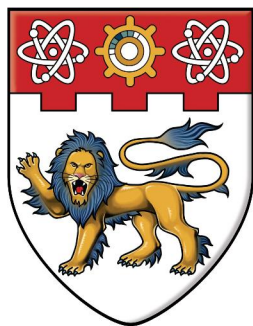
Thaker, Youg Raj

2009

CASPASE INTERACTION OF ANTI-APOPTOTIC LIVIN AS WELL AS THE VACUOLAR ATPASE (V-ATPASE) AND STRUCTURAL INSIGHTS INTO THE SUBUNIT *d* AND *a* OF THE YEAST V-ATPASE

YOUG RAJ THAKER

SCHOOL OF BIOLOGICAL SCIENCE

2009

Caspase interaction of anti-apoptotic Livin as well as the vacuolar ATPase (V-ATPase) and structural insights into the subunit *d* and *a* of the yeast V-ATPase

YOUG RAJ THAKER

School of Biological Sciences

A thesis submitted to the Nanyang Technological University
in partial fulfillment of the requirement for the degree of
Doctor of Philosophy

2009

Acknowledgements

My deepest and sincere gratitude goes to my supervisor A/Prof. (Dr.) Gerhard Grüber for his continuous guidance, scientific advice, making in me a strict discipline of science, and taking care of myself and my scientific interests when I needed it most. Without his generous support, kind heartedness and devotion to the science, I wouldn't have been able to complete this thesis. Many thank to A/Prof. Gerhard Grüber for giving me an opportunity to work under his guidance, and adopting me as a part of his group at a very critical time. This has been a great pleasure to work under the guidance of A/Prof. Gerhard Grüber. His attitude towards the life and science gave me an unforgettable experience, which will surely help me to succeed in the science and research.

I would also like to take this opportunity to thank A/Prof. Wu Mian for his initial guidance at School of Biological Science and helping me to initiate a research interest in apoptosis.

Special thanks go to A/Prof. Gerhard Grüber and A/Prof. Manfred Roessle for their help in collecting the Small Angle X-ray (SAXS) Data of the subunit *d* at EMBL, Hamburg Outstation (Germany). Appreciate help from A/Prof. Stephan Wilkens (Upstate Medical University, New York, USA) for providing high quality images of 3D electron micrographs of the V_O domain of clathrin coated vesicles and to Dr. Ardina Grüber for help and discussion with MALDI-TOF data analysis. I would like to extend my thanks to A/Prof. Thorsten Wohland for collaboration about subunits *a* and *d* FCS binding studies with the support of Dr. Pan Xiaotao from his lab. I am grateful to colleague Mr. Shovanlal Gayen for help with NMR spectroscopy and effective discussions and to all lab members for creating a lively environment and moral support. Thanks go to Dr. Cornelia Hunke for help with computer related problems. Again, I very much appreciate A/Prof. Gerhard Grüber for critical comments and reading this thesis several times. Thanks also go to everyone who helped in thesis reading and corrections.

Special thanks go to the Nanyang Technological University for providing me an opportunity to study in Singapore and financially supporting me.

I am extremely grateful to my girl friend, Manisha Mishra for her immense support and care in my life. Last but not least, my heartedly gratitude goes to my parents for selfless support, love and understanding during and before my PhD study in Singapore. I would also like to remember my grandfather for his kind heartedness, love and best wishes I am living with, who passed away during my PhD study at NTU (Singapore).

To my grandparents, parents and to all those who love me and care about me!

3. RESULTS………………………………………………………………...………**58**

3.1 CASPASE MEDIATE DEGRADATION OF LIVIN (ML-IAP) IN ARTS INDUCED APOPTOSIS AND THE CASPASE 3 TARGET SUBUNIT *d* OF EUKARYOTIC V₁V₀ ATPASE……………………………………………………...………**59**

3.2 STRUCTURAL AND BIOCHEMICAL CHARACTERIZATION OF SUBUNIT *d* OF THE VACUOLAR ATPASE OF *SACCHAROMYCES CEREVISIAE*....................**74**

List of figures

Introduction figures

Methods figures

Result figures

List of tables

Abbreviations

Apaf-1.. Apoptotic protease activating factor-1

ATP .... Adenosine triphosphate

ADP... Adenosine diphosphate

ARTS... Apoptosis Related protein in TGF- Signaling pathway

BID.. BH3-interacting Domain Death Agonist

BIR .... Baculovirus IAP Repeat

BSA... Bovine Serum Albumin

CED... Cell Death Defective

CD .... Circular Dichroism

DTT... Dithiothreitol

E. coli .... *Escherichai coli*

EDTA .... Ethylenediaminetetraacetic acid

EM... Electron Microscopy

Hepes... (4-(2-hydroxyethyl)-1-piperazineethanesulfonic acid)

IAP .... Inhibitor of Apoptosis Proteins

IPTG... Isopropyl- -D-thiogalactoside

MALDI... Matrix Assisted Laser Desorption Ionization

NEM... N-ethyl maleimide

MDR... Multidrug Resistant

NTA.. Nitrilotriacetic acid

NMR... Nuclear Magnetic Resonance

PAGE .... Polyacrylamide Gel Electrophoresis

PCR .... Polymerase Chain Reaction

PDB .... Protein Data Bank

P-loop .... Phosphate loop

RING.. Really Interesting New Gene

SAXS.. Small Angle X-ray Scattering

SDS .... Sodium dodecyl sulphate

STS .... Staurosporin

STV1 .... Similar to VPH1

tBID... truncated BID

TOF .... Time of Flight

TMR .... Tetra Methyl Rhodamine

TNF .... Tumor Necrosis Factor

TNFR.. Tumor Necrosis Factor receptor

Tris .... Tris-(hydroxymethyl) aminomethane

VMA .... Vacuolar Membrane V-ATPase

VPH1.. Vacuolar PH 1

V-ATPase .... Vacuolar ATPase

ZVAD-FMK .... Benzylocarbony-VAD-Floromethyl Ketone

Abstract

Apoptosis is a critical process to remove the non-functional and redundant cells regulated by pro- and anti-apoptotic factors. Perturbation of balance between pro- and anti-apoptotic components is the leading cause of several physiopathological conditions such as neurodegenerative and cancer malignancies. Here, the pro-apoptotic cellular protein, ARTS as well as an anti-apoptotic protein, Livin, a family member of inhibitor of apoptosis have been studied. Results showed that ARTS is not the target of Livin E3 ligase activity in apoptotic cells co-expressing ARTS and Livin. In turn, Livin was found to undergo cleavage in ARTS-promoted apoptosis which was independent of its self-ubiquitination activity, normally observed in healthy cells. The exhaustion of Livin during ARTS-promoted apoptosis could partially be suppressed by the caspase inhibitors, implying a possible role of caspases concomitant with high active caspase 7 levels found in ARTS-promoted staurosporine-induced apoptosis.

Not only Livin, caspase do cleave several important cellular components during apoptosis and here, I have identified subunit *d* of V-ATPase as a new target of caspase 3. V-ATPases do play critical role in health and disease by maintaining proper acid/base balance pH. Additionally, homogenous protein preparation of yeast subunit *d* protein was used to determine its first low resolution shape by small angle X-ray spectroscopy (SAXS), revealing two distinct domains of 6.5 nm and 3.5 nm widths forming a "boxing glove" shape. Using previously solved low resolution structure of V_O domain as a template, subunit *d* could be assigned inside the V_O, allowing its clear localization on the top of V_O domain of V-ATPase. Moreover, biochemical approaches of fluorophore labeling, tryptic digestion and MALDI-TOF analysis led to the identification of a cysteine bridge between Cys36 and Cys329. Changes to disulphide formation have been further studied by fluorescence- and circular dichroism (CD) spectroscopy. Various truncated forms of subunit *d* lacking one or more cysteine residues and a C329S substitution mutant revealed that only domain (d_{11-329}) containing all six cysteine residues was soluble, underlying the importance of the termini. Furthermore, using fluorescence correlation spectroscopy and nuclear magnetic resonance, revealed a close proximity of subunit G to subunit *d* as well as a very strong interaction between subunits a (*Vph1p_{1-388}*) and *d*, indicative of an extended peripheral assembly of *d* inside the enzyme.

Subunit *a* is not only involved in the proton conduction and regulatory process of reversible disassembly but has also been recently described as a pH sensor element of V-ATPase, where it was found to interact with ARNO (ADP-ribosylation factor Nucleotide site Opener), an activator

of small GTPase, Arf6 (ADP-ribosylation factor 6) in a pH dependent manner. To structurally characterize this pH sensing elements, an essential region (386-402 aa) of subunit *a2* (mouse V-ATPase) involved in ARNO binding has been studied and its three dimensional solution structure was determined. Further, 3D NMR structures of the ARNO PB (Poly Basic) domain in its unphosphorylated and phosphorylated forms at S^{392} have been solved, showing helix-loop-helix structures, with evident difference between the two forms, giving insights into the reported phosphorylation dependent binding to subunit *a2*.

1. Introduction

1.1 Apoptosis and V-ATPase

1.1.1 Overview of apoptosis

Apoptosis is a highly regulated mechanism of cell suicide where cell actively participates in its own demise. The term "apoptosis" was coined by Kerr *et. al.* in 1972 to symbolize the phenomenon of cell death that was associated with the genomic DNA fragmentation (KERR *et al.*, 1972). Apoptosis is associated with distinct morphological changes such as cell shrinkage, chromatin condensation, nuclear pykonesis, membrane blebbing, cell rounding, collapse of cytoskeleton and preservation of cell organelles and membranes (KERR *et al.*, 1972; REED, 2000). Eventually, the cell breaks into small membrane-bound fragments, called as "apoptotic bodies", that are rapidly engulfed by the neighboring phagocytes to prevent inflammatory reaction in the vicinity (WYLLIE *et al.*, 1980; HENGARTNER, 2000) (Figure IA). Release of apoptotic bodies inspired the word "apoptosis", a Greek term which means "to fall away from" (KERR *et al.*, 1972; HENGARTNER, 2000). The term programmed cell death (PCD) was used to describe the phenomenon of cell death at specific time and space, especially during the process of development (ELLIS and HORVITZ, 1986). Since nearly all PCD is apoptotic, the terms are used interchangeably.
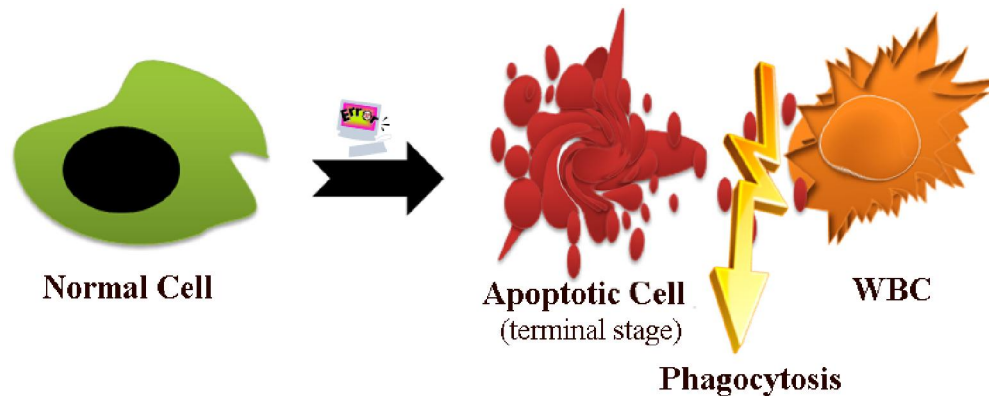
Figure I1. A cartoon representation of a cell undergoing apoptosis and being cleared by the phagocytic white blood cells (WBC). Due to the disruption of normal cell physiology by external or internal cellular insult, cell undergoes apoptosis. Apoptosis is a well coordinated and controlled phenomenon where the cell is broken into several membrane fragments known as "apoptotic bodies" that are produced from the membrane blebbings, a hallmark of apoptosis, without cell injury or inciting any inflammation in the vicinity.

Initially, apoptotic phenomenon was identified in the nematode *Caenorhabditis elegans* cell lineage and genetic studies, which distinguished a set of somatic cells that undergo PCD during normal development (SULSTON and HORVITZ, 1977; SULSTON *et al.*, 1983). Such observations led to the discovery of cell death molecular mechanism and identification of apoptotic proteins such as CED (cell death abnormal), CED-3, CED-4 and CED-9, where they were found to function as cysteine protease, pro-apoptotic factor and anti-apoptotic factor,

respectively (ELLIS and HORVITZ, 1986; HENGARTNER *et al.*, 1992; YUAN and HORVITZ, 1992; YUAN *et al.*, 1993). Homologs of these proteins have been recognized in other metazoans including mammals demonstrating apoptosis as a conserved mechanism of death in the organism. Apoptotic process is also believed to be present in the unicellular organisms such as budding yeast, *Saccharomyces cerevisiae* (FRÖHLICH and MADEO, 2001) (LUDOVICO *et al.*, 2001). Homologs of pro-apoptotic factors such as caspases have also been identified in yeast (MADEO *et al.*, 2002) (UREN *et al.*, 2000). Yeast has been used as an important genetic model in apoptotic studies (HAWKINS *et al.*, 1999; GUNYUZLU *et al.*, 2000). Apoptosis is regulated by an array of anti- and pro-apoptotic proteins and it is the balance between these two factors that determines the fate of cell - life or death (O'BRIEN and KIRBY, 2008). The PCD is also a vital genetic program during development and as an asset for the removal of non-functional cells of body to keep and maintain a state of homeostasis. The death machinery of cells is an extremely coordinated process with a fine tune and balance between different sub-programs operating simultaneously (HANGERTON, 2000). Deregulation of apoptosis results in various diseased conditions from cancers, heart failure to AIDS and neurodegenerative diseases (MATTSON, 2000; PERFETTINI *et al.*, 2005; NARULA *et al.*, 2006; ANDERSEN *et al.*, 2008; O'BRIEN and KIRBY, 2008). All pathways of apoptosis, guided by various pro-apoptotic factors result in the activation of various cysteine protease family members, called caspases, from their inactive zymogen forms (LI and YUAN, 2008). Initiator or upstream caspases activate downstream or effector caspases, culminating in the degradation of structural and functional units of cellular machinery (SALVESEN and DIXIT, 1997; EARNSHAW *et al.*, 1999; LI and YUAN, 2008). Caspases are the enzymes that recognize and cleave target substrates at aspartate residue (designated as P1) on a tetrapeptide motif (proximal residue towards N-terminus is designated as P4) (LI *et al.*, 1998; EARNSHAW *et al.*, 1999; JIANG and WANG, 2004). They can be grouped into initiator (upstream) caspases (for example, caspase-8 and 9) or effector (downstream) caspases (for example, caspase-3 and 7) according to the level at which they are activated during apoptotic chain of events. Upstream caspases activate downstream caspases that trigger cleavage of key cellular component pushing cell to a no-return point of death (EARNSHAW *et al.*, 1999; REED, 2000; RIEDL and SHI, 2004). Anti-apoptotic proteins prevent apoptosis either by inhibiting the pro-apoptotic proteins or by directly binding with caspases to block their activation (DEVERAUX and REED, 1999; HOLLEY *et al.*, 2002; BERGAMASCHI *et al.*, 2003; LISTON *et al.*, 2003).

Apoptosis signaling is either initiated from outside the cell by extracellular factors such as ligand fusion to cell surface receptors or from within the cells due to the damage of cellular components. In either case the final target is the activation of caspases. The activated caspases produce diverse results depending upon the target substrate, sequence and cleavage site (HENGARTNER, 2000). In most cases, a loss of function effect is produced such as cleavage of either a single polypeptide (for example, poly-ADP ribose polymerase) or a macromolecular assembly (for example, laminin network) (HENGARTNER, 2000). Caspase cleavage may also result in the gain of function effect, such as caspase 8 mediated cleavage of pro-apoptotic Bid to generate active truncated-Bid (tBid), removing its inhibitory domain (LI *et al.*, 1998). Caspases are mainly activated by four different pathways: (i) the cell surface death receptor-mediated pathway; (ii) the mitochondrial-mediated pathway; (iii) the endoplasmic reticulum (ER)-mediated pathway; and (iv) the granzyme B-mediated pathway (CREAGH *et al.*, 2003; WANG *et al.*, 2005).
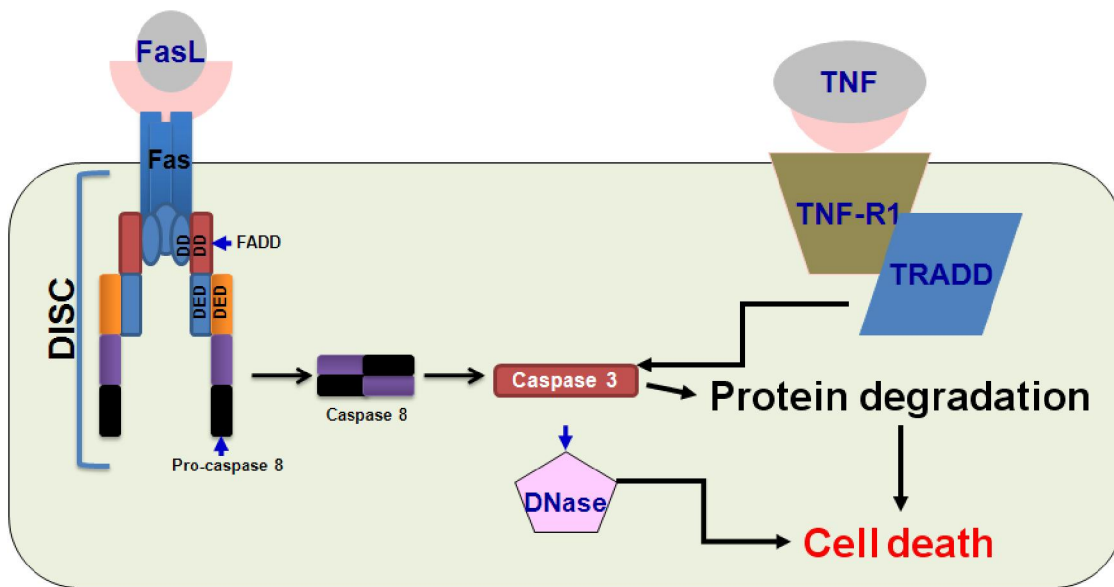
Figure I2: **Extrinsic pathway of caspase activation and cell death.** The receptor-mediated pathway, also known as extrinsic pathway, involves the activation of cell surface death surface by the ligand fusion resulting in the recruitment of adapter proteins (such as FADD to Fas receptor) which in turn binds to zymogen pro-caspase 8 via "death effector domain" (DED), resulting in its processing and maturation and initiation of the downstream events including activation of effector caspases such as caspase 3 culminating in cell death.

The extrinsic pathway (Figure I2) requires membrane receptors known as "death receptors" and apoptosis is initiated by the binding of corresponding "death ligand" (ASHKENAZI and DIXIT, 1998). These involve the proteins of TNF (Tumor Necrosis Factor) family of receptors such as CD95 (also called Fas), TNFR 1 (also called p55) characterized by the presence of an extra-cellular cysteine-rich domain and a cytosolic "death domain" (DD) (GRUSS and DOWER,

1995; NAGATA, 1997). After association with death ligand, the receptor undergoes conformational changes with subsequent binding of adaptor protein, Fas-associated death domain (FADD) or TNF-receptor associated death domain (TNFAAD) via homotyptic "death domain" interaction (NAGATA, 1997). Then, pro-caspase 8 is added to this assembly to form DISC (Death Inducing Signaling Complex) resulting in the generation of active caspase 8, which subsequently causes processing of caspase 3, the effector enzyme of apoptosis (GRUSS and DOWER, 1995; ASHKENAZI and DIXIT, 1998). In the second pathway (Figure I3), mitochondrial residential factors are released during apoptosis resulting in the activation of caspases (GREEN *et al.*, 1998). In response to neoplastic agents such as exposure to UV light, growth factor withdrawal and DNA damage, mitochondria become permeable and various factors residing in its compartments are released into the cytosol. These include cytochrome c, apoptosis inducing factor (AIF), and others such as Bcl-2 family members (GREEN *et al.*, 1998). Release of cytochrome c from mitochondria leads to the formation of caspase activation complex, known as, apoptosome (CREAGH *et al.*, 2003; MARTIN and ELKON, 2004; WANG *et al.*, 2005). Apoptosome recruits pro-caspase 9, converting it into an active form, which causes activation of downstream caspases 3, and 7 (GREEN *et al.*, 1998).
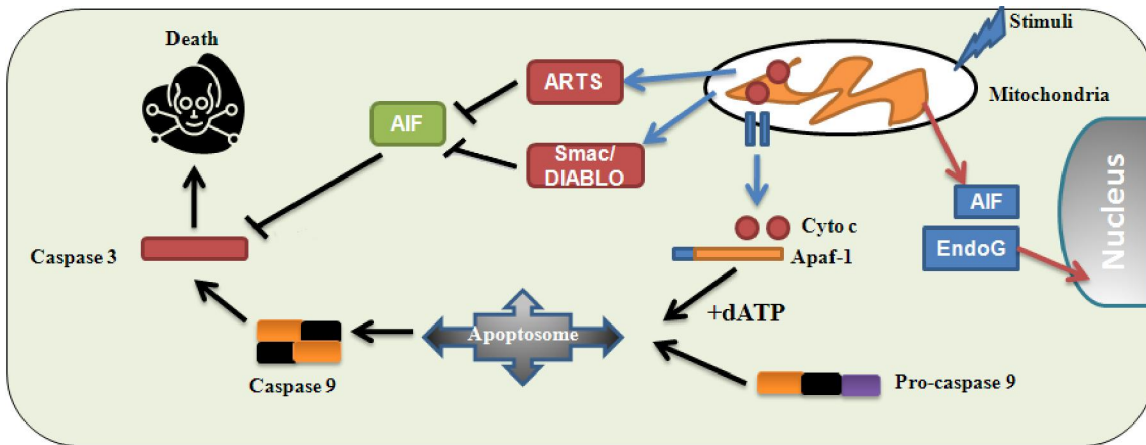
Figure I3. **The mitochondrial-mediated or the intrinsic pathway of apoptosis.** The mitochondrial pathway is initiated by internal cellular insults such as DNA damage and cell cycle arrest that leads to the permeablization of mitochondrial member, release cytochrome c and other polypeptides into the cytosol. Cytochrome c together with Apaf-1 (apoptotic protease activating factor-1) and pro-caspase 9 in presence of dATP promotes assembly of a macromolecule complex "apoptosome". Apoptosome activates caspase 9, which is capable of activating downstream effector caspases. Amplification of caspase cascade results in cellular apoptosis.

The third pathway of ER-mediated activation of caspases has been identified in response to ER stress, namely, accumulation of misfolded proteins in the ER, loss of calcium homeostasis, inhibition of N-glycosylation or ER/Golgi transport (FERRI and KROEMER, 2001; WANG *et al.*, 2005). Studies have shown activation of caspase 12 during ER stress, in a manner which was

independent of death receptor and mitochondrial pathways (NAKAGAWA *et al.*, 2000) concomitant with the release of cytochrome to activate cell death (WANG *et al.*, 2005). A new Bcl-2 family member, Bcl2/cb5 has been shown to inhibit the ER-stress mediated release of cytochrome c from the mitochondria (HAÌCKI *et al.*, 2000). However, ER pathway is less clear and is being actively studied to demonstrate its role in the progression of apoptosis. The fourth pathway is the granzyme B mediated activation of caspase 3. Granzyme B is a serine protease, which is injected by phagocytes into target cells infected with virus or tumor cells to initiate the processing and activation of pro-caspase 3 to its active form, that leads to cell death (TRAPANI and KWANG, 1998). However, it has been reported that granzyme B alone may not be able to fully mature caspase 3 and may require cytochrome c and other factors such as Smac/DIABLO, which are released from the mitochondria (SUTTON *et al.*, 2003).

1.1.2 ARTS role in programmed cell death

ARTS for "Apoptosis Related protein in TGF- Signaling pathway", is a septin-like protein product of the human septin H5/PNUTL2/CDCrel2b gene, identified in a retroviral insertional mutagenesis screen in TGF- mediated apoptosis (LARISCH *et al.*, 2000). This unique splice variant transcript of H5 septin gene encodes a protein of 32 kDa with a unique C-terminal 27 residues domain. Septin is a class of proteins that was first identified in the budding yeast associated with cytokinesis and cell division events (WEIRICH *et al.*, 2008). Septins are P-loop (Phosphate-loop) GTPases having conserved GTP binding domain, G1 (GxxxxG(S)K(T)), G3 (DxxG) and G4 (NKxD) motifs (BOURNE *et al.*, 1991; PAN *et al.*, 2007), with the exception of group 1A (found in mammals and close related to fungal septins), a predicted coiled-coil domain at the C-terminal and have been shown to form heteropolymeric complexes *in vitro* (FIELD and KELLOGG, 1999; WEIRICH *et al.*, 2008). In addition to the actively dividing cells, septins are also found in cell types such as neurons, thus this family of proteins may have diverse functions aside from the established role in cell shape modeling (via directly associating with the actin and membranes) (FATY *et al.*, 2002; WEIRICH *et al.*, 2008). More importantly ARTS retains a G1 motif (Walker A box or P-loop motif; GXSGXGKST) (SARASTE *et al.*, 1990), which is conserved in septin family as well as in other apoptotic proteins such as Apaf-1 (Apoptotic protease activating factor 1) and CED-4 (Cell Death abnormal) of drosophila (YUAN and HORVITZ, 1992) (HU *et al.*, 1998). Of the other two motifs (G3 and G4) common to most GTPases and other spetins, only G3 is preserved in ARTS. As demonstrated most recently, ARTS is the only septin family protein that localizes to mitochondria in healthy cells, and is

released into cytosol when apoptosis is triggered (LARISCH *et al.*, 2000; LARISCH, 2004). Released ARTS is capable of enhancing apoptosis and caspase activation in TGF- treated cells, via mostly unknown mechanisms (LARISCH *et al.*, 2000; LARISCH, 2004). Pro-apoptotic activity of ARTS was found to be dependent on its P-loop motif and a mutation in this domain (GKS to ENP) failed to induce apoptosis in response to TGF- treatment (LARISCH *et al.*, 2000). Its pro-apoptotic activity was also demonstrated by the reduced apoptotic response to TGF- in the cells, where endogenous ARTS was knocked-down by anti-sense ARTS construct (LARISCH *et al.*, 2000). In the cells induced to undergo apoptosis by TGF- treatment, a mitochondria-to-nucleus translocation of ARTS was seen which was absent in the P-loop mutant, thus the P-loop has been assumed essential for its apoptogenic activity (LARISCH *et al.*, 2000). In a later study by Yossi *el. al.*, (2004) it was found that ARTS is capable of promoting apoptosis in diverse cell types (for example, HeLa, COS-7, HL-60, K562, A549 and NRP154) in response to various pro-apoptotic stimuli (for example, staurosporin, etoposide, arabinoside, and Fas) (YOSSI *et al.*, 2004) and was not restricted to TGF- induction only as reported previously (LARISCH *et al.*, 2000). ARTS is also known to interact and target XIAP, a member of IAP family of proteins but the role of this interaction is not completely defined yet (YOSSI *et al.*, 2004). It has been found that ARTS release from the mitochondria is a caspase independent event (YOSSI *et al.*, 2004). Thus, release of ARTS from the mitochondria is an upstream process which occurs well before the release of Smac/DIABLO and cytochrome c like apoptogenic factors (YOSSI *et al.*, 2004). A remarkable downregulation in the levels of XIAP was observed in ARTS-promoted apoptosis, and therefore a function of ARTS homologous to the IAP antagonists Grim, Hid, and Reaper of Drosophila has been proposed (YOSSI *et al.*, 2004). ARTS is short lived protein and is kept at low levels through constant ubiquitin-mediated degradation in healthy cells (LOTAN *et al.*, 2005). On the other hand, in the cells induced to undergo apoptosis, ARTS levels are increased by the inhibition of its ubiquitin-mediated loss (LOTAN *et al.*, 2005). ARTS protein has been reported to be lost in majority of childhood acute lymphoblastic leukemia (ALL) patients and proposed as a tumor suppressor protein in childhood ALL (ELHASID *et al.*, 2004). Also a critical role has been assigned to ARTS as an important protein for late spermatogenesis in mice, supporting its important physiological role in caspase regulation through IAP inhibition (KISSEL *et al.*, 2005).

1.1.3 Role of anti-apoptotic IAPs in apoptosis

IAPs, on the other hand, is a group of anti-apoptotic proteins called as Inhibitors of Apoptosis Proteins. Besides, XIAP and LIVIN other members of IAP family are Survivin, c-IAP1, c-IAP2 etc. All members of this family are characterized by the presence of one to three tandem baculovirus IAP repeats (BIR) motifs and some of them including Livin possess a COOH terminal RING (Really Interesting New Gene) domain. The ~70 amino acid baculovirus IAP repeat was initially reported in the baculovirus genome, which caused suppression of apoptosis by a mechanism that involved modulation of the host apoptotic machinery (CROOK *et al.*, 1993). IAP family of proteins has been found conserved from single cell species of *Saccharomyces cerevisiae* to mammals characterized by the presence of atleast one BIR domain and apoptosis inhibitory effect (UREN *et al.*, 1998) (DEVERAUX and REED, 1999). IAPs have been shown to bind caspases *in vivo* to inhibit their activities (DEVERAUX *et al.*, 1997; ROY *et al.*, 1997; DEVERAUX *et al.*, 1998; DEVERAUX and REED, 1999). IAPs are the first known endogenous caspase inhibitors (DEVERAUX *et al.*, 1999).

IAP family members have been implicated in several physiological disorders where spinal muscular atrophy (SMA, a motor neuron degenerative disorder) was the first disease associated with the genetic deletion of NIAP gene characterized by the loss of neurons. Limiting the caspase activation in neurodegenerative diseases such as Alzheimer's and Parkinson's diseases by interference with IAPs has been proposed as potential therapeutic target (SALVESEN and DUCKETT, 2002; LISTON *et al.*, 2003). A deregulation in the apoptotic machinery can also result in the excessive survival of cells making them oncogenic and many of the anti-apoptotic factors including IAPs are found up regulated in cancerous cells (IMOTO *et al.*, 2001; DAI *et al.*, 2003; YANG *et al.*, 2003). In line with these observations chromosomal amplification of several IAP genes such as c-IAP1 and c-IAP2 have been identified in diverse cancerous cell lines (DAI *et al.*, 2003). Not to mention, a recently identified novel member of IAP, Livin/ML-IAP (Melanoma-IAP) has been found to be upregulated in melanomas making cells resistant to numerous apoptotic stimuli and chemotherapeutic agents such as 4-TBP, a skin damaging agent (VUCIC *et al.*, 2000). IAPs are being investigated as attractive targets for the treatment of various cancers, arising from their up regulation (LISTON *et al.*, 2003).

1.1.4 Livin function in apoptosis

Livin was identified as a novel human IAP protein consisting of a single BIR domain and C-terminus RING domain mainly expressed in the placenta, lymph node and fetal kidney and so

was called as KIAP (Kidney Inhibitor of Apoptosis Protein) (LIN *et al.*, 2000). KIAP was found to inhibit apoptosis induced by the over expression of pro-apoptotic Bax (LIN *et al.*, 2000). Subsequently, this novel human protein was identified as commonly over expressed protein in various melanoma cell lines and named as ML-IAP (Melanoma Inhibitor of Apoptosis Protein) (VUCIC *et al.*, 2000). Characterization of ML-IAP revealed its anti-apoptotic nature and potential to block apoptosis in response to various stimuli (for example, death receptor Fas ligation as well as chemotherapeutic agents), and its activity was found comparable to the previously characterized IAPs, viral p35 and human XIAP and c-IAP (VUCIC *et al.*, 2000). ML-IAP was found to inhibit the caspase 3 activity by direct association and also inhibit caspase 9 function, though it was not able to inhibit caspase- 1, 2, 6, 8 and weakly inhibited caspase 7 compared to c-IAP1 (VUCIC *et al.*, 2000), thus ML-IAP is considered as a weak inhibitor of caspases and apoptosis. Additionally, a third study by Kasof *et. al.* reported that LIVIN binds to unprocessed (45 kDa) inactive and processed (35 kDa) active forms of caspase-9 *in vivo*, and active forms of caspase-3 and -7 *in vitro* (KASOF and GOMES, 2001). Also recombinant Livin inhibited maturation of caspase 9 in the presence of activating factors, cytochrome c, Apaf-1 and dATP (KASOF and GOMES, 2001). Further it was observed that the use of anti-sense construct of Livin specifically initiated apoptosis in the cell lines expressing Livin mRNA, thus a novel strategy to induce apoptosis in cancerous cell lines was proposed (CRNKOVIC-MERTENS *et al.*, 2003). Further studies have shown that human tumor cells can be resensitized to apoptosis by viable si-RNA technology and Livin represents as important target (KASOF and GOMES, 2001; WANG and FU, 2004). Since then several potential studies have been done marking Livin as a very potential and promising therapeutic target for the treatment of cancer malignancies (ZHANG *et al.*, 2003; ANDERSEN *et al.*, 2004; DE GRAAF *et al.*, 2004; WANG and FU, 2004; SUN *et al.*, 2005; CRNKOVI -MERTENS *et al.*, 2006; CHANG and SCHIMMER, 2007; CRNKOVI -MERTENS *et al.*, 2007; LIU *et al.*, 2007; CAI *et al.*, 2008). Livin was found to be expressed in two isoforms, Livin and Livin , lacking a 18 amino acid BIR-RING connector with varied tissue specific distribution of the two isoforms (ASHHAB *et al.*, 2001). Low levels of only Livin were found in the brain and no expression was detected in the fetal tissues, where as high expression of the form could be detected in the fetal kidney and lower levels in the placenta and heart cells (ASHHAB *et al.*, 2001). The two isoforms of Livin also showed variation in their anti-apoptotic effect in response to various stimuli (ASHHAB *et al.*, 2001; NACHMIAS *et al.*, 2003). Livin- was found to efficiently block staurosporine induced apoptosis, whereas only Livin- could inhibit etoposide induced apoptosis (ASHHAB *et al.*,

2001; NACHMIAS *et al.*, 2003). In MeWo, a melanoma cells line, high levels of Livin are expressed and in a study by Nachmias *et. al.,* (2003) a specific cleavage of Livin   and   isoforms was observed in response to the apoptotic induction by staurosporine (NACHMIAS *et al.*, 2003). Cleaved products of Livin   (39 kDa) and Livin   (37 kDa) were named as p30-Livin   and p28- Livin , respectively (NACHMIAS *et al.*, 2003). Concomitantly, cleavage of Livin isoforms was found to be accompanied by the caspase 3 mediated fragmentation of PARP (Poly-ADP Ribose Polymerase), a hallmark of apoptosis, establishing a relationship between Livin cleavage, caspase 3 and apoptosis (NACHMIAS *et al.*, 2003). The cleavage was identified as the result of effector caspase 3 and 7 in both Livin   and   isoforms (NACHMIAS *et al.*, 2003). However, pan-caspase inhibitor was not able to completely block the caspase cleavage of Livin, thus, involvement of other mechanism was not excluded (NACHMIAS *et al.*, 2003). Importantly, cleavage site of Livin was identified at the N-terminus sequence $DHVD_{52,}$ and cleaved product did not only lose the anti-apoptotic activity but additionally gained a pro-apoptotic effect compared to the wild type (NACHMIAS *et al.*, 2003). Newly exposed N-terminal sequence after caspase cleavage as well as RING domains were identified essential for the observed pro apoptotic effect of truncated Livin (NACHMIAS *et al.*, 2007). In a more recent study about the cleavage of Livin during apoptosis induction, it was found that Livin is cleaved in response to various stimuli and only specific mutation of $DHVD^{52}$, Asp52 to Ala or deletion of the adjacent region (53 – 61 residue) abrogated the caspase cleavage, whereas the mutation of Asp52 to Glu did not affect caspase cleavage *in vivo* (YAN *et al.*, 2006). Also, inhibition of caspase mediated cleavage by pan-caspase inhibitor, ZVAD-fmk, was sensitive in 4-TBP but not to UVB or Cisplatin induced apoptosis (YAN *et al.*, 2006). These results established a complicated nature of IAP regulation and a possible involvement of non-canonical caspases or recognition of non-canonical caspase cleavage sites in Livin. Elimination of IAP mediated caspase inhibition is an essential step in the execution of apoptosis and the one described mechanism is the targeted attack by mitochondrial proteins Smac/DIABLO released with cytochrome c during apoptosis (DU *et al.*, 2000; VERHAGEN *et al.*, 2000). Caspase mediated cleavage of Livin during apoptosis is the second mode of mechanism, by which barrier posed by IAP can be removed (DEVERAUX *et al.*, 1999). Cleavage of XIAP during apoptosis has been found, where XIAP was cleaved into (i) a fragment containing BIR 1 and 2 domains, which retained anti-apoptotic activity, however, at a significantly lower level compared to full length XIAP and (ii) a second fragment consisting of remaining portion of XIAP, BIR 3 domain and RING domain, was found to have gained a prominent pro-apoptotic activity (DEVERAUX *et al.*,

1999). Livin has been also reported to interact with Smac/DIABLO during apoptosis and promotes its degradation via ubiquitin proteosome pathway (MA *et al.*, 2006). Livin itself is known to undergo auto-ubiquitination in healthy cells, to maintain minimum threshold levels for normal physiological processes within the cells (MA *et al.*, 2006). In more recent studies, ARTS appears to act upstream of Smac/DIABLO to promote apoptosis, by directly inhibiting IAP activity (YOSSI *et al.*, 2004). However, the regulation of IAP proteins is much more complicated phenomenon, and little data exist about the role of pro-apoptotic ARTS and IAPs (for example, Livin) in the process of apoptosis. Lastly, cellular acidity is a common feature observed at the onset of apoptotic conditions and V-ATPases have been directly implicated in apoptosis. Increased V-ATPase expression has been associated with delayed apoptosis (GOTTLIEB *et al.*, 1995). On contrary, specific inhibitors of V-ATPase cause cell death by apoptosis (NISHIHARA *et al.*, 1995) (JIAKE XU, 2003). In recent years, certain novel apoptotic genes have been identified that do form part of V-ATPase complex (ANDERSON and WILLIAMS, 2003; LI *et al.*, 2006). Subunit B2 isoform of human V-ATPase has been reported as an important anti-apoptotic factor and it's over expression resulted in apoptotic cell death protection of HEK 293 cells to serum withdrawal or staurosporine treatment (LI *et al.*, 2006). These studies indicate that V-ATPase, besides its primary proton function, is obviously involved in diverse processes of cells. However, roles of most other subunits of V-ATPase in processes other than ATP cleavage/proton transport remained to be discovered.

1.2   Eukaryotic V_1V_O ATPase (V-ATPase)

1.2.1 Function and regulation of V_1V_O ATPase

ATP (adenosine triphosphate) is a well known and precious universal energy currency of the biological cell and is utilized as energy molecule to drive most physio-chemical activities in the cell that are dependent on energy. ATP powers processes such as nerve conduction, maintenance of correct acidity in cytoplasm and vacuoles, active transport, muscle contraction, bioluminescence, signaling, perception of pain and taste and many other uncountable and beautiful processes of life, making this small molecule an incredible and magical entity in the cell. Chemical energy of ATP is stored in high potential phosphoanhydride bonds and removal of terminal phosphate during ATP hydrolysis liberates energy to drive potentially unfavorable reactions. ATP was discovered by Karl Lohmann in 1921 and later in 1941 (LIPMANN, 1941).
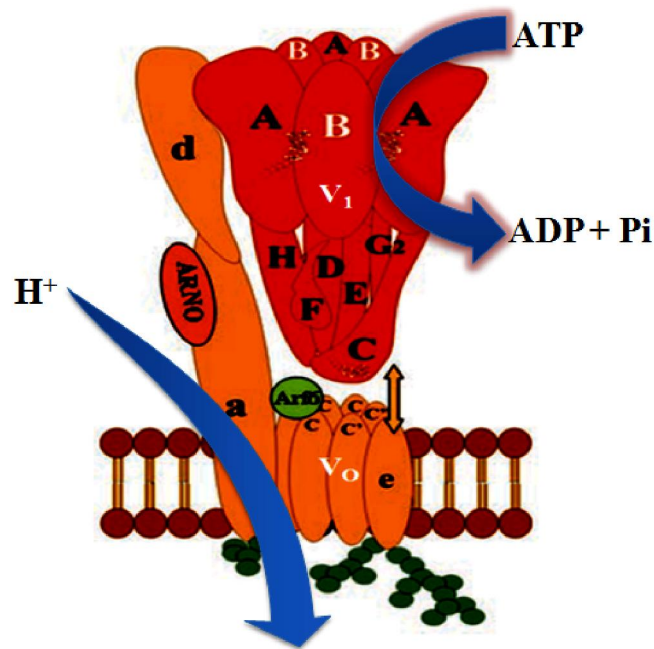
Figure I4. Energy released during ATP hydrolysis on the V_1 catalytic domain of V-ATPase is used to drive the proton transport across the intracellular or plasma membrane (V_O domain) to acidify the respective cellular compartments and generate the proton gradient across the membrane that is used for the endo- and exocytic protein trafficking as well as coupled transport via anti- and symporters such as electrophretic uptake of malate in the plant cell vacuoles, electrophoretic transport of Cl^- across endosomal membranes via Cl^-/H^+ anti-porter (ClC-5) and uptake of neurotransmitter via VMAT.

V-ATPase (vacuolar ATPase) is a multi-subunit motor protein and the most fundamental unit of cell (Figure I4). Vacuolar ATPases were initially identified in the yeast vacuolar membrane preparation experiments and named as Mg^{2+}-ATPase, and eventually reported as an important marker of these organelles (KAKINUMA *et al.*, 1981). It came to be known as Mg^{2+}-ATPase for its Mg^{2+} dependent ATP hydrolysis activity (KAKINUMA *et al.*, 1981). Mg^{2+}-ATPases differed from the mitochondrial ATPase in pH optimum and sensitivity to inhibitors (KAKINUMA *et al.*, 1981). Contrary to mitochondrial ATPase, Mg^{2+}-ATPases activity was not inhibited by ADP (KAKINUMA *et al.*, 1981). Mg^{2+}-ATPase was characterized as the proton (H^+) translocating ATPase and responsible for generating an electrochemical potential of proton difference across the membrane, demonstrated by the use of florescence quenching dyes in presence of ATP. It was also shown that this system acts as potential energy donating system for the secondary processes of amino acid uptake as well as ions uptake through antiporters (KAKINUMA *et al.*, 1981). Later, another study demonstrated that clathrin coated vesicles also contain such proton pumping machines, which are responsible for generating low pH inside the vesicles, that is required for dissociation of receptor-ligand complex inside the cytoplasm, release of virus

genome, and various other proteins and hormones which have been endocytosed by the plasma membrane in the form of coated vesicles (FORGAC *et al.*, 1983).

Inherent catalytic activity of V-ATPases result in the liberation of energy from the hydrolysis of ATP into ADP and Pi (Figure I1) that is utilized to transport the protons (H^+) across diverse membranes to generate an electrochemical potential (H^+), which in turn is used to drive various secondary transports via symporters and antiporters as well as channel mediated transports (BEYENBACH and WIECZOREK, 2006). V-ATPase, as the name suggests is present on the endo-membrane systems such as vacuoles, Golgi, lysosomes, secretory vesicles, storage vesicles, synaptic vesicles and endosomes, with increasing examples of V-ATPase being associated with the plasma membrane such as osteoclasts, male reproductive tract and kidney intercalated cells, to regulate the acidic environment inside and outside the cell, respectively (BROWN and BRETON, 2000; NISHI and FORGAC, 2002; BEYENBACH and WIECZOREK, 2006; BRETON and BROWN, 2007; YAO *et al.*, 2007; GRÜBER and MARSHANSKY, 2008). V-ATPases are lineal coordinators of several physiological processes such as intracellular protein trafficking, targeting and degradation, enzyme maturation in lysosomes, accumulation and secretion of neurotransmitters, receptor mediated endocytosis besides the functions linked to their plasma membrane presence such as membrane energization, bone resorption, acid secretion by macrophages, acid secretion and protein reabsorption of kidney cells, maintenance of pH for sperm maturation and keeping sperms in immotile state during its passage through vas deferens and epididymis are few of the functions that can be ascribed to V_1V_O ATPases (NELSON and HARVEY, 1999; BROWN and BRETON, 2000; BEYENBACH and WIECZOREK, 2006; GRÜBER and MARSHANSKY, 2008).

Vacuolar ATPases are also obligatory components in the mid gut alkalization of lepidopteran insects such tobacco hornworm (*Manduca sexta*) larva and mosquito *(Aedes aegypti)* larva mid gut, where pH can go beyond 11 with the aid of V-ATPase (LEPIER *et al.*, 1994; WIECZOREK *et al.*, 1999; ZHUANG *et al.*, 1999). Mid gut goblet cells plasma membrane of tobacco hornworm contains high amounts of V-ATPases which generate an electrochemical gradient of protons (H^+) via ATP dependent primary transport. The generated proton gradient is then coupled to the anti-porter $2H^+/K$ to transfer K^+ to the midgut, producing a high alkalinization (LEPIER *et al.*, 1994). Such mechanism also established that proton motive force (pmf) is an alternative to sodium motive force for energizing the animal plasma membranes (LEPIER *et al.*, 1994). High mid gut pH in the insects is thought to help in the breakdown of dietary tannins, to aid in the absorption process (ZHUANG *et al.*, 1999).
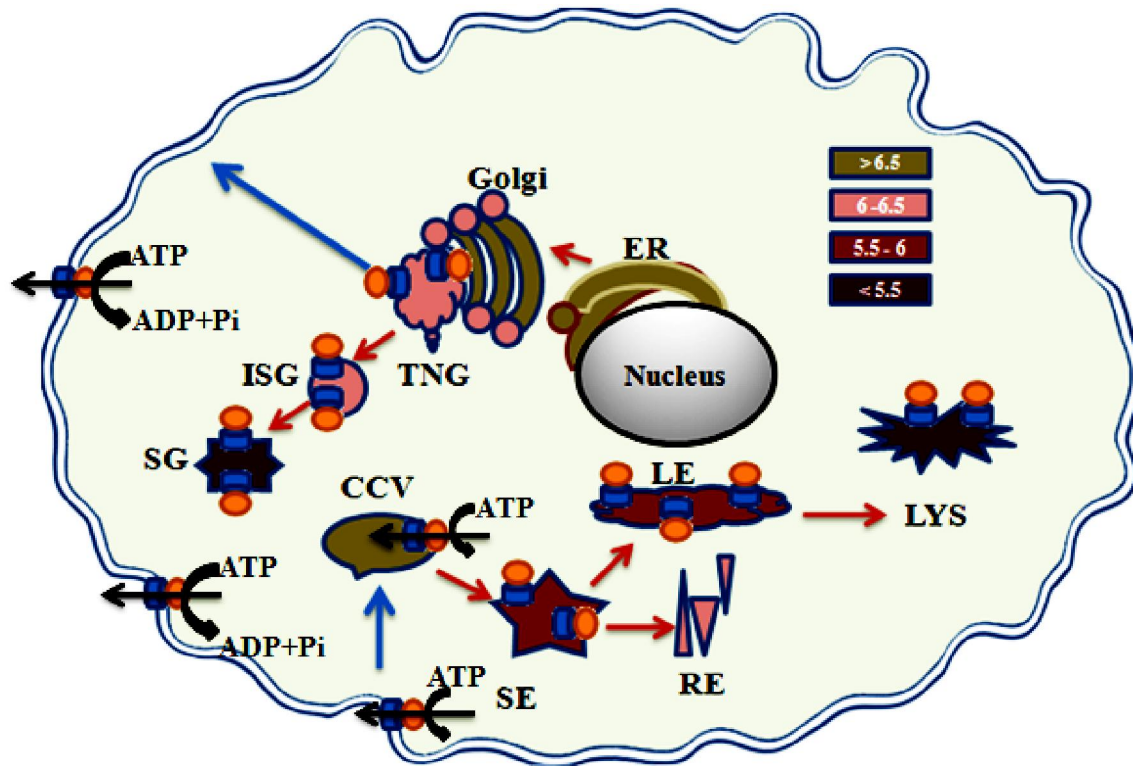
Figure I5: **V-ATPase in the endocytic and the exocytic membrane traffic.** Endocytosed cargo (for example, hormones) in clathrin coated vesicles (CCV) is taken up by the sorting endosomes (SE, also called as early endosomes) where lower pH allows the dissociation of receptor and ligand from each other. Recycling membranes are either directly transported back to the plasma membrane or routed back through specialized recycling endosomes (RE). Other part of sorting endosomes containing ligand and fluid phase proteins are delivered to the late endosomes (LE) and finally to the lysosomes (LYS). pH gradually decreases with passage of cargo enroute to the lysosomes, the most acidic compartment. In the secretory or biosynthetic pathway, the membrane or secretory proteins are sorted after post translational modification and maturation in endoplasmic reticulum (ER). Modified and properly folded proteins are then targeted to the cis-Golgi and finally via cis-face cargo enters into the Golgi and buds off via trans-Golgi network (TGN). Several post translational modifications are achieved in the Golgi complex. Proteins are then delivered to immature secretory granules (ISG) and finally to the secretory granules (SG) followed by fusion with the plasma membrane. In some polarized cells, proteins are directly targeted from the TGN to respective destination via distinct carriers. Distribution of V-ATPase complex is shown on the endosomal and secretory system as well as on the plasma membrane (for example, mid-gut cells of *Manduca sexta* and proximal tubular cells of kidney). V-ATPase is responsible for the generation and maintenance of pH inside celluar compartments they are present on as well as on the extracellular environment when present on the plasma membrane.

Vacuolar ATPases also play essential role in the accumulation of neurotransmitter at the nerve endings and during the synaptic activity, when presynaptic vesicles are docked to the synaptic membrane and neurotransmitters are released via membrane fusion channel formed by the merger of two opposing V_O domain of V-ATPase (MOREL, 2003). Under such conditions free V_O sectors are generated by established regulatory phenomenon of reversible disassembly, where soluble V_1 domain dissociates from membrane V_O sector to inhibit V-ATPase activity (KANE, 1995; KANE, 2000; BEYENBACH and WIECZOREK, 2006). Membrane ligation occurring via V_O domain has also been studied in the yeast vacuolar fusion process as an important step of vesicle unification (PETERS *et al.*, 2001). Other than this, the membrane fusion process has also

been studied in *D. melanogaster* and *C. elegans* and has been found as a separate function of V-ATPase independent of its proton pumping activity (FORGAC, 2007). More recently, a more diverse and unexpected function of V-ATPase in the left-right symmetry during the development in *Xenopus* has been reported (ADAMS *et al.*, 2006). This mechanism is conserved in chick and zebra fish and appears as an early upstream event in the process of development (ADAMS *et al.*, 2006).

The roles of V-ATPase in the physiological processes other than proton pumping is extensively growing and a very important function of pH sensing has been assigned to V-ATPase very recently (HURTADO-LORENZO *et al.*, 2006). During this study, V-ATPase was found to directly associate with Arf6 (ADP-ribosylation factor 6), a low molecular GTPase and ARNO (ADP-ribosylation Factor Nucleotide site Opener), a GEF (GTP/GDP Exchange Factor) of Arf6, via subunit *c* and subunit *a2* of the mouse V-ATPase, respectively (HURTADO-LORENZO *et al.*, 2006). Arf interacts with ARNO on the scaffold provided by V-ATPase in a pH dependent manner and disruption resulted in the reversible inhibition of endocytosis and block of protein trafficking between early and late endosomes (MARANDA *et al.*, 2001; HURTADO-LORENZO *et al.*, 2006). Arf and ARNO proteins are essential for various other signaling pathways such as cytoskeleton organization, maintenance of Golgi structure and function, synaptic transmission, epithelial cell migration and many more (SANTY and CASANOVA, 2001) (FRANCO *et al.*, 1998; ASHERY *et al.*, 1999). V-ATPase thus forms a vital platform to communicate between intracellular components, regulating them, and establishing a defined network of processes to attain right physiology within and outside the cellular milieu.

V-ATPases are not only critical to maintain proper physiological conditions for efficient growth, proliferation and functioning of diverse cell types but also involved in various disease conditions that have been reported including cancer and diabetes. Extracellular acidity has been implicated as an important factor in the cellular invasiveness, tumor proliferation and metastasis (SENNOUNE *et al.*, 2004; SENNOUNE and MARTINEZ-ZAGUILAN, 2007). It has been seen that cancerous cells that are highly metastatic in nature have increased V-ATPase density compared to the cells that exhibit low metastatic rate. Metastatic cells also exhibit enhanced plasma membrane V-ATPase activity to maintain proper cellular acidity, whereas lowly metastatic cells use the ubiquitous Na^+/H^+ and HCO_3^- based H^+ pumps (SENNOUNE *et al.*, 2004). Thus, the excessive expression of the plasma membrane V-ATPase gives the cells an edge in the increased proliferation and metastatic activity (SENNOUNE and MARTINEZ-ZAGUILAN, 2007). The cancerous cells have high acidic outside and more alkaline internal

cytosolic environments (SENNOUNE and MARTINEZ-ZAGUILAN, 2007). Since, cellular acidity is associated with apoptosis (GOTTLIEB *et al.*, 1995; LAGADIC-GOSSMANN *et al.*, 2004), cancerous cells must develop a counter mechanism to maintain an alkaline pH for extensive proliferation (SENNOUNE and MARTINEZ-ZAGUILAN, 2007). The poorly engiogenic cells of diabetes mellitus exhibit decreased plasma membrane V-ATPase and thus have reduced proliferative and invasive properties (SENNOUNE and MARTINEZ-ZAGUILAN, 2007). V-ATPase is reportedly also involved in multi-drug resistance (MDR) (SENNOUNE *et al.*, 2004). MDR is associated with the altered cytosolic acid/base homeostasis and certain cell types (for example, HL60) have shown the efflux of doxorubicin drug in an energy dependent manner, and use of specific V-ATPase inhibitors caused the accumulation of drug (SENNOUNE *et al.*, 2004). V-ATPase is also an essential component in the initiation of apoptosis. Again, pH is a critical factor to trigger cell death and studies have shown that apoptosis is preceded by the rise in celluar acidity, due to the non-functioning of V-ATPase (GOTTLIEB *et al.*, 1995). Inhibition of V-ATPase by specific inhibitors such as bafilomycin A1 causes cellular apoptosis (NISHIHARA *et al.*, 1995; JIAKE XU, 2003),(YOSHIMOTO and IMOTO, 2002). Apoptotic death of Neutrophils under *in vitro* culture condition is reported, that can be delayed by the presence of G-CSF (Granulocyte Colony Stimulating Factor) via a mechanism which involved the up regulation of V-ATPase (GOTTLIEB *et al.*, 1995).

V-ATPase (V_1V_O ATPase) is composed of two main structural and functional components, head piece V_1, which forms catalytic core and V_O domain, forming the proton channel of enzyme, respectively (GRÜBER, 2003; GRÜBER and MARSHANSKY, 2008). Most V-ATPases are composed of 14 well defined subunits and some accessory subunits (SMITH *et al.*, 2003; GRÜBER and MARSHANSKY, 2008; MARSHANSKY and FUTAI, 2008). The V_1 sector is composed of eight subunits in the stoichiometry of $A_3:B_3:C:D:E_{2-3}:F:G_{2-3}:H_x$ (OHIRA *et al.*, 2006; GRÜBER and MARSHANSKY, 2008; KITAGAWA *et al.*, 2008; RISHIKESAN *et al.*, 2009). $A_3:B_3$ forms the core of catalytic center that is responsible for the hydrolysis of ATP. V_O is mostly membrane embedded hydrophobic region of the complex, composed of six different subunits, $a_1:d_1:c_{4-5}:c'_1:c''_{1:}e$ in yeast V-ATPase (FORGAC, 2007; GRÜBER and MARSHANSKY, 2008) and an additional hydrophobic subunit *e* has recently been identified (SAMBADE and KANE, 2004; COMPTON *et al.*, 2006). In higher eukaryotes, *c'* subunit is missing but accessory subunits Ac45 (SUPEK *et al.*, 1994; JANSEN *et al.*, 1998) and M8-9 (LUDWIG *et al.*, 1998; DEMIRCI *et al.*, 2001) are found attached to the V_O domain. A heavily glycosylated V_O associated subunit M9.7 has been identified in midgut and Malpighian tubules

of *M. sexta* (MERZENDORFER *et al.*, 1999). Various subunits of V-ATPase are expressed in different isoforms, especially in higher eukaryotes, multicellular complex organism, to achieve the target specific functions (GOGARTEN *et al.*, 1992; KARET, 2005). These include subunit *d* (NISHI *et al.*, 2003), subunit G (SUN-WADA *et al.*, 2003), subunit C (MURATA *et al.*, 2002; SUN-WADA *et al.*, 2003), subunit *a* (KARET, 2005; NISHI, 2005), and E (STROMPEN *et al.*, 2005). In *Paramecium tetraurelia*, 17 isoforms of subunit *a* have been identified, representing the largest isoform for any of V-ATPase subunit (WASSMER *et al.*, 2006). In yeast, however, all subunits are encoded in single isoform by their respective single genes (as shown in table below), with the exception of subunit *a*, which is produced in two different isoforms, Vph1 (vacuole specific) (MANOLSON *et al.*, 1992) and Svt1 (Golgi specific) (MANOLSON *et al.*, 1994).

Domain	Subunits	Yeast Gene	MW (kDa)	Subunit Function
V_1	A	*VMA1*	70	Catalytic site, coupling, peripheral stalk
	B	*VMA2*	60	Non-catalytic, regulatory, actin and aldolase binding
	C	*VMA5*	40	Activity, assembly, reversible dissociation, actin binding
	D	*VMA8*	34	Assembly
	E	*VMA4*	33	Activity, assembly, peripheral stalk, RAVE, aldolase binding
	F	*VMA7*	14	Activity, assembly
	G	*VMA10*	13	Activity, assembly, peripheral stalk
	H	*VMA13*	50	Regulator subunit, assembly
V_O	*a*	*VPH1, STV1*	100	Proton pumping, targeting, assembly, peripheral stalk
	d	*VMA6*	40	Coupling, peripheral stalk, activity
	c	*VMA3*	17	Proton transport, bafilomycin binding
	c'	*VMA11*	17	Proton transport
	c''	*VMA16*	21	Proton transport
	e	*VMA9*	9	unknown

Table 1. **Subunit composition of the catalytic V_1 and proton translocating V_O domains of V-ATPase.** *Saccharomyces cerevisiae* V-ATPase subunit genes are shown along with respective molecular masses of each subunit. Subunit function (adapted from different original research article, see text for references and detailed function of each subunit) is also shown.

V-ATPase has mechanistic and overall structural similarities to F_1F_O and A_1A_O ATP synthases; however, they have remarkable diversities in subunit composition, functioning as well as modes of regulation (GRÜBER and MARSHANSKY, 2008). V-ATPases are exclusively ATP dependent proton pumps, in contrast to F/A-type ATP synthases, which produce ATP at the expense of proton motive force (pmf) under physiological conditions in eukaryotes and archae, respectively (GRÜBER and MARSHANSKY, 2008). Also, V-ATPases are regulated by

reversible disassembly phenomenon causing dissociation of V_1V_O ATPase into individual sectors, V_1 and V_O in response to various extracellular conditions such as glucose deprivation (KANE, 1995). Such regulatory mechanism is absent in the A type and F type ATP synthases.

1.2.2 Structural feature of V_1V_O ATPase

The ~570 kDa peripheral, soluble domain of V-ATPase is dressed in a hexameric fashion at the top, formed by the alternating arrangement of subunit A and B, around a central cavity which occupies an asymmetric seventh mass forming the central stalk (RADERMACHER *et al.*, 2001; GRÜBER, 2003). Subunit A and B, which are homologous to the subunits and , respectively, of the related F_1 ATPase domain of F_1F_O ATP synthase, are responsible for the catalytic activity (GRÜBER, 2003; BEYENBACH and WIECZOREK, 2006). The subunits are also involved in the regulation and assembly of the complex. Other than this subunit B is also involved in the binding of actin (CHEN *et al.*, 2004) (HOLLIDAY *et al.*, 2005) and aldolase (LU *et al.*, 2003). Subunit C has been shown important in the regulation of reversible disassembly of V_1 from V_O during physiological stress, such as deprivation of glucose from the media or a drop in the ATP to ADP ratio (ARMBRÜSTER *et al.*, 2005; BEYENBACH and WIECZOREK, 2006; HONG-HERMESDORF *et al.*, 2006). Subunit C is the only component of V_1V_O ATPase that is lost during this physiological regulatory process when V_1 pops-off from V_O, via binding to the actin cyskelton (ARMBRÜSTER *et al.*, 2005; VITAVSKA *et al.*, 2005; BEYENBACH and WIECZOREK, 2006). Besides, mutational analysis of subunit C has demonstrated a critical role to balance the activities like V_1V_O assembly as well as ATPase activity (CURTIS *et al.*, 2002). Vma5p (subunit C) also binds WNK kinase and undergoes phosphorylation (HONG-HERMESDORF *et al.*, 2006). Thus, C subunit is an important protein that communicates with the signaling pathways and regulatory mechanism of V-ATPase to attain maximum favorable physiological order within the cell. Subunit D of V_1 domain encodes an 32 kDa protein in yeast designated as Vma8p (GRAHAM *et al.*, 1995), and its disruption resulted in the typical *vma* phenotype, where mutants were unable to grown at neutral pH 7.5 and on non fermentable carbon sources but exhibiting normal growth at pH 5.0 (GRAHAM *et al.*, 1995). Moreover, *vma8* mutants failed to assemble the V_1 onto the V_O sector besides, subunit D alone was also unable to assemble with V_O in the absence of fully assembled V_1 domain (GRAHAM *et al.*, 1995). Also subunit D has been shown not required for ATP hydrolytic activity in presence of Ca^{2+} and methanol induced Mg^{2+} -dependent ATPase activity (COSKUN *et al.*, 2004) however, the detailed role(s) of subunit D is still a matter of debate. Other subunits of V-ATPase including

subunit E and G are debated to be present in multiple copies per complex (OHIRA *et al.*, 2006; KITAGAWA *et al.*, 2008). Mutational analysis have demonstrated essential role of subunit E in the assembly and catalytic activity of A_3B_3 (OWEGI *et al.*, 2005). Subunit E has also been shown in close proximity to the catalytic subunits A, B and to subunit D (in nucleotide dependent manner) and also known essential for the ATPase activity as well as E subunit conformational changes in presence of Ca^{2+}ATP and -ADP are reported in *M. sexta* V_1 ATPase (GRÜBER *et al.*, 2000). N-terminus domain of subunit E form 19-39 amino acid has been recently mapped to bind with subunit G (RISHIKESAN *et al.*, 2008), whereas the C-terminus of E is believed to have a regulatory function in V_1V_O ATPase (OWEGI *et al.*, 2005). Subunit G is required for ATPase activity and assembly of V_1V_O and mutations can partially inhibit the reversible disassembly (CHARSKY *et al.*, 2000). Of the remaining two subunits F and H of V-ATPase, subunit F is involved in V_1V_O assembly (GRAHAM *et al.*, 1994; NELSON *et al.*, 1994; AVIEZER-HAGAI *et al.*, 2003), whereas subunit H is essential regulatory component and believed to inhibit the V-ATPase activity of dissociated V_1 domain during the process of reversible disassembly (PARRA *et al.*, 2000; SAGERMANN *et al.*, 2001; JEFFERIES and FORGAC, 2008). The studies with *M. sexta* V_1 ATPase domain has shown that subunit C, F and H dissociation increases the hydrolyzing activity of the V_1 (RIZZO *et al.*, 2003), thus they do not form the core of ATPase active V_1 subcomplex.

1.2.3 Subunit *d* of V-ATPase

Subunit *d* was initially observed as a 39 kDa protein in purified H^+-ATPase chromaffin granule membrane preparation (WANG *et al.*, 1988). An antibody raised against this protein cross-reacted to various membrane preparations from other sources as well, which suggested the sequence homology amongst subunit *d* from diverse origins that has been conserved through the evolution, pointing to the essential role of this protein in the H^+-ATPase (WANG *et al.*, 1988). However, no function of this protein was reported but studies revealed that mild treatment with chaotropic agents failed to remove it from the membrane, so a membrane integral perspective and an ancillary function was suggested (WANG *et al.*, 1988). Later it was shown that a fraction of V_1 subunits can assemble in absence of Vo that lacks subunit *d*, and association of such V_1 (–subunit *d*) with membrane V_O can partially restore proton pumping. However, the complex as a whole was very unstable to detergent solubilization and immunoprecipitation, establishing a structural and functional role of subunit *d* (PUOPOLO *et al.*, 1992). Also, it was observed that addition of subunit *d* during reassembly of V_1V_O increased the ATPase activity by two fold,

indicative of a vital role of subunit *d* in accomplishing the maximal activity of V_1V_O complex (PUOPOLO *et al.*, 1992). This study also reported that functional assembly of V_1V_O requires the presence of 34 kDa subunit E (PUOPOLO *et al.*, 1992). In the absence of E subunit about 50% higher activity could be achieved compared to the condition when subunit *d* was lacking, and about 75 – 80% activity compared to fully assembled V-ATPase (PUOPOLO *et al.*, 1992). Thus disruption of subunit *d* was more lethal than subunit E presenting the functional significance of this protein in V-ATPase activity and assembly. Nevertheless, both subunits were required to attain the maximal activity. VMA6 gene of *Saccharomyces cerevisiae* was cloned and characterized to synthesize a 345 amino acid, 36 kDa protein which remained non-integrally associated with the membrane V_O sub complex (BAUERLE *et al.*, 1993). Discrepancy in the molecular weight was attributed to the overall acidic nature of the protein, whereby it was termed as 36 kDa protein based on its behavior on SDS PAGE, against a predicted molecular mass of 39.8 kDa (BAUERLE *et al.*, 1993). Further it was demonstrated that disruption of VMA6 gene results in a typical *vma* phenotype (BAUERLE *et al.*, 1993). Null mutants of Vma6p were defective in the vacuolar acidification, and isolated membranes did not show any detectable V-ATPase activity (BAUERLE *et al.*, 1993). Also it was seen that endogenous subunit *d* levels remained unaffected by the V_1 subunits but protein level was reduced several folds on the disruption of membrane *vma3* subunit, hence the stability of subunit *d* was rather dependent on the membrane subunits (BAUERLE *et al.*, 1993). In contrast, in the yeast cells lacking subunit *d*, V_1 peripheral subunits were unable to reach and attach the vacuolar membranes (BAUERLE *et al.*, 1993). Characterization of subunit *d* in wild type membrane preparations showed that protein can be removed only by the harsh treatments of chaotropic agents, 5 M urea or solution of Na_2CO_3 at pH 11.5 (BAUERLE *et al.*, 1993). However, these did not remove the remaining V_O subunits (*a,c,c',c''*) (BAUERLE *et al.*, 1993). Again, sequence analysis of Vma6p did not show any obvious putative transmembrane regions in its primary sequence (BAUERLE *et al.*, 1993). Thus, a membrane V_O perspective of subunit *d* came into origin and its essential role in the regulation and assembly of V-ATPase started emerging (BAUERLE *et al.*, 1993). Moreover, tryptic digestion experiments indicated that subunit *d* is exposed in the native complex and its sensitivity to digestion was increased in the membranes stripped of V_1 domain (ZHANG *et al.*, 1992). Membrane reconstitution experiments with subunit *d* and subunit *a* of V_O have demonstrated that they do not form a functional proton channel and presence of 17 kDa subunit *c* is indispensable for proton conduction in fully assembled complex (ZHANG *et al.*, 1994). Different isoforms of subunit *d* have been identified in higher eukaryotes (NISHI *et al.*, 2003;

SUN-WADA *et al.*, 2003; SMITH *et al.*, 2005), whereby they are expressed in tissue specific and developmental stage specific manner (SMITH *et al.*, 2005; SATO *et al.*, 2006). However in yeast single copy gene, VMA6 encodes a single form of subunit *d*, Vma6p (BAUERLE *et al.*, 1993). In mouse V-ATPase two isoforms of subunit *d* (*d1* and *d2)* have been identified (NISHI *et al.*, 2003). Whereas *d1* isoform was ubiquitously expressed in all the tissues and the expression of *d2* was mainly observed in the kidney and to lower levels in the lung, skeletal muscles, heart and testis (NISHI *et al.*, 2003). Only *d1* isoform was able to complement the *vma* phenotype of yeast cells lacking Vma6p, and *d2* isoform containing cells exhibited unstable V-ATPase and reduced proton pumping (NISHI *et al.*, 2003). Variation was also seen in the coupling efficiency between the two isoforms and Vma6p, indicative of a possible role of subunit *d* in the coupling (NISHI *et al.*, 2003). Thus, both isoforms exhibited differences in the formation and stabilization of a functional V-ATPase complex that might be important with respect to their observed tissue specific expression. Further studies showed that *d2* expression was restricted to the kidney and bone cells and could be co-localized with tissue specific *a4* and *a3* subunits, respectively (SMITH *et al.*, 2005). More recent studies have demonstrated that subunit *d* couples ATP hydrolysis with proton conduction across the membranes (OWEGI *et al.*, 2006). Various truncations from the N- or C-terminus destabilized the protein *in vivo* and a functional assembly of V_1V_O was inhibited (OWEGI *et al.*, 2006). Significant level of ATPase activity was dropped in the single point mutants C329A and E317A of subunit *d* of yeast V-ATPase besides the loss of coupling, showing the importance of full length protein in the assembly and activity of the complex *in vivo* (OWEGI *et al.*, 2006). Structural features of subunit *d* of V-ATPase have remained elusive as well as its binding partners. Some studies have revealed association between subunit A and subunit *d* in immunoprecipitation experiments (SHAO and FORGAC, 2004) but there is no further data in this direction. Also, the relationship between subunit *d* and other subunits of V_1 and V_O domains have remained largely unknown till now. Low resolution electronic microscopic structure of V_O domain from clathrin coated vesicles have shown peculiar mass on the luminal side, proposed to be parts of the subunit *d* and subunit *a* (WILKENS and FORGAC, 2001), but due to the absence of structural data about these subunits, an unambiguous assignment of these masses is lacking. Some data also suggest that subunit *d* and subunit *a* might be more extended and possibly components of peripheral stalk (FORGAC, 2000; CLARE *et al.*, 2006), but no conclusive studies have been done so far and subunit *d* remained to be one of the least, structurally as well as functionally, studied subunit of V-ATPase. Structural and biochemical studies can provide vital data about V-ATPase architecture and in

particular, the emerging role of subunit *d* in the diseased conditions and prominent future drug target. Subunit *d* has been associated with impaired osteoclast fusion and bone formation (LEE *et al.*, 2007). Genetic studies with mice showed that subunit *d* is required for osteoclast fusion and maturation (LEE *et al.*, 2007). Osteoclasts are the type of bone cells which are responsible for bone reabsorption, and the loss-of-function of subunit *d* resulted in the excessive bone mass (LEE *et al.*, 2007). This study also provided important genetic data showing that the inhibition of subunit *d* provides vital therapeutic target to stimulate bone formation in disease conditions such as osteoporosis, by specifically interrupting a single, VMA6, encoding subunit *d* protein (LEE *et al.*, 2007).

1.2.4 Subunit *a* of V-ATPase

Subunit *a* of V-ATPase has been shown to play a critical role in the process of proton conduction (KAWASAKI-NISHI *et al.*, 2001). Subunit *a* isoforms have been also demonstrated essential for the targeting of V-ATPase to the specific organelle (NISHI and FORGAC, 2000; KAWASAKI-NISHI *et al.*, 2001). Four isoforms of subunit a (*a1,a2,a3,a4*) found in mice and man are expressed in organelle on different endomembranes or plasma membrane defined by specific function of the cell type (TOYOMURA *et al.*, 2000; OKA *et al.*, 2001; SUN-WADA *et al.*, 2006). Remarkably, 17 different isoforms of subunit *a* are found in *Paramecium tetraurelia*, and its C-terminus was implicated in the specific targeting, which was also studied using florescence labeling of subunit *a* and localization to different compartments of cells revealed highly specialized functional targeting (WASSMER *et al.*, 2006). Subunit *a* is a established *bona fide* protein of V_O domain and was initially identified in the clathrin coated vesicles and the chromaffin granules as a 120 kDa protein which was partially exposed to the cytosolic face of the membrane due to free labeling with lactoperoxidase-catalysed radioiodination (APPS *et al.*, 1989). But unlike other peripheral stalk subunits, *a* subunit could be labeled by hydrophobic probes indicating that a second domain of subunit *a* is rather membrane embedded (APPS *et al.*, 1989). Subsequent analysis of various membrane preparations from diverse plant and animal origin confirmed that subunit *a* consists of a cytoplasmic N-terminal hydrophilic charged domain, and a C-terminal membrane hydrophobic domain (PERIN *et al.*, 1991). A gene encoding the *Saccharomyces cerevisiae* subunit *a* was identified in the vacuolar acidification mutant, vph1-1 (vacuolar pH 1) (PRESTON *et al.*, 1989). Mutants showed the absence of bafilomycin sensitive ATPase activity and defective proton pumping as well as loss of V_1 peripheral subunits from the membranes (MANOLSON *et al.*, 1992). The gene *VPH1* was then

cloned from the   gt11 expression library and independently by the complementation of vph1-1 mutation as well (MANOLSON *et al.*, 1992). Disruption of *VPH1* was not crucial for the survival of yeast but mutants showed defects in assembly and activity of V-ATPase (MANOLSON *et al.*, 1992).

In the meantime, a functional homolog of Vph1p was identified in yeast, named as Stv1p (Similar to Vph1p), showing more than 50% identity to Vph1p (MANOLSON *et al.*, 1994). Defective phenotype of   VPH1 mutants could be rescued by the over expression of STV1 gene, thus *STV1* was able to functionally complement the phenotypes arising from the deletion of *VPH1* (MANOLSON *et al.*, 1994). However, neither of the two deletions independently caused *vma* type phenotype, as had been observed on the disruption of peripheral subunits such as subunits A and B, and only a partial defective growth pattern was seen in   VPH1 yeast, whereas   STV1 cells showed normal phenotype (MANOLSON *et al.*, 1994). Nevertheless, double disruption of both *VPH1* and *STV1* resulted in the typical *vma* phenotype (MANOLSON *et al.*, 1994).

Site directed mutagenesis experiments done by Ling Xh *et. al*., established that charged residues in the transmembrane (TM) region of yeast subunit *a* (Vph1p) are essential for proton conduction, especially the E789Q mutation in TM7 helix, which completely abolished both the proton transport and the ATPase activity but did not affect the subunit stability and complex assembly (LENG *et al.*, 1996). Other two mutations in the helix TM6 (R735L) and helix TM5 (Q634L) destabilized Vph1p besides other mutations in the polar residue, demonstrating that subunit *a* is required for both assembly as well as proton pumping activity of V-ATPase (LENG *et al.*, 1996). Additional mutation experiments showed that negative charge of E789 and positive charge at H743 are not absolutely required for proton transport or V-ATPase activity as indicated earlier (LENG *et al.*, 1998).

 Trypsin cleavage experiments indicated that Vph1p is exposed in V-ATPase and more interestingly its susceptibility to cleavage in the presence of ATP and divalent cations varied (LANDOLT-MARTICORENA *et al.*, 1999). Higher cleavage could be observed in the presence of divalent cations plus ATP than ATP alone (LANDOLT-MARTICORENA *et al.*, 1999). But observed differences in the cleavage sensitivity disappeared when V_1 was stripped off from the membranes (LANDOLT-MARTICORENA *et al.*, 1999). These results showed that subunit *a* adapts single conformation in the absence of V_1 domain and structural changes are accompanied during catalysis in V_1 (A_3:B_3) sector and possibly transmitted to the V_O via subunit *a,* thus physically linking catalytic sector, V_1 with proton channel, $V_{O.}$ To understand the topology and

transmembrane helices orientation of Vph1p, single cysteine residue containing forms of subunit *a* were prepared by mutagenesis and their orientation was studied by the use of either membrane impermeable sulfhydryl reagent, AMS (4-acetamido-4'- maleimidylstilbene-2,2'-disulfonic acid) or membrane permeable, MBP 3'-(N-maleimidylpropionyl) biocytin (MBP) (LENG *et al.*, 1999). Conclusion from these results showed a nine transmembrane helix model with amino- and carboxy terminus located on the cytoplasmic and luminal sides of the membrane, respectively (LENG *et al.*, 1999). Additional mutation studies unequivocally identified R735 in helix TM7 as an absolute requirement for the proton conduction and a non conservative mutation of R735 resulted in the defective assembly and loss of activity and proton conduction in yeast V-ATPase (KAWASAKI-NISHI *et al.*, 2001). Later, using cysteine mediated cross-linking it was shown that TM7 helix R735 is in contact with E145 in the TM4 of c and c' and TM2 of c'' of yeast V-ATPase and association is vital for the transfer of proton to luminal side of the membrane (KAWASAKI-NISHI *et al.*, 2001; WANG *et al.*, 2004). Based on these data, a swiveling interaction model between the helices of subunit *c* and *a,* controlling the flux of proton into hemi-channel was proposed (WANG *et al.*, 2004). Later, a model built upon the NMR structure and dynamic studies of a TM7 region peptide, involved in the proton conduction, showed that this 25 amino acid region formed two helices separated by a ball-and-joint type two amino acid linker that controls the opening and closing of proton hemi-channel in the subunit *a* during proton conduction (DUARTE *et al.*, 2007).

Besides the identified two isoforms in yeast (Vph1p and Stv1p), several isoforms were identified in higher eukaryotes as well (for example, four isoforms in mouse and human (*a1-a4*) and three isoforms in chicken (*a1-a3*)), expressing in tissue and developmental stage specific manner (MATTSSON *et al.*, 2000; NISHI and FORGAC, 2000; TOYOMURA *et al.*, 2000; OKA *et al.*, 2001). Yeast V-ATPase containing different isoforms of subunits *a* differ in the coupling and reversibly disassembly (KAWASAKI-NISHI *et al.*, 2001). Thus, possibility of different isoforms role in the targeting of V-ATPase was very much evident which was additionally confirmed by the chimeric experiments performed with the *Saccharomyces cerevisiae* Vph1p (vacuole specific) and Stv1p (Golgi specific) isoforms (KAWASAKI-NISHI *et al.*, 2001). A chimeric protein containing N-terminal of Golgi isoform Stv1p and C-terminal of vacuole isoform, Vph1p, was targeted to the Golgi and the complex did not showed reversible dissociation in response to glucose depletion (KAWASAKI-NISHI *et al.*, 2001), demonstrating that information for correct targeting is located on the N-terminus of subunit *a* and different isoforms have varied response to physiological conditions (KAWASAKI-NISHI *et al.*, 2001). Whereas the COOH-

terminus has been shown to be involved in the assembly and activity of V-ATPase (LENG *et al.*, 1998). Thus, different isoforms containing V-ATPase exhibit function in the context of its location, making V-ATPase a functionally and regulatory diverse complex in cellular milieu. NH_2-domain, on the other hand, has been also proposed to possibly form the peripheral stator connecting V_1 with V_O to prevent energy loss through futile rotation of V_1 with respect to V_O and reportedly suggested to interact with subunit A and subunit H (LANDOLT-MARTICORENA *et al.*, 2000). Non-homologous region (NHR), a stretch of unique 90 amino acids of subunit A, found only in the V-ATPase and the A-ATP synthase, is also know to interact with a domain consisting of subunit *d* and *a*, linking the two opposite subcomplexes, V_1 with V_O (SHAO and FORGAC, 2004), but detailed studies remain to be done. Subunit G3 of man V-ATPase has been demonstrated to interact with the subunit *a4* from kidney cells as well as from other organs, further indicating possible V_1 to V_O connection via subunit *a* (NORGETT *et al.*, 2007). *a4* isoform is mainly expressed in the kidney cells (OKA *et al.*, 2001). Mutations in the gene encoding subunit *a4* have been associated with distal (or type 1) renal tubular acidosis (dRTA) (WAGNER *et al.*, 2004), (STEHBERGER *et al.*, 2003). Mutation in the *a3* isoform leads to a severe form of infantile malignant osteopetrosis, characterized by defective osteoclast bone resorption (FRATTINI *et al.*, 2000; KORNAK *et al.*, 2000). This disease is associated with the loss of hearing and visual impairment (KORNAK *et al.*, 2000). Also reported finding with genetic models showed that the mutations in subunit *a* arising in disease conditions such as impaired glycosylation and cutis laxa, indicating the important role of this protein in processing and transport at the Golgi apparatus (KORNAK *et al.*, 2008). Beside the classical role of V-ATPases to acidify the cellular compartments, additional phenomenon such as membrane fusion has been attributed to them in novel findings that have shown involvement of subunit *a* in the process of microglia cells mediated phagocytosis of dead neurons in the brain (PERI and NÜSSLEIN-VOLHARD, 2008). Moreover, physiological importance of V-ATPase in the kidney proximal tubule (PT) cells has been demonstrated, with the use of specific inhibitors of V-ATPase (for example, bafilomycin and concanamycin) and acidification uncouplers (for example, NH_4Cl) (MARSHANSKY, 2007). A flurophore labeled albumin protein (Alexa495-albumin) was used to follow the endocytic pathway (Figure I6), and treatment of mentioned inhibitors or uncouplers strongly abolished the mouse PT albumin uptake (Figure I6) (MARSHANSKY, 2007). Pathophysiological conditions such as Dent's disease and related Fanconi's syndrome are associated with deficient protein reabsorption and proteinuria in the kidney PT cells (HURTADO-LORENZO *et al.*, 2006). Phenomenon of endosomal V-ATPase

mediated trafficking has now been understood in more detail, with the findings, that endosomal pH directly regulates vesicular signaling proteins; ARNO and Arf6, to control endosomal degradative pathways (HURTADO-LORENZO *et al.*, 2006).
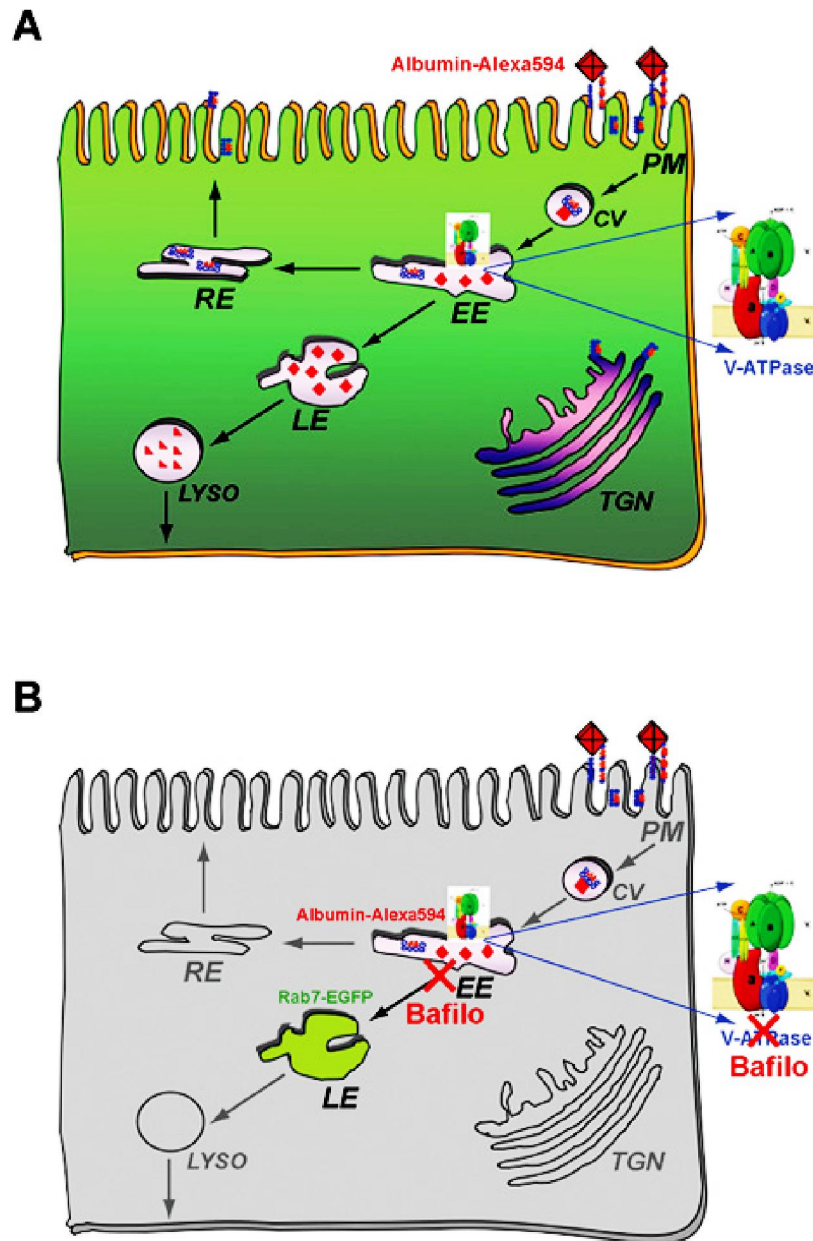
Figure 16: **Role of V-ATPase in the endosomal trafficking and degradation pathways of kidney proximal tubule (PT) cells. (A)** Megalin and cubilin are multi ligand receptors on the PT cells involved in the reabsorption of low molecular weight proteins (for example, albumin) (MARSHANSKY, 2007). Uptake of Alexa594 flurophore labeled albumin (red squares) is shown and its passage through early endosomes (EE) and late endosomes (LE) occurs in a pH dependent manner, generated by V-ATPase (MARSHANSKY, 2007). PM = Plasma membrane; CV = clathrin-coated vesicles; TGN = trans-Golgi network; RE = recycling endosome **(B)** Experimental approach that was used in the study of membrane trafficking between early and late endosomes. LE was labeled with green florescence, Rab7-EGFP. Use of bafilomycin blocked the cargo, albumin alexa594, passage between early and late endosomes. Recently, mechanism of this membrane transport has been understood to involve V-ATPase and small GTPase ARNO to modulate the endosomal trafficking and degradation pathways in a pH dependent manner, making V-ATPase a novel component of pH sensing machinery (HURTADO-LORENZO *et al.*, 2006). The figure has been adapted from the review by Vladimir Marshansky (MARSHANSKY, 2007).

Subunit *a2* has been demonstrated as an essential component of this endosomal sensory machinery to control the protein targeting and degradation in the early endosomes in a pH dependent manner in a collective response with the Arf6 and its cognate exchanger ARNO (HURTADO-LORENZO *et al.*, 2006). Subunit *a2* of mouse V-ATPase was found to directly interact with ARNO and subunit *c* with Arf6 in a pH dependent manner and disruption of this interaction resulted in the reversible abrogation of endocytosis (MARANDA *et al.*, 2001; HURTADO-LORENZO *et al.*, 2006). Loss of endosomal acidification resulted in the failure of formation of carrier vesicles to transport the cargo between early and late endosomes, resulting in the accumulation at early endosomes and inhibition of endocytosis (HURTADO-LORENZO *et al.*, 2006) (MARSHANSKY, 2007). ARNO is a guanine nucleotide exchange factor that is responsible for the GTP/GDP exchange on the small GTPase protein, Arf 6 (ADP-ribosylation factor 6) to activate and regulate its activities (FRANCO *et al.*, 1998). ANO/Arf6 is involved in the regulation of endosomal vesicular trafficking (MARSHANSKY and FUTAI, 2008), cytoskeleton organization (MOSS and VAUGHAN, 1998), lipid modification and rearrangement (MASSENBURG *et al.*, 1994; SANTY and CASANOVA, 2001), cell motility (FRANCO *et al.*, 1999), membrane recycling (TURNER and BROWN, 2001), regulated exocytosis in the neuroendocrine cells (ASHERY *et al.*, 1999), and more interestingly carrier vesicle coat formation that is required to bud off vesicles from the early endosomes (MARANDA *et al.*, 2001; HURTADO-LORENZO *et al.*, 2006). ARNO is also known to undergo protein kinase C (PKC) mediated phosphorylation *in vivo* at S392, however the function of this modification has remained largely unknown, as phosphorylation did not cause the activation of ARNO (SANTY *et al.*, 1999).

In spite of the fact that subunit *a* has been very considerably studied during these years and vital roles have emerged in the diverse functions of V-ATPase and in particular the subunit a, but structural and biochemical data is scant. Also, its structural and positional insights inside V-ATPase complex are not very well understood and the interacting partners have not been studied thoroughly. Emerging role(s) of this enzyme with respect to the signaling proteins such as ARNO are also at very premature stages.

1.3 Goals of this thesis

i) ARTS, is a novel protein, and one of the least characterized pro-apoptotic proteins in the apoptotic machinery. Its role(s) in the process of apoptosis is not completely defined and the mechanism associated with its pro-apoptotic effect in cells remains to be elucidated. Here, I have studied ARTS in the perspective of Livin, an anti-apoptotic protein of IAP family. IAPs are known to inhibit apoptosis, whereas pro-apoptotic ARTS is the causative agent of cell death in response to diverse stimuli. Anti-apoptotic Livin is a known E3 ligase which promotes the ubiquitin mediated degradation of several target proteins during apoptosis. The project was initiated to characterize the role of this activity of Livin, if any, to ARTS in apoptotic cells. During this investigation, rather a cleavage of Livin was found during ARTS-promoted apoptosis. The observed cleavage of Livin has been further studied to explore the possible pathway involved. During the investigation of cellular apoptosis, we found subunit d of V-ATPase as a novel, previously unreported target of caspase 3. Its further characterization by biochemical and biophysical techniques formed the second objective of my work.

ii) Subunit d of V-ATPase is a pivotal protein required for V_1V_O assembly, and coupling of ATP hydrolysis to proton transport across the endo- or plasma membranes. Moreover, I identified this protein as a new substrate of caspase 3, an apoptosis executioner enzyme. However, no known structural information is available about this protein to further characterize and understand its structural-functional aspects in cell physiology. Also, the information about the binding associates of subunit d in V_1 and V_O domains is least characterized besides its localization inside V_1V_O complex remained elusive. The goals of this project were to over express and produce the recombinant protein, which could be used to derive the structural and biochemical information. Other than that, subunit d assembly inside V_1V_O is not understood. Therefore to get further insights into this aspect, NMR, FCS and SPR techniques have been used to characterize the neighboring proteins in association with subunit d of V-ATPase.

iii) Besides the fundamental proton pumping machine, V-ATPase has been demonstrated as a hinging point between the intracellular pH sensing and recruitment of signaling proteins ARNO and Arf6, which regulate the intracellular membrane trafficking and degradation pathways besides other functions like organization of cytoskeleton and cell motility. Subunit a is directly involved in this signaling pathway by interacting with ARNO in a pH dependent manner. To get further cognition of subunit a, soluble N-terminus domain of yeast subunit a (Vph1p

isoform), $a_{1\text{-}388}$ was successfully produced and studied. Several other proteins of this N-terminal domain of yeast and mouse subunit a have been examined as well. The project objective was to solve the 3D structures of vital regions of subunit $a2$ and ARNO, which do interact to each other. The achievements include the solution 3D NMR structures of ARNO-PB (polybasic) domain in phosphorylated and non-phosphorylated forms, and 3D structure of subunit $a2_{386\text{-}402}$ of mouse V-ATPase.

2.   Materials and methods

2.1 Materials

2.1.1 Chemicals

All the chemicals used in the current study were of at least analytical grade. Chemicals were purchased from the following companies:

Buffers and salts	Sigma (St. Louis, MO, USA),USB (Sampscott,MA), Calbiochem (Darmstadt, Germany), Fluka (Sigma, Buchs Germany), Roth (Karlsruhe, Germany), Serva (Heidelberg, Germany)
Pefabloc^{SC}	BIOMOL (Hamburg, Germany)
PMSFSigma (St. Louis, MO, USA)	
Protease inhibitor tablets (EDTA free)	Roche (Mannheim, Germany)
DTT Hoefer (San Francisco, CA, USA)	
Ni^{2+}-NTA	QIAGEN (Hilden)
^{15}NH^{4}Cl Cambridge Isotopes Lab (USA)	
^{13}C Glucose	Cambridge Isotopes Lab (USA)
LB Media	BD (Sparks, MD, USA)
Electrophoresis Chemicals	
(Agarose, SDS, Glycine, APS etc.)	Bio-Rad (Hercules, CA, USA)
Antibiotics	Calbiochem, Sigma and Gibco (Invitrogen)
IPTG Fermentas	
BSA GERBU (Heidelberg, Germany)	

2.1.2 Molecular biology materials

2.1.2.1 Templates, primers and peptides

Genomic DNA	*Saccharomyces cerevisiae* (AH104 strain)
Primers 1st Base and Research Biolabs (Singapore)	
Peptides NTU proteomics core facility (Singapore)	

2.1.2.2 Enzymes and kits

Pfu and T4 DNA Polymerase	Fermentas (Glen Burnie, MD, USA)
NcoI, SacI, XhoI, NdeI, EcoRI, SalI	Fermentas and New England Biolabs
T4 DNA Ligase	Fermentas and NEB

CIAPFermentas (Glen Burnie, MD, USA)

Caspase 3   Sigma (St. Louis, MO, USA)

Miniprep Plasmid Kit   Qiagen (Hilden, Germany)

Nucleobond AX mediprep Kit   MN & Co (Düren, Germany)

2.1.2.3 Cell Lines, Yeast and *E. coli* strains

Mammalian Cell lines: 293T, COS7, HeLa

Saccharomyces cerevisiae: AH104

Escherichia coli: DH5 , BL21 (DE3), Rosetta^{TM} 2 (DE3), Rosetta-gami^{TM} 2 (DE3), NovaBlue (Novagene; Darmstadt, Germany)

2.1.2.4 Vectors

pET-9d1 (GRÜBER *et al.*, 2002)

pET-24 (+)   Novagene (Darmstadt, Germany)

pSUMO Lifesensors (Malvern, PA)

pcDNA3.0-Flag   Invitrogen (Carlsbad, CA)

pEGFP-C1   Clontech (Mountain View, CA)

2.1.2.5 Antibodies

mAb anti-GFP, mAb anti-Actin   Santa Cruz

mAb anti-ARTS

mAb anti-Flag

rabbit mAb anti-Flag   (St. Louis, MO, USA)

pAb anti-GFP Sigma

Rat mAb anti-Caspase 7

Agarose conjugated mouse anti-Flag

p-Ab-anti-GFP   Clontech (Mountain View, CA)

2.1.2.6 Caspase inhibitors

Pan-caspase inhibitor, ZVAD-FMK   Sigma (SL, Missouri, USA)

Caspase-9 inhibitor, Z-LEHD-FMK   Sigma (SL, Missouri, USA)

Caspase 3 inhibitor V, Z-DQMD-FMK   Calbiochem (EMD biosciences, La Jolla, CA)

Proteosome inhibitor, MG132   Sigma (SL, Missouri, USA)

2.1.3   Chromatography

2.1.3.1 Ion exchange

RESOURCE^{TM} Q

SOURCE^{TM} 30Q   GE Healthcare (Uppsala, Sweden)

Mono^{TM} Q, Mono^{TM} S

2.1.3.2 Gel filtration

Superdex 75 HR (10/30)   GE Healthcare (Uppsala, Sweden)

2.1.3.3 Instruments and accessories

Akta FPLC, Akta Prime   GE Healthcare (Uppsala, Sweden)

Millex Filters (0.45 µM)   Millipore (Bradford, USA)

Syringe, needles and accessories   BD Biosceinces

2.1.3.4 Protein concentration, estimation and dialysis

Centriprep YM30, YM10   Millipore (Co-cork, Ireland)

Amicon ulta (3-30kDa)   Millipore (Co-cork, Ireland)

Protein estimation: BCA Assay Kit   Pierce (Rockford, IL, USA)

Protein estimation: Bradford reagent   Bio-Rad

Dialysis Spectra Por^{R}CE membranes   Roth (Karlsruhe, Germany)

2.1.4 Other instrumentation

PCR Thermocycler:

Biometra T personal   Biometra

Biometra T gradient   Biormetra

Micropulser Electroporator   Bio-Rad

Ultraspec 2100 Pro Spectromphotometer Amersham Biosciences

Sonoplus Sonicator   Bendelin

GS-800 Calibrated Densitometer   Bio-Rad

2.1.5 Softwares

Vector NTI 10.3.0	Invitrogen
SPARKY 3.110	University of California (San Francisco, USA)
Topspin 1.3	Bruker
CAYANA 2.1, 3.0	Kimmo Paakkonen and Peter Günter (Japan)
TALOS 98.040	(CORNILESCU *et al.*, 1999)
Quantity One	Bio-Rad

Construct	Template	Primer sequence (5'-3')
Livin	c-DNA Library	L-P1: CGGAATTCCATGGGACCTAAAGACAGTGCCAAG
		L-P2: CGGTCGACCTAGGACAGGAAGGTGCGCACGCG
Livin-C124A	Livin	L-P1: CGGAATTCCATGGGACCTAAAGACAGTGCCAAG
		L-P2: CGGTCGACCTAGGACAGGAAGGTGCGCACGCG
		L-P3: CAGGACAAGGTGAGGGCCTTCTTCTGCTATGGGGGC
		L-P4: AGCAGAAGAAGGCCCTCACCTTGTCCTGATG
Livin RING	Livin	L-P1: CGGAATTCCATGGGACCTAAAGACAGTGCCAAG
ARTS	c-DNA Library	A-P1: CGGAATTCCATGATCAAGCGTTTCCTGGAG
		A-P2: CGGTCGACCTAGTGGCAGCCCTGCCCCTG

Subunit *d* (Vma6p) constructs from *Saccharomyces cerevisiae*

d (wt)	Forward	CATGCCATGGTAATGGAAGGCGTG
	Reverse	CGTTCGAGCTCTCAATAAACGGAAATATAATTG
d (C329S)	Reverse	TTCTTTCTCTTTGATTTCGAGCTCTCAATAAAC GGAAATATAATTGTTGATTTGTGCTATTGA
d $_{38-345}$	Forward	CATGCCATGGTTACGTTGGAAGATC
d $_{1-298}$	Reverse	CGTCGAGCTCTCAATCTCTACATAGTTCC
d $_{11-345}$	Forward	CATGCCATGGTAGGGTTTATTGAAGGTG
d $_{1-328}$	Reverse	CGTCGAGCTCTCATTCAGCAATCCAG
d $_{11-189}$	Reverse	CGTCGAGCTCTCATAAATAAGCCTTGTAC
d $_{38-189}$	Forward	CATGCCATGGAAGACTTCTACAATTTTGTCAC
d $_{190-328}$	Forward	CATGCCATGGAAGACTTCTACAATTTTGTCAC

Subunit *a* (Vph1p) constructs from *Saccharomyces cerevisiae* genome

a $_{1-388}$	Forward	TTTCTCCATGGCAGAGAAGGAGGAAGCGATTTTTCG
	Reverse	
a $_{1-388(C)}$	Reverse	TTTGAGCTCAGCAAGTAAACTTGTTAGTTCTGT GGAAGGTAGGTGG
a $_{1-323+C}$	Forward	TTTCTCCATGGCAGAGAAGGAGGAAGCGATTTTTCG
	Reverse	G
a $_{1-81}$	Forward	TTTCTCCATGGCAGAGAAGGAGGAAGCGATTTTTCG
	Reverse	AG
a $_{182-323+C}$	Forward	G
	Reverse	GCTTCTGTAAACTATGTCACTGGTGTCATTGC

Subunit *a* (STV1p) constructs from *Saccharomyces cerevisiae* genome

STV1 $_{1-450}$	Forward	CATACATATGAATCAAGAAGAGGCTATATTCCGGTC
	Reverse	TACATCTCGAGTTCTTTATATGTTGCGATACCGTATG
STV1 $_{1-351}$	Reverse	TACATCTCGAGGTGTATAACGAGCAGTTCTGTG

Subunit *a* constructs from *mouse a2 isoform*

a2 1-58	Forward	TATTCCATGGGCTCTCTCTTCCGCAG
		GATGCGAGCTCTTAACACCTCTTTACCTCAC
a2 1-133	Reverse	CATACGGAGCTCTCACCTCAGCATGTG
a2 134-393	Forward	CATGCCATGGATACGAAGACCTTCCTC
a2 1-393	Reverse	AGCTGCGAGCTCTCATTCTCTGTAACTCC

PEPTIDES

E 18-38	NKMQAFIRKEAEEKAKEIQLK
E 1-20	MSSAITALTP NQVNDELNKM
aN-22*	YGVGSYREVNPALFTII
ARNO*	VSVDPFYEMLAAKKRISVKKKQEQP
ARNO(p)*	VSVDPFYEMLAAKKRIS(*p*)VKKKQEQP

***Table 2* Livin, ARTS and V-ATPase constructs, primers, and peptides**: List of constructs and their respective forward and reverse primers, mostly synthesized either at *1st Base Pte Ltd*, Singapore or *Research Biolabs Pte Ltd*, Singapore. ARTS and Livin constructs were kindly provided by Prof. Wu Mian. List of peptides used in study are shown. * Peptides were generously provided by Prof. Vladimir Marshansky (*Harvard University, MGH, Boston*). If not indicated the peptides have been synthesized at NTU Proteomics core facility.

2.2 Methods

2.2.1 Yeast genomic DNA isolation

Reagents

YPD:	*1% Yeast Extract*
	2% Peptone
	2% Dextrose

Harju buffer:	*2% Triton X-100,*
	1% SDS
	100 mM NaCl
	10 mM Tris-HCl, pH 8.0
	1 mM EDTA

Enzyme:	*RNase*

Genomic DNA of *Saccharomyces cerevisiae* was isolated as described below (HARJU *et al.*, 2004). 1.5 ml of liquid *Saccharomyces cerevisiae* (AH104) culture was grown for 20 – 24 h at 30 °C in YPD media. Cells pellet down by centrifugation at 10,000 × g for 5 min. 200 µl of Harju buffer was added and tubes immersed in a dry ice-ethanol bath for 2 min and immediately transferred to a 95 °C water bath for 1 min. Last two steps repeated once and tubes were vortexed for 30 seconds. 200 µl of chloroform added and vortexed for 2 min followed by centrifugation for 3 min at room temperature, 14,000 × g. Upper aqueous phase was transferred to a micro centrifuge tube containing 400 µl ice-cold 100% ethanol, mixed thoroughly by inversion and incubated at room temperature for 5 min. Centrifuged 5 min at room temperature, 14,000 × g. Supernatant removed gently with pipette tip aspiration and pellet washed with 0.5 ml 70% ethanol by centrifuging for 5 min at room temperature, 14,000 × g. Supernatant discarded. Air-dried pellets resuspended into 25 – 50 µl TE (pH 8.0). 0.25 µl RNase cocktail added to the samples (final concentration 0.125 U RNAse A) to get rid of RNA contamination. Quality and concentration of the sample was estimated from 0.7% DNA agarose gel.

2.2.2 PCR cloning and mutagenesis of ARTS, Livin, subunit *d* and subunit *a* constructs

2.2.2.1 Vector preparation

Reagents

Luria-Bertani (LB) media:	*10 g/l Tryptone*
	5 g/l Yeast Extract
	5 g/l NaCl

DNA Purification:	*Qiagen Kit*
Plasmid Isolation:	*Nucleobond AX Kit*
Enzymes:	*EcoRI, SalI, XhoI, NdeI,Nco I, Sac I, CIAP*

(A)

(B)

(C)

(D)

***Figure M1*. Vector maps**: (**A**) pcDNA3-Flag (Invitrogen) (**B**) pEGFP-C1 (Invitrogen), (**C**) modified pET-9d1 (+) (GRÜBER *et al.*, 2002) and (**D**) pET-24a(+) (Novagene; Darmstadt, Germany) vectors showing full map and unique multiple cloning sites (MCS) that has been used to clone various genes and their different truncated and mutated forms (Table 1).
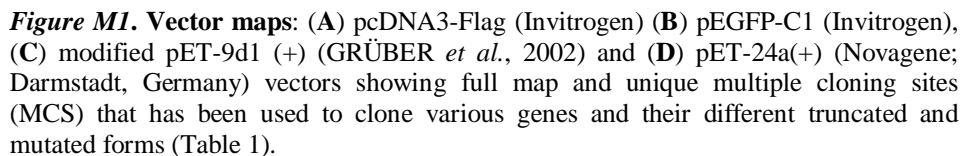
500 ml overnight culture of DH5 /vector was harvested and plasmid DNA was purified by using the Nucleobond AX or Qiagen midi-prep kit as per the manufacturer's protocol. Isolated plasmid was checked for quality on 0.7% agarose gel and quantity was determined by spectrophotometric absorption at 260 nm. Plasmid was digested with respective vector specific restriction enzymes in sequential manner at 37 °C and the extent of digestion was confirmed by running 1 μl sample on 1% agarose gel. Restriction mixture was purified at the end of each cycle

(Qiagen purification kit). Finally, the double digested pET9-d(+) (GRÜBER *et al.*, 2002) was dephosphorylated with CIAP (Fermentas, MD, USA) for 30 min, 37 °C. Concentration of final product was estimated spectrophotometrically as described above.

2.2.2.2 Cloning and mutagenesis of Livin and ARTS constructs

Full length Livin gene fragment was amplified from HeLa cDNA library by PCR using primer pair L-P1/L-P2. PCR product was digested with *EcoRI* and *XhoI* enzymes, and dephosphorylated with CIAP enzyme (Fermentas, MD, USA). The purified fragment was subcloned into *EcoR /Xho* sites of pCDNA3/Flag (Figure M1) to prepare Flag-tag Livin (Flag-Livin). A cDNA fragment coding for Livin RING (residues 1 – 239) was generated by PCR reaction using primers L-P1/L-P9. Amplified product was digested and ligated with vector pCDNA3/Flag as described above for Flag-Livin construct (for details of protocol see section 2.2.2.3). PCR-mediated mutagenesis with primer pairs L-P1/L-P4 and L-P3/L-P2 was used to generate Livin point mutant Livin-C124A. Mutations created were further verified by DNA sequencing. Using similar strategy as explained for Livin, full length ARTS gene fragment was amplified from HeLa cDNA library by PCR using primer pair A-P1/A-P2. The amplified fragment was subcloned into *EcoR /SalI* sites of pEGFP-C1 to make a GFP-fusion ARTS (GFP-ARTS). I am thankful to Dr. Li Ma (USTC, China) for help with the creation of constructs.

2.2.2.3 Cloning and mutagenesis of subunit *d* (VMA6) constructs

Isolated pure genomic DNA of *Saccharomyces cerevisiae* strain AH104 was used as template for the amplification of subunit *d* gene (VMA6). PCR reaction was setup in a total volume of 50 µl on ice as mentioned below with the appropriate concentration of constituents as:

```
Pfu buffer (10x) ........................................... 5 µl
DNTP's (2mM) ...................................... 1.5 µl
Primers (100uM) ............................... 2 x 0.5 µl
Template (gDNA ........................................ 1 µl
MilliQ water ............................................. 41 µl
Pfu DNA polymerase ................................. 1 µl
```

Reaction contents were properly mixed and kept on ice all the time. PCR thermocycler (Biometra T personal) was preheated to 95 ºC before reaction tubes were placed inside the machine. Following PCR thermocycler program was used for the amplification:

```
Lid Temp..............................................99 °C
Initial denaturation..............................95 °C        3 – 5 min
Denaturation.......................................95 °C        0.5 – 1 min ⎤
Annealing .................................... 50 – 68 °C       0.5 – 1 min ⎬ x 30-40
Extension............................................72 °C         1 – 2 min ⎦
Final extension ...................................72 °C        5 – 10 min
Hold ....................................................4 °C
```

The amplified PCR product was stored at -20 °C before proceeding to the next step. 5 µl of PCR amplified product was applied onto the analytic agarose gel (1%) to check the quality of amplified product. If the product was sufficiently pure, remaining reaction mixture was applied onto preparative agarose gel and purified by gel extraction kit (QIAGEN) as per the manufacturers protocol and finally eluted in 30 – 50 µl volume of water or Tris/HCl (pH 8) buffer. The purity of gel extracted PCR product was estimated by running 1 µl sample on 1% analytical agarose gel. Purified DNA was double digested overnight at 37 ºC and re-purified by enzyme reaction purification kit from QIAGEN. Subsequently, ligation reaction between vector and amplified PCR product was setup as:

```
Ligase buffer (10x)............................ 1.5 µl
Vector (V)......................................... 50-100 ng
Insert (I) ........................................... variable (1:1-1:5 V: I ratio)
Ligase................................................ 1 µl
MilliQ water..................................... variable
Total.................................................. 15 µl
```

Ligation mixture was incubated at room temperature for 40 – 60 min or alternatively left overnight at 4 ℃. The reaction was terminated by precipitation of DNA from rest of the reaction contents by adding 85 µl of MilliQ to a 100 µl of total volume. To it, 1 ml of butanol was added and mixed thoroughly by inversion several times and centrifuged at 13,000 rpm (Eppendorf mini-centrifuge) for 10 min. Supernatant was aspirated gently and pellet resuspended in 150 µl of 70% ethanol and centrifuged again for 5 min. Supernatant was discarded and pellet dried and re-dissolved in 10 µl of EB buffer (Qiagen) or MilliQ water. 5 – 10 µl of ligation mixture was transformed into DH5 cells as described below in section 2.2.3. Several colonies were picked from transformation plate and plasmid DNA was isolated (Qiagen mini-prep kit) for double digestion to confirm the ligation. Size of insert and vector were compared with appropriate controls and markers. Verified plasmid was finally transformed into BL21 (DE3) or Rosetta-gami[TM]2 (DE3) or Rosetta [TM]2 (DE3) cells for protein expression. All BL21 and Rosetta protein expression strains were purchased from Novagene (Darmstadt, Germany).

2.2.2.4 Cloning of other constructs

The similar strategy was used for the cloning of several other constructs of subunit *d* and subunit *a* of yeast and mouse V-ATPase. Primers and constructs for all constructs used in current studies are described in detail under materials section (Table 1). STV1$_{1-450}$ gene was cloned into pET-24a(+). Initially direct cloning method via ligation to the double digested linearized vector, pET-24a(+) did not work so an alternative strategy by insert the gene into the GT-GFP-TOPO vector pCDNA 3.1 (TOPO TA kit; Invitrogen) was used. STV1$_{1-450}$ PCR product was amplified and extracted from the gel as described above. Pure DNA fragment with intact restriction sites was ligated to pCDNA 3.1 using T/A ligation strategy as per the manufacturer's instructions. Inserted gene was then released from the pCDNA 3.1 vector by double digestion with *NdeI and XhoI.* Released fragment was gel purified (Qiagen gel purification kit) and re-ligated with linearized pET-24a(+) vector (double digested with *NdeI and XhoI,* and dephosphorylated with CIP). Subsequent steps were same as explained above in section 2.2.2.3.

2.2.3 Electroporation transformation

Reagents

SOB media: 20 g/l Tryptone
5 g/l Yeast Extract
0.58 g/l NaCl
0.18 g/l KCl
10 ml Mg solution (1M MgCl$_2$.6H$_2$O, 1M MgSO$_4$)
SOC media: SOC
100 mM Glucose

Electroporation was done for the transformation of plasmid into electro-competent cells. Electro-competent cells were prepared as per the protocol from Current Protocols in Molecular Biology (Wiley InterScience) manual. 1 – 50 ng of plasmid was added to 80 – 100 μl of competent cells and incubated on ice for 5 – 10 min. Electroporation was done at constant voltage of 2500 V (Micropulser Electroporator, Bio-Rad) and cuvette was immediately placed back on ice for 1 min followed by addition of LB or SOC (SOB + 100 mM Glucose) media was added to 1 ml and mixture incubated at 37 °C for 1 h. Appropriate dilutions were prepared before plating out on antibiotic selection plates.

2.2.4 Cell Culture and transfection

293T and COS7 cells were cultured in GlutaMax DMEM (Dulbecco's Modified Eagle's Media) (Invitrogen, Carlsbad, CA, USA) media supplemented with 10% FBS (Fetal Bovine

Serum) (Invitrogen, Carlsbad, CA, USA) 100 μg/ml penicillin and 100 μg/ml streptomycin (Invitrogen, Carlsbad, CA, USA) and 1X MEM sodium pyruvate (Gibco, Invitrogen). HeLa cells were cultured in GlutaMax DMEM (Invitrogen) supplemented media with additional 1X non-essential amino acids. Cell lines were maintained at 37 ºC in 5% CO_2 environment. Transfections were performed using nucleic acid transfecting reagents Lipofectamine 2000 (Invitrogen Carlsbad, CA, USA) and FuGENE 6 (Roche, Indianapolis, IN) as per the manufacturer's specifications.

2.2.5 Western blotting and Bradford protein quantification

Reagents

Blot transfer buffer: *25 mM Tris/HCl pH 8.3*
                         192 mM Glycine
                         20% Methanol
PBS: *10 mM sodium phosphate pH 7.4*
                         150 mM NaCl

Proteins were separated on 12% resolving SDS-polyacrylamide gel at 200 V constant for 45 min and transferred onto transfer buffer equilibrated nitrocellulose or 100% methanol activated PVDF membrane (Amersham) by wet transfer method (Bio-Rad). Membrane was blocked with 8% non-fat milk (NFM) in PBS-T (PBS; 0.1% Tween-20) for 1 h at room temperature, washed with PBS-T three times for 10 min each followed by incubated with primary antibody (diluted in 2% NFM prepared in PBS-T) for additional 1 h at room temperature. After primary antibody binding, membrane was washed as above and incubated with HRP-conjugated secondary antibody for 1 h at room temperature. Membrane was washed again with PBS-T three times for 10 each at room temperature. Membrane was partially dried with Whatman paper to prepare for the development. Western blot was developed using chemiluminescent method with ECL Plus^{TM} or Lumigen LMA 6 reagents (GE Healthcare, UK) as per the manufacturer's specifications on Kodak X-ray film development station in dark room. For stripping and re-probing of membranes, Restore Western Blot Stripping Buffer (Peirce; Thermo Scientific) was used to strip the membranes at room temperature for 30 min followed by washing three times in PBS.

Protein quantification was done with Bradford assay using Bio-Rad Bradford reagent with at least three independent replicates for each sample. BSA (Bio-Rad) was used as standard (20 – 140 μg) for protein quantification. Samples were incubated at room temperature for 5 min in Bradford reagent and absorbance reading taken at 595 nm as per the manufacturer's protocol

(Bio-Rad). Reading were averaged and plotted against BSA standard to estimate the protein concentration.

2.2.6 Co-immunoprecipitation (Co-IP)

Reagents

RIPA lysis buffer:	*50 mM Tris/HCl pH 7.4*
(Radio-Immunoprecipitation Assay)	*1% Triton*
	150 mM NaCl
	1 mM EDTA
Leupeptin:	*1 µg/ml (final conc.)*
Aprotinin:	*1 µg/ml (final conc.)*
PMSF:	*1 mM (final conc.)*
Mini complete protease inhibitor:	*1 tablet/30 ml*

Cells were cultured in 100 mm dishes for 24 h before transfection. Whole cell protein lysates were prepared using RIPA complete lysis buffer, with leupeptin and aprotinin (1µg/ml each), freshly prepared 1mM PMSF (Phenyl Methane Sulphonyl Fluoride, a serine protease inhibitor) dissolved in DMSO and Mini-complete Protease Inhibitor (Roche). Lysates were immunoprecipitated overnight at 4 ℃ with agarose or spherose conjugated antibodies. Immunoprecipitates were captured by pulse centrifugation at 4 ℃ (20 sec at 10,000 x g). Supernatant was discarded and beads were washed with ice-cold RIPA buffer 4 times for 3 min each. After final wash beads were resuspended in 30 µl of 5X SDS loading buffer and boiled at 95 ℃ for 4 min.

2.2.7 Apoptosis induction

Apoptosis was induced with either 100 µM of etoposide, a topoisomeras II inhibitor, for 16 – 24 h, or staurosporine (STS; 1 µM), a non-specific kinase inhibitor for 4 – 10 h. Cultured and transfected cells were initiated to undergo apoptosis following treatment with either etoposide or staurosporine, which specifically block essential activities of cells to bring them into the stress so that the execution apoptotic events do occur.

2.2.8 Ubiquitination *in vivo* assay

HeLa cells were cultured in 100 mm dishes for 24 h before transiently transfected with mentioned plasmids. Lipofectamine 2000 (Invitrogen) was used for transfection. Cells were allowed to express the respective transfected genes for 24 h followed by treatment with 20 µM MG132 (Z-Leu-Leu-Leu-aldehyde; cell permeable proteosome inhibitor) (Sigma) prepared in

DMSO, for 8 or 12 h. Cells were harvested and whole cell lysates prepared in RIPA complete lysis buffer with protease inhibitor (Mini Complete, Roche), 1μg/ml Leupeptin (N-acetyl-L-leucyl-L-leucyl-L-argininal; a serine/cysteine protease inhibitor) (Sigma), 1μg/ml Aprotinin (a serine protease inhibitor protein) (Sigma) and freshly prepared 1mM (final concentration) PMSF, prepared in DMSO. Lysates were subjected to immunoprecipitation over night in cold room followed by 3 – 5 times washing with RIPA buffer to get rid of non-specific bound materials. Immunoprecipitates were mixed 30 μl with 5X SDS loading buffer (Bio-Rad), heated at 95 ℃ for 5 min and loaded onto SDS polyacrylamide gel (12%) followed by western blotting as described in section 2.2.5.

2.2.9 Caspase inhibition assay

Caspase inhibition assays were performed as described previously (KARLSSON *et al.*, 2004; KARLSSON J., 2004). The COS7 cells transfected with respective plasmids were cultured for 24 h before treating with 40 μM each of pan-caspase (ZVAD-FMK), caspase 8 (Z-LETD-FMK), caspase 8 (Z-LEHD-FMK) or caspase 3 (Z-DQMD-FMK) inhibitors. 12 h later apoptosis was induced by addition of 1 μM staurosporine (Sigma) to culture media of respective experimental plates. Caspase inhibitor concentration was kept to a maximum of 40 μM, as higher concentrations have been reported to also inhibit Calpain (WATERHOUSE *et al.*, 1998; BLOMGREN *et al.*, 2001; BLOMGREN K., 2001), a family of calcium dependent, non-lysosomal cysteine proteases, which are vital for functions such as cell division, cell motility and cell specific signal transduction functions (GOLL *et al.*, 2003). Cell lysates were prepared as described in section 2.2.5. Protein amounts from each lysate were normalized by Bradford assay (section 2.2.5). Samples were loaded on 12% SDS gel followed by blotting onto nitrocellulose membrane (Amersham). Western was done with anti-GFP and anti-Flag antibodies as described in section 2.2.5.

2.2.10 Caspase 3 cleavage assay of subunit *d* and C of V-ATPase

Reagents
1X Reaction buffer: *50 mM Hepes, pH 7.4*
     100 mM NaCl
     1 mM EDTA
     10 mM DTT
     0.1 % CHAPS

Blot transfer buffer: *25 mM Tris base*
     192 mM Glycine

TBSN buffer:	*20 mM Tris/HCl pH 7.5*
	500 mM CaCl2
Reaction buffer APP:	*50 mM Tris/HCl*
	100 mM NaCl
	50 mM MgCl$_2$

NBT stock solution I:	*75 mg/ml NBT (Nitro Blue Tetrazolium)*
	70 % DMF (Dimethylformamide)

BCIP stock solution II: 50 mM BCIP (5-bromo-4-chloro-indolyl phosphate) in 100% DMF

Pure recombinant subunit *d* and subunit C proteins of yeast V-ATPase were used for the *in vitro* digestion reaction, using recombinant caspase 3 enzyme (Sigma, St. Louis, USA). 0.5 U of enzyme was supplemented in a reaction volume of 10 µl containing 10 – 30 µmoles of substrate. Reaction was properly mixed and tubes were sealed with parafilm and incubate at 37 ºC for 1 – 10 h. For His-pull down, the reaction mixture was incubated with 100 µl Ni^{2+}-NTA beads at 4 ºC at a constant rotation on rotator (Neolab). Beads were washed 2 times with reaction buffer and resuspended in 20 µl SDS loading buffer and heated at 95 ºC for 15 min. Beads were spinned down by centrifugation at 14,000 x g for 5 min and supernatant was loaded onto 17% SDS gel. Protein was transferred onto nitrocellulose membrane by semi-dry blotting procedure at a constant voltage of 1 V/cm^2 for 1 h. Prior to transfer the membrane was pre equilibrated in transfer buffer for 5 – 10 min. Membrane was stained with reversible Ponceau S stain (0.2% Ponceau S; 3% TCA) to confirm the transfer and prepare the membrane for antibody probe. Ponceau S stain was complete removed with TBSNT (TBSN; 0.05% Tween-20) buffer wash. Membrane was blocked with 3% gelatin in TBSNT at room temperature for 1 h and washed with TBSNT buffer three times for 5 min each. AP-conjugated Ni^{2+}-NTA (Qiagen) was incubated with membrane for 1 h in TBSNT 1% gelatin buffer (1:1000 dilution) at room temperature or overnight in cold room at constant shaking. The blot was developed by standard procedure using 45 µl of NBT stock solution I and 35 µl of BCIP stock solution II in 10 ml of total reaction buffer APP. The blot was developed away from direct light and immediately dried and scanned.

2.2.11   Protein production

2.2.11.1 Induction test

Reagents
4X Lysis buffer: 250 mM Tris/HCl, pH 6.8
*   9.2 % SDS*
*   40 % Glycerol*
*   0.2 % Bromophenol Blue*

At least 5 – 10 single colonies were randomly picked from selection plates and grown to OD_{600} of 0.6 - 0.7 at 37 °C and constant shaking at 170 – 200 rpm on Infors HT Minitron shaker. Protein induction was initiated by the addition of 0.5 – 1 mM IPTG, depending on the characteristics of protein being produced and the conditions that have been optimized for respective protein, for 2 – 3 h at 30 – 37 °C. Respective controls were left uninduced under identical conditions. Cells were pellet down and resuspended with 50 µl of 1X lysis buffer in presence of 1 mM DTT. Resuspended cell mass was heated at 95 ºC for 5 min and 15 – 20 µl of each sample was loaded onto a 17% SDS polyacrylamide gel. A representative induction gel is shown below in figure M2.

Subunit d		Subunit E_{1-69}		Subunit E_{39-233}		Subunit a_{1-72}	
-	+	-	+	-	+	-	+
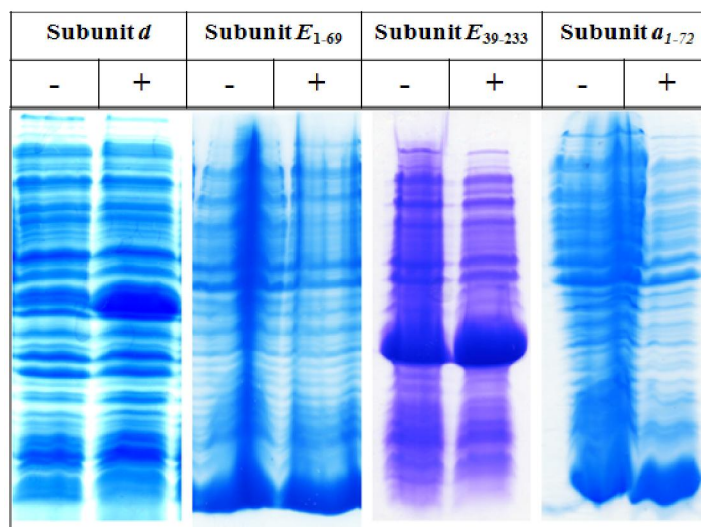
Figure M2. **Induction test**: uninduced (-) and induced (+) samples from few representative proteins used in the current study. Induction was done with 0.5 – 1 mM IPTG at 37 °C. Whole cell lysate was prepared by heating cells in 1X lysis buffer at 95°C for 5 min and followed by electrophoresis on a 17% SDS gel.

2.2.11.2 Solubility test

Reagents

> *IM Pefabloc^{SC}*
> *100 mM PMSF*
> *1.25 M DTT*

After successful induction of proteins with appropriate concentration of IPTG at the optimized temperature and shaking conditions, solubility of the produced proteins was tested in various buffers as shown below. 50 ml of culture was grown and induced with IPTG. Cells were pellet down into 5 equal fractions by centrifuging at 10,000 x g for 10 min. Freshly prepared protease inhibitors Pefabloc^{SC} (2 – 8 mM) in water and/or 1 – 2 mM PMSF (dissolved in isopropanol) were added. Reducing agent such as DTT (1 mM) or -mercaptoethanol (1 mM)

were used in some preparations. Resuspension was sonicated at 20% power with KE 76 tip of sonicator (Bandelin Sonoplus) three times for one min each with a cooling interval of two min between each cycle. Supernatant was then separated from the pellet by centrifugation at 10,000 x g, transferred to a fresh tube and pellet resuspended in the same buffer. All the steps were carried on ice. 10 – 15 µl of pellet and supernatant were loaded onto a 17% SDS gel.

50 mM Tris/HCl 500 mM NaCl, pH 7.5		50 mM HEPES 150 mM NaCl, pH 7.0		50 mM MES 150 mM NaCl, pH 6.5		50 Tris/HCl 150 mM NaCl, pH 8.0	
P	**S**	**P**	**S**	**P**	**S**	**P**	**S**
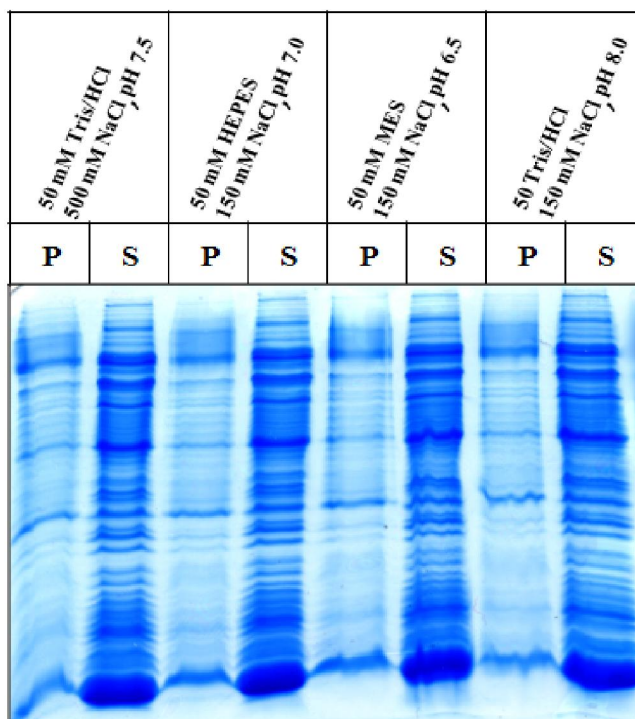
Figure M3. **Solubility test**: A 17% SDS gel showing solubility test results from a representative protein, E_{1-69}. Pellet (P) and supernatant (S) in various buffers is shown on the gel representing preponderance of protein in the supernatant of various buffers.

2.2.12 Protein production and purification of subunit *d* and subunit *a*

2.2.12.1 Subunit *d* (Vma6p)

VMA6 gene inserted into His₃-pET-9d vector was transformed into either BL21 or Rosetta-gami™ 2 (DE3) *E. coli* cells for initial protein expression. Rosetta-gami™ 2 cells expressing Vma6p (subunit *d*) were used for subsequent studies described here. Rosetta-gami™ 2 cells have combined features of Rosetta 2 and Origami 2 containing rare tRNA codons used by eukaryotic protein and enhanced disulphide formation. Since subunit *d* is a yeast eukaryotic protein and has six cysteine residues so Rosetta-gami™ 2 was the most appropriate host for expression. Following growth of His₃/subunit *d* to an optical density of 0.6 – 0.7, protein expression was induced by the addition of IPTG to a final concentration of 1 mM and the

temperature dropped to 30 °C for 3 – 4 h. Cells were harvested by centrifugation at 8,000 x g for 15 min and immediately frozen with liquid nitrogen to stored at -80 °C.

The process of protein purification was started by dissolving cells in 50 mM Tris/HCl; 500 mM NaCl; pH 7.5. All the steps proceeded on ice with minimum time delays. 1 mM DTT and 4 mM Pefabloc^{SC} used as reducing agent and protease inhibitor, respectively. DNAase was added to the preparation involving larger cell mass. Cells were sonicated at 50% power with KE 76 tip for three times of one min each with a gap of two min between each cycle. Lysate was clarified by centrifugation at 10,000 x g for 35 min and by passing through a 0.45 µm syringe filter. Appropriate amount of Ni^{2+}-NTA matrix (Qiagen) to cell ratio was equilibrated with buffer, mixed with clarified lysate and incubated at 4 °C for 3 h on a Neolab rotator. His-tagged protein was eluted with an imidazole gradient (25 – 200 mM), prepared in 50 mM Tris/HCl; 500 mM NaCl; pH 7.5, by gravity flow at 4 °C in presence of appropriate protease inhibitors (Pefabloc^{SC}). Elution was done in tubes containing 10 mM EDTA. 20 µl from each fraction was loaded onto SDS gel to check the fractions containing protein of interest. Identified fractions, containing the protein were pooled together, concentrated using YM30 (30 kDa cut-off) centricon and subsequently diluted 10 times with 50 mM Tris/HCl; pH 7.5 and applied to Source^{TM} 30Q ion-exchanger column at a constant flow rate of 2 ml/min in buffer A (50 mM Tris/HCl; 50 mM NaCl; pH 7.5). The protein was eluted with a linear gradient of buffer B (50 mM Tris/HCl; 1M NaCl; pH 7.5). Main peak-half fractions were pooled and concentrated to required volume and checked for purity on a SDS PAGE. All SDS gels were stained with Coomassie Brilliant Blue R250. Protein concentration was determined by BCA assay as per manufacturer's instructions.

The same procedure was followed for the expression and purification of other subunit d constructs such as d_{11-345}

2.2.12.2 Subunit a_{1-388}

Subunit a_{1-388} containing N-terminal His-tag was produced by over expression in Rosetta-gami^{TM} 2 cells and purified using the 2-step protocol as described above in section 2.2.12.1. The first step involved enrichment of His-tagged subunit a_{1-388} protein by specifically binding to Ni^{2+}-NTA matrix and the second step employed ion-exchange chromatography using Resouce^{TM} Q column (GE Healthcare), to get rid of remaining impurities, as described above in section 2.2.12.1. Identical set of buffers were used as mentioned in section 2.2.12.1.

2.2.13 Protein quantification by BCA

The protein concentration estimation was done by bicinchoninic acid assay (BCA; Pierce, Rockford, IL, USA) as per the manufacturer's instructions. BSA (0 – 250 µg/ml) was used as standard. Each dilution of protein was measured in triplicate. Optical density was measured at 562 nm against blank.

2.2.14 Circular dichroism (CD) spectroscopy of proteins and peptides

Circular dichroism spectroscopy measures the difference between the absorption of right- and left handed circularly polarized light, arising due to the symmetry of particular molecule under consideration. Circular dichroism can be used to determine the secondary structure contents of protein in far – UV range where peptide bond acts as active chromophore. I measured steady-state CD of proteins in 0.1 mm quartz Hellma cell (60 µl volume) at 18 ℃ on CHIRASCAN spectropolarimeter (Applied Photophysics) instrument at a step resolution of 1 nm from 180 – 260 nm far UV range of spectrum under continuous purging of N_2 gas. Protein samples were buffer exchanged, reduced or oxidized by appropriate protocols before measurements. Each protein sample was measured in triplicates at a concentration of 2 mg/ml and buffer reading were taking before and after protein sample. Averaged buffer base line was subtracted from average protein values using in built Chirascan software. Initial millidegree units were converted into mean molar residue ellipticity with the help of Chirascan software by giving appropriate cell path length, molecular weight, number of amino acid residues and protein concentration values. Final plotting was done in MS Excel (2003).

2.2.15 Determination of molecular weight by size exclusion chromatography

A standard set of proteins (GE Healthcare) of known molecular weight were used to calibrate the Superdex S75 (10/30) gel filtration column. Standard proteins and their respective molecular masses are BSA (67 kDa), ovalbumin (45 kDa), -cymotrypsinogen (25 kDa), ribonuclease A (13.7 kDa). All proteins were chromatographed at identical conditions and constant flow rates (0.5 ml/min). The K_{av} parameter was determined ($K_{av} = (V_e - V_0)/(V_t - V_0)$; where V_e represents the elution volume, V_0 the void volume, and V_t the total bed volume). The K_{av} values for standard proteins were plotted as a function of the logarithm of molecular mass, and the resulting calibration curve was used to derive the molecular mass of Vma6p (subunit *d*).

2.2.16 Intrinsic tryptophan fluorescence spectroscopy

Intrinsic fluorescence of protein can arise from aromatic residues tryptophan, tyrosine and phenylalanine (Figure M4A-B). Intrinsic fluorescence act as valuable native tools that can be used to monitor the structural and environmental changes in proteins. Tryptophan is most commonly monitored for native florescence because of its much stronger intensity and higher quantum yield than tyrosine and phenylalanine (Figure M4A-B). All tryptophan fluorescence experiments were measured at 20 °C in a Varian Cary Eclipse spectrofluorimeter with an excitation at 295 nm and emission from 310 – 380 nm. Excitation and emission band passes were set to 5 nm. An average of at least three readings from each sample was used to subtract from respective buffers.

(**A**)
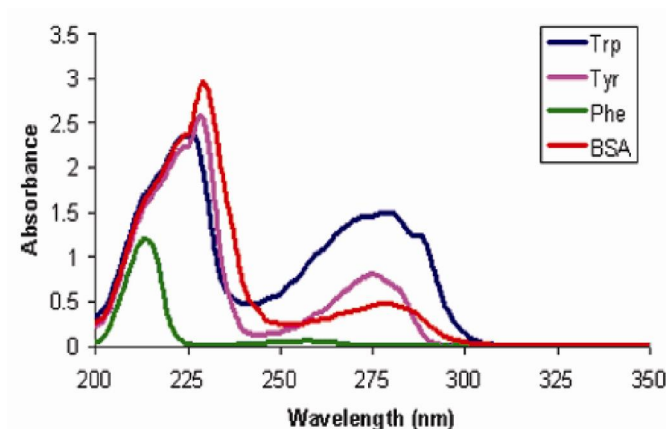
(**B**)

	Lifetime	Absorption		Fluorescence	
		Wavelength	Absorptivity	Wavelength	Quantum
Tryptophan	2.6	280	5,600	348	0.20
Tyrosine	3.6	274	1,400	303	0.14
Phenylalanine	6.4	257	200	282 .	0.04

Figure M4. **Native protein fluorescence.** (**A**) Characteristic fluorescence spectrum of aromatic residues (**B**) life time in nanoseconds, absorption and emission wavelengths are given in nanometers (http://dwb.unl.edu/Teacher/NSF/C08/C08Links/pps99.cryst.bbk.ac.uk/projects/gmocz/fluor.htm).

2.2.17   Disulphide bond formation analysis in subunit *d*

2.2.17.1 CuCl₂ cross-linking

To induce zero length disulphide bond cross-linking protein was treated with 100 µM $CuCl_2$ for 30 min rotating (Neolab rotator) at 4 °C. The reaction was terminated by addition of EDTA to a final concentration of 1 mM. Sample was mixed with DTT free 3X SDS loading buffer (Bio-Rad) and observed for cross-links on Coomassie stained SDS gel.

2.2.17.2 TMR and NEM fluorophore labeling, tryptic digestion and MALDI-TOF analysis

Subunit *d* protein samples were labeled with either TMR (Tetra Methyl Rhodamine; 486.91 Da) or NEM (N-ethyl Maleimide; 125.13 Da) fluorophore dye for 30 min in cold room in dark to avoid the bleaching. TMR and NEM are the thiol-reactive dyes which do bind to the cysteine residues. The reaction was setup using 4 µg of subunit *d* protein in presence of 1 µM final concentration of TMR or NME in 50 mM Tris, 300 mM NaCl, pH 7.5 buffer. To probe for the cysteine residues involved in cross-link formation by $CuCl_2$, labeled subunit *d* was digested and analyzed by MALDI-TOF and a map of peptides was generated to identify the possible disulphide linked peptides. The band of subunit *d* treated with $CuCl_2$, DTT and TMR, respectively, was cut from the gel and destained overnight with a solution of 50 mM ammonium bicarbonate, 40% ethanol. The protein was digested in gel with trypsin (Promega) according to Roos (ROOS *et al.*, 1998) except that the bands had been washed three times with acetonitrile before drying them in a speed vacuum concentrator. Digested samples were desalted with a ZipTip$_{C18}$ (Millipore) and eluted with CHCA- (10 mg/ml -cyano-4-hydroxycinnamic acid in 50% acetonitrile, 0.1% trifluoroacetic acid) or FA- (8 mg/ml 3-methoxy-4-hydroxycinnamic acid in 50% acetonitrile, 0.1% trifluoroacetic acid) matrix solution. 1-2 µl of matrix-analyte solution was spotted onto the MALDI plate and allowed to dry (HONG-HERMESDORF *et al.*, 2006). Peptide mass mapping was performed by matrix assisted laser desorption-ionization/time-of-flight mass spectrometry (MALDI-TOF MS) using a Voyager-DE STR Biospectrometry Workstation) at Protein and Proteomics Center, NUS (Singapore). The peptide map was acquired in reflectron positive-ion mode with delayed extraction at a mass range of 900 – 8 000 Da. The instrument was calibrated using a calibration mixture (Applied Biosystems). For interpretation of the protein fragments, the PEPTIDEMASS (MARC R. WILKINS, 1997) program available at Expasy web site (www.expasy.ch/tools/peptide-mass.html) was used.

2.2.18 Small angle X-ray scattering (SAXS) and data analysis

The synchrotron radiation X-ray scattering data were collected by A/Prof. Gerhard Grüber, following standard procedures on the X33 beam line (BOULIN *et al.*, 1986; BOULIN *et al.*, 1988) of the EMBL Hamburg on the storage ring DORIS III of the Deutsches Elektronen Synchrotron (DESY) using a MAR345 image plate with online readout (MarResearch, Norderstedt, Germany). The scattering patterns from subunit *d* at protein concentrations of 0.8 and 12.7 mg/ml were measured using a sample - detector distances of 2.4 m, covering the range of momentum transfer $0.1 < s < 4.5$ nm^{-1} ($s = 4$ $sin($ $)/$, where   is the scattering angle and   =

0.15 nm is the X-ray wavelength). A sample volume of 60 µl was disposed in a small cuvette (1mm thickness) with thin polystyrene windows (20 µm) and two repetitive measurements of 120 sec of the same protein solution were performed in order to check for radiation damage. No aggregation was found during the initial 120 sec exposure. The data were normalized to the intensity of the incident beam; the scattering of buffer was subtracted and the different curves were scaled for concentration. All the data processing steps were performed using the program package PRIMUS (KONAREV *et al.*, 2003). The forward scattering *I(0)* and the radius of gyration R_g were evaluated using the Guinier approximation (GUINIER and FOURNET, 1955) assuming that at very small angles (*s < 1.3/R_g*) the intensity is represented by *I(s) = I(0) exp(-(sR_g)^2/3)*. These parameters were also computed from the entire scattering patterns using the indirect transform package GNOM (SVERGUN, 1994), which also provide the distance distribution function *p(r)* of the particle. The molecular mass of subunit *d* was calculated by comparison with the forward scattering from the reference solution of bovine serum albumin (BSA).

Low resolution models of the *d* subunit were built using two *ab initio* methods. The program DAMMIN (SVERGUN, 1992; SVERGUN, 1994) represents the protein shape as an ensemble of M>>1 densely packed beads inside a search volume (a sphere of diameter D_{max}). Each bead belongs either to the protein (index=1) or to the solvent (index=0), and the shape is thus described by a binary string of length M. Starting from a random string, simulated annealing (SVERGUN, 1992) is employed to find a compact configuration of beads minimising the discrepancy χ between the experimental $I_{exp}(s)$ and the calculated $I_{calc}(s)$curves:

$$\chi^2 = \frac{1}{N-1}\sum_{j}\left[\frac{I_{\exp}(s_j)-cI_{calc}(s_j)}{\sigma(s_j)}\right]^2$$

where *N* is the number of experimental points, *c* is a scaling factor and *σ(s$_j$)* is the experimental error at the momentum transfer *s$_j$*.

In a more versatile *ab initio* approach implemented in the program GASBOR (SVERGUN *et al.*, 2001) the protein is represented as a collection of dummy residues (DR). Starting from randomly positioned residues, a chain-compatible spatial distribution of DR's inside the search volume is found by simulated annealing. The DR method permits an enhanced resolution, but the number of residues must be known *a priori*. For the subunit *d* ten GASBOR reconstructions were performed using 350 amino acid residues. These ten independent models were analyzed using the programs DAMAVER (SVERGUN *et al.*, 2001) and SUBCOMB (SVERGUN *et al.*, 2001).

These packages align all possible pairs of models and identify the most probable model giving the smallest average discrepancy with the rest. An averaged model is computed by aligning all other models with the most probable one, computing the density map of beads and drawing the threshold corresponding to the excluded particle volume. The DAMMIN and the GASBOR approach resulted in similar models and the averaged DR model was used for further interpretations.

In order to compare the experimental data of subunit *d* with the atomic structure of the stalk subunit C of the A_1A_O ATP synthase from *T. thermophilus*, the SAXS parameters of the high resolution model of subunit C (PDB entry 1r5z) (BERNSTEIN *et al.*, 1977) were extracted from its structure using the program CRYSOL (SVERGUN *et al.*, 1995).

2.2.19 Nuclear magnetic resonance (NMR) spectroscopy

Nuclear magnetic resonance is a power technique to study the structural and functional aspects of macromolecules such as proteins. NMR can be used to determine the structure of protein in solution and to study biochemical and biophysical properties such as protein-ligand interaction to demonstrate new binding partners as well as to map the binding regions down to single amino acid level. Specific nuclei such as hydrogen, one of the most receptive and abundant NMR active nuclei besides other isotopes such as ^{15}N, ^{13}C, ^{31}P etc. can be observed in magnetic resonance. Any nuclei having odd number of protons and neutrons, which exhibits net intrinsic magnetic momentum and angular momentum, can be defined as NMR active. All the NMR experiments were collected on Bruker Avance 600 or 700 MHz machines at NTU NMR core facility.

2.2.19.1 ^{15}N single and ^{13}C ^{15}N double labeling of proteins

Reagents:

Minimal Media (M9): *42 mM Na_2NPO_4*
22 mM KH_2PO_4
8.5 mM NaCl
1 g/L $^{15}NH_4Cl$
0.1 mM $CaCl_2$
2 mM $MgSO_4$
10 g D-Glucose
30 μM $FeCl_3$
5 ng/l Thiamin
Antibiotic
LB Media

For NMR experiments, either single (^{15}N) or double (^{13}C ^{15}N) labelled recombinant proteins were produced in *E. coli* BL21 (DE3) and purified as explained above using established protocols. Following protocol was used for growing the cells in M9 minimal media. 50 ml of overnight culture was pellet down at low centrifugal force at room temperature and washed two times with LB media following a final wash in 1X M9 media and resuspended in 10 ml M9. 1 ml of final resuspension was inoculated per 500 ml and cells were shaken at 37 ℃ till an OD_{600} of 0.6 - 0.7 was achieved and culture was induced with 1 mM IPTG for 3 – 5 h or alternatively induced overnight at 25 ℃. Cells were harvested and frozen in liquid nitrogen and stored at – 80 ℃ till purification.

2.2.19.2 One dimensional (1D) ^{1}H and multi- dimensional (2D, 3D) ^{13}C-^{15}N NMR spectroscopy

1D NMR spectrum of various proteins was collected at temperatures ranging from 288 K to 298 K on core facility Avance 600 or 700 MHz instruments (Bruker, Billerica, MA). Unlabeled or labelled protein sample in appropriate buffer such as phosphate (pH 6.8) was used in presence of 10 % D_2O (v/v) to record the spectrum. Protein concentration varied from 100 to 500 μM. In multi-dimensional experiments, ^{15}N labelled proteins in 90% H_2O and 10% D_2O in 25 mM PO_4 (pH 6.8) buffer was used to collect 2D spectrum such as HSQC (Hetero nuclear Single Quantum Coherence), which was used for assignment and binding studies in subsequent stages of analysis and experiments, respectively. Other 2D experiments used in current studies were 2D NOESY and 2D TOCSY for peptide data collection. Appropriate pulse calibrations and other parameters including temperature, buffer, and protein concentration were optimized before making final measurements. All spectra were recorded on in house cryo-probed Bruker Avance 600 or Bruker Avance 700 machines. ^{15}N-^{13}C labelled samples were utilized to collect 3D spectra such as HNCO, HNCACO, CBCA(CO)NH, HNCACB, HNCA, 3D ^{15}N -NOESY-HSQC, H(CCO)NH in 10% (v/v) D_2O lock signal. The 3D ^{15}N-NOESY-HSQC used mixing time of 200 ms (tm=200ms). All experiments recorded made use of pulsed-field gradients for coherence selection and artefact suppression utilizing gradient sensitivity enhanced schemes. Quadrature detection in the indirectly detected dimensions was achieved using either the States/TPPI (time-proportional phase incrementation) or the echo/anti-echo method. Baseline corrections were applied wherever necessary. The proton chemical shift was referenced to the methyl signal of DSS (2, 2-dimethyl-2-silapentane-5-sulphonate [Cambridge Isotope Laboratories]) as an external reference to 0 ppm. The ^{13}C and ^{15}N chemical shifts were

referenced indirectly to DSS. All the NMR data were processed using Bruker Avance spectrometer in-built software Topspin and NMR pipe (F. DELAGLIO *et al.*, 1995). Peak-picking and data analysis of the Fourier transformed spectra were performed with the SPARKY program (KNELLER and GODDARD, 1997).

To elucidate the 3D structure of the peptides such as $a2_{386-402}$, $ARNO_{375-400}$ and $ARNO_{375-400(phos)}$, data were collected on Bruker Avance at 600 MHz by dissolving appropriate amounts (1 – 2 mM) in 50 mM phosphate buffer pH 6.8 or MilliQ water and TFE-d$_3$ (2,2,2 Tri Fluro Ethanol, deuteriated). 10% D$_2$O was used to lock the NMR signal in each experiment. The one dimensional (1D) and two dimensional (2D) ^{1}H NMR spectra including total correlation spectroscopy (TOCSY) and nuclear overhauser enhancement spectroscopy (NOESY) were obtained at the temperature of 288 K to 298 K proton frequency. TOCSY and NOESY spectra of the peptide were recorded with mixing times of 80 ms and 200 – 400 ms, respectively. All the NMR data were processed using Bruker Avance spectrometer in-built software Topspin. Peak-picking and data analysis of the Fourier-transformed spectra were performed with SPARKY 3.1 program (KNELLER and GODDARD, 1997). Assignments were carried out according to classical procedures including spin system identification and sequential assignment (WÜTHRICH, 1986). Dihedral angle restraints were calculated from chemical shifts using torsion angle likelihood obtained from shift and sequence similarity (TALOS) (WÜTHRICH, 1986) and over all secondary structures were predicted from the chemical shift index (CSI) (WISHART *et al.*, 1992) and NOE pattern. Structure calculations was done by using Cyana 2.1 or Cyana 3 program package which uses simulated annealing with molecular dynamics in torsion angle space (HERRMANN *et al.*, 2002). Final Cyana ensemble structures were visualized by MOLMOL program (KORADI *et al.*, 1996).

2.2.19.3 Binding studies with NMR

Interaction studies were performed between various proteins using highly precise and reproducible technique of NMR. Binding studies with NMR have the advantage of monitoring interactions at single amino acid level. ^{1}H-^{15}N heteronuclear single quantum coherence (HSQC) spectrum of labeled protein was used as starting point, recording the spectrum at optimized condition, followed by addition of ligand protein in increasing amount at appropriate temperature and buffer conditions, recording a series of ^{1}H-^{15}N heteronuclear single quantum coherence (HSQC) spectra. Usually a constant amount (100 µM) of ^{15}N labeled protein was used, adding unlabeled binding partner in increasing amounts to a molar ration of 1:1 – 1:2 in most cases and

changes in chemical shift were monitored in HSQC spectrum. Experiment was performed on Bruker Avance 600/700 machine using Topspin for acquisition and processing of spectra. Respective spectra were overlapped to monitor chemical shift changes, further analysis were done in SPARKY (KNELLER and GODDARD, 1997).

2.2.20 Florescence correlation and florescence cross correlation spectroscopy (FCS, FCCS) binding studies

Fluorescence correlation spectroscopy was performed on a LSM-FCS system (ConfoCor 3, Zeiss, Jena, Germany) and on a custom-built LSM-FCS system on Olympus® FV300 at Biophysical Fluorescence Lab in NUS using TMR (Tetramethylrhodamin) labeled subunit d and unlabeled subunit a_{1-388}. The experiments have been performed in a collaborative project with the cooperation of Dr. Pan Xiaotao from A/Prof. Thorsten Wohland's laboratory at NUS. The labeling experiments were done in 50 mM Tris, 300 mM NaCl, pH 7.5 buffer for 10 min at room temperature, reaction was stopped by the addition of 1 mM DTT and excess of free flurophores were removed by buffer exchanged. All steps were carried out in dark to avoid the bleaching of dye. The 514 nm laser line of a 8 mW argon/2 ion laser was focused into the aqueous solution using a water immersion objective (C-Apochromat 40 ∕ 1.2 W, korr UL-Vis-IR, Zeiss). FCS was performed on 30 µl droplets on Nunc 8 well-chamber cover glasses (Nunc, Denmark). The following filter sets were used for TMR labeled subunit d: MBS (main beam splitter): HFT514/633 (Hauptfarbteiler, main color splitter); EF (emission filter): none; EF2: BP 530-610 IR (band pass filter); DBS (dichroism beam splitter): mirror, DBS2: plate, DBS3: Mirror. Pin hole size was kept at 90 µm^2 and laser transmission set to 6%.

The florescence cross-correlation experiments (FCCS) were done using TMR labeled subunit d and Cys5 labeled subunit a_{1-388}. Additional 633 nm laser line was used in the following beam path: MBS: HFT514/633; EF (emission filter): none, EF2: BP 655-710 (band pass filter) IR. Out-of-focus fluorescence was rejected by a 75 µm pinhole in the detection pathway, resulting in a confocal detection volume of approximately 0.25 fl. Fluorescence autocorrelation functions were measured for 30 s each with twenty repetitions. Solution of 1 – 10 nM TMR and Cy5 in buffer were used as references and for calibration of the ConfoCor 3 system. The determination of the binding constants only required calculation of the relative amounts of free labeled subunit d with the short diffusion time, in comparison with an increase of the diffusion time. The increase of the diffusion time is caused by the increment of the size of the complex caused by the interaction with subunit a_{1-388} according to the Stokes–Einstein relation. Therefore, the diffusion time for

free fluorescently labeled subunit *d* was measured independently using a one-diffusion-coefficient model, and kept fixed during fitting of all the FCS data for subunit *d* and subunit a_{1-388} binding experiments. A standard autocorrelation two-diffusion-coefficient normalized triplet model was used for fitting (FCS-LSM software, ConfoCor 3, Zeiss). The calculations were performed using ConfoCor 3 software version 4.2, Microsoft Excel 2003, Igor Pro 6.0 (Wavemetrics Inc.) and Origin 7.5 (Origin Lab, Northampton, MA, USA).

2.2.21 Surface plasmon resonance (SPR) binding studies

Binding affinity of subunit a_{1-388} with subunit *d* of V ATPase was determined by surface plasmon resonance (SPR) at 25 ºC using a Biacore 3000 instrument (Biacore AB, Uppsala, Sweden) and the experiment was performed by Yin Hoe (A/Prof. Susana G. Shochat's lab, NTU). Subunit *d* was covalently immobilized on a carboxymethylated sensor surface (CM5, research grade) using amine coupling chemistry. The surfaces were activated with 0.2 M EDC (N-ethyl-N'-[3-(diethylamino) propyl] carbodiimide) and 50 mM NHS (N-hydroxysuccinimide) for 7 min. The subunit *d* protein was coupled to the desired level and deactivation of the surface was performed using 1 M ethanolamine-HCl (pH 8.5) for 7 min, at a flow-rate of 10 ml/min. The reference surface was treated in the identical way as the ligand surfaces except that protein injection was omitted. For the determination of kinetic parameters, subunit a_{1-388} was passed above the reference and protein surfaces in duplicates of five to seven concentrations (60 – 1000 nM), in HBS (10mM Hepes buffer; pH 7.4, 150 mM NaCl; 3.4 mM EDTA and 0.005% P-20), at a flow rate of 30 µl/min. Surfaces were regenerated using the same flow-rate by a 15 µl injection of 50 mM NaOH. The level of immobilization was chosen to avoid mass transfer limitation in the experiment. Sensorgrams were fitted using the simple 1:1 Langmuir binding fit model, the association rate constants (*ka*) and dissociation rate constant (*kd*) were fitted simultaneously by rate equation (1), and the equilibrium dissociation rate constant was calculated according to equation (2). The BIAevaluation 4.1 software was used for data analysis.

$$dR/dt = k_a \; x \; C \; x \; (R_{max} - R) - k_d \; x \; R \; \dots\dots\dots\dots\dots\dots\dots\dots\dots\dots\dots(1)$$

whereas C is the concentration of the analyte (e.g. subunit *a* in *a/d* binding) and R is the response unit (RU).

$$K_D = k_d/k_a \dots\dots\dots\dots\dots\dots\dots\dots\dots\dots\dots\dots\dots\dots\dots\dots\dots\dots\dots\dots (2)$$

3. Results

3.1 Caspase mediated degradation of Livin (ML-IAP) in ARTS induced apoptosis and the caspase 3 target subunit *d* of eukaryotic V_1V_o ATPase
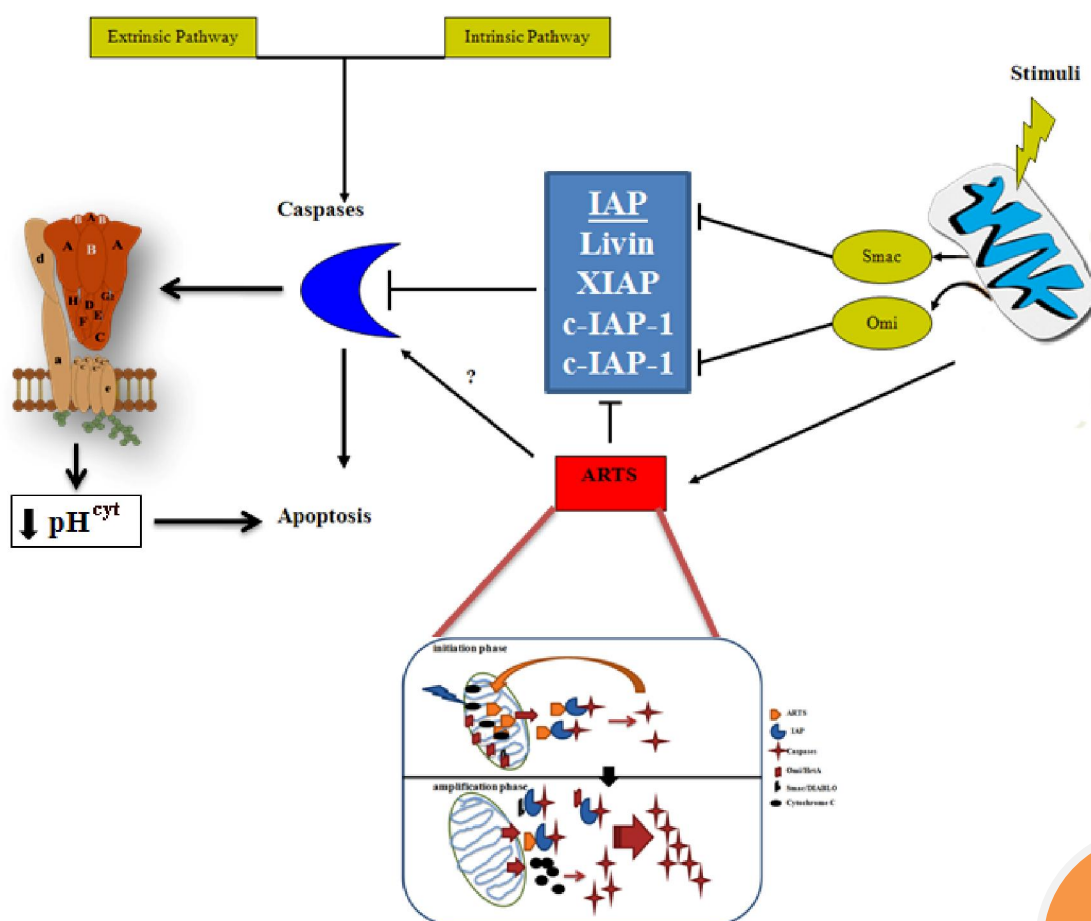
Apoptosis is a conserved mechanism of cell death which is regulated by the delicate balance of pro- and anti-apoptotic factors in development and maintenance of tissue homeostasis (ZHAOYU and EL-DEIRY, 2005). Defects in apoptosis may result in several physiological disorders causing either excessive accumulation such as in cancer and restinosis or loss of cells in AIDS, neurodegeneration, heart failure like diseases (REED, 2000). ARTS (Apoptosis Related Protein in the TGF-b Signaling pathway), a member of Septin family of proteins, is the novel and least characterized pro-apoptotic protein, which induces the cells to undergo apoptosis in response to various extra-cellular stimuli (LARISCH *et al.*, 2000; YOSSI *et al.*, 2004). Septin family of proteins are GTPases involved in a variety of cellular functions such as cytoskeleton assembly, cellular morphogenesis and cell division (FIELD and KELLOGG, 1999; FATY *et al.*, 2002). ARTS also contains a P-loop motif (phosphate binding), which can act as potential nucleotide binding domain (LARISCH *et al.*, 2000). Livin or K/ML-IAP (Kidney/Melanoma Inhibitor of Apoptosis Protein) (KASOF and GOMES, 2001), on the other hand, is a member of IAP (Inhibitor of Apoptosis Protein) family of proteins and a key repressor protein of apoptosis, preferentially expressed in melanoma cells, rendering them resistant to apoptosis (ASHHAB *et al.*, 2001; KASOF and GOMES, 2001). IAP is an emerging family of proteins which can suppress apoptotic activity by directly binding to caspases (SALVESEN and DUCKETT, 2002). However, under the circumstances when cells are marked to undergo apoptosis, the activity of IAP must be abrogated to allow the initiation of cell death (MARTIN, 2002). Several pro-apoptotic proteins have been found to promote apoptosis at least in part by directly inhibiting IAPs (HOLLEY *et al.*, 2002). The direct role of caspases in the cleavage of IAPs is also reported, where caspases have been found to remove the inhibition barrier posed by XIAP (X-linked Inhibitor of Apoptosis), an apoptosis suppressor (DEVERAUX *et al.*, 1997). Nevertheless, more detailed information is needed to complete the underlying mechanism governing the regulation of IAPs in survival and death. Here, I describe the studies with human ARTS and Livin proteins in apoptosis. The results of this chapter have been partially obtained in an ongoing collaborative project with A/Prof. Wu Mian.

3.1.1 Livin does not act as E3 Ligase to ARTS

IAP family members such as XIAP (KAUR *et al.*, 2005; MORIZANE *et al.*, 2005) and Livin (MA *et al.*, 2006) have been reported to act as E3 ligase (activity of RING domain) and promote degradation of target proteins via ubiquitin proteosome pathway. Also, ARTS regulation by XIAP (X-linked Inhibitor of Apoptosis Protein) has been recently found, where E3

Ligase XIAP promoted the degradation of ARTS via ubiquitination proteosome pathway (LOTAN *et al.*, 2005). So to investigate if such E3 ligase active, Livin, does also promotes ARTS degradation *in vivo,* I co-transfected GFP-ARTS and Flag-Livin vectors into the COS7 cells and 24 h post transfection, proteosome inhibitor, MG132 (20 µM, 8 h) was added, to allow the accumulation of polyubiquitinated ARTS (Figure 1A). Cell lysates were immunoprecipitated with anti-ARTS antibody and western blotting was done using anti-GFP antibody. The results inferred from the figure 1A indicate that ARTS is ubiquitinated *in vivo* and MG132 causes accumulation of ARTS polyubiquitinated forms. However, there was no further increase in ARTS ubiquitination in the presence of Livin, rather a slight decrease was observed when compared to ARTS alone control (Figure 1A). In a similar experiment, when Livin RING, lacking E3 ligase active RING domain, was co-transfected with ARTS, no significant changes could be detected (Figure 1A). RING domain of Livin is essential for the E3 ligase activity (VAUX and SILKE, 2005), which is responsible for ubiquitination of target proteins as well as auto or self-ubiquitination of Livin. ARTS polyubiquitination has been known to regulate its threshold levels in healthy cells, to maintain a normal cellular activity and prevent apoptosis induction by excessive free ARTS in the cytoplasm of healthy cells (LOTAN *et al.*, 2005). As per these observations, ARTS must be degraded in healthy cells and prevented from degradation in apoptotic cells so that it can promote cell death in cells that have been marked for death by certain external or internal insult. To understand the degradation pattern of ARTS in apoptosis, transfected cells were induced to undergo apoptosis by treating with STS (staurosporine; 1 µM) for 4 h followed by the addition of MG132 (20 µM) for additional 8 h. As shown in western blot (Figure 1B), ARTS was not ubiquitinated in apoptotic cells. Again, in the conditions where ARTS was co-transfected with Livin (wild type), Livin RING (– RING domain) or Livin C124A (BIR domain mutated, BIR domain is essential for anti-apoptotic activity of IAPs), no significant changes could be observed (Figure 1B). Thus, the results point to the conclusion that Livin did not act an E3 ligase and ARTS was prevented from ubiquitination during apoptosis. However interestingly, a decrease in Livin levels was seen in the control lysate (GFP-ARTS + Flag-Livin co-transfected cells), when equal amount of lysates were probed with anti-Livin antibody, as shown in figure 1B (*bottom panel; lane 3*). However, no such decrease in Livin levels was found in non-apoptotic condition (Figure 1A) (*bottom panel; lane 3*). A significant decrease in Livin C124A mutant can be explained due to the instability of this mutant, because C124 is critical for overall folding of Livin (MA *et al.*, 2006), but downregulation in Livin levels could not be explained. Following experiments were designed to understand this phenomenon.

(A)

(B)
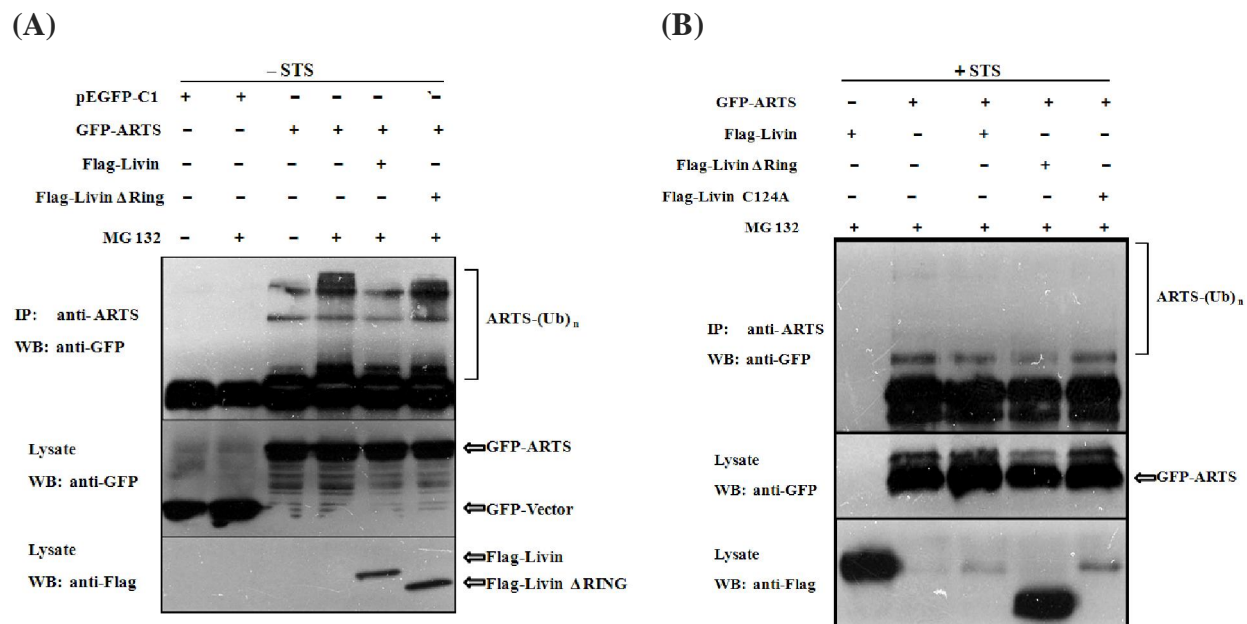
***Figure 1.* ARTS ubiquitination *in vivo*. (A)** HeLa cells were transfected with GFP-vector control or co-transfected with GFP-ARTS and either Flag-Livin or Flag-Livin Ring. 24 h later cells were treated with MG132 (20 µM) for 8 h before harvesting. Whole cell lysates were subjected to IP with anti-ARTS antibody. In non-apoptotic cells ARTS was found to be ubiquitinated and the presence of Livin did not enhanced ubiquitination rather a slight decrease was observed in ARTS poly-ubiquitination patterns. **(B)** Culture HeLa cells were transfected with mentioned plasmids and 24 h post-transfection cells were induced to undergo apoptosis by STS (1 µM) treatment for 4 h. Results showed that ARTS ubiquitination was completely inhibited in apoptotic cells and presence of Livin could not promote its degradation.

3.1.2 Livin cleavage into 10 kDa fragment during ARTS-promoted apoptosis

To examine the Livin degradation phenomenon observed in section 3.1.1 in detail, HeLa cells were co-transfected with GFP-ARTS (0.5 µg) plus Flag-Livin (2 µg) for 24 h when apoptosis was induced with the addition of STS to the culture media at a final concentration of 1 µM. A 10 kDa cleaved fragment of Livin was detected in protein lysates of cells transfected with ARTS plus Livin for 20 h and induced to undergo apoptosis by STS for 4, 6, 8 or 10 h as shown in figure 2. However, cells transfected with Livin alone under identical conditions did not produce the 10 kDa fragment, but depletion in Livin protein levels could be observed. Appearance of Livin cleaved fragment in ARTS-promoted apoptosis and absence of such cleavage pattern in native conditions (only Livin transfected cells) raises the possibility that Livin might be degraded by different pathways in the presence and absence of ARTS. Cleavage of Livin in apoptotic cells has been reported (NACHMIAS *et al.*, 2003), where it was found that after cleavage Livin not only loses its anti-apoptotic function but also gains a pro-apoptotic effect (NACHMIAS *et al.*, 2003). Livin has 14 aspartate residues in its protein sequence (Figure 2B), which can act as preferred substrate sites for caspases (cysteinyl aspartate proteinases). Caspases

do recognize and cleave their substrates at tetra-peptide sequences after conserved aspartate residue at fourth position (SALVESEN and DIXIT, 1997). Potential caspase cleavage sites have been indicated in figure 2B.

(A)
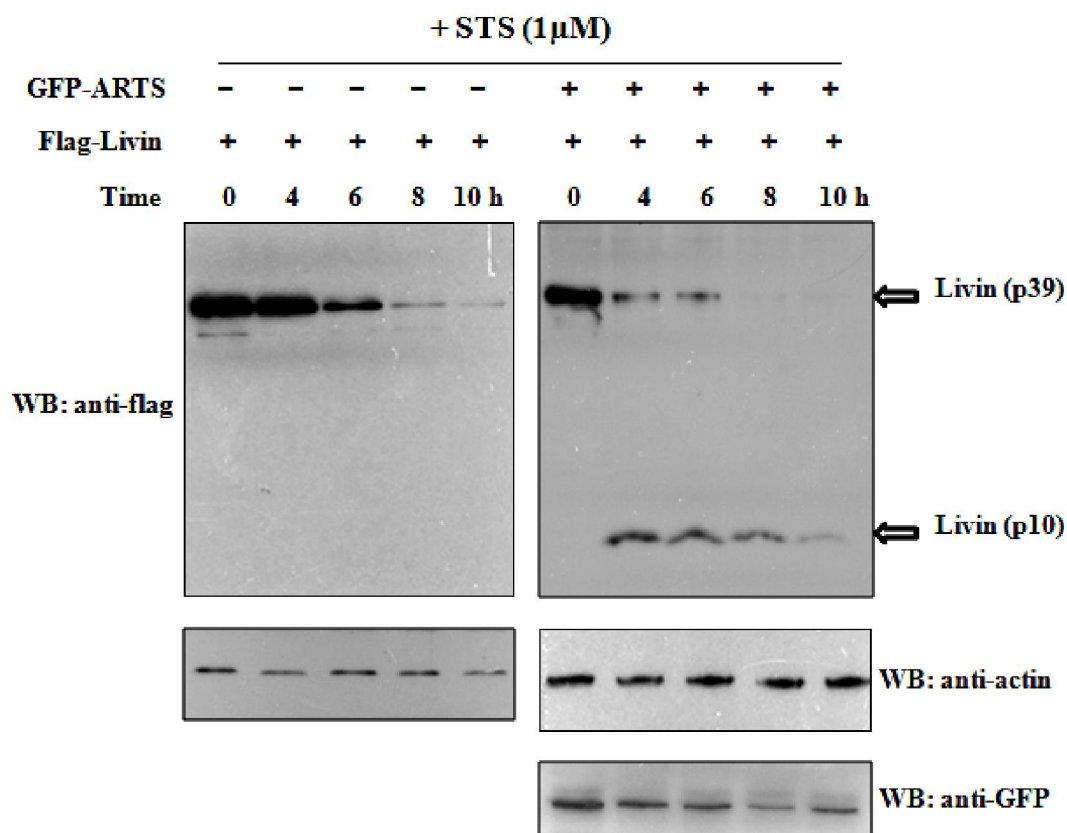
(B)
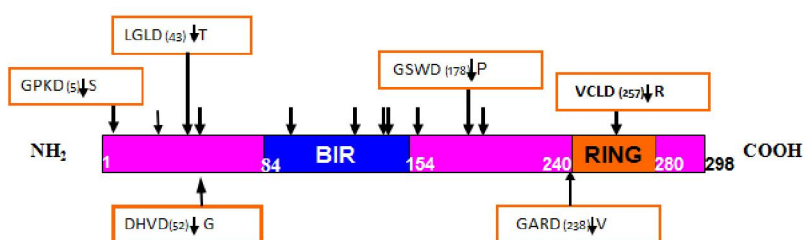
***Figure 2*. Livin cleavage into 10kD fragments in ARTS apoptosis.** (**A**) A 10 kDa fragment of Livin was produced during ARTS induced apoptosis. COS7 cells transfected with GFP-ARTS (0.5 µg) and Flag-Livin (2 µg) were treated with STS for 4 – 10 h, respectively in individual plates before harvesting (0 h represents untreated STS control) (**B**) Schematic representation of potential caspase cleavage sites. Caspase 8 and 9 potential cleavage sites have been highlighted in boxes. Remaining unconventional possible non-canonical sites have been marked by arrows only. Caspase 3 and 7 cleavage site is located at 52 residues position from NH_2 terminus (indicated amino acid positions are roughly to the scale).

3.1.3 Livin is degraded independent of ubiquitin-proteosome pathway

To probe the pathway involved in Livin degradation, two possibilities were taken into consideration: first, self or auto-ubiquitination due to the presence of E3 ligase RING domain (MA *et al.*, 2006) and second one, the enzyme cleavage by the caspases (NACHMIAS *et al.*, 2003; YAN *et al.*, 2006). Both mechanisms have been established by previous studies with IAPs (NACHMIAS *et al.*, 2003; YANG and DU, 2004), however, not in the context of ARTS or cellular apoptotic conditions. To examine these pathways, HeLa cells were co-transfected with Flag-Livin plus either GFP-ARTS or GFP-vector (control) for 24 h when cells were treated with MG132 (20 µM) for additional 12 h. To induce apoptosis, cells were treated with STS (1 µM) for 4 h or left untreated before the addition of MG132. Cells were harvested and whole cell lysates were prepared for respective experiments as described in method section 2.2.8 and proteins were quantified by Bradford assay (section 2.2.5). These lysates were used for anti-Flag immunoprecipitation followed by western blotting that was done using anti-Flag antibodies. The results are shown in figure 3, where Livin was found to undergo auto (self)-ubiquitination in non-apoptotic cells (Figure 3, *lane 1*), being slightly reduced in apoptotic (*lane 2*) and non-apoptotic ARTS transfected cells (*lane 3*), with significant amounts of intact wt-Livin in all three. Although Livin levels were slightly reduced in non-apoptotic cells in presence of ARTS in comparison to other two lanes (*lane 1 and 2*), but in apoptotic conditions, most of the Livin was depleted in presence of ARTS (*lane 4*), which was not accompanied by the appearance of extra polyubiquitinated forms of Livin. Extra ubiquitination would be expected if it is degraded via ubiquitin proteosome pathway.
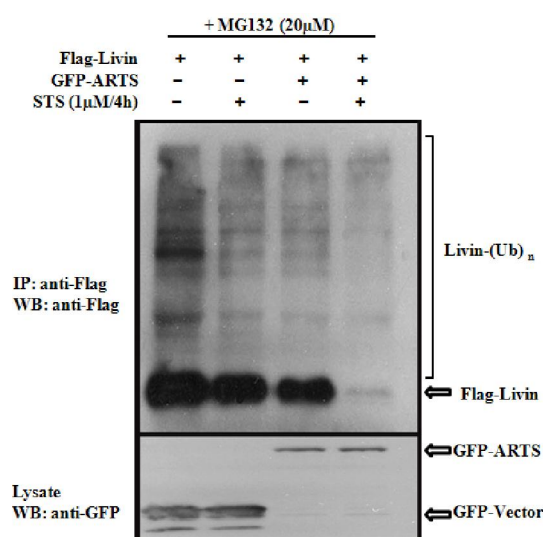
Figure 3. **Livin degradation is independent of Ubiquitin-proteosome pathway.** HeLa cells were co-transfected with Flag-Livin plus either GFP-vector or GFP-ARTS and treated with 20 µM MG132 for 12 h. Further, cells were either left untreated or treated with 1 µM STS for 4 h as shown in figure. Immunoprecipitation and western blotting was carried out with anti-Flag antibody.

3.1.4 Caspase inhibitors can prevent Livin degradation

Results from section 3.1.3 indicated that ubiquitin-proteosome may not be involved in the observed Livin degradation in the apoptotic cells (STS treated) that co-express Livin and ARTS. To further examine the observed phenomenon of Livin degradation and the likely role of caspases, COS7 cells were transiently transfected with Flag-Livin alone or with GFP-ARTS. Cells were cultured for 12 h in the presence of various caspase inhibitors (pan-caspase and specific caspase 3, 8 and 9 inhibitors) before apoptosis was initiated with STS for 4 – 10 h. The concentration of caspase inhibitors was kept below 50 µM to avoid the inhibition of Calpain (WATERHOUSE *et al.*, 1998; BLOMGREN K., 2001), a family of calcium dependent cysteine proteases vital for various cellular activities such as cell division and motility. Protein was extracted as described in section 2.2.8 and quantified with at least three independent replicates and analyzed by anti-Flag western blotting. In the first set of experiment, the general non-specific caspase inhibitor, ZVAD-FMK, was added to the cells, transfected with Livin or Livin plus ARTS for 12 h, then 1 µM STS was added for 0 – 10 h. Results in figure 4 revealed that pan-caspase inhibitor can block Livin degradation and most of the Livin (> 90%) could be recovered at 4 h time slot. About 50% of Livin could be prevented at 6 – 10 h following the STS treatment.

(A)   **(B)**
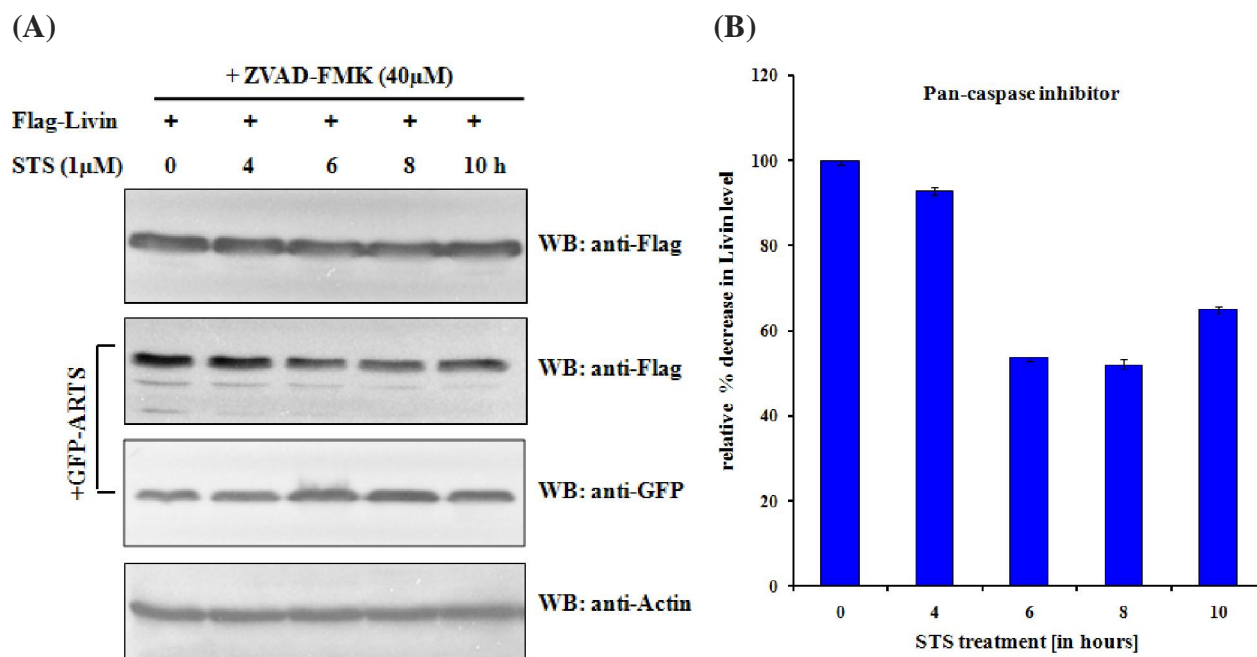
***Figure 4.* Caspase inhibitor ZVAD-FMK can block Livin degradation during ARTS induced apoptosis. (A)** COS7 cells were transfected with either Flag-Livin or co-transfected with GFP-ARTS and Flag-Livin. 24 h later cells were treated with 40 µM pan-caspase inhibitor, ZVAD-FMK for another 12 h. 1 µM STS was added to induce apoptosis in cells for 4, 6, 8 and 10 h (0 h represents no STS treatment). Livin levels were quantified by anti-Flag western blot. Actin served as endogenous loading control. GFP western blot was used for GFP-ARTS expression control. (**B**) Graph showing average relative percent of Livin protected from degradation with respect to control, in the presence of pan-caspase inhibitor.

Such observations are in conformity with the existing hypothesis for ARTS dependent apoptosis, where ARTS is thought to release the IAP mediated inhibition of caspases. Activated caspases do in turn target additional IAP molecules, as well as causing the release of other mitochondrial factors such as Smac/DIABLO in the late stages of apoptosis, taking the execution a step ahead (cover page) (LARISCH, 2004).

Inhibition in Livin degradation could be seen in presence of pan-caspase inhibitor, as shown in figure 4. Further in this direction, specific inhibitors of caspase – 8 (Z-LETD-FMK), – 9 (Z-LEHD-FMK.TFA) and – 3 (Z-DQMD-FMK) (Figure 5) were used. Final concentration of all the inhibitors were kept at 40 µM in individual plates for 12 h. Cells were harvested at 0, 4, 6, 8 and 10 h time intervals following the STS treatment. Normalized amounts of protein were loaded from each sample into the individual lanes of SDS gel (12%) and analyzed by anti-Flag western blotting. Following the use of specific inhibitors, caspase 8 inhibitor was found to be as efficient as pan-caspase inhibitor at 4 h of STS treatment (Figure 5B) but degradation beyond 4 h was much faster and could not be blocked efficiently. STS untreated Livin levels were considered as 100% and all figures are relative to it. Only 55% and 25% of the Livin was prevented from degradation at 4 and 6 h respectively following treatment with caspase 9 specific inhibitor (Z-LEHD-FMK.TFA), however almost 90% and 40% could be prevented from degradation in the presence of caspase 8 specific inhibitor (Z-DQMD-FMK) (Figure 5A-C). Results in figure 5D demonstrate that caspase 3 inhibitor was unable to prevent Livin down regulation at 8 and 10 h following STS treatment, however, it can partially prevent at 4 h and 6 h time interval. Earlier data about Livin cleavage by caspase 3, 7 and possibly caspase 9 do exist (NACHMIAS *et al.*, 2003; YAN *et al.*, 2006), with additional recent reports supporting the fact that Livin might be cleaved by non-canonical caspases (YAN *et al.*, 2006), consistent with the results obtained here, where Livin cleavage did show the involvement of more than one type of caspase. Such findings have also demonstrated that endogenous Livin is cleaved into 29 and 10 kDa fragments during apoptosis, abrogating its anti-apoptotic activity (NACHMIAS *et al.*, 2003). Furthermore, a role of endogenous ARTS cannot be ruled out in such observation. The results here also demonstrate that Livin can be the target of more than one type of caspase during apoptosis in the presence of pro-apoptotic ARTS.

(A)
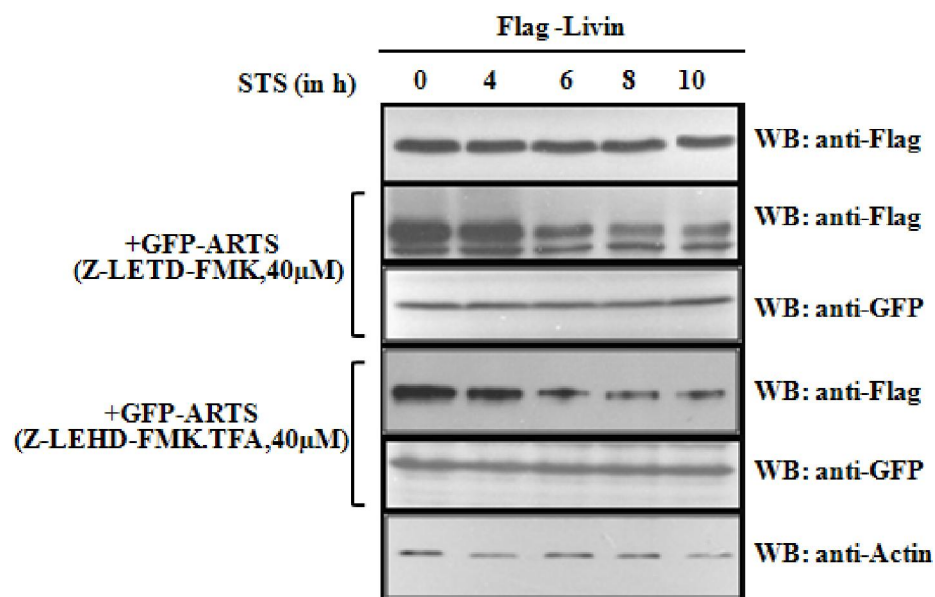
(B)
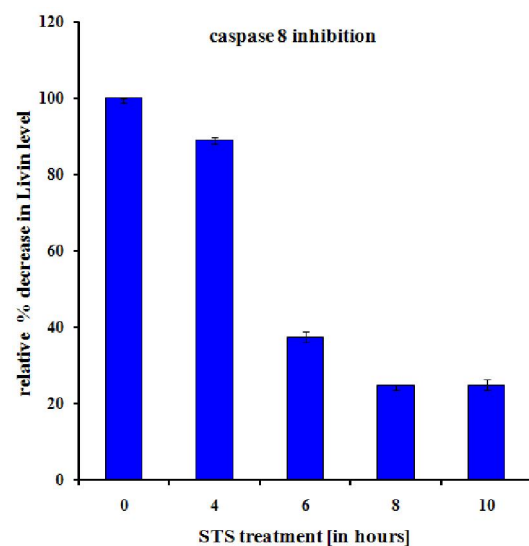
(C)
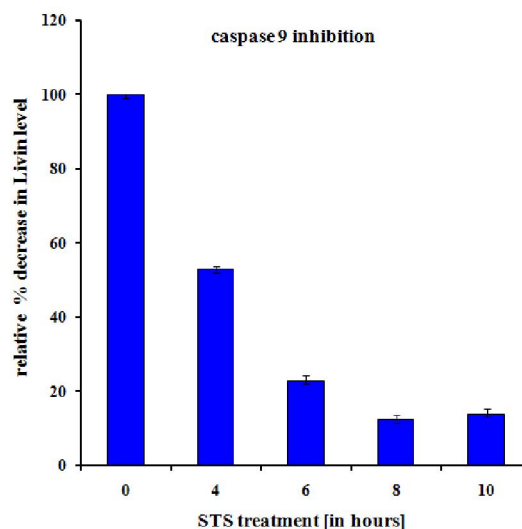
Figure 5. **Inhibition of caspase 8 and -9 mediated Livin degradation in ARTS apoptosis**. (**A**) Cells were transiently transfected with Flag-Livin (control) or co-transfected with Flag-Livin plus GFP-ARTS. Transfected cells were further treated with 40 μM each of caspase 8 inhibitor (Z-LETD-FMK) or caspase 9 inhibitors (Z-LEHD-FMK.TFA) individually for 12 h followed by STS (1 μM) treatment for 4 – 10 h (0 h shows STS untreated control). Western blot was done using anti-Flag antibody. (**B – C**) Diagrams shows the relative percentage of Livin that could be prevented from degradation in the presence of specific caspase -8 and -9 inhibitors respectively.

(D)

(E)
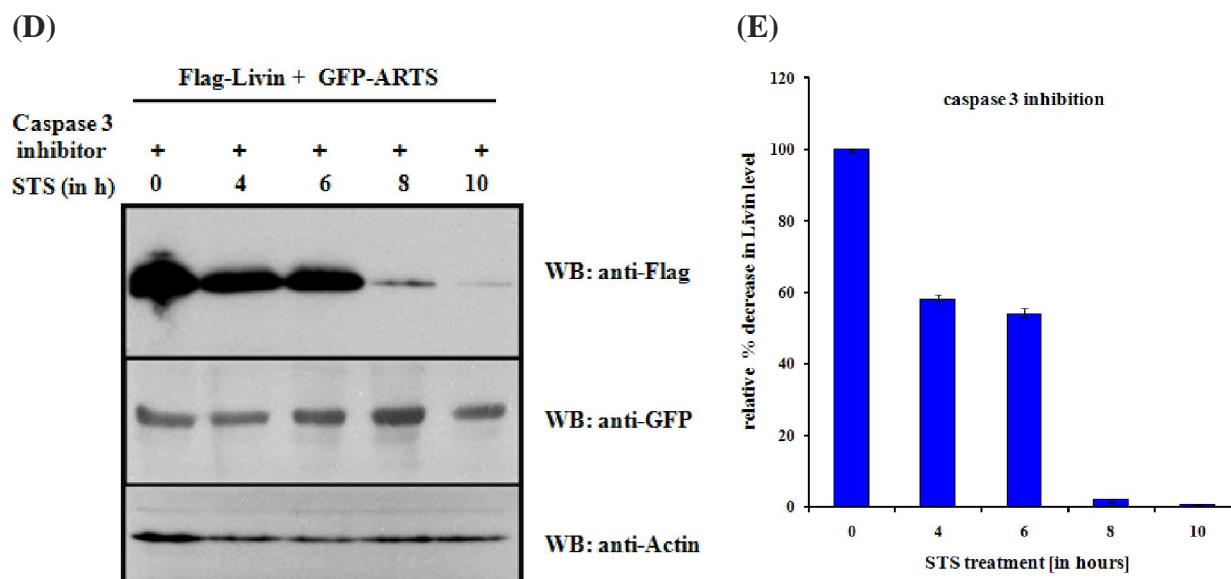
***Figure 5 cont.* Inhibition of caspase 3 mediated Livin degradation in ARTS apoptosis. (D)** Results obtained when Flag/Livin and ARTS co-transfected cells were cultured in the presence of caspase 3 inhibitor and induced to undergo apoptosis for 4 – 10 h following treatment with STS (0 h is untreated control). **(E)** Bar diagram showing the relative percentage of Livin levels with respect to control, when caspase 3 inhibitor is added.

3.1.5 Increased active caspase 7 (20 kDa) levels in apoptotic cell co-expressing ARTS and Livin

Since no specific inhibitor of caspase 7 is available, the active caspase 7 (p20) levels were examined in the COS7 cells transfected with Flag-Livin (control) or Flag-Livin plus GFP-ARTS and treated with STS or left as untreated controls. Results inferred from figure 6 indicate that active caspase 7 levels were up regulated in the apoptotic cells co-transfected with GFP-ARTS and Flag-Livin compared to control cells (Livin or Livin + STS). No active caspase 7 was found in Flag-Livin transfected non-apoptotic cells. The direct participation of caspase 7 in the cleavage of Livin could not be confirmed due to the absence of caspase 7 specific inhibitor. Nevertheless, caspase 7 may be the potential candidate of Livin cleavage in accord with its established role in the cleavage of Livin at $DHVD_{(52)}$ position (NACHMIAS *et al.*, 2003; NACHMIAS *et al.*, 2007).

Role of caspases as the terminators of cellular structural and functional units during apoptosis is well established. However, function of V-ATPases in apoptosis; whether V-ATPase complex structure is demolished by caspases, which subunits are targeted, remain unknown and an open question to be explored. In this direction, I have identified an essential subunit (*d*) of V-ATPase as a new substract of active caspase 3, as described below in section 3.1.6.

(A)
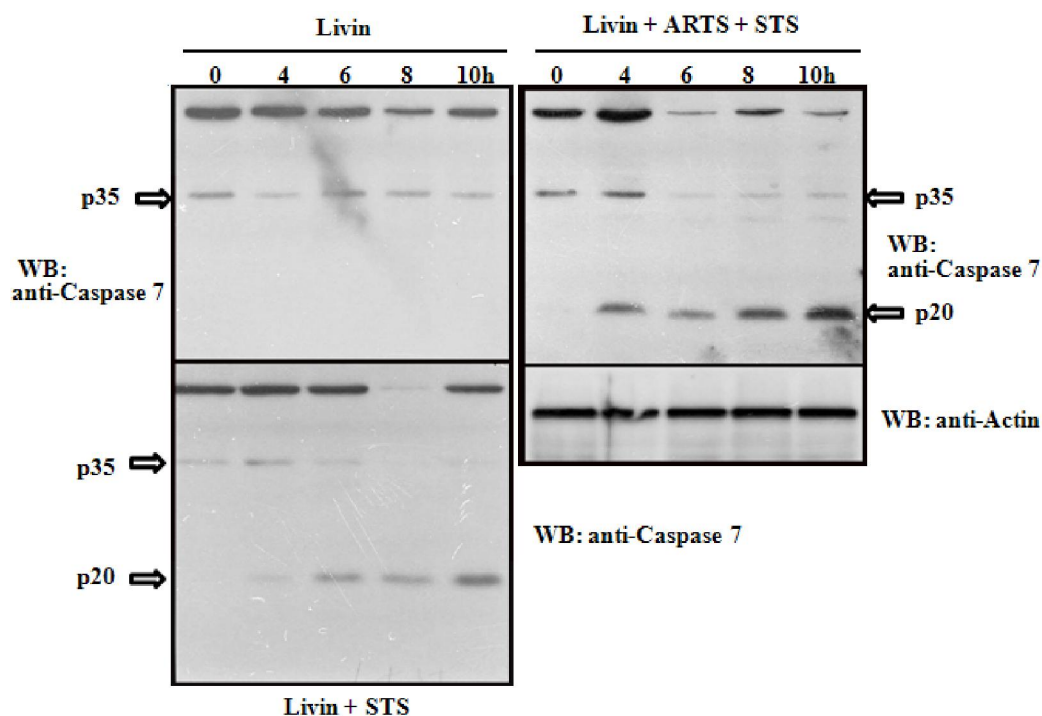
(B)
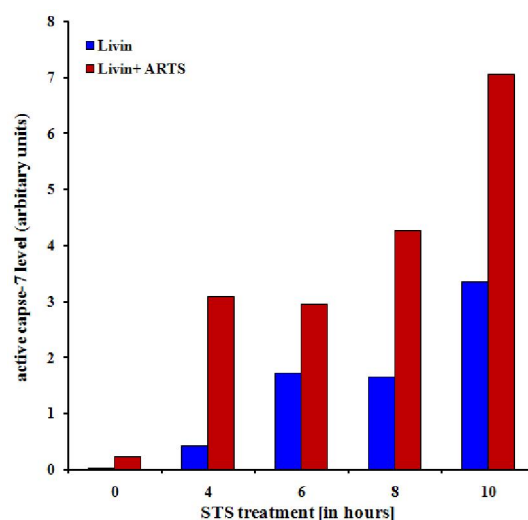
Figure 6. **Active Caspase 7 levels were up regulated during Livin/ARTS-promoted apoptosis.** (**A**) COS7 cells were transfected with Flag/Livin or Flag/Livin plus GFP/ARTS and samples were collected at 4 - 10 h after induction of apoptosis with STS (0 h is STS untreated control). Equal amount of proteins were loaded and probed with anti-caspase 7 antibody. (**B**) Graphical representation of active caspase 7 levels (p20) in ARTS and Livin co-transfected or Livin alone (control) transfected apoptotic cells.

3.1.6 Identification of subunit *d* of V-ATPase as caspase 3 target

V-ATPases do play vital role to maintain various physiological processes and regulate a delicate balance of pH (FORGAC, 2007; KANE, 2007; GRÜBER and MARSHANSKY, 2008). Acidification of cells during apoptosis is a general feature, which does occur in response to both extrinsic and intrinsic pathways of apoptosis and is believed to play critical role in the initiation

of apoptosis and several anti-apoptotic agents act via alkalization of cytoplasmic pH (GOTTLIEB *et al.*, 1995; GOTTLIEB *et al.*, 1996; LAGADIC-GOSSMANN *et al.*, 2004).

Owing to the importance of V-ATPase function in maintaining delicate balance between cell survival and death (apoptosis), I tried to identify the potential targets of caspases in this multi-subunit complex (V_1V_O ATPase). In the search of caspase 3 cleavage targets in the vacuolar ATPase, I used *in vitro* digestion screening to test various subunits of this multi-complex protein. Subunit *d* (THAKER *et al.*, 2007) and subunit C (ARMBRÜSTER *et al.*, 2004; ARMBRÜSTER *et al.*, 2005) are the two very important subunits of V_1V_O ATPases which are involved in the coupling of ATP cleavage to proton pumping as well as in the reversible disassembly, a physiological regulatory processes of V_1V_O ATPase (ARMBRÜSTER *et al.*, 2005; OWEGI *et al.*, 2006). Within V_1V_O ATPase, both subunit *d* and subunit C are believed to be exposed onto the surface which makes them readily accessible to mild proteolysis in clathrin coated vesicles (ADACHI *et al.*, 1990; VITAVSKA *et al.*, 2003; ARMBRÜSTER *et al.*, 2005; HONG-HERMESDORF *et al.*, 2006). Subunit *d* also remains associated with catalytic A subunit (SHAO and FORGAC, 2004; THAKER *et al.*, 2009) and stalk subunit G (RISHIKESAN *et al.*, 2009) forming a structural and mechanistic interface between V_1 and V_O domains (THAKER *et al.*, 2009). Such kind of arrangements within the whole complex make subunit *d* and subunit C an attractive target for caspases to destabilize the whole complex, which can lead to loss of cellular pH homeostasis and initiation of cell catastrophe by apoptosis.

Recombinantly produced and purified subunit His_3-*d* (Chapter 3.2) (THAKER *et al.*, 2007) and subunit His_3-C (ARMBRÜSTER *et al.*, 2005) (kindly provided by Ms Ying LI, former FYP student in our lab) of yeast V-ATPase were used to test their susceptibility to caspase 3 enzyme activity (section 2.2.10). Equal amounts of proteins were digested by caspase 3 followed by His-pull down on Ni^{2+}-NTA column and subsequently western blotting of the eluant was done with AP-conjugated Ni^{2+}-NTA as described in section 2.2.10. The results obtained showed no cleavage products of subunit *d* or subunit C (Figure 7). Interestingly, the densitometric analysis of the western bands revealed that protein quantity in subunit *d* dropped by almost 40 percent (Figure 7B-C), which was also observed on the ponceau stained membrane (Figure 7A).

(A)

(B)

(C)
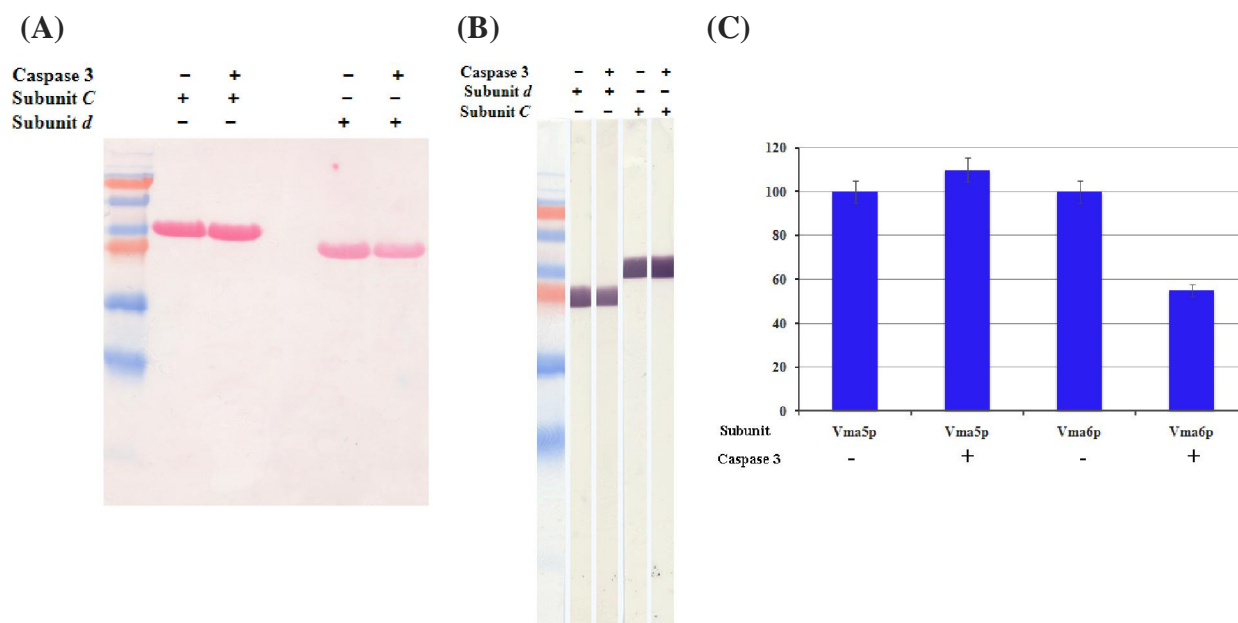
Figure 7. **Caspase 3 mediated cleavage of subunit *d*.** Equal amounts of recombinantly produced and purified subunit *d* and subunit C was treated with caspase 3 or left untreated as control for three h at 37 ℃, respectively, followed by His-pull down on Ni^{2+}-NTA column, western transfer onto nitro-cellulose membrane and ponceau staining **(A)** and membrane was probed with AP-conjugated Ni^{2+}-NTA for His-detection (**B**). (**C**) The densitometric quantitation (Quantity One software; Bio-Rad) of proteins after caspase 3 digestion with standard deviation shown from two independent experiments.

Since no cleaved subunit *d* fragment could be detected during His-pull down experiments as shown in figure 7 the digestion was repeated under identical conditions where subunit *d* was digested for 3 h and 10 h respectively at 37 ℃ along with a negative control where no caspase 3 was added. In contrast to making His-pull down, reaction was stopped by the addition of 5x SDS loading buffer and immediately loaded onto the 17% SDS gel and visualized by Coomassie staining as shown in figure 8A. Similarly, under identical conditions subunit C was digested for 10 h and the reaction mixture was loaded onto a SDS gel as described for subunit *d* (Figure 8A). Digestion of subunit *d* (Figure 8A) showed a prominent cleaved band running below the native band (marked as cleaved subunit *d* in lane 3 – 4), whereas no digestion or degradation of protein was observed in control experiment (Figure 8, *lane 2*). In contrast, no cleavage of subunit C could be observed. These results indicate that subunit *d* is the target of caspase 3.

(A)

(B)
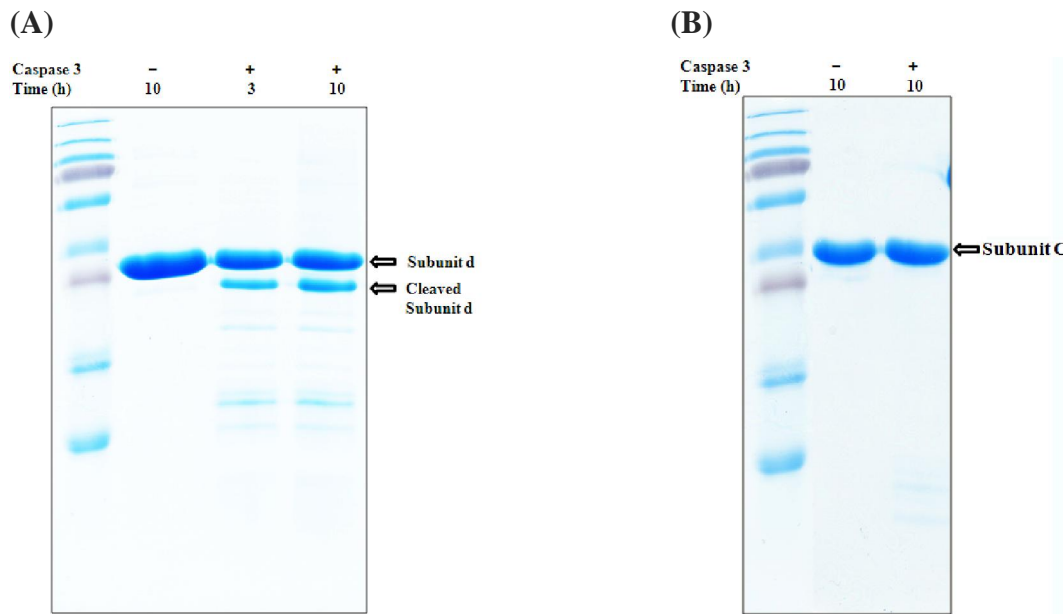
Figure 8. **Caspase 3 mediated cleavage of vacuolar ATPase subunit *d* and subunit *C*.** (**A**) Equal amounts of pure His$_3$-subunit *d* protein were digested with caspase 3 for 3 and 10 h at 37 ℃ (*lane 3,4*) or left untreated (*lane 2*) as negative control. Reaction was terminated with the addition of SDS buffer and samples were loaded onto 17 % SDS gel and run at a constant current of 10 - 15 mA. Gel was stained with Coomassie stain for 10 min and then destained. (**B**) Equal amounts of His-subunit *C* were digested with caspase 3 under identical conditions as described for subunit *d* (*lane 3*) or left untreated as negative control (*lane 2*).

To further characterize the caspase 3 cleavage site in subunit *d*, N-terminal protein sequencing was done at the Protein and Proteomics Centre (National University of Singapore). The protein was digested for 10 h at 37℃ and transferred onto a PVDF membrane at 70 V for 1 h as described in section 2.2.10. Membrane was stained with Coomassie followed by thorough destaining and drying. Results indicate that protein was cleaved at D50 from the NH$_2$-terminus at the sequence ^{47}**SSTD Y**^{51} (Figure 9). Caspases do cleave their targets at the tetra-peptide sequences after aspartic acid residue at P4 position (EARNSHAW *et al.*, 1999) and caspase 3 does recognize the classical motif DEVD in most substrates with strong tendency of aspartic acid residue at P4 position (EARNSHAW *et al.*, 1999). However, caspase 3 also recognizes motifs with varying sequences known as non-canonical sites in diverse cellular substrates (KIPP *et al.*, 2000). In the search of identified subunit *d* caspase 3 motif, it was found that this motif is also present in the Geminin protein, which is involved in the regulation of cell cycle and differentiation, where it has been shown to be used as caspase 3 cleavage site (ROUKOS *et al.*, 2007). In subunit *d*, the identified motif, SSTD is therefore a non-canonical caspase 3 site.
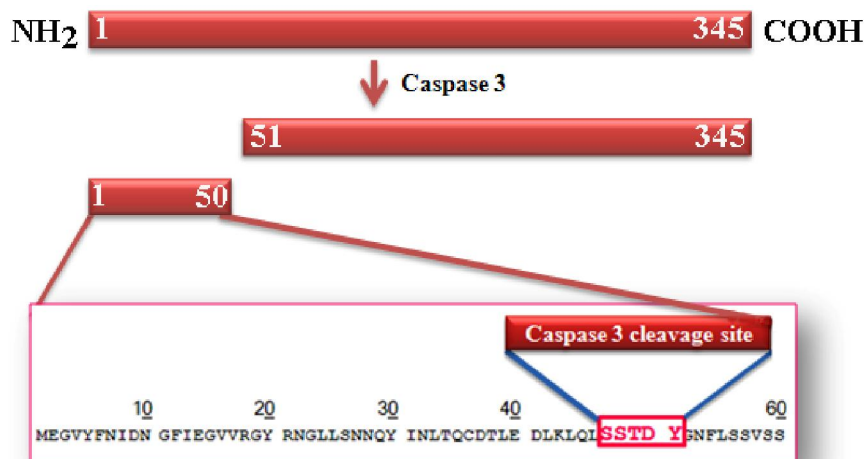
***Figure 9.* Schematic representation of the caspase 3 cleavage site in subunit *d*.** N-terminal sequencing of caspase 3 cleaved subunit *d* showed that recognition motif is present at D50 from N-terminus and the actual sequence was formed by 47 **SSTD** 50 residues, which was recognized and cleaved by caspase 3 as shown in the figure. Sequence of whole N-terminal fragment is shown (BAUERLE *et al.*, 1993; THAKER *et al.*, 2007).

3.2   Structural and biochemical characterization of subunit *d* of the vacuolar ATPase of *Saccharomyces cerevisiae*
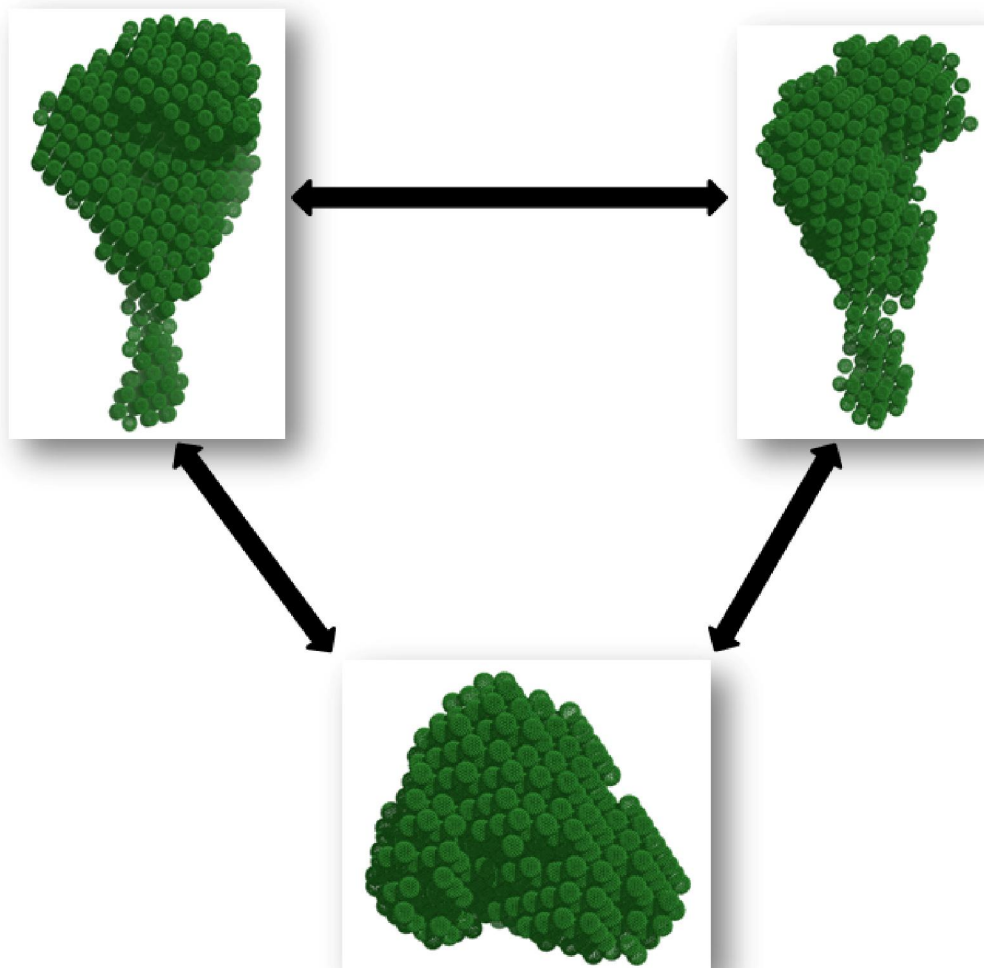
Vacuolar ATPases are composed of several subunits which together form V_1 (subunits A-H) and V_O (subunits *a,d,c,c',c''*) domains of the fully functional V_1V_O complex (THAKER *et al.*, 2007; GRÜBER and MARSHANSKY, 2008). Subunit *d* (BAUERLE *et al.*, 1993; ZHANG *et al.*, 1994; NISHI *et al.*, 2003; SMITH *et al.*, 2005) is part of membrane embedded V_O, the proton translocating domain. It is encoded by a single gene *VMA6* as the only isoform, known as Vma6p (BAUERLE *et al.*, 1993) with obvious absence of transmembrane anchors (BAUERLE *et al.*, 1993). This poorly characterized subunit remains firmly attached to V_O in functional reversibly disassembled states (KANE, 1995) and can be removed from V_O upon harsh treatments alone (5 M urea or sodium carbonate at pH 11.5) (BAUERLE *et al.*, 1993) suggesting that subunit *d* is a *bona fide* part of V_O domain. However, precise contribution of subunit *d* to V_1V_O ATPase function is predominantly unclear, although it has been suggested to be essential for the coupling of ATP hydrolysis and proton transport and functional assembly of V_1 and V_O (NISHI *et al.*, 2003; OWEGI *et al.*, 2006). Therefore, this subunit had been characterized using various biophysical techniques giving important structural and biochemical insights.

3.2.1 Cloning, production, optimization and purification of subunit *d* (Vma6p

VMA6, the subunit *d* of *Saccharomyces cerevisiae,* was successfully cloned in modified pET9-d1 expression vector (GRÜBER *et al.*, 2002) as described in section 2.2.2.3. Yeast genomic DNA was used as template to PCR amplify the *VMA6* gene and clone into pET-9d1 expression vector as described in detail under 2.2.2.3. Since the amino acid sequence of subunit *d* contains six cysteine residues, expression was carried in routinely used host BL21 (DE3) as well as Rosetta-gami[TM] 2 (DE3) *E. coli* strains. Rosetta-gami[TM] 2 (DE3) carries additional combined features of Rosetta 2 and Origami 2, containing rare t-RNA codons and enhanced disulphide formation capability, respectively. Various optimization and screening tests revealed that the protein is produced in high quantity and quality, when expressed in Rosetta-gami[TM]2 cells at 30 °C for 3 h with 1 mM IPTG (0.1 – 1 mM IPTG concentration was used to optimize the expression level). Furthermore, a comparative study was done to determine the production and solubility rates of subunit *d* in BL21 (DE3) and Rosetta-gami[TM]2 (DE3) *E. coli* strains, which showed that higher quantities of native folded protein can be produced in Rosetta-gami[TM]2 cells (Figure 10).
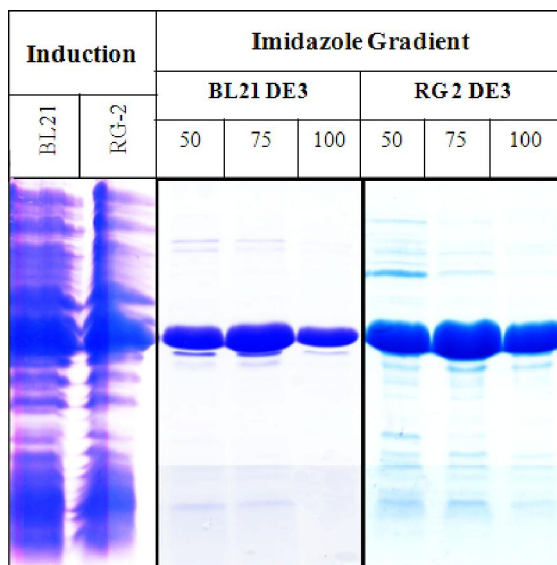
***Figure 10*. Comparative analysis of the His$_3$-*d* production rate in BL21 and Rosetta- gami^{TM} 2 cells.** Induction and isolation of protein in the soluble fraction from host BL21 DE3 and Rosetta-gami^{TM} 2 (DE3) is shown, respectively. Equal amounts of cells induced under identical conditions were analyzed. 50-100 mM imidazole fractions of Ni^{2+}-NTA are shown on a 17% SDS gel.

Recombinant subunit *d* protein was purified as described under section 2.2.12.1. In the first step of purification, His$_3$-*d* protein was enriched by Ni^{2+}-NTA affinity chromatography and bound protein was eluted with 0 – 200 mM imidazole gradient (Figure 11A). Distinct bands of subunit *d* protein were identified in the fractions 75 mM to 125 mM on SDS gel (Figure 11A). To remove residual minor contaminations and imidazole, protein was additionally applied onto an anion-exchange column RESOURCE^{TM} Q. Prior to injecting on the column, identified fractions were diluted 10 times in 50 mM Tris/HCl, pH 7.5 buffer to a final NaCl concentration of 50 mM for effective binding to the column material. Elution was done with a linear gradient of buffer A (50 mM Tris/HCl, 50 mM NaCl, pH 7.5) and buffer B (50 mM Tris/HCl, 1 M NaCl, pH 7.5). A single distinct and sharp peak around 28 – 33% of buffer B gradient (Figure 11B) contained His$_3$-subunit *d*/Vma6p. Peak half volume, as shown in figure 11B, was pooled, concentrated and subsequently applied onto an SDS gel (insert; Figure 11B) to check the purity and quantity of the recombinant protein. Analysis of the isolated protein by SDS polyacrylamide gel and MALDI mass spectrometry revealed the high purity of this protein, and confirmed the sequence-based predicted mass of 40.6 kDa, including the His$_3$-tag (THAKER *et al.*, 2007).

(A)   **(B)**
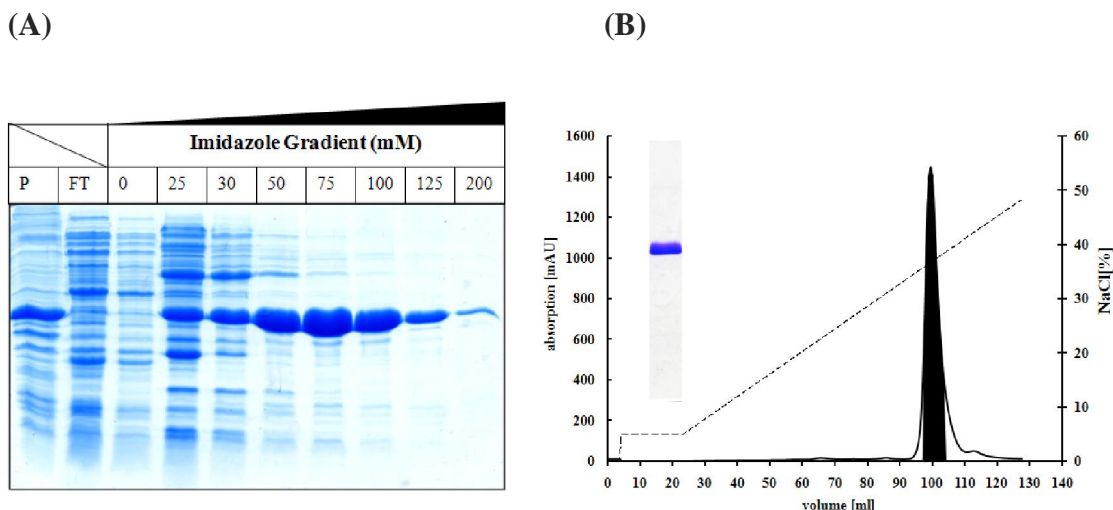
***Figure 11.* Purification of subunit *d.* (A)** Ni^{2+}-NTA purification of His$_3$-subunit *d*/Vma6p (2 g of Rosetta-gami^{TM} 2 cells) in 50 mM Tris/HCl, 500 mM NaCl, pH 7.5 buffer, elution was done with 0 - 200 mM imidazole. 15 μl of sample was applied on a 17% SDS gel from each fraction. (**B**) Purification of protein by a linear gradient of NaCl on anion exchange column Resource Q (6 ml). 50 - 100 mM Ni^{2+}-NTA fractions were pooled and applied at a constant flow rate of 2 ml/min in buffer A (50 mM Tris/HCl, 50 mM NaCl, pH 7.5). Insert shows 1 μl of anion exchange purified protein on 17 % SDS gel. (P=Pellet (insoluble fraction), FT=Flowthrough (unbound fraction)) (THAKER *et al.*, 2007).

3.2.2   Secondary structure and folding analysis of subunit *d*

3.2.2.1 One dimensional NMR analysis

One dimensional NMR spectrum of subunit *d* recorded in 25 mM phosphate buffer (pH 6.8) showed that the protein was nicely folded, as concluded from the characteristic pattern of peaks and good dispersion of resonance lines amide protons (6 to 10 ppm), -protons (3.5 to 5 ppm), and uphill shifted methyl protons (-0.5 to 1.0 ppm) (PAGE *et al.*, 2005) (Figure 12).
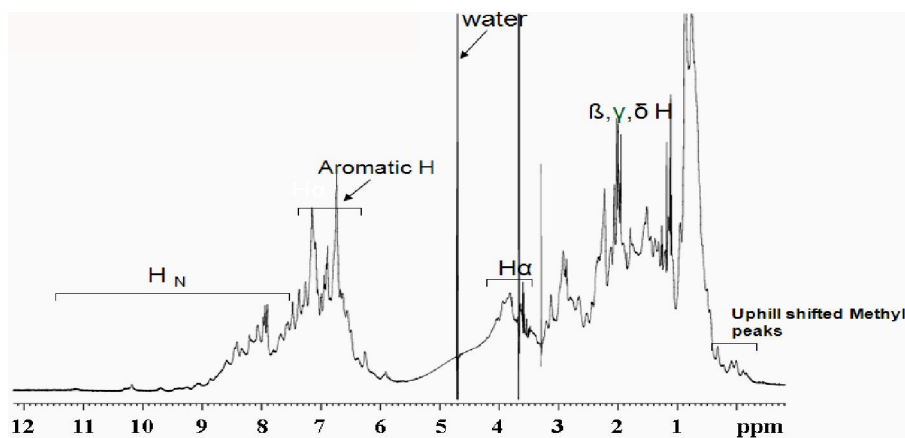
Figure 12. One dimensional NMR spectrum of subunit *d* recorded at 288 K in 25 mM PO$_4$ buffer (pH 6.8) on Bruker Avance 600 MHz machine. Nice dispersion of resonance peaks in HN region, -protons and uphill shifted methyl peaks are the characteristics of natively folded protein. Strong peaks at 4.7 ppm represents water signal (THAKER *et al.*, 2007).

3.2.2.2 CD spectroscopy of subunit *d*

2 mg/ml of pure subunit *d* protein was used to record the CD spectrum from 190 – 260 nm (Figure 13A) as described above in section 2.2.14. The minima of at 222 and 208 nm and the maximum at 192 nm indicated the presence of -helical secondary structures in the protein. Several computer based methods were used to analyze the raw data from measured CD spectrum (PROVENCHER and GLÖCKNER, 1981; ANDRADE *et al.*, 1993; SREERAMA and WOODY, 2000; PER *et al.*, 2001). The calculated average secondary structure content was 58% -helix and 36% random coil. This result is in agreement with the predicted secondary structure calculated from the primary amino acid sequence analysis, using online software package at PSIPRED server (http://bioinf.cs.ucl.ac.uk/psipred/) (MCGUFFIN *et al.*, 2000) (Figure 13B). The molar ellipticity values at 208 nm and at 222 nm were 23621.5 deg cm^2/dmol and 23658.3 deg cm^2/dmol, respectively, in a ratio of about 1.0. Since non-interacting helices typically give ratios of around 0.8, whereby interacting ones have ratios close to 1.0, the CD spectrum indicated that many of the residues in subunit *d* were in -helical interactions (THAKER *et al.*, 2007).
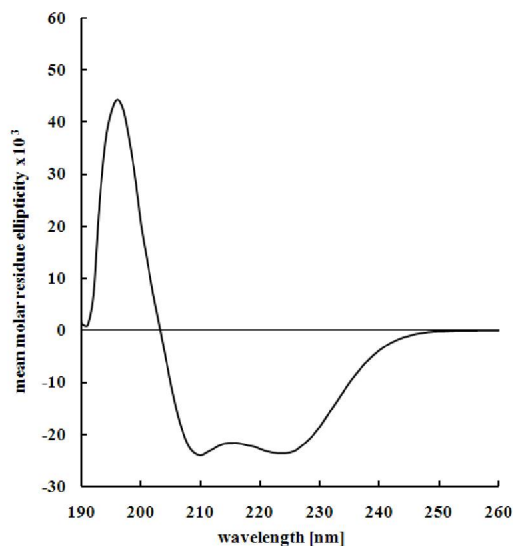
(A) **(B)**
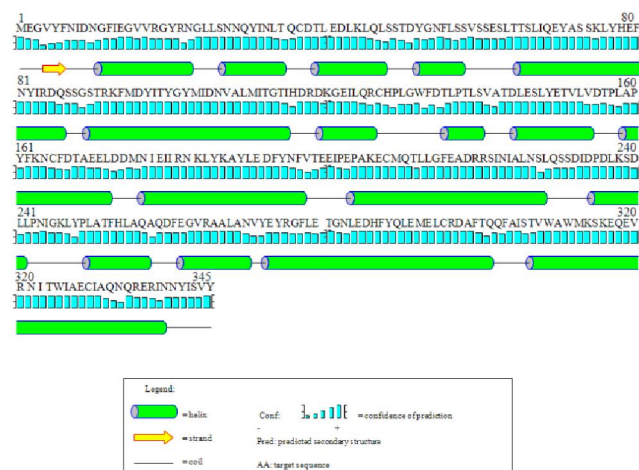
Figure 13. **CD spectroscopy of subunit *d*. (A)** Subunit *d* (wt, 1-345 aa) CD spectrum measured at 18 °C in a Hellma quartz cuvette (60 μl volume) on Chirascan spectropolarimeter (Applied Photophysics) at a step resolution of 1 nm in the far UV range of the spectrum (THAKER *et al.*, 2007) and **(B)** predicted secondary structure by online PSIPRED software, which uses a position specific scoring matrices generated by PSI-BLAST for secondary structure calculation by a two stage neural network algorithm (MCGUFFIN *et al.*, 2000).

3.2.3 Determination of native molecular weight and overall dimensions of subunit *d*

3.2.3.1 Gel filtration of subunit *d*

To determine the native molecular mass and overall shape of subunit *d,* a calibration curve of *Kav* values, a representative of size and elution volume factors, was generated for the

proteins of known molecular mass as described in section 2.2.15. Subunit *d* under identical conditions was eluted between BSA and ovalbumin as shown in figure 14A. Calculated *Kav* values of standard proteins were plotted against logarithm of respective molecular masses as plotted in figure 15B. Comparison of the Kav for *d* versus standards suggested a native molecular mass of approximately 47 ± 3 kDa (Figure 14) (THAKER *et al.*, 2007).

(A)
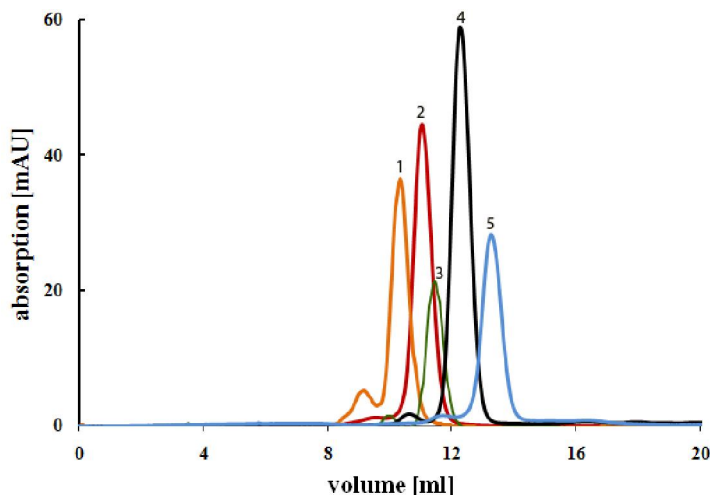
(B)
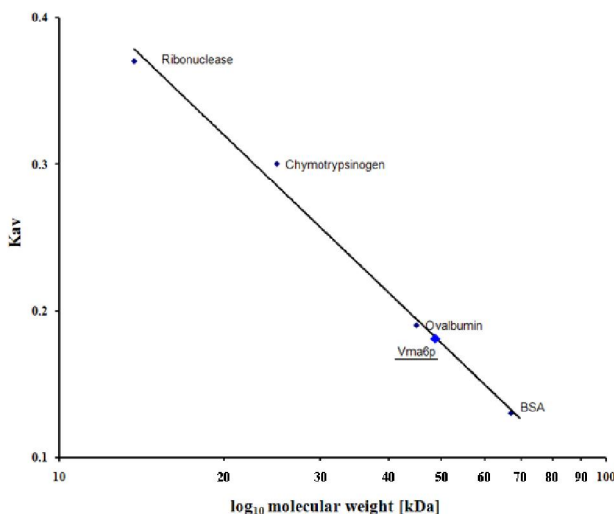
Figure 14. **Native molecular mass determination of subunit *d*. (A)** Elution profile of a set of standard proteins used as molecular size markers were BSA (67 kDa; *peak 1*), ovalbumin (45 kDa; *peak 3*), - chymotrypsinogen A (25 kDa, *peak 4*) and ribonuclease A (13.7 kDa; *peak 5*) against subunit *d* (*peak 2*) on a Superdex S75 (10/30) gel filtration column. **(B)** Elution profile and column dimensions were used to determine the *Kav* value as described in section 2.2.15. The *Kav* value of subunit *d* (Vma6p) is indicated by blue diamond (THAKER *et al.*, 2007).

3.2.3.2 Small angle X-ray scattering data of subunit *d*

SAXS pattern from solution of subunit *d* was recorded and processed as described under section 2.2.18. Final composite curves are shown in figure 15. The initial portion of the

scattering curve in the Guinier presentation is well approximated by a straight line (insert Figure 15A), suggesting that the protein is monodisperse. The radius of gyration R_g and the maximum dimension D_{max} of subunit d are 2.74 ± 0.01 nm and 11 nm, respectively, revealing that d is an elongated particle in solution and monomeric by comparison with the BSA standard at protein concentrations of 0.9 mg/ml and 12.7 mg/ml for subunit d and 3 mg/ml for BSA. Comparison of scattering curves of subunit d with standard protein BSA yields an approximate molecular mass of 46 ± 4 kDa in concordance with the gel filtration derived native molecular mass (section 3.2.3.1) (THAKER *et al.*, 2007). Qualitative analysis of the distance distribution function suggests that d consists of a major part yielding a principal maximum in the distance distribution function, p(r) at around 3.1 nm (Figure 15B) whereas the separated protuberance domain giving rise to a shoulder from 6.5 nm to 11 ± 0.2 nm.
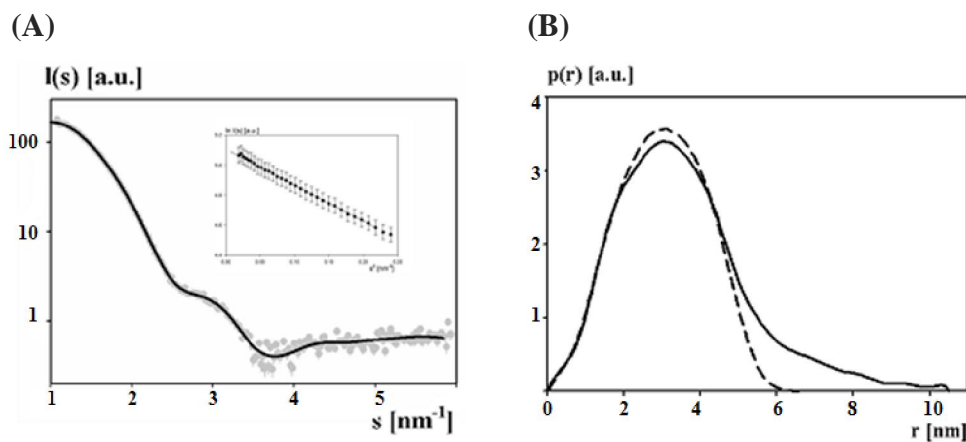
Figure 15. **SAXS data of subunit *d*.** X-ray solution scattering (SAXS) composite curves of subunit *d* recorded at 0.8 and 12 mg/ml concentrations in 50 mM Tris/HCl (pH 7.5), 340 mM NaCl either in the presence or absence of 1 mM DTT. The experimental SAXS curve from subunit *d* (full circles with error bars); scattering from typical *ab initio* model of subunit *d* (solid line) computed by the program GASBOR. Insert shows Guinier plot with linear fit (**A**). (**B**) Distance distribution function curves of subunit *d* (full line) and high resolution subunit C of *T. Thermophilus* A_1A_O ATP synthase (pdb 1r5z, dashed lines), respectively (THAKER *et al.*, 2007).

3.2.4 Low resolution shape and domain structure of subunit *d* (Vma6p)

The gross structure of subunit *d* was restored *ab initio* from the scattering pattern in figure 15A using the shape determination program DAMMIN (SVERGUN, 1992; SVERGUN, 1994; SVERGUN, 1999) and the dummy residues modeling program GASBOR (SVERGUN *et al.*, 2001) as described in section 2.2.18. The two approaches yielded similar results. In the following results, the models obtained with GASBOR are presented, which yield good fits to the experimental data in the entire scattering range (a typical fit displayed in figure 15A with a discrepancy = 2.32). Ten independent reconstructions yielded a reproducible structure which is displayed in figure 16.

(A) **(B)** **(C)**
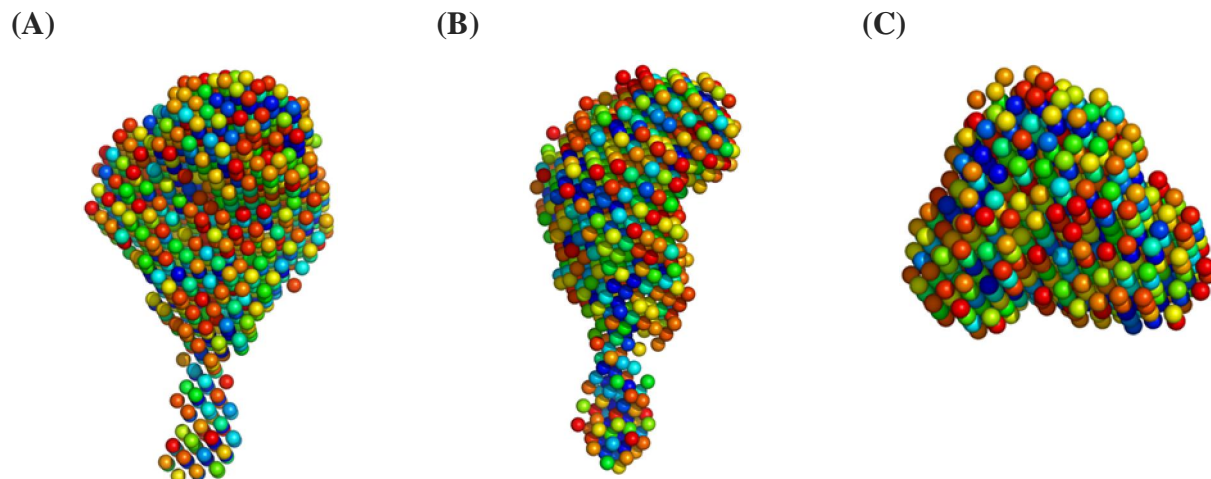
Figure 16. **Low resolution structure of subunit *d*.** **(A)** Low resolution shape of subunit *d* determined from the SAXS data, collected at 0.8 and 12.7 mg/ml, using shape determination programs DAMMIN and GASBOR as described in section 2.2.18. The structures in **(B)** and **(C)** are rotated by 90º along x- and y-axis respectively (THAKER *et al.*, 2007).

Subunit *d* appears as a boxing glove-shaped molecule with two distinct domains. The major domain has dimensions of about 6.5 x 5.0 nm, and in the side view 6.5 x 4.5 nm, whereby the protuberance is about 3.5 nm in length and 2.0 nm in width (THAKER *et al.*, 2007). To investigate the location within the V_O subcomplex, the shape of subunit *d* was superimposed onto previously solved low resolution structure of V_O from bovine brain clathrin-coated vesicles determined by single particle analysis of negatively stained electron micrographs (WILKENS and FORGAC, 2001). Analysis revealed remarkable similarities to the elongated mass located above the cytoplasmic site of membrane-embedded V_O domain of the bovine brain clathrin-coated vesicles (Figure 17) (THAKER *et al.*, 2007).

(A) **(B)** **(C)**
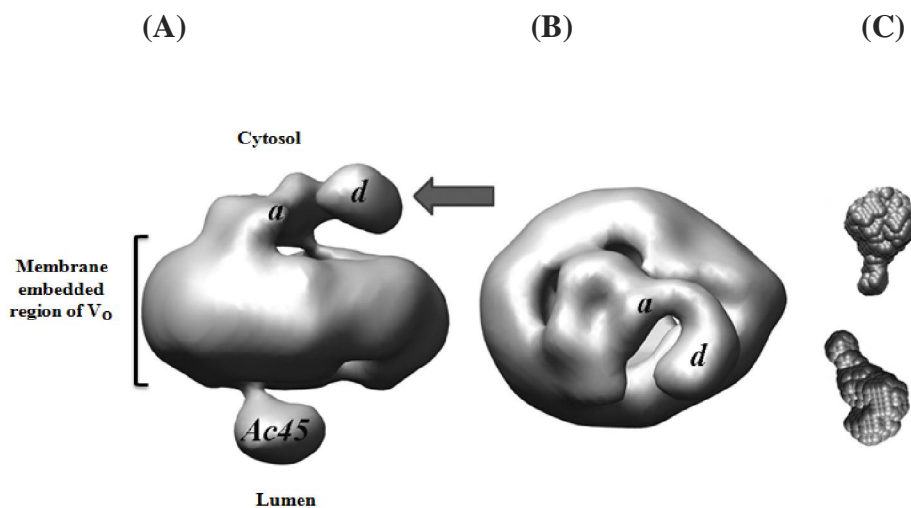
Figure 17. **Subunit *d* in the context of V_O domain of V-ATPase**. Localization of subunit *d* shape onto previously solved 3D electron structure of V_O domain (WILKENS and FORGAC, 2001) from bovine brain clathrin-coated vesicles determined by single particle analysis of negatively stained micrographs (A, B). A clear assignment of previously unknown structure (arrow) can now be made to subunit *d* determined low resolution shape (C)(THAKER *et al.*, 2007).

3.2.5 Investigation of disulphide bond formation in subunit *d*

Vma6p (subunit *d*) of *Saccharomyces cerevisiae* V-ATPase has six cysteine residues in its primary amino acid sequence (Figure 19). Analysis and alignment of the sequence with related subunit *d* from higher eukaryotes showed high level of sequence conservation, with a particular interest of three cysteine residues ($Cys_{36,127,329}$), which were found to be conserved among all eukaryotic subunit *d* described so far (Figure 19) (THAKER *et al.*, 2007).

3.2.5.1 Examination of disulphide formation by cross-linking and mutagenesis

In order to gain insight into the disulphide bonds of subunit *d*, the protein was treated with $CuCl_2$, a known zero length thiol cross-linker (OGILVIE *et al.*, 1997; SCHULENBERG and CAPALDI, 1999; COSKUN *et al.*, 2002; COSKUN *et al.*, 2004), to monitor the formation of cross-links between neighboring cysteine residues on SDS gel under reducing and non-reducing conditions as described in section 2.2.17. When applied onto a polyacrylamide gel, the disulphide containing proteins migrated faster than their respective reduced correlatives, which revealed that the disulphide containing form is more compact (SVERGUN *et al.*, 2000) (Figure 18). However, the non-reduced sample migrated as diffused band (Figure 18; *lane 2*). Reduction of cysteine residues with dithiothreitol in non-oxidized samples produced a defined band at expected position (Figure 18; *lane 3*). When subunit *d* was supplemented with 100 µM $CuCl_2$, the protein migrated further down (Figure 18; *lane 2*) and reduction with DTT produced a defined band again (Figure 18, *lane 4*). Changes in the migration behavior of subunit *d* upon oxidation and reduction gave initial intimation about the possible disulphide bond formation in subunit *d*. Reduced migration of DTT treated protein can be either imparted to larger hydrodynamic volume or alternatively to a lower net negative charge (THAKER *et al.*, 2007).
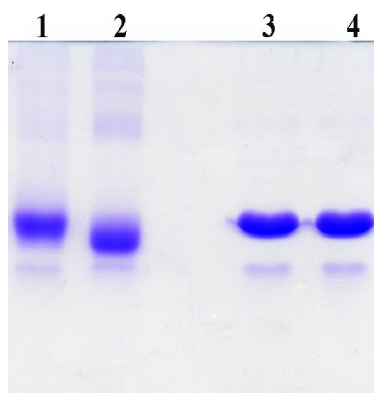
Figure 18. Migration pattern of subunit *d* on 17% SDS gel on treatment with zero length cross-linker $CuCl_2$ in non-reduced (*lane 2*) and reduced (*lane 4*) environment. Native non-oxidized non reduced (*lane 1*) and non-oxidized reduced (*lane 3*) are also shown. (THAKER *et al.*, 2007).

```
S.cerevisiae    (1)  ---------MEGVYFNIDNGFIEGVVRGYRNGLLSNNQYINLTQCDTLED
D. discoideum   (1)  MGLFGGRKHGGLFTFNKDDGYLEAILRGFKKGILSRADYNNLCQCDNLED
    M. sexta    (1)  ---------MKGCIFNIDAGYLEGLCRGFKCGILKQSDYLNLVQCETLED
    N. crassa   (1)  ---------MEGLLFNVNNGYIEGIVRGYRNSLLTSTNYTNMTQCESIDD
    Consensus   (1)           MEGLIFNIDNGYIEGIVRGFKNGILSNSDYINLTQCDTLED
                     51                                              100
S.cerevisiae   (42)  LKLQLSSTDYGNFLSSVSSESLTTSLIQEYASSKLYHEFNYIRDQSSGST
D. discoideum  (51)  MKMHFISTDYGDFLAGEPSP-IHTTTIAEKATGKLVSEFNHIRNQAVEPL
    M. sexta   (42)  LKLHLQGTDYGTFLANEPSP-LSVSTIDDKLREKLVIEFQHLRNHSVEPL
    N. crassa  (42)  LKLQLG-PAYGDFLASLPPK-PSTSALAAKTTDKLVSEFRYVRANAAGSL
    Consensus  (51)  LKLQL STDYGDFLASEPSP LSTSTIAEKATDKLVSEFNHIRNQAVGSL
                     101                                             150
S.cerevisiae   (92)  RKFMDYITYGYMIDNVALMITGTIHDRDKGEILQRCHPLGWFDTLPTLSV
D. discoideum (100)  STFMDFISYGYMIDNVVLLITGTLHERDISELVDKCHPLGLFKSMATLSV
    M. sexta   (91)  STFLDFITYSYMIDNIILLITGTLHQRPISELIPKCHPLGSFEQMEAIHV
    N. crassa  (90)  AKFMDYLTYGYMIDNVALLITGTLHERDTRELLERCHPLGWFETMPVLCV
    Consensus (101)  STFMDFITYGYMIDNVALLITGTLHERDISELLDKCHPLGWFETMPTLSV
                     151                                             200
S.cerevisiae  (142)  ATDLESLYETVLVDTPLAPYFKNCFDTAEELDDMNIEIIRNKLYKAYLED
D. discoideum (150)  VHNVADLYNNVLIDTPLAPYIQGCLS-EEDLDEMNNEIIRNTLYKAYLED
    M. sexta  (141)  AATPAELYNAVLVDTPLAPFFVDCIS-EQDLDEMNIEIIRNTLYKAYLEA
    N. crassa (140)  ATNIEELYNSVMIETPLAPYFKSSLS-LQDLDELNIEIVRNTLYKNYLED
    Consensus (151)  ATNIEELYNSVLIDTPLAPYFK CLS EQDLDEMNIEIIRNTLYKAYLED
                     201                                             250
S.cerevisiae  (192)  FYNFVT---EEIPEPAKECMQTLLGFEADRRSINIALNSLQSSDIDPDLK
D. discoideum (199)  FYNYCK----YLGGQTELIMSDILKFEADRRSINITINSFGATELSKDDR
    M. sexta  (190)  FYDFCK----QIGGTTADVMCEILAFEADRRAIIITINSFG-TELSKDDR
    N. crassa (189)  FYHFVNTHPDMAGTPTAEVMSELLEFEADRRAINITLNSFG-TELSKADR
    Consensus (201)  FYNFVK   D IGGPTAEVMSEILAFEADRRAINITINSFGATELSKDDR
                     251                                             300
S.cerevisiae  (239)  SDLLPNIGKLYPLATFHLAQAQDFEGVRAALANVYEYRGFLETG------
D. discoideum (245)  EKLYPSLGLLYPEGTSKLGKAEDVDQVRGILEVYSTYRNFFSDGVNNE--
    M. sexta  (235)  AKLYPRCGKLNPDGLAALARADDYEQVKAVAEYYAEYSALFEGAGNNVGD
    N. crassa (238)  KKLYPNFGQLYPEGTLMLSRADDFEGVRLAVEGVADYKSFFDAAGLGGGP
    Consensus (251)  AKLYPNIGKLYPEGTA LARADDFEQVRAALE YAEYRAFFEAAGNN G
                     301                                             350
S.cerevisiae  (283)  --------------NLEDHFYQLEMELCRDAFTQQFAISTVWAWMKSKEQ
D. discoideum (293)  -------------KSLEDSFFEHEVHLNRMAFEDQYGYGVFYAYIKLREQ
    M. sexta  (285)  -------------KTLEDKFFEHEVNLNVHAFLQQFHFGVFYSYLKLKEQ
    N. crassa (288)  SGPGNMGGGGTEGKSLEDMFYQKEMEISKMAFTRQFTYAIVYAWVKLREQ
    Consensus (301)             KSLED FFQHEMELNRMAFTQQFAYGVVYAWIKLKEQ
                     351                   377
S.cerevisiae  (319)  EVRNITWIAECIAQNQRERINNYISVY
D. discoideum (330)  EIRNIVWIAECISQNMKQKMNQYIPIF
    M. sexta  (322)  ECRNIVWISECVAQKHRAKIDNYIPIF
    N. crassa (338)  EIRNITWIAECIAQNQKERINNYISVF
    Consensus (351)  EIRNIVWIAECIAQNQKEKINNYISIF
```

Figure 19. **Alignment of subunit *d* primary sequence from *S. cerevisiae, D. discoideum, M. sexta, and N. crassa.*** Conserved cysteine residues are highlighted in blue foreground, non-conserved cysteine residues are shown in bright green foreground and partially conserved cysteine in light green. Vector NTI advance 10 (Invitrogen) software was used for the sequence analysis and alignment using AlignX algorithm (THAKER *et al.*, 2007).

3.2.5.2 Characterization of cysteine residues in disulphide bond formation by tryptic digestion and matrix-assisted laser desorption/ionization mass spectroscopy

To identify and distinguish the cysteine residues involved in disulphide bond formation, a combination of tryptic digestion and MALDI-TOF analysis was used. Protein was treated with thiol reactive TMR (Tetra Methyl Rhodamine, 486.91 Da) or less bulky, NEM (N-ethyl Meleimide, 125.13 Da) dyes to label the surface or the more buried free cysteine residues, respectively, as described in section 2.2.17.2. Figure 20 shows a UV scanned SDS polyacrylamide gel picture of non-reduced TMR (*lane 1*) and NEM (*lane 2*) labeled subunit *d*, respectively.
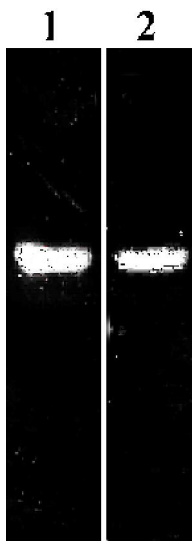
Figure 20. **Labeling of free cysteine residues**. UV fluorescence gel of TMR (*lane 1*) or NEM (*lane 2*) labeled subunit *d* used to characterize the cysteines of subunit *d* by tryptic digestion and MALDI-TOF peptide fingerprinting as described in section 2.2.17.2.

The bands of the TMR-labeled subunit *d*, and Cu^{2+}- and DTT-treated protein respectively, were cut out for in-gel tryptic digestion and MALDI-TOF analysis. Using a variety of available software packages for mass fingerprinting, 32 peptides covering 72% of the subunit *d* sequence were identified. As summarized for proteins larger than 900 Da in table 3, the four TMR-labeled proteins $_{164}$NCFDTAEELDDMNIEIIR$_{181}$, $_{206}$ECMQTLLGFEADR$_{218}$, $_{206}$ECMQTLLGFEADRR$_{219}$ and $_{277}$GFLETGNLEDHFYQLEMELCR$_{297}$ could be determined, indicating that the Cys residues 165, 207 and 296 are accessible in the protein. No bound fluorophor could be detected in the peptide $_{121}$GEILQRCHPLGWFDTLPTLSVATDLESLYETVLVDTPLAPYFK$_{163}$. A mass of 4412.96 Da was found and unequivocally identified as a cross-link product, occurring via the peptides $_{19}$GYRNGLLSNNQYINLTQCDTLELK$_{43}$ and $_{322}$NITWIAECIAQNQR$_{335}$, including the Cys_{36} and Cys_{329}. When *d* was supplemented with Cu^{2+} as a zero-length cross-linker, an

additional tryptic fragment of 6971.90 Da was generated, which is formed by the disulphide bridge of the two Cys residues 127 and 165 of the peptide $_{121}$GEILQRCHPLGWFDTLPTL SVATDLESLYETVLVDTPLAPYFKNCFDTAEELDDMNIEIIR$_{181}$ (Table 3). By comparison, no cross-link product but smaller fragments of the N- and C-terminal part of *d* occured in the presence of the reducing agent DTT (THAKER *et al.*, 2007).

To exclude the possibility that Cys$_{36,127,329}$ might not have been labeled in the TMR-treated protein, because of their inaccessibility to the TMR molecule or disulphide cross-link formation during the preparation of the digests for MALDI-TOF experiment, subunit *d* in the absence of DTT was labeled with the small alkylating agent N-ethyl maleimide (section 2.2.17.2), which has been successfully used for characterization of disulphide bond formation in protein folding studies (MEZGHRANI *et al.*, 2001). Similar peptides of the trypsin cleaved, NEM-labeled *d* could be determined as has been obtained with the TMR marked subunit *d*, including the peptides $_{19}$GYRNGLLSNNQYINLTQCDTLELK$_{43}$ and $_{322}$NITWIAECIAQNQR$_{335}$ (Table 3). The main difference between the NEM- and TMR labeled protein was given by the detection of the NEM labeled residue Cys$_{127}$, which became accessible for the smaller maleimide, NEM (THAKER *et al.*, 2007) (Table 3).

Subunit *d*	Start residue	End residue	Measured mass	Sequence
Non-reduced TMR	1	18	2059.32	MEGVYFNIDNGFIEGVVR
	19-43	322-335	4412.96	$_{19}$GYRNGLLSNNQYINLTQCDTLELK$_{43}$*
				$_{322}$NITWIAECIAQNQR$_{335}$*
	44	75	3443.72	LQLSSTDYGNFLSSVSSESLTTSLIQEYASSK
	85	93	964.99	DQSSGSTRK
	121	163	4850.65	GEILQRCHPLGWFDTLPTLSVATDLESLYETVLV
				DTPLAPYFK
	164	181	2625.35	NCFDTAEELDDMNIEIIR**
	206	218	1996.72	ECMQTLLGFEADR**
	206	219	2152.9	ECMQTLLGFEADRR**
	219	238	2053.26	SINIALNSLQSSDIDPDLK
	267	276	1169.30	AALANVYEYR
	277	297	3028.84	GFLETGNLEDHFYQLEMELCR**
	298	316	2245.58	DAFTQQFAISTVWAWMKSK
CuCl$_2$-Treated	1	18	2059.32	MEGVYFNIDNGFIEGVVR
	22-43	322-335	4034.55	$_{22}$NGLLSNNQYINLTQCDTLELK$_{43}$*
				$_{322}$NITWIAECIAQNQR$_{335}$*
	44	75	3443.72	LQLSSTDYGNFLSSVSSESLTTSLIQEYASSK

	93	118	2954.42	FMDYITYGYMIDNVALMITGTIHDR
	121	181	6971.90	GEILQRCHPLGWFDTLPTLSVATDLESLYETVLV
				DTPLAPYFKNCFDTAEELDDMNIEIIR*
	206	218	1510.72	ECMQTLLGFEADR
	206	218	1666.90	ECMQTLLGFEADRR
	219	238	2053.26	SINIALNSLQSSDIDPDLK
	248	266	2176.46	LYPLATFHLAQAQDFEGVR
	267	297	3696.12	AALANVYEYRGFLETGNLEDHFYQLEMELCR
	298	314	2030.33	DAFTQQFAISTVWAWMK
DTT-Treated	1	18	2059.32	MEGVYFNIDNGFIEGVVR
	22	43	2394.68	NGLLSNNQYINLTQCDTLELK
	44	75	3443.72	LQLSSTDYGNFLSSVSSESLTTSLIQEYASSK
	85	93	964.99	DQSSGSTRK
	92	120	3325.86	KFMDYITYGYMIDNVALMITGTIHDRDK
	121	163	4850.56	GEILQRCHPLGWFDTLPTLSVATDLESLYETVLVDTPLAPYFK
	164	181	2141.35	NCFDTAEELDDMNIEIIR
	187	205	2275.50	AYLEDFYNFVTEEIPEPAK
	206	238	3694.15	ECMQTLLGFEADRRSINIALNSLQSSDIDPDLK
	248	266	2176.46	LYPLATFHLAQAQDFEGVR
	317	335	2301.56	EQEVRNITWIAECIAQNQR
	322	335	1659.88	NITWIAECIAQNQR
Non-reduced NEM	1	18	2059.32	MEGVYFNIDNGFIEGVVR
	19-43	322-355	4412.96	$_{19}$GYRNGLLSNNQYINLTQCDTLELK$_{43}$*
				$_{322}$NITWIAECIAQNQR$_{335}$*
	44	75	3443.72	LQLSSTDYGNFLSSVSSESLTTSLIQEYASSK
	121	163	4489.87	GEILQRCHPLGWFDTLPTLSVATDLESLYETVLVDTPLAPYFK
				***
	164	181	2264.55	NCFDTAEELDDMNIEIIR***
	206	218	1635.94	ECMQTLLGFEADR***
	206	219	1792.12	ECMQTLLGFEADRR***
	219	238	2053.26	SINIALNSLQSSDIDPDLK
	267	276	1169.30	AALANVYEYR
	277	297	2668.06	GFLETGNLEDHFYQLEMELCR***

*   Peptides involved in disulphide formation via Cys residues
**   Peptides labeled with TMR
*** Peptides labeled with NEM

Table 3. **Peptide fingerprinting of trypsin digested subunit *d*.** MALDI-mass spectrometry analysis of peptides of subunit *d*, labeled with TMR and NEM, respectively, as well as the $CuCl_2$ - and DTT- treated protein (THAKER *et al.*, 2007).

3.2.6   Spectroscopic investigations of secondary structure alterations in subunit *d*

3.2.6.1 Intrinsic tryptophan fluorescence spectroscopy

Changes in the disulphide formation were observed by MALDI-TOF analysis (section 3.2.5). In addition, these structural alterations were further analyzed by intrinsic tryptophan fluorescence spectroscopy measurements. Subunit *d* has four tryptophan residues, one at the N-terminus (Trp_{132}), and the other three at positions $Trp_{311,313,326}$ which can be used as native probes to monitor the conformational changes. Protein tryptophan spectra were measured in native non-oxidized, oxidized ($CuCl_2$), and reduced (DTT) conditions as shown in figure 21. An average of at least three readings with buffer baseline correction showed that subunit *d* had emission maxima at 337 nm and addition of DTT causes a net increase in the quantum yield without any noticeable shift in the emission wavelength of the spectrum, reflecting an increase in the surrounding polarity. Oxidation of cysteine residues with $CuCl_2$ decreased the quantum yield with slight shift towards the red end of spectrum showing maximum emission at 341 nm (Figure 21) meditative of the decreased polar environment surrounding tryptophans (THAKER *et al.*, 2007).
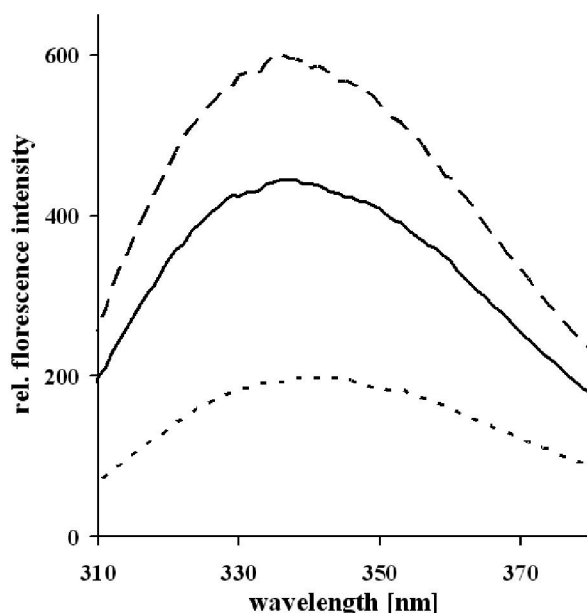
Figure 21. **Intrinsic tryptophan fluorescence.** Averaged and buffer subtracted spectrum of subunit *d* (__), in $CuCl_2$ oxidized (---) and DTT reduced state (…) is shown. Experiments were recorded at 20 ℃ on a Varian Cary Eclipse spectrofluorimeter with excitation set at 295 nm and fluorescence emission recorded between 310 – 380 nm (band pass 5 nm) (THAKER *et al.*, 2007).

3.2.6.2 Circular dichroism spectroscopy

Differences in the left and right handed circularly polarized light measured by CD can be used to monitor the secondary structural alterations in the proteins. A similar approach was used

to monitor the alterations in subunit *d*. Prior to each reading the sample was treated with 100 µM CuCl$_2$ or 1 mM DTT or left untreated as control. After appropriate incubations, CD was recorded and processed as described under section 2.2.14. As displayed in figure 22, slight variations in secondary structure were observed in the reduced and the non-reduced conditions. However, significant differences appeared when protein was cross-linked with CuCl$_2$, displaying a decrease in the helicity due to additional disulphide bond. By comparison, the $_{222}/_{208}$ ratio of the reduced and Cu-treated protein is 0.99 and 0.97, respectively (THAKER *et al.*, 2007).
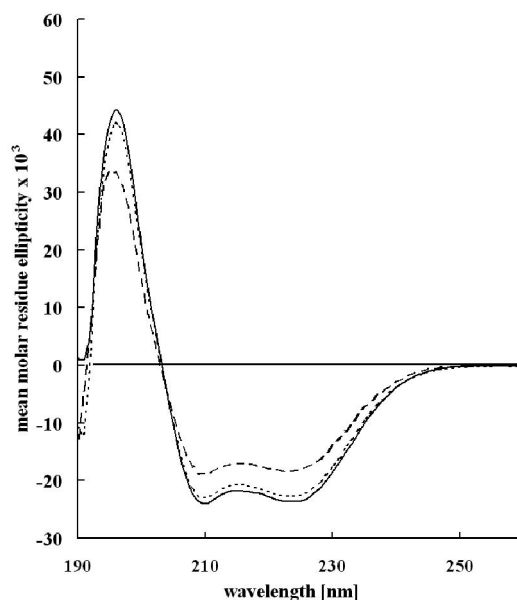
Figure 22. Circular dichroism spectrum of subunit *d* from *Saccharomyces cerevisiae* V-ATPase in the presence (··) and absence (—) of 1 mM DTT and after 100 uM CuCl$_2$-treatment (--) (THAKER *et al.*, 2007).

3.2.6.3 3D Structure alterations studied by SAXS

To probe whether the alterations of secondary structure in different states (reduced and non-reduced) were accompanied by changes in the tertiary structure, a series of SAXS measurements were recorded in defined conditions (section 2.2.18). However, the recorded spectra did not show any significant variations from the standard measurement (Figure 15A), demonstrating that no observable disparity occurs in the tertiary shape of the protein at this resolution, however, minor alterations cannot be excluded due to the resolution limit of SAXS.

3.2.7 Biochemical and structural features of subunit *d* mutants

To further study secondary and tertiary structure alterations and implication of disulphide bond formation between Cys$_{36}$ and Cys$_{329}$, several mutants of subunit *d* (Figure 23A), which carried N- and C-termini deletions (d_{11-345}, d_{38-345}, d_{1-328} and d_{1-298}), point mutation (d_{C329S}) or

missing both N- and C-terminal regions of varying lengths (d_{11-189}, d_{38-189}, $d_{190-328}$) were generated. The lack of 37 (d_{38-345}) residues at the N-terminus and 17 (d_{1-328}) or 47 (d_{1-298}) residues from the C-terminus, as well as missing regions from both ends (d_{11-189}, d_{38-189}, $d_{190-328}$) resulted in a low production of proteins, which was either insoluble or unstable as indicated below in figure 23B results. More importantly, a point mutation C329A also resulted in insoluble protein (Figure 23B). Figure 23B shows a representative buffer from each solubility experiment as: The subunit *d* constructs that produced soluble proteins and could be purified in homogenous preparations are highlighted in blue colour (Figure 23A). A summary of traits exhibited by various constructs of subunit *d* is described in table 4.
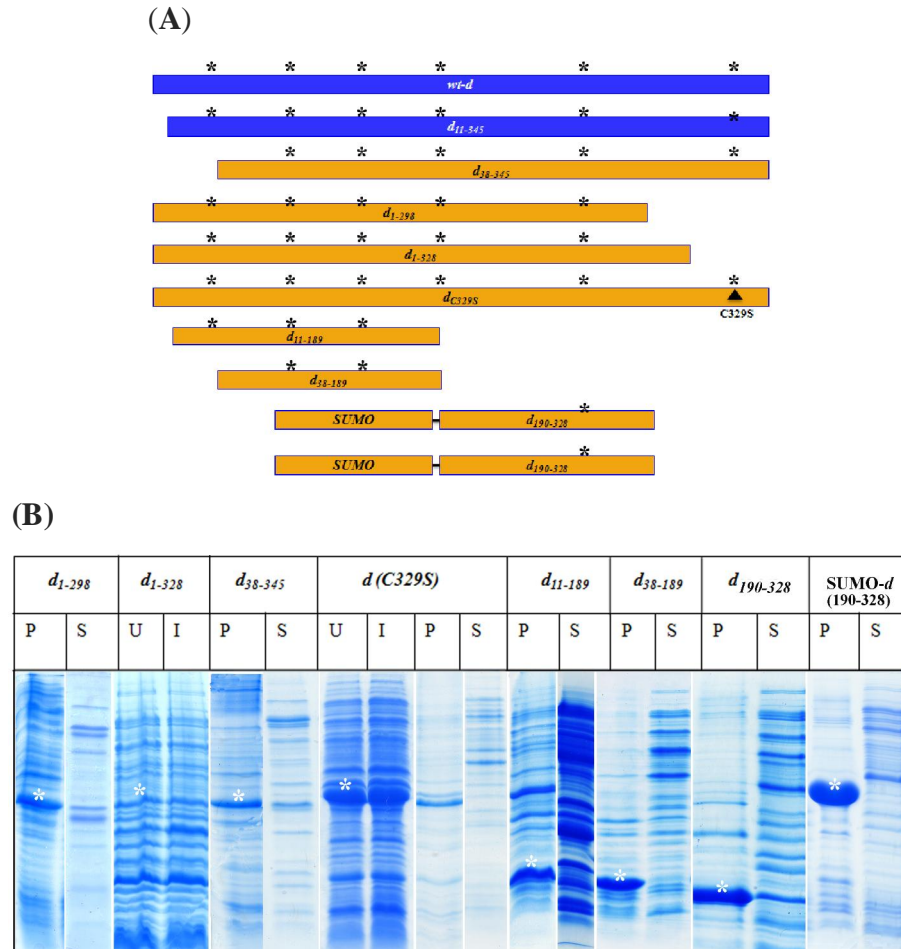
***Figure 23.* Subunit *d* mutants.** Various constructs carrying deletions of various lengths from N- or C-termini or both or point mutation were generated (**A**) to probe the importance of cysteine bridge (Cys$_{36}$-Cys$_{329}$), cysteine positions in primary sequence are indicated by *. Constructs of subunit *d* that could be successfully produced and purified are shown in blue. (**B**) 17% SDS polyacrylamide gels showing various mutant proteins that were poorly produced and/or less stable and insoluble. Samples from the induction test (U and I) and solubility test (P and S) are shown. Expected molecular weight of respective mutants is indicated by asterisks (white). (P = Pellet, S = Soluble, U = Uninduced, I = Induced). Only full length proteins (d_{wt}; Figure 11) and the construct having all cysteines intact (d_{11}-$_{345}$; Figure 24) could be successfully produced and purified. Representative solubility gels are shown from buffer 50 mM Tris, 500 mM NaCl, pH 7.5 except mutant $d_{190-328}$ which used 50 mM Tris, 200 mM NaCl, pH 9.0 buffer.

	Production	Solubility	Stability
d(wt)	++	++	++
d (C329S)	+	-	-
d_{38-345}	-	-	-
d_{1-298}	+	-	- -
d_{11-345}	++	++	++
d_{1-328}	-	-	-
d_{11-189}	+	-	-
d_{38-189}	+	-	-
$d_{190-328}$	+	+	-
$d_{190-328}^{SUMO}$	++	-	-

Table 4. **Summary of the traits of various subunit *d* mutants.** Characteristics of mutant proteins of subunit *d*, carrying various tranucations or point mutations. Solubility, stability and production traits are compared with respect to wild subunit *d*. Protein that could be properly expressed are highlighted in the blue font.

The only truncated construct which could be purified was d_{11-345}, lacking the first 10 residues (Figure *24*). Consequently, d_{11-345} was isolated by Ni^{2+}-NTA and anion-exchange chromatography (insert Figure 24B). CD spectrum has been studied with the purified protein indicating an -helical content of 62% and 30% random coil and a $_{222}/_{208}$ ratio of 0.99 (Figure 24B). Production and quality of this protein was comparable to the wild type subunit *d*. Besides, d_{11-345} protein also displayed similar biochemical behavior as shown by the wild type subunit *d* in presence of $CuCl_2$ and DTT.

The results from the studies with mutant proteins of subunit *d* gave an interesting insights into this protein, where the only proteins having intact Cys_{36} and Cys_{329} could be purified, demonstrating the importance of disulphide bond between C- and N- termini in the stability and structural folding of protein during synthesis. Since the point mutant C329S was also unstable, which further supported the importance of N- and C- termini in the formation of a stable tertiary structure during the protein synthesis (THAKER *et al.*, 2007).

(A)

(B)
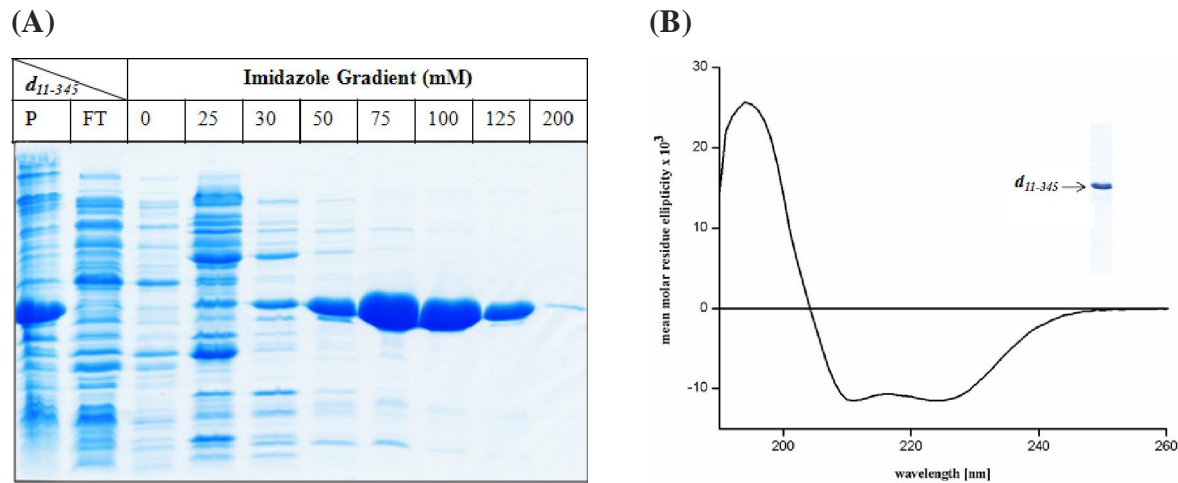
Figure 24. **Isolation, purification and analysis of $d_{11\text{-}345}$ mutant.** SDS gel showing the Ni^{2+}-NTA eluted samples by an imidazole gradient from 0 – 200 mM (**A**). (**B**) Far UV-CD spectrum of the truncated form. (Insert), SDS gel shows a sample of the Resource Q (6 ml) purified recombinant $d_{11\text{-}345}$ protein used in the CD spectroscopy measurement.

Additionally, several shorter constructs with deletions from both N- and C-termini ($d_{11\text{-}189}$, $d_{38\text{-}189}$, $d_{190\text{-}328}$) were generated (section 2.2.2.3) in the hope to get some further insight into the structure and biochemical properties of subunit *d*. None of the proteins were stable and little or no production was observed as summarized in table 4. To exclude the fusion-dependent interferences in the properties of expressed subunit *d* mutants, a SUMO (Small Ubiquitin Related Modifier) (BUTT *et al.*, 2005) fusion construct of $d_{190\text{-}328}$ was prepared. The over expressed SUMO-$d_{190\text{-}328}$ protein was also insoluble, that could not be used for further studies relevant to the shape and properties of subunit *d* observed in this study (THAKER *et al.*, 2007) (Figure 23B). Nonetheless these data showed indispensability of the termini for synthesis and stability of subunit *d*.

3.2.8 Assembly of subunit *d* with subunit G by NMR spectroscopy

Since subunit *d* and subunit G of V-ATPase have been shown to interact with each other in the immunoprecipitation experiments (JONES *et al.*, 2005), attention was focused to map the domain and amino acids of G involved in *d*/G assembly, in a collaborative approach with Mr. S. Rishikesan from our laboratory. Recombinant N-terminal fragment of subunit G ($G_{1\text{-}59}$) (produced and purified from *E. coli* by S. Rishikesan) was used to monitor the binding with subunit *d* using heteronuclear single quantum spectroscopy (HSQC) NMR technique, where ^{15}N labeled subunit $G_{1\text{-}59}$ was used to record the spectrum and monitor the changes in the chemical shift of amino acid peaks. Addition of recombinant unlabeled subunit *d* to the ^{15}N labeled subunit G caused remarkable changes in the spectrum of $G_{1\text{-}59}$, indicative of complex formation between

the two. As shown in figure 25, only N-terminal regions of amide resonances of the free G_{1-59} subunit were weakened progressively upon the addition of increasing amounts of *d* subunit. Binding of *d* subunit induced a structural change in the G_{1-59}, which is in chemical exchange on an intermediate rate, with respect to the NMR timescale. This caused loss of NMR signals in the resonances affected by the binding (RISHIKESAN *et al.*, 2009). The signal losses observed were indicative of complex formation and resulted from the formation of either a stable, large molecular weight complex or a complex with an exchange rate between the free and bound forms that is similar to the chemical shift difference (KAY *et al.*, 1996). Intensity of interaction was quantitatively evaluated by plotting the intensity of peak ratio [G_{FREE}/G_{BOUND}] at a molar ratio of 0.5 to subunit *d* (B). Intensity perturbations were seen in the N-terminal region of G_{1-58} in the amino acid residues 7 – 34 (RISHIKESAN *et al.*, 2009).

(A)

(B)
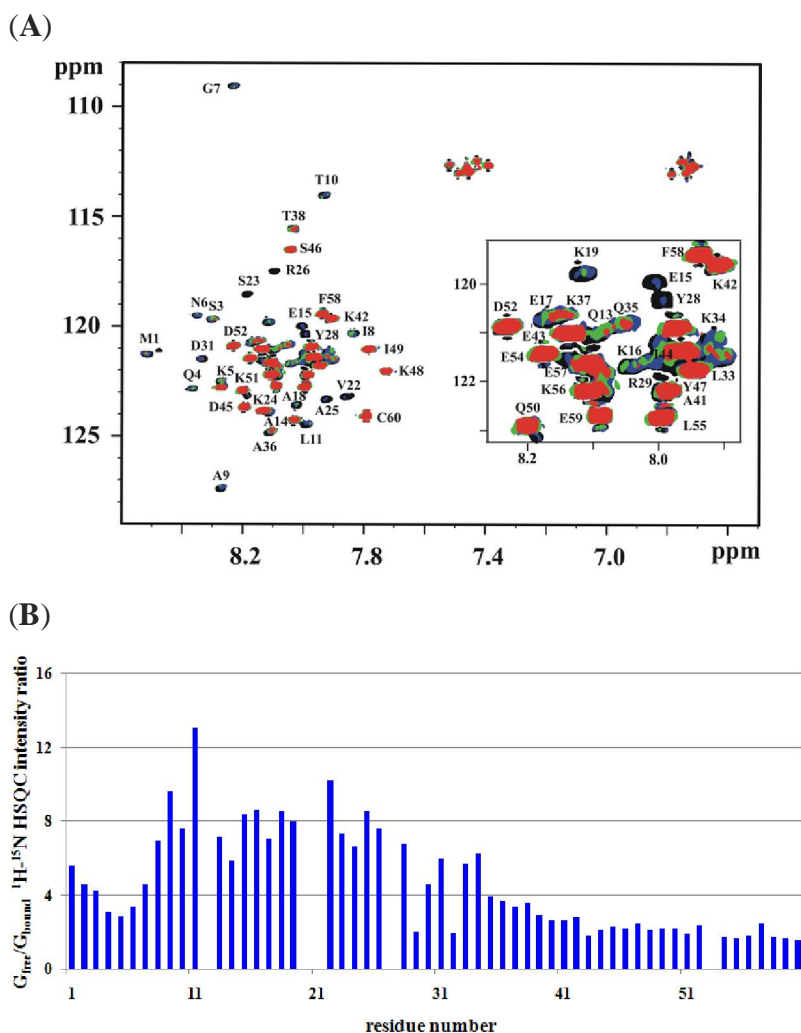
Figure 25. **Subunit *d* binding to subunit G_{1-58} of yeast vacuolar ATPase. (A)** A series of titration experiments were done where 15N-labeled G_{1-59} was added with varying concentration of subunit *d*. Concentrations of unlabelled *d* subunit are 0 mM (*black*), 0.125 mM(*blue*), 0.159 (*green*) and 0.187 (*red*). **(B)** Graphical representation of change in the intensity of HSQC spectrum of subunit G_{1-59} when unlabeled subunit *d* was added. Decrease in the intensity of peak is proportional to the height of bar (RISHIKESAN *et al.*, 2009).

3.3 Structural and biochemical characterization of subunit *a* of the vacuolar ATPase
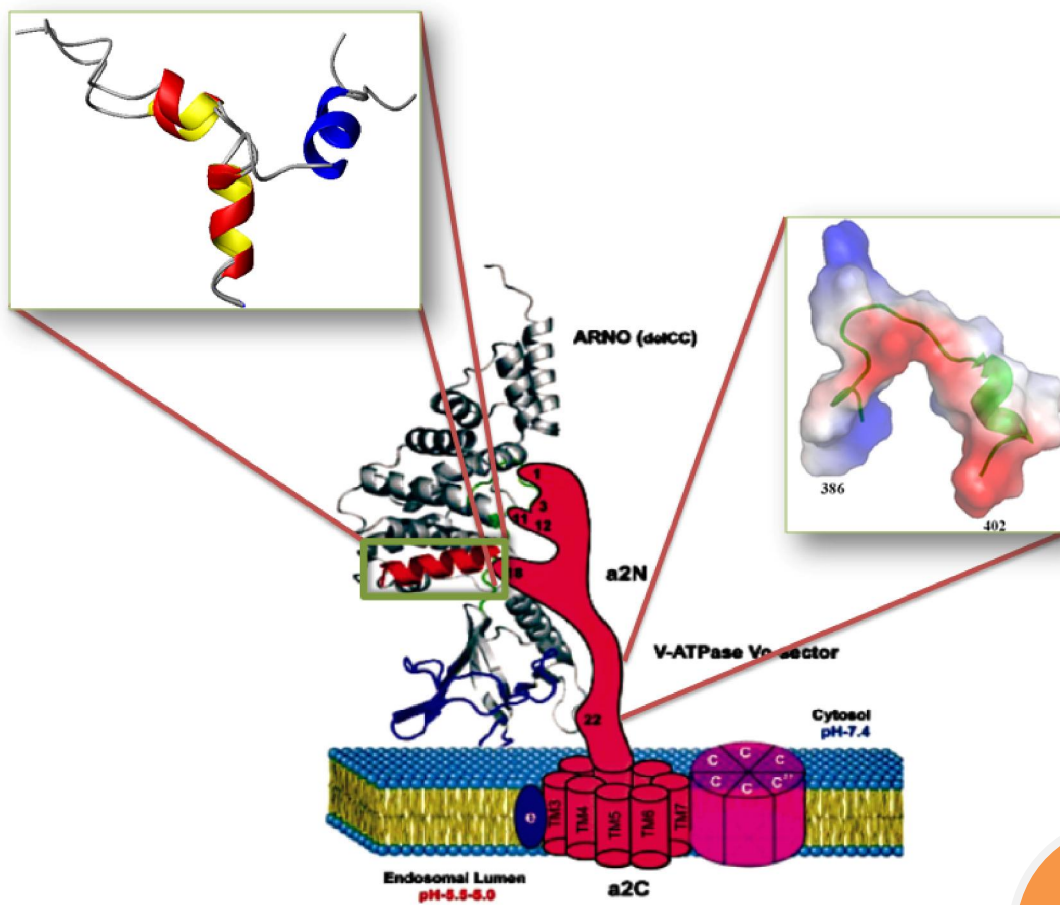
Subunit *a* from *Saccharomyces cerevisiae* vacuolar ATPase (V-ATPase) was identified as product of the *VPH1* (Vacuolar pH 1) gene, which was cloned by the complementation of vph1-1 mutation, giving rise to a 95 kDa protein called as Vph1p (MANOLSON *et al.*, 1992). The disruption of *VPH1* gene was shown to cause defects in V_1V_O assembly and vacuolar acidification (MANOLSON *et al.*, 1992). These results showed that subunit *a* is an indispensable unit of the vacuolar ATPase, required for the association of V_1 catalytic domain to proton channel V_O domain to restore the fully functional enzyme (MANOLSON *et al.*, 1992). Subunit *a* contains a hydrophilic N-terminal domain and a membrane embedded C-terminal region (LENG *et al.*, 1999). Here, I initiated studies with the hydrophilic N-terminal domain of the subunit *a,* to characterize this region of *Vph1p* by various biophysical techniques.

3.3.1 Cloning, production and purification of subunit a_{1-388} and $a_{1-388(C)}$

A fragment of gene *VPH1,* coding for 1 – 388 region of primary sequence, represented as a_{1-388} (Figure 28B) was cloned from the *Saccharomyces cerevisiae* genome by PCR method and ligated to the His_3-pET9d-1 vector (GRÜBER *et al.*, 2002) to be produced as His-fusion protein as described in detail under section 2.2.12.2. Subsequently, the pET 9-d1/ a_{1-388} was transformed into the BL21 (DE3) and Rosetta-gami^{TM} 2 (DE3) expression hosts for initial optimization steps and subsequent expression was done in the Rosetta-gami^{TM} 2 (DE3) cells. Additionally, a point mutant A388C construct of subunit *a* ($a_{1-388(C)}$), introducing a cysteine residue at the COOH terminus was generated for thiol-specific labeling with cysteine reactive fluorophor dyes. Flurophore labeled proteins were used for binding studies in the fluorescence correlation spectroscopy (FCS). Protein expression and purification methodology for both constructs is described in detail under section 2.2.12.2, whereby the protein was purified in two steps via Ni^{2+}-NTA affinity chromatography and ion exchange chromatography as shown in figure 26-27, respectively. Proteins were checked for the purity on SDS polyacrylamide gel and concentrations were determined by BCA assay (section 2.2.13).

(A)

(B)
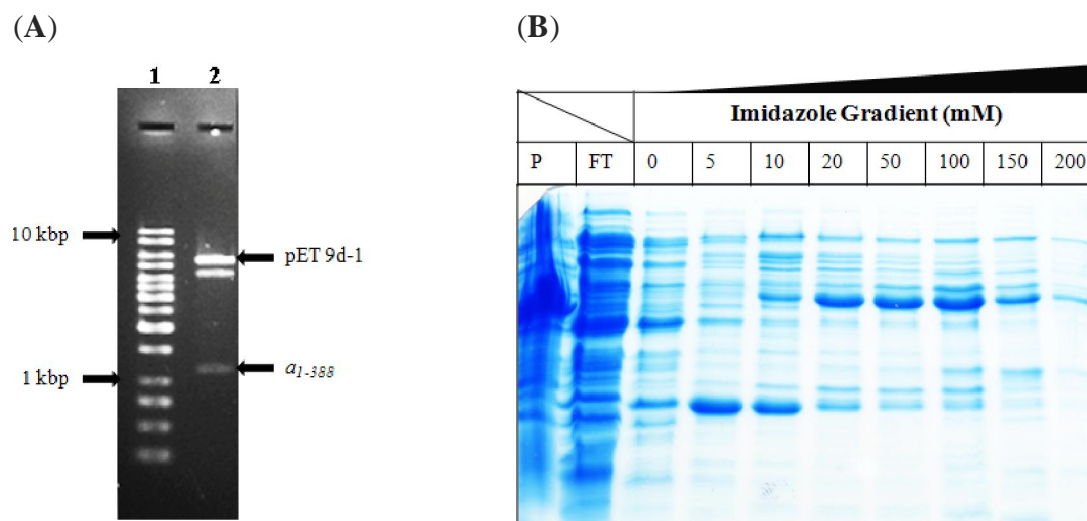
Figure 26. **Cloning, production and purification of subunit a_{1-388} and $a_{1-388(c)}$.** **(A)** DNA agarose gel (1 %) picture showing double restriction digestion with *NcoI* and *SacI* enzymes of one selected clone obtained after ligation of PCR fragment a_{1-388} to pET9d-1 (released insert and vectors are shown by arrow) in *lane 2* and *lane 1* contains 1 Kb marker (O Gene Ruler; Fermentas) and **(B)** Ni^{2+}-NTA affinity enrichment of protein from whole cell lysate in buffer 50 mM Tris/HCl, 500 mM NaCl, pH 7.5 using an imidazole gradient (0 – 200 mM) for elution of Ni^{2+}-NTA bound protein. Fractions from 20 – 100 mM imidazole were pooled together for further purification step as shown below in figure 27.
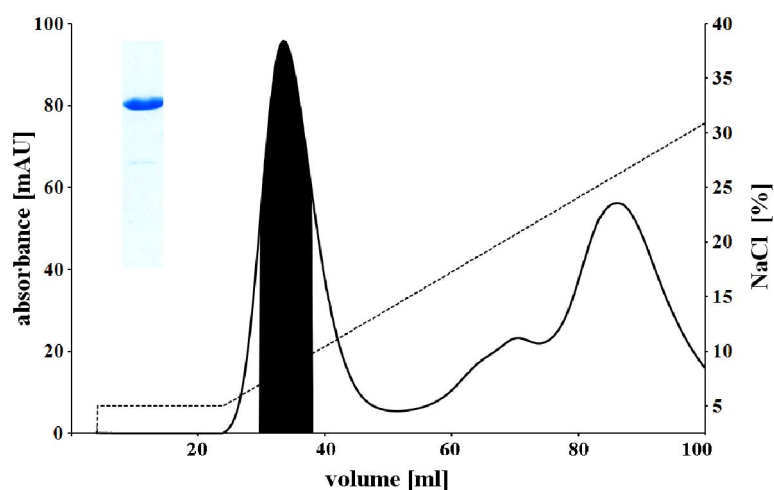
Figure 27. **Ion-exchange purification of subunit a_{1-388}.** Protein containing fractions of Ni^{2+}-NTA from a_{1-388} protein were pooled, diluted with 50 mM Tris, pH 7.5 to reduce the salt concentration to 50 mM and applied onto the anion exchange column (Resouce Q, 6 ml) for additional purification step. Protein bound to column media was eluted using a linear gradient (---) of buffer A (50 mM Tris/HCl, 50 mM NaCl, pH 7.5) and B (50 mM Tris/HCl, 1 M NaCl, pH 7.5) resulting in the protein separation as a sharp peak, containing the pure protein (shaded peak area volume was pooled). Insert shows 1 µl of pure eluted protein applied on a 17% SDS gel.

3.3.2 Secondary structural characteristics of subunit a_{1-388}/$a_{1-388(C)}$

To characterize the secondary structure content of subunit a_{1-388}, a circular dichroism spectrum of the purified protein (2 mg/ml) was recorded in buffer 50 mM Tris/HCl, 100 mM NaCl, pH 7.5 as described in section 2.2.14. Analysis of the CD spectrum shows minima at 222 and 208 nm and a maximum at 192 nm, which are the characteristics of -helical proteins. Further, the secondary structure of subunit *a* was predicted by online analysis with PSIPRED algorithm, which uses a two stage neural network for analysis of the position specific scoring matrices generated by PSI-BLAST (MCGUFFIN *et al.*, 2000), showing the protein is mostly -helical in nature with a helical content of 48%, 38% random coil and 12% -sheet (Figure 28).

(A)

(B)
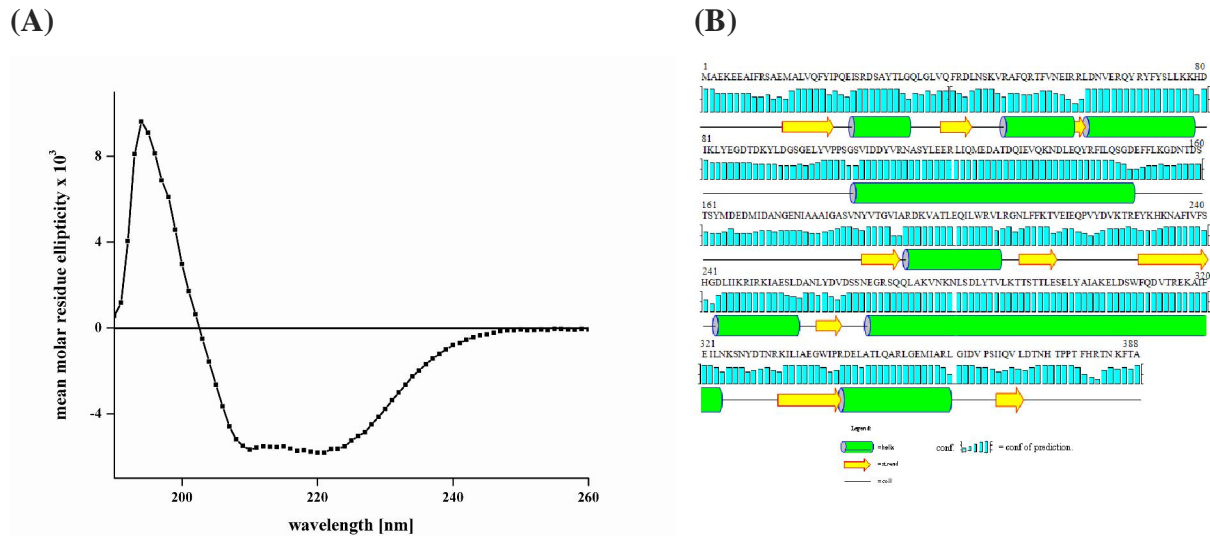
Figure 28. **Secondary structure analysis of subunit a_{1-388}.** (**A**) Circular dichroism spectrum of subunit a_{1-388} measured at 2 mg/ml protein concentration in buffer 50 mM Tris, 500 mM NaCl, pH 7.5 in a Hella quartz cuvette (120 µl) at a step resolution of 1 nm. The spectrum was recorded on Chirascan spectropolarimeter instrument (Applied Photophysics). (**B**) Secondary structure analysis by online algorithm PSIPRED shows that the protein is a mixture of -helix and -sheet. PSIPRED algorithm uses PSI-BLAST results for secondary structure analysis by a two stage neural network frame (MCGUFFIN *et al.*, 2000).

3.3.3 Fluorescence correlation spectroscopic experiments of subunit a_{1-388}/$a_{1-388(C)}$ with subunit *d*

Initially, TMR labeled subunit *d* was used to measure the binding with unlabelled subunit a_{1-388} using the technique of fluorescence correlation spectroscopy, which measures the diffusion time of labeled protein. Subunit *d* was labeled with TMR dye at room temperature for 10 min and the reaction was inactivated by the addition of 1 mM DTT. FCS measurements with TMR labeled protein *d* with unlabeled subunit a_{1-388} indicated significant changes in the diffusion time when compared to *d* subunit alone, the measured mass change ratio was 2.03, which means the mass of measured protein doubles, suggesting that *d* binds to a_{1-388} as shown in figure 29A.

There was no difference in the results between incubation and non-incubation measurements (Figure 29B). The concentration had no effect on the results; basically, 50 nM and 100 nM of protein *d* showed the same trend. Detailed data interpretations are tabulated in table 4 indicative of interaction between the two proteins. Due to almost similar molecular mass of two proteins (41.2 kDa for *d* verses 45.8 kDa for a_{1-388}) and possible aggregation of the protein, as the number of particles in solution decreased during measurements (Figure 29B), a new subunit *a*/Vph1p construct $a_{1-388(C)}$ carrying a cysteine residue at C-terminus was cloned. The purified protein was labeled with Cy5 fluorescence dye as described in section 2.2.20, to be used in fluorescence cross correlation spectroscopy (FCCS) measurements. The FCCS was recorded with TMR-*d* and Cy5-a_{1-388}, which also demonstrated that two proteins do associate with each other as shown in figure 29D. However, quality of the data could not be improved due to the aggregation of the formed complex and almost similar mass of the two proteins but these initial results obtained gave first impression that two proteins might associate with each other. To overcome these problems, proteins were studied in a label free system, surface plasmon resonance (SPR) as described below in section 3.3.4.

(A)

(B)
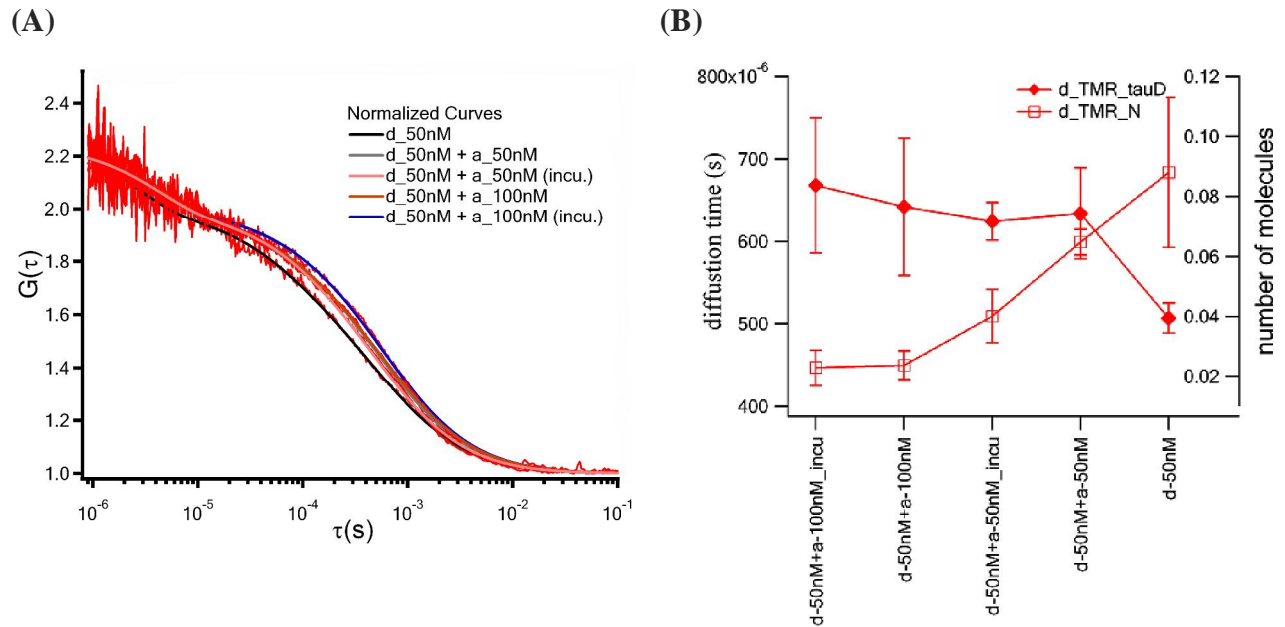
Figure 29. **Fluorescence correlation spectroscopy of subunit a_{1-388} and subunit *d*.** (A) Fluorescence correlation normalized and fitted curves of subunit *d* (50 nM, TMR labeled) in presence of unlabeled a_{1-388} (50 – 100 nM) when samples were either incubated at 37 °C for 10 min or measured without incubation (details in figure legend). (B) Graph showing the trend of diffusion (tauD in seconds) indicative of binding between two proteins with increasing diffusion time, and graph also shows the mean particle number (N) in solution.

(C)

(D)

Figure 29 contd. (**C**) Shows intensity fluctuation tracks when subunit *d* is added with subunit *a*. (**D**) Fluorescence cross correlation spectroscopy results obtained with TMR-*d* and Cy5-*a* labeled samples, normalized correlation curves showing the ratio of diffusion time (G( )), indicative of binding between the subunits *d* and a_{1-388}.
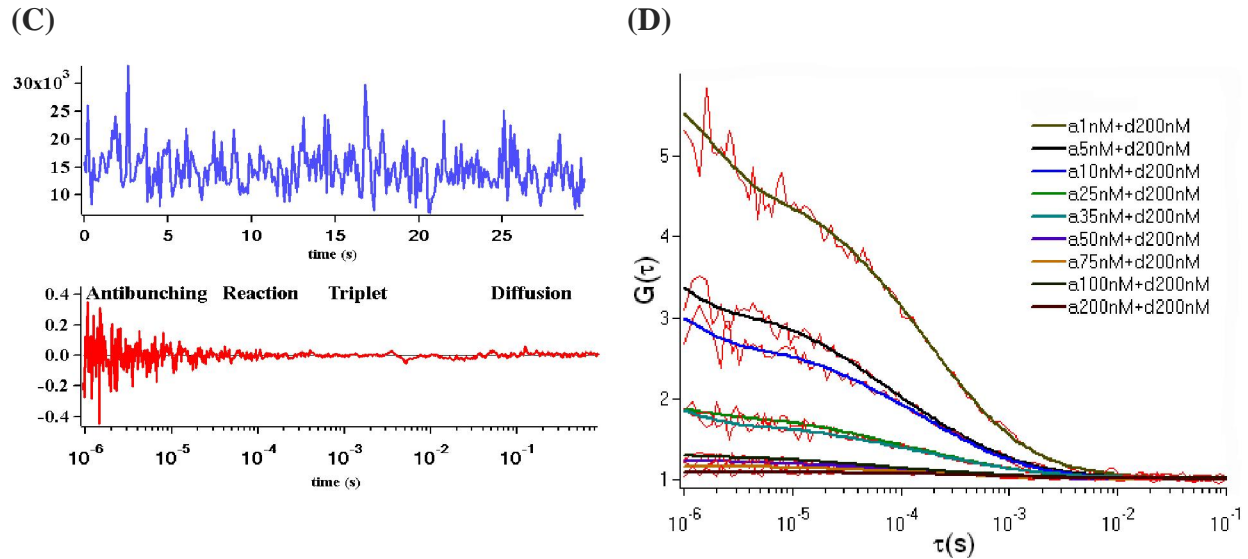
S.No.		d_TMR_tauD	d_TMR_tauD_Std	d_TMR_N	d_TMR_N_Std
1	**d-50nM**	5.07E-04	1.83E-05	8.80E-02	2.51E-02
2	**d-50nM+a-50nM**	6.34E-04	5.54E-05	6.48E-02	4.28E-03
3	**d-50nM+a-50nM_incu**	6.25E-04	2.25E-05	4.01E-02	8.91E-03
4	**d-50nM+a-100nM**	6.42E-04	8.32E-05	2.36E-02	4.76E-03
5	**d-50nM+a-100nM_incu**	6.68E-04	8.20E-05	2.28E-02	5.79E-03

Table 5. Statistics of the binding between subunit *d* (*d*_TMR) and subunit a_{1-388} obtained from the analysis of FCS experimental data as shown in the fitted data curves in figure 29A (tauD, Std and N represent diffusion time (s), standard and number of particles, respectively.

3.3.4 Interaction of subunit a_{1-388} with subunit *d* of yeast vacuolar ATPase studied by surface plasmon resonance

Surface plasmon resonance (SPR) is a real time binding analysis technique which can be used to monitor the interaction between a surface immobilized protein and its ligand in a label free environment (JONSSON *et al.*, 1991; CHAIKEN *et al.*, 1992; KARLSSON *et al.*, 1994). SPR experiment were done by Mr. Yin Hoe in a collaborative project with A/Prof. Susana G. Shochat's laboratory. Subunit *d* in HBS buffer (10 mM Hepes buffer, pH 7.4, 150 mM NaCl, 3.4 mM EDTA and 0.005% P-20) was covalently immobilized on a carboxymethylated sensor surface using amine coupling chemistry at 25 ºC as described in detail in section 2.2.21. For the determination of kinetic parameters, subunit a_{1-388} was passed above the reference and protein surfaces in duplicates of five to seven concentrations (18.7 – 300 nM), in HBS at a flow rate of 30 µl/min. The data were fitted by simple 1:1 Langmuir fitting model as described in method section 2.2.21. The measured affinity kinetics between subunit *d* and subunit *a* are shown with

standard error from four independent experiments in parentheses. An association rate constant $k_a = 7.7 \, (\pm 1.1) \times 10^3 \, M^{-1} s^{-1}$ and dissociation rate constant $k_d = 4.4 \, (\pm 1.2) \times 10^{-4} \, s^{-1}$ was obtained. Consequently, dissociation constant (k_d/k_a) of $K_d = 6.0 \, (\pm 1.8) \times 10^{-8}$ M was calculated for subunit *d* and *a* binding. The chi^2 was within 1% of Rmax from the fit as displayed in figure 30. These data suggest strong interaction between subunit *a* (N-terminal domain) and subunit *d* of V-ATPase from *Saccharomyces cerevisiae* in line with the FCS results (section 3.3.3) and biochemical characteristics of subunit *d,* which remains firmly associated with the V_O domain despite the absence of transmembrane regions (BAUERLE *et al.*, 1993).
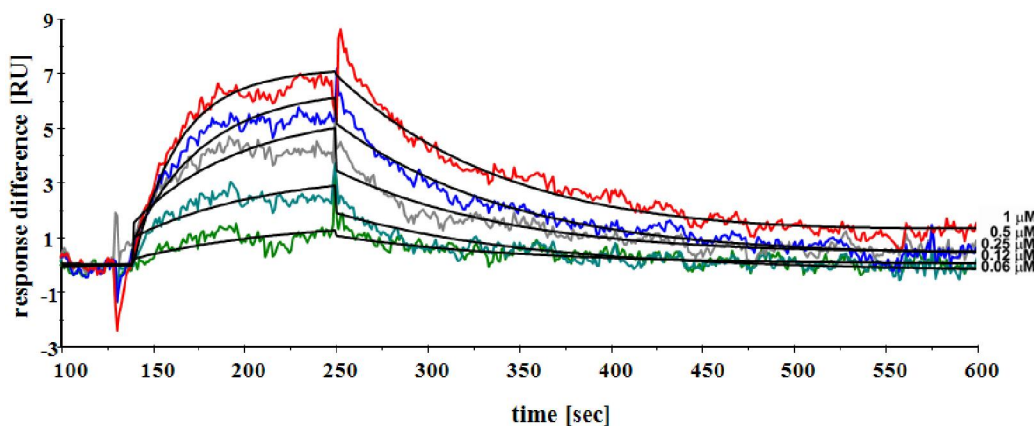
Figure 30. **Subunit a_{1-388} and subunit *d* interaction by SPR.** Surface plasmon resonance was used to measure the binding affinity of subunit a_{1-388} with wild type subunit *d* of yeast vacuolar ATPase. Subunit *d* was covalently immobilizing onto a carboxymethylated sensor surface in HBS (10 mM Hepes buffer, pH 7.4, 150 mM NaCl, 3.4 mM EDTA and 0.005% P-20) buffer and subunit a_{1-388} was passed over the reference and experimental surface at a constant flow rate of 30 µl/min. Sensorgrams were fitted using the simple 1:1 Langmuir binding fit model (THAKER *et al.*, 2009).

3.3.5 Crystallization of subunit a_{1-388} of Vph1p isoform of yeast V-ATPase

Pure protein subunit a_{1-388} was used to set up the crystals in Hampton Research crystal screen HR-110 and HR-130 for initial screening with a protein concentration of 10 – 15 mg/ml in 2 µl droplets (1 µl protein + 1 µl mother liquor) per well in hanging drop plates containing 1 ml of mother liquor base. Initially a kind of phase separation (Figure 31A) was observed in condition containing 0.1 M Hepes sodium pH 7.5, 2% PEG 400, 2 M ammonium sulfate. Optimization of this condition by varying precipitant, salt concentration and changing buffer or pH in various grid screens resulted in the formation of needle clusters (Figure 31C). Additional optimization was performed with varying protein concentration and replacement of salt, which resulted in little improvements in the needle bunches (Figure 31D). Attempts were also made by using additional grid screens, Additive Screen^{TM}, Index Screen^{TM}, Salt Screen^{TM} besides micro-

and macro-seeding at various steps. However, additional conditions have to be tried in future experiments.
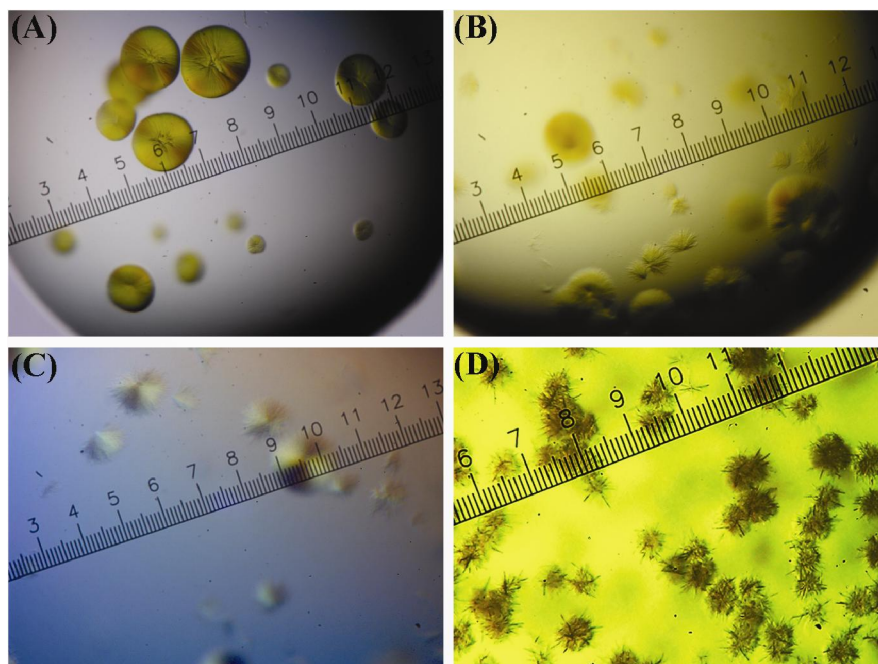
Figure 31. **Crystallization and optimization of subunit a_{1-388}.** Crystallization trials of subunit *a* protein were made in hanging drop plates as 2 μl droplets (1 μl of protein + 1 μl of mother liquor) in a 1 ml well volume. Screening with Crystal Screen HR-110 (Hampton Research) resulted in the phase separation (**A-B**) in condition 0.1 M Hepes sodium pH 7.5, 2% PEG 400, 2 M ammonium sulfate which was further optimized with grid screens that resulted in needle clusters (**C-D**).

3.3.6 Cloning, production and purification of subunit *a* (*VPH1*) constructs a_{1-323}, $a_{182-322}$ and a_{1-81}

In order to map the binding domain of subunit *a* that is required for its interaction with subunit *d* and to get the diffractable quality crystals, various N-terminal domain deletion mutants of subunit *a* were cloned using PCR method by direct amplification from genomic DNA of *Sacchromyces cerevisiae* using forward and reverse primers as detailed in table 2 and methodology as described in section 2.2.2. The successfully cloned constructs a_{1-323}, $a_{182-322}$ and a_{1-81} proteins were induced for overproduction of protein in the *E. coli* BL21 (DE3) and Rosetta-gami^{TM} 2 (DE3) expression hosts. Results inferred from the figure 32 showed that the proteins were insoluble, poorly expressed and/or instable. The proteins were further optimized to get soluble fractions by inducing at different temperatures ranging from 15 – 37 ℃ with varying amounts of IPTG from 0.1 – 1 mM in different host strains. Moreover, several buffer conditions with varying buffers types and salt concentrations at different pH values (see Figure M3 for few

buffer compositions) were used for solubilization of the produced proteins. But, no further improvements could be achieved (Figure 32). Even the shorter construct (a_{1-81}) of subunit a could not be solubilized and was rather more unstable with prominent degradation visible on the SDS polyacrylamide gel, revealing that some minimum length of protein might be required to attain proper folding and stability. In comparison, longer constructs (a_{1-323} and $a_{182-322}$) were slightly more stable but completely insoluble (Figure 32).
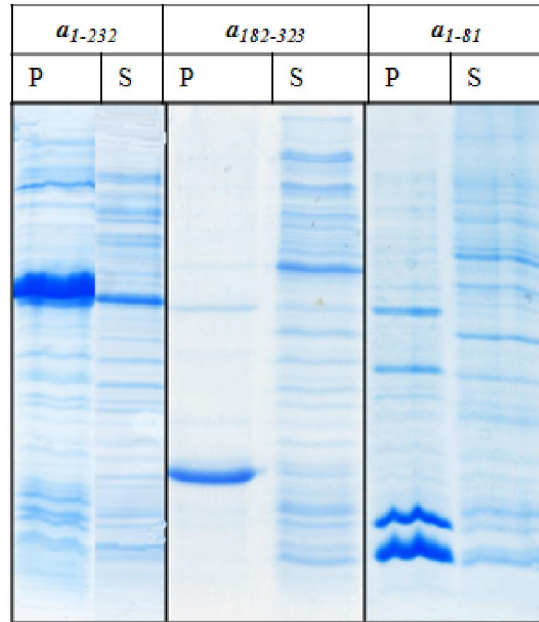
Figure 32. Expression and solubility of N-terminal Vph1p constructs. Mutant proteins were produced under various conditions in different buffers with varying temperature and IPTG levels. Figure shows the production, solubility and stability of construct in one selected buffer condition. P represents pellet and S represents supernatant on a 17% SDS polyacrylamide gel (20 µl/lane).

3.3.7 Cloning, production and purification of STV1 isoform of subunit *a* of *Saccharomyces cerevisiae*

Yeast vacuolar ATPase system has been shown to contain two subunit *a* isoform proteins, known as Vph1p and Stv1p (Similar to Vph1p), which are targeted to different organelles, (MANOLSON *et al.*, 1992; MANOLSON *et al.*, 1994). Stv1p is mostly found on the Golgi membrane V-ATPase (MANOLSON *et al.*, 1994) whereas Vph1p is present on the vacuolar membranes of V-ATPase (MANOLSON *et al.*, 1992). Like Vph1p, the Stv1p is also a membrane integral protein with N-terminal hydrophilic region exposed on the cytosolic face and C-terminal trans-embedded into the lipid bilayer (MANOLSON *et al.*, 1994). Stv1p has 54% identity with Vph1p and has been described as functional homolog of Vph1p in different organelles (MANOLSON *et al.*, 1994). The presence of different isoforms can have an important

role in targeting, assembly and regulation of vacuolar ATPase in organelle specific manner (MANOLSON *et al.*, 1994). Since N-terminal domain of isoform Vph1p was shown to interact with *d*/Vma6p in the present study (section 3.3.3 –3.3.4) and in order to demonstrate whether such assembly also occurs with its homolog isoform, Stv1p, a N-terminal fragment $Stv1p_{1-450}$ was cloned from the yeast genome using primers as described in table 2 and details of cloning strategies are described in section 2.2.2. Protein expression and production was done as described for the Vph1p (section 3.3.1). Results of expression and solubility experiments showed that the construct is poorly expressed and the produced proteins were not soluble (Figure 33). Several optimization steps with expression, induction and buffer conditions were used to get soluble fraction of proteins with on further betterment.
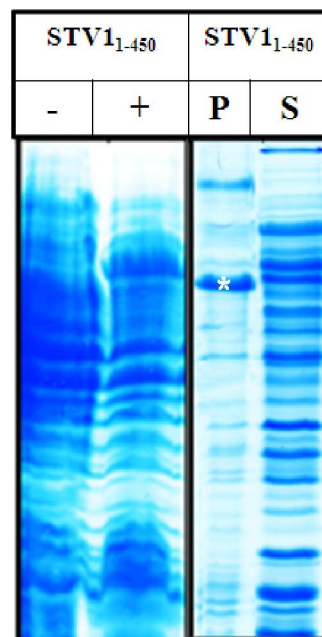
Figure 33. **Induction and expression of yeast V-ATPase subunit *a* isoform Stv1p$_{1-450}$.** SDS gel showing induction of proteins yeast isoform Stv1p (- and + represent uninduced and induced samples respectively). Cells were induced with 0.5 – 1 mM IPTG for 3 h at 37 ºC. The protein was tested for solubility in various buffers; one representative buffer is shown (P and S for pellet and supernatant respectively). Protein band on pellet lane are shown by *.

3.3.8 Cloning, induction and expression of subunit *a2* isoform from mouse V-ATPase

Mouse V-ATPase has four isoforms *a1*, *a2* and *a3* and more recently identified *a4,* which can be further expressed in different alternatively spliced variants. Subunit *a1* is mostly expressed in brain, whereas subunit *a2* is present in kidney and liver cells, *a3* in heart, lung, liver, spleen, brain and kidney (NISHI and FORGAC, 2000). A fourth isoform *a4* is mainly expressed in kidney and liver tissue cells and studies revealed that it is also essential for renal acid/base homeostasis (OKA *et al.*, 2001). Subunit *a2* has been recently described as putative endosomal pH sensor involved in the protein trafficking between early and late endosomes

regulated by its direct interaction with ARNO (ADP Ribosylation factor Nucleotide site Opener) in a pH dependent manner at early endosomal membranes (HURTADO-LORENZO *et al.*, 2006; MARSHANSKY, 2007). Due to its recently emerged crucial roles, various constructs of subunit *a2* NH_2-domain were created (Table 2). PCR cloning was done from the cDNA clones kindly provided by Prof. Vladimir Marshansky (MGH, Harvard University, Boston, USA). Due to the difficulties encountered in the amplification, $a2_{1-58}$ and $a2_{134-393}$ fragments were amplified using nested PCR strategy which made use of *a2* cDNA template amplifying 1 – 393 amino acid sequence region with its flanking primers in the first set of PCR and subsequent PCR was done with respective gene primers to receive the pure product. The amplified product was inserted into pET-9d1 vector as described in section 2.2.2 using set of primers described in table 2. Various clones from respective constructs were selected for further protein production. Successful clones were further analyzed for solubility of protein as described in detail under section 2.2.11.2, using various buffer compositions. However, results after several optimizations of temperature, host, IPTG concentration and buffer conditions showed that none of the produced proteins were soluble (Figure 34).
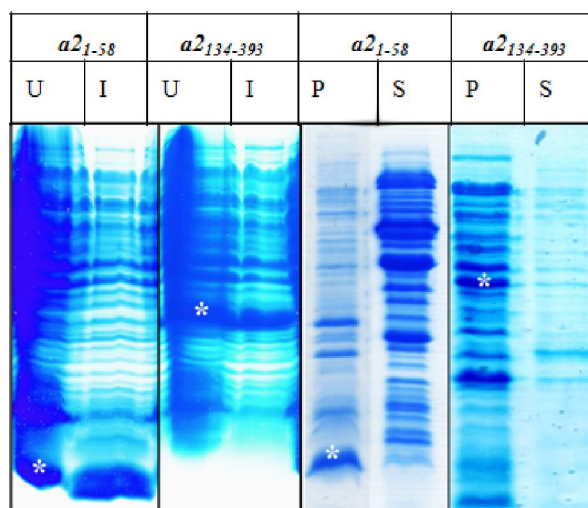
Figure 34. **Induction and expression of mouse subunit *a* constructs; $a2_{1-58}$ and $a2_{134-393}$.** N-terminal mouse *a2* proteins, $a2_{1-58}$ and $a2_{134-393}$ were expressed in BL21 as shown in *lanes 1 -2* (U and I represent uninduced and induced samples) at 37 C for 3 h with 1 mM IPTG. Successful clones were further checked for the solubility of protein in various buffers. One representative buffer is shown here in *lanes 3 – 4* for respective constructs (P and S represent pellet and supernatant, respectively). Respective position of proteins bands on SDS gel (17%) are shown by *.

3.3.9 NMR solution structure of subunit $a2_{386-402}$ of mouse V-ATPase *a2* isoform

To further characterize and study V-ATPase subunit *a*, attention was focused to the important regions of the protein and a short length peptide was kindly provided by Prof. Vladimir Marshansky (MGH, Harvard University, Boston, USA) which I used for structural

studies using high resolution NMR techniques. The region 386 – 402 of mouse V-ATPase subunit *a2* isoform have been recently shown essential for binding to the ARNO protein (Figure 47) (MERKULOVA *et al.,* 2009), regulating vital physiological processes of protein trafficking and degradation at the cellular level in a tightly co-ordinated and regulated manner (HURTADO-LORENZO *et al.*, 2006; MARSHANSKY, 2007). Secondary structure prediction of this region of protein shows a flexible region between two helices and the peptide length is mostly predicted to be unstructured with C-terminal helix as shown in figure 35 (MCGUFFIN *et al.*, 2000). The peptide was dissolved in water and NMR experiments were recorded on 700 MHz Bruker Avance spectrometer at a peptide concentration of 1 mM.
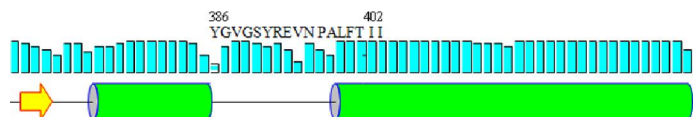
Figure 35. **Secondary structure prediction of a region involving peptide *a2*386-402 of mouse V-ATPase**. Secondary structure predictions show that majority of region is unstructured with C-terminus strongly -helical forming a sandwich between two helical bundles that is essential for interaction with ARNO protein. Secondary structure prediction was performed by online PSI-PRED server which uses PSI-BLAST in its dual neural network analysis.

3.3.9.1 Assignment of V-ATPase *a2*386-402

Amino acids in the primary sequence of peptide *a2*386-402 were sequentially assigned as per the standard procedure described in method section 2.2.19.2. 2D TOCSY and 2D NOESY raw data was processed using in-built Topspin software (Bruker). NOESY and TOCSY experiments were recorded at a mixing time of 300 ms and 60 ms respectively. 2D NOESY experiments recorded at 250 ms and 400 ms did not show any variation. All the amino acids were sequentially assigned as demonstrated in figure 36, showing the assigned HA region of the 2D NOESY spectrum. Primary sequence amino acid marking was followed by the assignment of cross peaks by overlaying TOCSY and NOESY spectra. Identified cross peaks in HN-HN region are displayed below in the figure 37A designating -helical content in the peptide. HN–HN, H – HN(i, i+3), H –HN(i, i+4), and H –H (i, i+3) connectivities were plotted from the assigned NOESY spectrum (Figure 37B) indicative of -helical formation in the C-terminus.
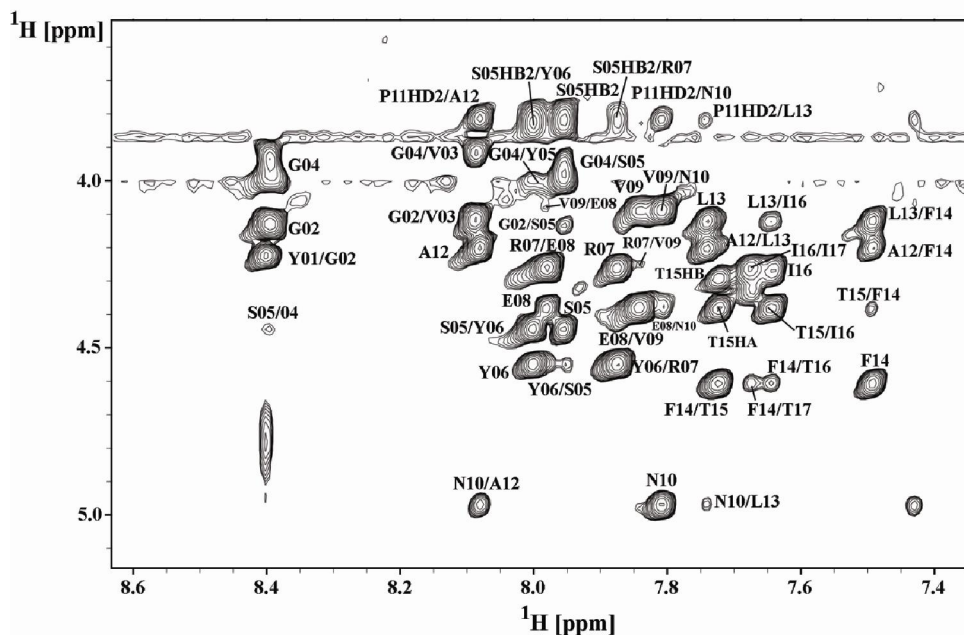
Figure 36. **2D NOESY spectrum of subunit *a2* peptide *a2*_{386-402} showing -proton peaks.** All peaks were sequentially assigned from homonuclear two dimensional NOESY and TOCSY spectra as per the standard procedure described in section 2.2.19.2. TOCSY and NOESY experiments were recorded on 700 MHz Avance Bruker machine with mixing time of 300 ms and 80 ms, respectively, at a peptide concentration of 1 mM dissolved in 50% deuteriated TFE-d3.
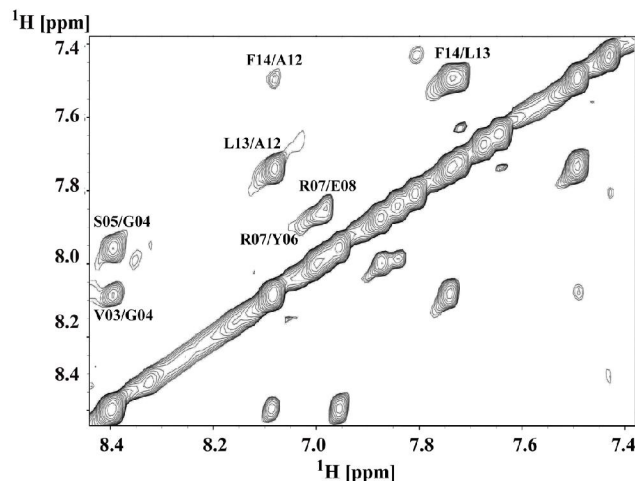
(A)   **(B)**
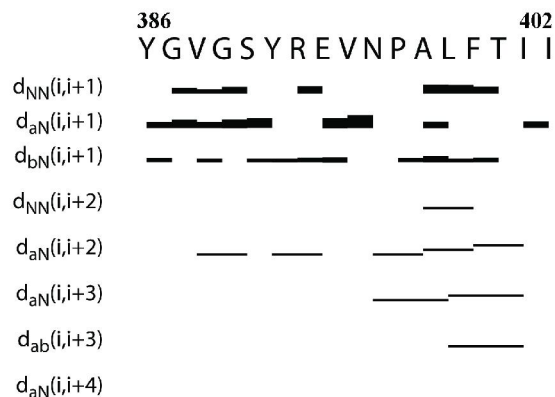
Figure 37. **(A) Assignment of cross-peaks in the NOESY spectrum of subunit *a2* peptide *a2*_{386-402}.** Figure shows NOESY cross-peaks in the HN-HN region of spectrum. Peak picking was done in Sparky 3.110 software and cross peaks were identified based on TOCSY spectrum**. (B)** Showing the NOESY connectivity plot of peptide *a2*_{386-402} indicative of the residues connected in space revealing the presence of helical structure in the C-terminus of the peptide.

3.3.9.2 Structure calculation of subunit *a2*_{386-402}

Data from assigned 2D NOESY spectra, torsion angle calculated from HA values by TALOS software and primary amino acid sequence were used as input for the automated

structure calculation by Cyana 3.0 package (HERRMANN *et al.*, 2002). Initial output was further refined by excluding the torsion angle strains and calculations done solely based on the NOESY data. In total an ensemble of 30 calculated structures resulted in an overall mean root square deviation (RMSD) of 0.68 ± 0.29 Å (Figure 38). All these structures have energies lower than -100 kcal mol^{-1}, no NOE violations greater than 0.3 Å and no dihedral violations greater than 5º. The summary of the statistics for 30 structures are shown in table 6. The calculated structure displays a flexible N-terminal region and an -helical C-terminus as shown in figure 38A, representing an overlay of 30 calculated structures. Even though the peptide has flexible N-terminus region, which is in line with the predicted secondary structure as calculated from the primary amino acid sequence (Figure 35), the overall structure has high consistence of maintaining the conformation, which is also reflected in the RMSD and cross-peaks in this region and indicative of a structure, which might be essential for specific interactions with other proteins. The PDB structure was further analyzed by PDBSum online software (LASKOWSKI *et al.*, 2005) and the analysis of surface cavities and clefts (Figure 38D) revealed that the protein structure might be essential for the interaction with other partners via its large cleft formed by the flexible region in the N-terminus, which is sandwiched between two helical ends (LASKOWSKI *et al.*, 1996). The structure gives important insights into this region of subunit *a,* an important component of the vacuolar ATPase.

(A) **(B)**
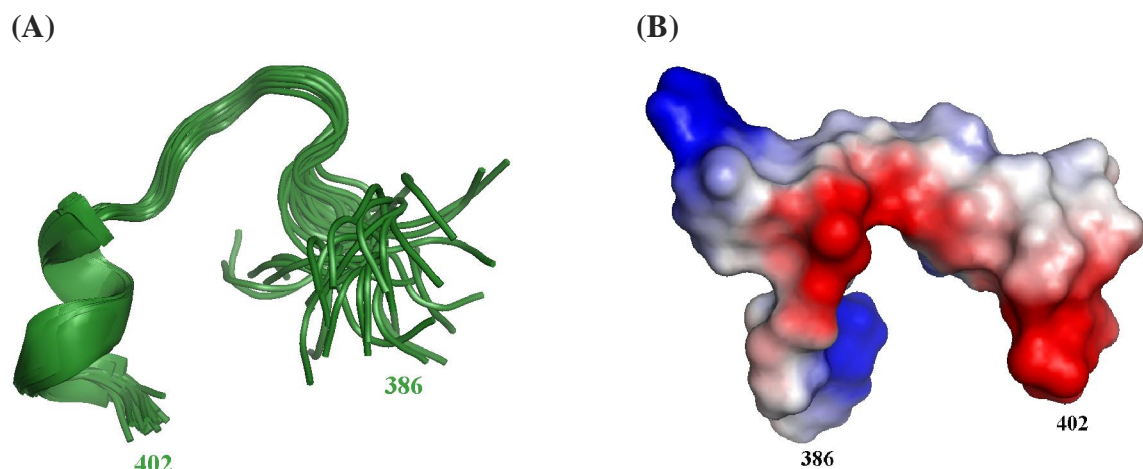
Figure 38. **3D NMR structure of peptide** *a2$_{386-402}$.* (**A**) Cartoon representation of the NMR structure of peptide *a2$_{386-402}$* showing superimposition of 30 structures calculated by Cyana 3.1 package revealing an unstructured N-terminus and helical C-terminus. The figure **B** shows the molecular surface electrostatic potential of peptide *a2$_{386-402}$* generated by Pymol (DELANO, 2001), where the positive potentials are drawn in blue and negative in red.

(C)   **(D)**

Figure 38. contd. (**C**) Overlay of cartoon and electrostatic surface potential of peptide and (**D**) surface cavities and cleft generated by PDBSum online software at EMBL (LASKOWSKI *et al.*, 2005) which uses PDB structure file to generate the output, showing the cavity in the upper panel and clefts in the lower panel, which might be essential for interaction with other proteins (LASKOWSKI *et al.*, 1996).
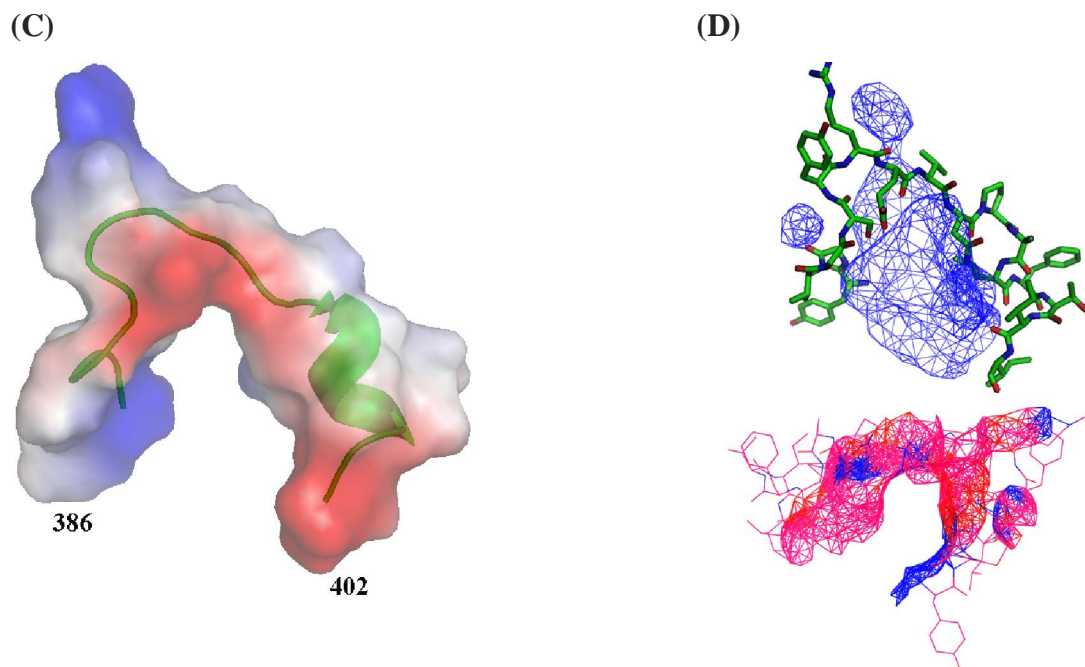
Distance restraints

Total	175
Intraresidue (i – j = 0)	45
Sequential (|i-j| = 1)	79
Short-range (i-j) <=1	124
Medium-range ($2 \leq |i-j| \leq 4$)	51
Long-range ($|i-j|$ 5)	0
Average number of violations	
Distance violations > 5 Å	0
Ramachandran plot[2] (%)	
Residues in most favoured regions	59.7
Residues in additionally allowed regions	31.9
Residues in generously allowed regions	8.3
Residues in disallowed regions	0.0
Average RMSD to Mean (Å) Backbone (C , C , and N)	0.68 ± 0.29

Table 6. **Structural statistics for mouse V-ATPase subunit *a2* peptide *a2*$_{386-402}$**

3.3.10 Structure of ARNO₃₇₅₋₄₀₀ and ARNO₃₇₅₋₄₀₀ (phos)

ARNO, a guanine nucleotide exchange factor (GEF) of small GTPase Arf6, is an essential component of endocytic regulatory machine and together they form key components of vesicular transport in eukaryotes (CHARDIN *et al.*, 1996; KLARLUND *et al.*, 1997; MEACCI *et al.*, 1997; FRANK *et al.*, 1998).   Previously it was reported that ARNO together with Arf6 are recruited from cytosol to endosomal membranes and the process was dependent on acidification caused by V-ATPase (MARANDA *et al.*, 2001) but the molecular mechanism remained elusive and the link between ARNO/Arf6 and V-ATPase remained unknown until more recently ARNO was found to directly associate with subunit *a2* isoform of V-ATPase and Arf6 with c-subunit of V-ATPase (HURTADO-LORENZO *et al.*, 2006). ARNO/*a2* interaction was intra-endosomal acidification-dependent and disruption caused reversible inhibition of endocytosis (MARANDA *et al.*, 2001). Arf6-GEF, ARNO protein consists of three domains: an N-terminal coiled-coil domain, a central catalytic sec7 domain, and a C-terminal PH domain (CHARDIN *et al.*, 1996) and a COOH-terminal polybasic sequence (NAGEL *et al.*, 1998). As demonstrated recently, the short 26 amino acid poly-basic region binds with *a2* and its interaction was dependent on the phosphorylation status at S392, whereby only the unphosphorylated form could assemble with the *a2* subunit (MERKULOVA *et al.*, 2009). To understand the structural changes accompanied with the phosphorylation status, I have solved the structures of ARNO₃₇₅₋₄₀₀ in its non-phosphorylated and phosphorylated forms by solution NMR spectroscopy.

3.3.10.1 Amino acid residue assignment for structure calculation of ARNO₃₇₅₋₄₀₀ and ARNO₃₇₅₋₄₀₀(phos)

2D NOESY and 2D TOCSY experiments were recorded at a mixing time of 300 ms and 80 ms respectively. 2D NOESY experiments recorded at 250 ms and 400 ms did not showed any variation. All raw data was processed using in-built Topspin software (Bruker). The amino acids in the primary structure of both ARNO peptides were assigned using standard procedure described in method section 2.2.19.2. All the amino acids were sequentially assigned using both NOESY and TOCSY data. Figure 39 shows the assigned NH region of the 2D NOESY spectrum. Primary sequence amino acid marking was followed by the assignment of cross peaks by overlaying 2D TOCSY and 2D NOESY spectra. Identified cross peaks in HN-HN region are shown below in the figure 39A and C, designating -helical structure in the peptide. HN–HN, H –HN(i, i+3), H –HN(i, i+4), and H –H (i, i+3) connectivities were plotted from the assigned NOESY spectrum (Figure 39B,D).

(**A**)
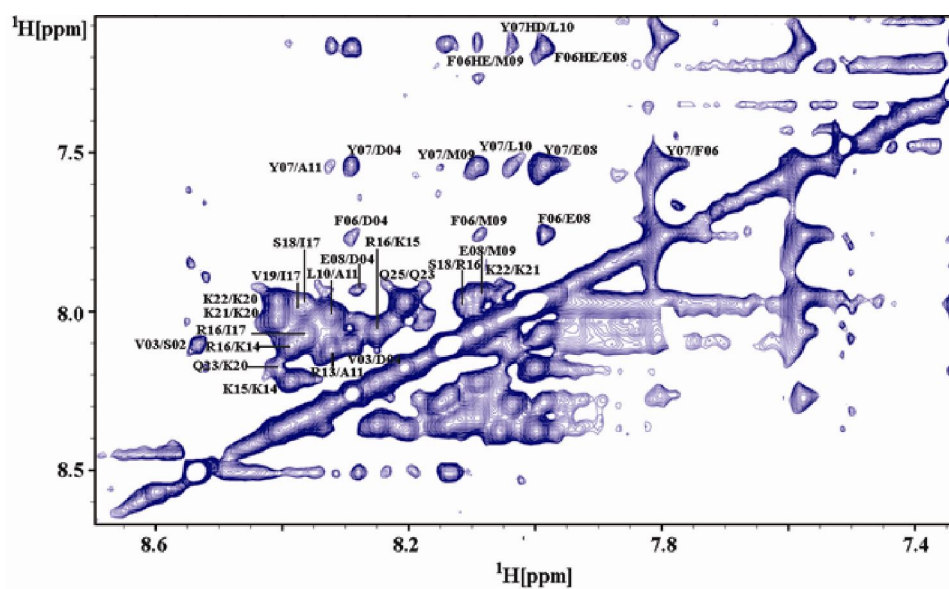
(**B**)

(**C**)
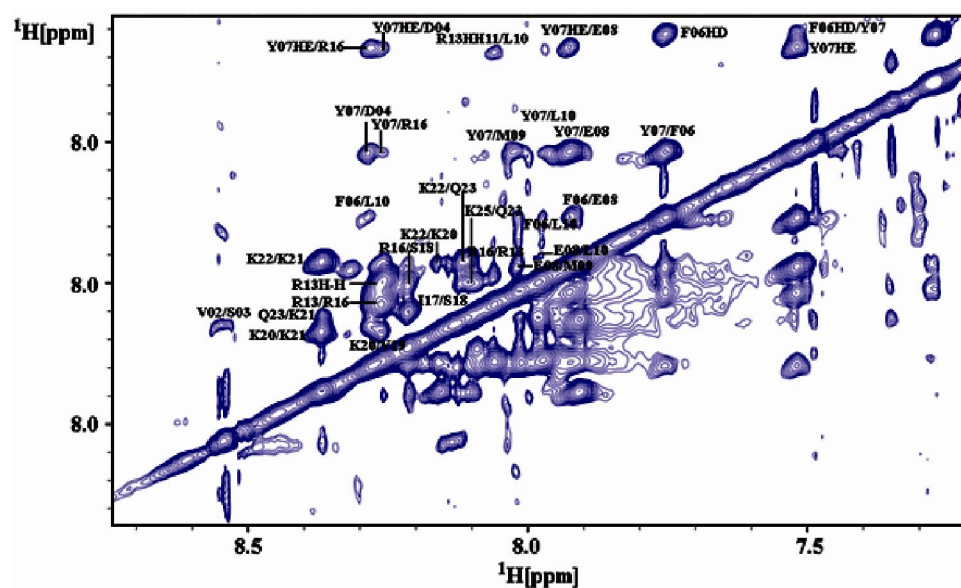
(D)

Figure 39. (**A-D**) **Assignment of cross-peaks in the NOESY spectrum of ARNO₃₇₅₋₄₀₀ and ARNO₃₇₅₋** **₄₀₀(phos)**. Figures **A** and **C** show NOESY cross-peaks in the HN-HN region of ARNO₃₇₅₋₄₀₀ and ARNO₃₇₅₋ ₄₀₀(phos) spectrum respectively. Peak picking was done in SPARKY 3.1 software and cross peaks were identified with reference to 2D TOCSY spectrum. (**B, D**) Showing the NOESY connectivity plot of ARNO₃₇₅₋₄₀₀ and ARNO₃₇₅₋₄₀₀ (phos), indicative of the residues connected in space revealing the presence of helical structures and stability of the region. Thickness of the connectivity bars is proportional to the intensity of the NOEs.

3.3.10.2 Structure calculation of ARNO₃₇₅₋₄₀₀ and ARNO₃₇₅₋₄₀₀(phos)

Data from assigned 2D NOESY spectra and primary amino acid sequence were used as an input for the automated structure calculation by Cyana 2.1 package (HERRMANN *et al.*, 2002). In total an ensemble of 20 calculated structures resulted in an overall mean root square deviation (RMSD) of 0.69 Å for non-phosphorylated ARNO₃₇₅₋₄₀₀ and 0.378 Å for ARNO₃₇₅₋ ₄₀₀(phos) (Figure 40). All these structures have energies lower than -100 kcal mol^{-1}, no NOE violations greater than 0.3 Å and no dihedral violations greater than 5º. Summary of the statistics for 20 structures are shown in table 7. The calculated structure ARNO₃₇₅₋₄₀₀ forms a stable N-terminus region with helix extending from 378-384, followed by a short loop from 385-387 and a second helix between 388-391 and third unstable 3₁₀-helix from 394-397 (Figure 40A-B). Reminder of C-terminus was mostly flexible (Figure 40A). Structural regions of ARNO₃₇₅₋₄₀₀ are also reflected in the NOE plot (Figure 39B). First helix is bent with an angle of 84.6º to second helix and a distance deviation of 77º is present between second and third helix of ARNO₃₇₅₋₄₀₀. Electrostatic potential surface analysis showed that the peptide is strongly basic in nature (Figure 40B), suggestive of its name, the poly-basic region of ARNO (NAGEL *et al.*, 1998; SANTY *et al.*, 1999).

Structural assignment and calculation of ARNO₃₇₅₋₄₀₀(phos), on the other hand, revealed that the phosphorylated form of ARNO forms a very stable structure in solution (Figure 40C-D).

Analysis showed that it forms a helix-loop-helix structure (Figure 40C) with a bent of 96º between the two helices. The first -helix at the N-terminus extends from 377-384 and second at the C-terminus from 390-396 (Figure 40C). The loop between the two helices extended from residues 385-389. Electrostatic surface potential as displayed in figure 40D was similar to that of the unphosphorylated form (Figure 40B).

(A)

(B)

(C)

(D)
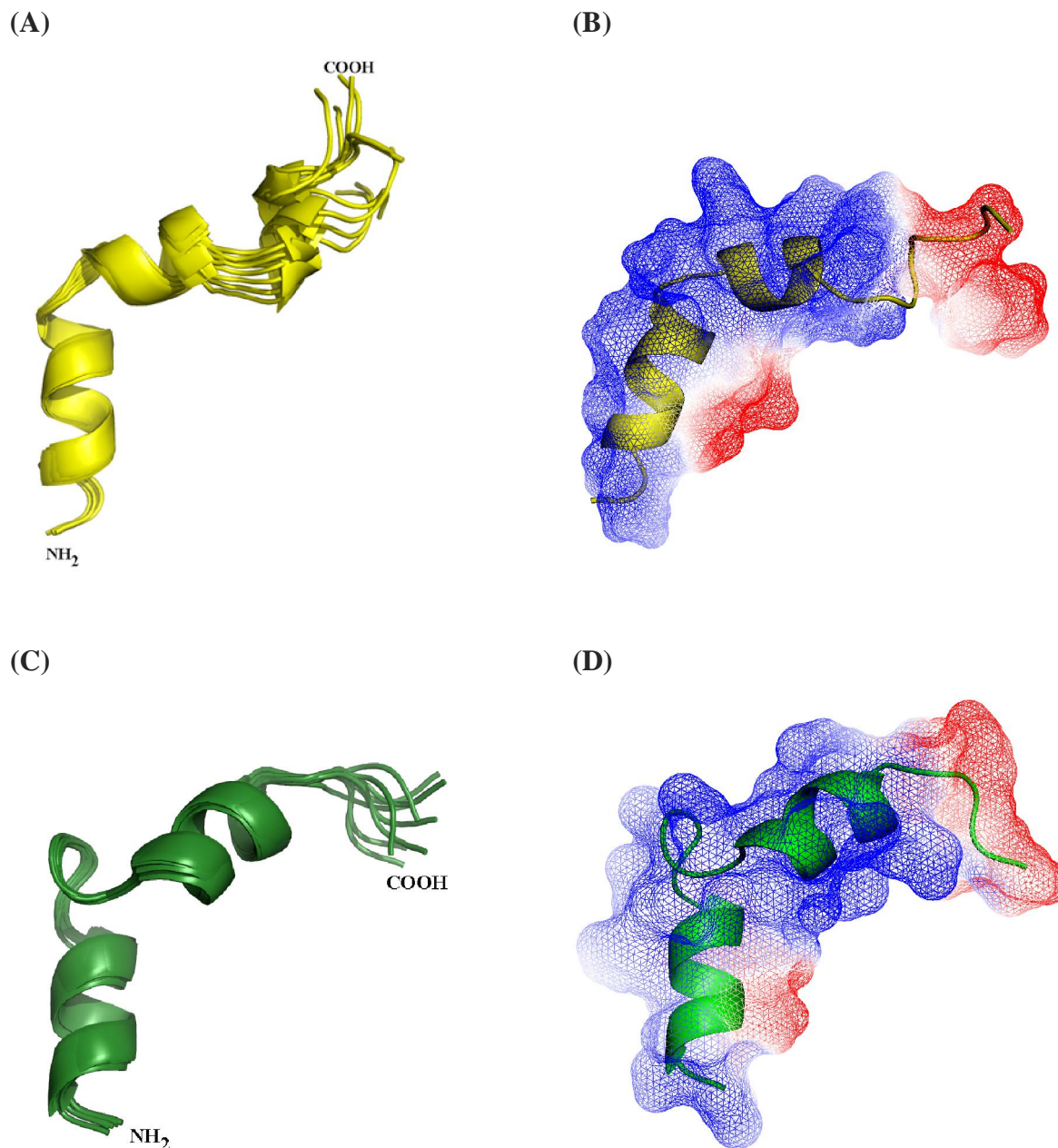
***Figure 40.* 3D NMR structure of peptide ARNO$_{375-400}$ and ARNO$_{375-400(phos)}$.** (**A-B**) Cartoon representation of the NMR structure of peptide ARNO$_{375-400}$, showing superimposition of 10 structures calculated by Cyana 3 package revealing an -helical N-terminus and a partially folded C-terminus. Figure **B** shows the qualitative molecular surface electrostatic potential of ARNO$_{375-400}$ calculated by Pymol 0.99rc6 (DELANO, 2001) which makes averaging of charges over a small region of space using a quasi-Columbic-shaped convolution function implemented in Pymol (http://www.pymol.org/). The positive potentials are drawn in blue and negative in red. (**C-D**) 3D structure of ARNO$_{375-400(phos)}$ showing an overlay cartoon of 10 structures and electrostatic surface potential of peptide is shown in figure D calculated as above.

3.3.10.3 Structural variation between non-phosphorylated (ARNO$_{375-400}$) and phosphorylat--ed (ARNO$_{375-400(phos)}$) forms of ARNO

Regulation of various proteins by phosphorylation/dephosphorylation is well established and play central role in the regulation of various processes in cellular physiology. Here, I have solved the structure of ARNO poly-basic region domain structure in its non- and phosphorylated form (Figure 40). Both forms displayed a helix-loop-helix structure with obvious difference accompanied by the phosphorylation at serine 392. The non-phosphorylated form displayed only a stable N-terminal helical domain (Figure 40A) and a short loop whereas only minor part of C-terminus could form the helix and most of the regions showed strong flexible tendency. On the other hand, the phosphorylated form of this poly-basic domain of ARNO formed a completely stable helix-loop-helix structure as shown in figure 40C. Structural comparisons as shown in the figure 41 have been done. Superimposition of the two structures in the native (red) and phosphorylated (blue) form via N-terminus 1-10 residues (Figure 41 A) showed a nice fitting in this region with root mean square deviation of 0.68 Å but the C-termini of both peptides showed the remarkable differences. Also the loop region in the phosphorylated form was more extended and adopted a different geometry in comparison to the non-phosphorylated form. Structural variations were also evident among different molecules of the same form of non-phosphorylated ARNO$_{375-400}$ (Figure 40A-B). An alignment via N-terminus of two peptides resulted in a distance deviation of 105° between the C-termini of non-phosphorylated ARNO$_{375-400}$ and phosphorylated form. Superimposition of the structure over the whole length of domain showed very poor similarities with RMSD values exceeding 2.5 Å. Though the ARNO$_{375-400(phos)}$ maintained two helices and a loop structural configuration, the non-phosphorylated ARNO$_{375-400}$ displayed tendency to form two -helices in the C-terminus besides the additional -helix at N-terminus common to both the structures. In comparison thus ARNO$_{375-400}$ forms two loops between three helices whereas the ARNO$_{375-400(phos)}$ form one loop between two -helices configurations. The structural comparisons between the phosphorylated and the unphosphorylated forms of ARNO$_{375-400}$ also demonstrated that phosphorylation influenced the structural changes in the C-termini, resulting in the disruption of -helix in the non-phosphorylated ARNO at S392. A continuous helix formation at S392 in ARNO$_{375-400}$(phos) and break of helix at same position in ARNO$_{375-400}$ is indicative of possible electrostatic stabilization of negatively charged S392 by adjacent basic lysine residues (ERRINGTON and DOIG, 2005).

(A)

(B)

(C)

(D)

(E)
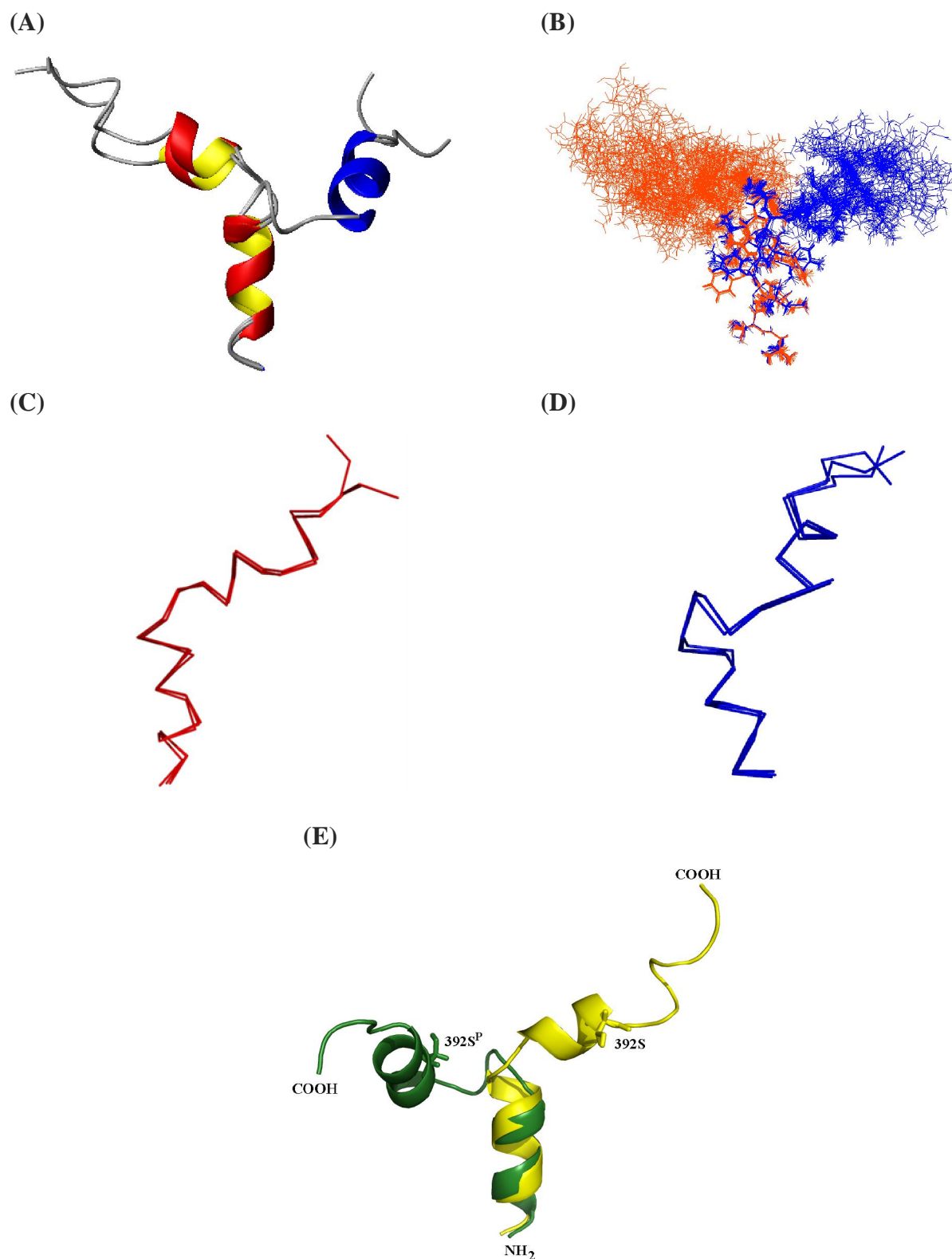
***Figure 41*. Structural comparison of ARNO$_{375\text{-}400}$ and ARNO$_{375\text{-}400 \text{ (phos)}}$.** (**A**) Superimposition of ARNO$_{375\text{-}400}$ (red) and ARNO$_{375\text{-}400 \text{ (phos)}}$ (blue) over the N-terminus (bottom region of structure) showed nice overlap but remarkable differences were seen in the C-terminus and loop regions, (**B**) shows the line diagram of figure A with evident flexibility of C-terminus in ARNO$_{375\text{-}400.}$ (**C-D**) Ribbon diagram of ARNO$_{375\text{-}400}$ (red) and ARNO$_{375\text{-}400(phos)}$ (blue), respectively, revealing the superimposition of three structures in each. (**E**) Structural changes at S392. Disruption of -helix at S392 was observed in the non-phosphorylated form of ARNO$_{375\text{-}400}$ (yellow). On the other hand, the phosphorylated ARNO$_{375\text{-}400}$ (green) displayed a continuous helix at S392.

Distance restraints	ARNO$_{375-400}$	ARNO$_{375-400(phos)}$
Total	316	305
Intraresidue (i – j = 0)	96	80
Sequential (|i-j| = 1)	102	98
Short-range (i-j) <=1	198	178
Medium-range ($2 \leq |i-j| \leq 4$)	118	102
Long-range ($|i-j|$ 5)	0	25
Average number of violations		
Distance violations > 5 Å	0	0
Ramachandran plot[2] (%)		
Residues in most favoured regions	81.4	88.0
Residues in additionally allowed regions	18.6	12.0
Residues in generously allowed regions	0.0	0
Residues in disallowed regions	0.0	0.0
Average RMSD to Mean (Å) Backbone (C , C , and N)	0.698	0.378

Table 7. **Structural statistics for ARNO$_{375-400}$ and ARNO$_{375-400\ (phos)}$**

4. Discussion

4.1 Caspase mediated degradation of Livin (ML-IAP) in ARTS induced apoptosis and the caspase 3 target subunit *d* of eukaryotic V_1V_O ATPase

Apoptosis is an essential molecular process that decides the fate of cell: to die or not (REED, 2000). ARTS is an unusual Septin family protein (LARISCH *et al.*, 2000), a group of GTPases involved in structuring cell shape, morphogenesis and division (FIELD and KELLOGG, 1999). ARTS is the least characterized pro-apoptotic protein that is released from mitochondria into the cytosol and subsequently translocates to nucleus during apoptosis (LARISCH *et al.*, 2000). A summary of apoptotic events and role of ARTS in summarized in figure 43. ARTS regulation via ubiquitination has been previously found in the cells under non-apoptotic conditions (LOTAN *et al.*, 2005). ARTS is a short lived protein ($t_{1/2}$~30 min) and is also suspected to constantly leak from mitochondria to cytosol in healthy cells (LOTAN *et al.*, 2005). However, whether ARTS does also undergo ubiquitination during apoptosis and if there is role of Livin is less understood. Livin protein is an E3 ligase, that undergoes self-ubiquitination in healthy cells and is also responsible for ubiquitination of proteins such as Smac/DIABLO, a pro-apoptotic protein released from mitochondria during apoptosis (MA *et al.*, 2006).

Here in this study, effect of Livin on ARTS in healthy or apoptotic cellular conditions was examined, where I found that E3 ligase activity of Livin did not promote ubiquitin proteosome mediated degradation of ARTS in either of the two circumstances (Figure *1*A, page 62). Basal level accumulation of ARTS polyubiquitination forms, however, could be found in the non-apoptotic cells that were unaffected by the Livin presence. Observed ubiquitination of ARTS in non-apoptotic conditions may be attributed to previously reported ubiquitin proteosome pathway (LOTAN *et al.*, 2005). Under identical conditions, when cells were induced to undergo apoptosis, no ubiquitination of ARTS could be seen (Figure 1B, page 62) and even basal levels, as detected in the non-apoptotic cells, disappeared. ARTS is known to be protected from ubiquitination during apoptosis (LOTAN *et al.*, 2005). Thus, based on these results it can be concluded that Livin does not act as E3 ligase to ARTS in apoptotic or non-apoptotic cells and role of any other IAP member remains to be studied.

During ARTS ubiquitination experiments, Livin levels were found to get rapidly depleted in apoptotic conditions in the presence of ARTS (Figure 1B, page 62). Further studies were done to examine the changes in the Livin levels at different time points as shown in the figure 2A (Page 63). A significant decrease in Livin levels were noted during STS induced apoptosis in presence of ARTS (Figure 2A, page 63). Although Livin degradation was also observed in apoptotic cells in absence of ARTS but half life was more stable compared to ARTS presence. Thus, ARTS

appears to enhance the degradation of Livin in apoptotic cells. More importantly, a 10 kDa fragment of Livin was produced in presence of ARTS in apoptotic stress, was absent in the control. This also raises the possibility that Livin might be degraded by different pathways in the presence or absence of ARTS in apoptotic cells. To evaluate the pathway involved in Livin down regulation during ARTS-promoted apoptosis, two possible hypothesis were speculated; (i) ubiquitin-proteosome pathway dependent upon the E3 ligase activity of Livin resulting in its self-mediated degradation and (ii) protease pathway involving caspases, the effector molecules of apoptosis, which cleave their substrates at tetra peptide sequence after aspartate residue (SALVESEN and DIXIT, 1997; NACHMIAS *et al.*, 2003; YAN *et al.*, 2006). Ubiquitin-proteosome pathway might play a role due to the presence of the RING domain in Livin which promotes self-ubiquitination in IAPs. As assessed from results obtained from the experiment to evaluate the first hypothesis, I found that Livin undergoes ubiquitin mediated degradation in non-apoptotic cells in compliance with the previously reported findings (MA *et al.*, 2006), but its ubiquitination was reduced when cells were treated with STS to undergo apoptosis (Figure 3, page 64). Ubiquitination was further diminished in ARTS presence (no STS treatment) (Figure 3, page 64). In contrast, a heavy depletion was seen in the Livin levels in presence of ARTS (STS treated cells) (Figure 3, *lane 4*) but more importantly, no increase of its polyubiquitinated forms could be observed. Also, these results reveal that Livin was degraded even if the proteosome pathway was blocked by MG132 treatment (Figure 3, page 64). Two major observations: first, there was no concomitant increase in Livin poly-ubiquitination which might correlate with the observed degradation; secondly, degradation of Livin was not prevented by MG123. Thus, the observed downregulation of Livin during ARTS-promoted apoptosis appears to be independent of ubiquitin proteosome pathway and the proposed first hypothesis seemed less likely true. The decrease detected in absence of ARTS, which did not produce 10 kDa fragment, appears to be the result of proteosome pathway as shown in figure 3, as well as the reported unstable behavior of Livin, which is constantly degraded via the proteosome pathway (MA *et al.*, 2006). Additionally, in earlier studies it has been reported that during caspase mediated apoptosis, the proteosome pathway becomes inhibited (SUN *et al.*, 2004), thus the cleavage/degradation pattern of Livin found in ARTS apoptosis, might be result of caspase cleavage. To examine the second hypothesis, where I speculated possible role of caspases in the observed cleavage and depletion of Livin, various caspase inhibitors were used (Figure 4-5, pages 65, 67). These results indicated that Livin could be rescued from degradation by pan-caspase inhibitor ZVAD-FMK and more than 90% of the Livin was prevented from degradation at 4 h following apoptotic induction,

while more than 50% was left at 6 – 8 h time slot (Figure 4, page 65). Inhibition of degradation by non-specific caspase inhibitor ZVAD-FMK indicates that caspases might be involved in the observed degradation/cleavage of Livin in ARTS-mediated apoptosis. Furthermore, to examine which member of this class of proteases is involved, specific caspase inhibitors of caspases were employed. The caspase 8 inhibitor Z-LETD-FMK showed significant recovery in the Livin levels at 4 h, which was comparable to pan-caspase inhibition, but inhibition beyond 4 h was not very efficient and Livin was degraded (Figure 5, page 67). Caspase 9 and 3 inhibitors could also partially prevent Livin degradation. ARTS is thought to regulate caspase activity by releasing IAP-mediated inhibition of caspases (LARISCH, 2004; YOSSI *et al.*, 2004) and results obtained here supports this model. IAP inactivation has been demonstrated to be important for execution of cell death (YOSSI *et al.*, 2004). Drosophila IAP antagonist proteins Reaper, Grim and Hid have been reported vital for releasing caspase inhibition and cell death and their absence can prevent cells from virtual apoptosis (JI YOO *et al.*, 2002) (HOLLEY *et al.*, 2002). Although there is no detectable similarity between ARTS and drosophila antagonist (JI YOO *et al.*, 2002) yet ARTS may be an important IAP antagonist in mammalian system owing to its emerging role in apoptosis. Besides Livin cleavage, high levels of active caspase 7 were found during ARTS induced apoptosis directly correlating with Livin degradation. Although direct involvement of caspase 7 could not be ascertained in this study but caspase 7 cleavage site at $DHVD_{(54)}$ in Livin has been reported (NACHMIAS *et al.*, 2003). Livin cleavage into 10 kDa fragment is known to result in the loss of its anti-apoptotic affect (NACHMIAS *et al.*, 2003) as well as reported important for its proper localization inside the cell to exert a pro-apoptotic affect after the cleavage (NACHMIAS *et al.*, 2007).

Involvement of more than one caspases in the cleavage of Livin cannot be ruled out since Livin has 14 aspartate residues in its protein sequence (Figure 2B, page 63) which may act as preferred substrate sites for cysteine proteases, caspases. $DHVD_{52}$ in Livin protein sequence is reported Caspase -3 and -7 cleavage site (NACHMIAS *et al.*, 2003). Group II caspases (Caspase -2, -3, and -7) prefer for DXXD tetramer sequence in their substrates where as group III caspases (Caspase -8, -9) prefer aliphatic amino acid at P4 position (fourth residue towards N-terminus from C-terminus aspartate) (EARNSHAW *et al.*, 1999). Accordingly, potential caspase -8 and -9 cleavage sites are GPKD $_{(5)}$ LGLD $_{(43)}$, GSWD $_{(178)}$, GARD $_{(238)}$ and VCLD $_{(257)}$ are shown in figure 2B (boxed cleavage sites). Subscripts refer to aspartate residue position from N-terminus of Livin. Also, Caspase 3 has been shown to cleave various substrates at different unconventional sites (SAMEJIMA *et al.*, 1999; AFFAR *et al.*, 2001; BASU *et al.*, 2002). Thus,

in addition to the preferred caspase cleavage sites other non-conventional sites located at 23, 96, 120, 138, 161, and 185 aspartate residue positions from N-terminus may also be utilized during its cleavage. 10 kDa fragment may be the product of $DHVD_{52}$ as has been reported (NACHMIAS *et al.*, 2003). These findings are in confirmation with the reports that proteosome is inhibited during apoptosis (SUN *et al.*, 2004). This may explain inhibition of Livin autoubiquitination and its degradation via caspases, as well as ARTS protection from ubiquitination during apoptosis. ARTS is a pro-apoptotic protein and is expected to be more stable during apoptosis than anti-apoptotic proteins, in order to execute cell death. Results also points out that the cleavage might be the result of non-canonical caspases or multiple non-canonical cleavage sites in line with the previously reported findings, which showed that mutation of Livin at caspase 3 cleavage site Asp(52) to Glu did not abolish the caspase activity to Livin (YAN *et al.*, 2006) indicative of non-canonical caspase (or recognition sequence) role.
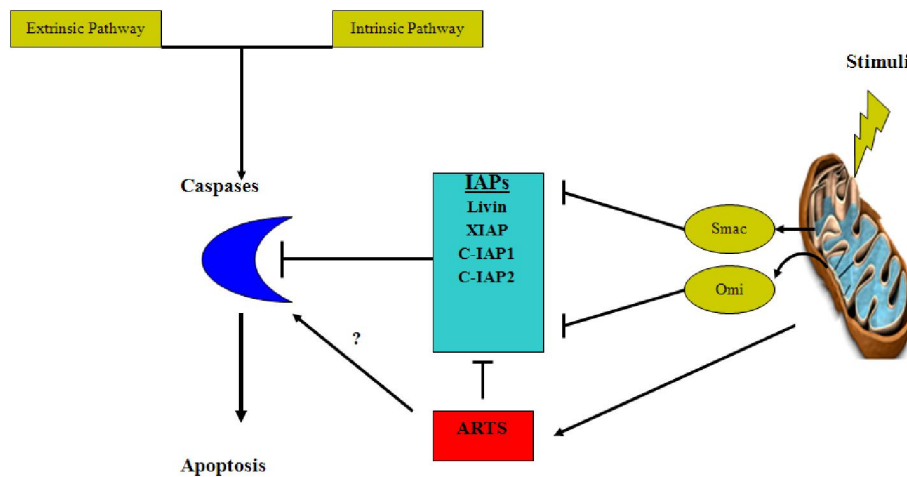
Figure 42. Apoptosis is characterized by the activation of the effector enzymes known as caspases, which leads to the dismantling of cellular processes that is associated with the morphological and biochemical changes observed during apoptosis. Caspases are activated by two different pathways; extrinsic pathway involving cell surface receptor stimulation and intrinsic pathway involving defects within the cells such as DNA damage or cell cycle arrest (REED, 2000; ZHAOYU and EL-DEIRY, 2005). IAPs are anti-apoptotic proteins and their activities are modulated by the factors released from the mitochondria such as Smac/DIABLO and ARTS resulting in the activation of caspases, concomitantly degrading the anti-apoptotic IAPs.

Under normal physiological conditions, caspase are present in their zymogen inactive forms and activated forms are subjected to inhibition by IAPs. ARTS release during apoptosis is a caspase independent event, and its discharge from mitochondria to cytosol results in possible removal of caspase inhibition, by targeting IAPs, resulting in caspases activation as an initial event of ARTS-mediated apoptosis (Figure 43). Activated caspases then promote caspase dependent events including release of pro-apoptotic factors from mitochondria, which is followed by amplification phase where several caspases are activated (Figure 43). This is a proposed model

based on the results obtained here. More work will be required to fully understand the whole mechanism. In conclusion the regulation of apoptosis by IAPs is more complicated phenomenon and awaits more discoveries.
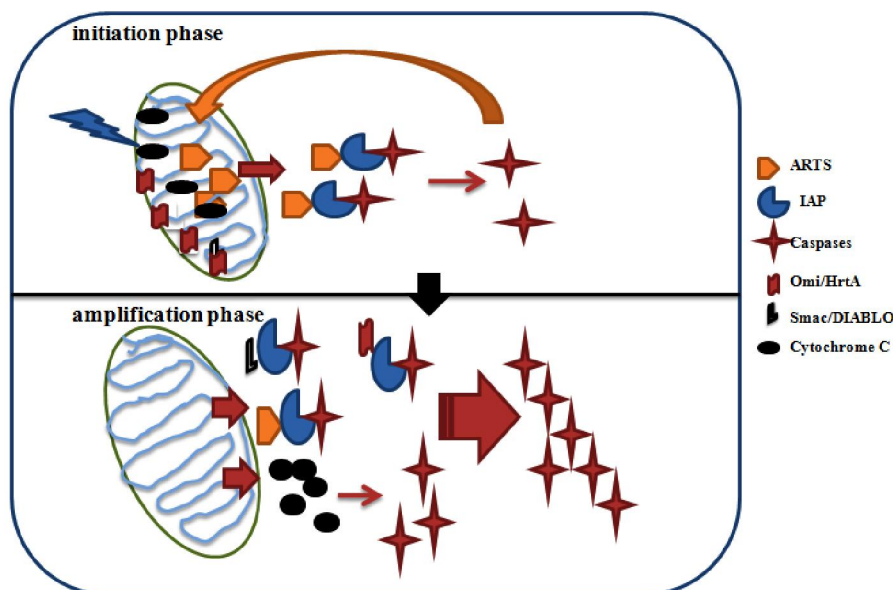
***Figure 43.* ARTS in apoptosis.** Apoptosis stimuli results in the release of ARTS from the mitochondria and its association with the IAPs such as XIAP (LOTAN *et al.*, 2005). The association results in the release of caspase inhibition and so their activation. The activated caspases do cause further amplification of the degradative processes by their action on the mitochondria which results in the release of pro-apoptotic protein such as Smac/DIABLO. Such hypothesis has been proposed in the previous studies with XIAP and results described here show the degradation of Livin in ARTS mediated apoptosis. Thus a common mechanism of ARTS apoptosis is anticipated.

Vacuolar ATPases (V_1V_O ATPases) are inevitable part of cellular machinery and they regulate the acid/base balance via their proton pumping activity. Vacuolar ATPases are composed of several subunits (at least 14 in yeast V-ATPase) arranged in two major sub domains, V_1 and V_O (GRÜBER and MARSHANSKY, 2008). Cellular acidity is an essential parameter within the cells, an increase in the acidity of the cell is associated with apoptosis and is believed to trigger initiation phase of cell death by apoptosis (PARKHIROTO *et al.*, 2003; LAGADIC-GOSSMANN *et al.*, 2004). Several anti-apoptotic agents act via alkalization of the cell pH and use of specific inhibitors of V-ATPases results in apoptotic death of cells (LONG *et al.*, 1998). Intracellular acidosis amounting to the pH of 0.3 – 0.4 is detected when cells are exposed to UV light, treated with Staurosporin, Etoposide and other agents that cause cellular apoptosis (LAGADIC-GOSSMANN *et al.*, 2004), which implies that function of V-ATPases is hindered during apoptosis. In short, they are vital for cell survival and disruption of function causes apoptosis and they are being discussed as hot candidates for cancer therapeutics (HIROTO *et al.*, 2003; BOWMAN and BOWMAN, 2005). The roles of V-ATPases in apoptosis is an emerging new field, and subunit *d* and subunit C are pivotal constituents of V_1V_O ATPase which are

involved in the coupling of ATP cleavage to proton conduction, V_1V_O assembly as well as in the regulation of reversible disassembly phenomenon (IWATA *et al.*, 2004; ARMBRÜSTER *et al.*, 2005; OWEGI *et al.*, 2006). More importantly, both subunits are believed to be exposed on the surface of the complex, due to their observed cleavage upon mild proteolysis (ADACHI *et al.*, 1990; BAUERLE *et al.*, 1993; ARMBRÜSTER *et al.*, 2004). During the process of reversible disassembly of V_1 from V_O portion, subunit C is the only component that is lost from V_1 domain (SUMNER *et al.*, 1995; PARRA and KANE, 1998; KANE, 2000) and is also known to interact with the actin cytoskeleton (VITAVSKA *et al.*, 2003; VITAVSKA *et al.*, 2005). Owing to the diverse roles of subunit *d* and subunit C they were chosen to test their caspase cleavage. Initial results obtained showed that the cleavage of subunit His_3-*d* do occurs at the N-terminus of protein as cleaved fragment did not bind to Ni^{2+}-NTA column as shown in 7A (Page 71). The cleavage site was further confirmed by N-terminal protein sequencing, resulting in the identification of $_{47}$**SSTD** Y_{51} motif, in line with the results obtained from His-pull down assay (Figure 7,8; page 71,72). Since V-ATPases are vital for maintaining cellular homeostasis between various functions, cleavage of an essential component can induce the destabilization and loss of proton pumping activity of V_1V_O complex resulting in the collapse of vital activities and cell death. This is in parallel with the fact that the potential targets among the activated caspase during apoptosis are essential components of cells such as mitochondria and vacuolar systems (RICCI *et al.*, 2004). Again, V-ATPases have recently been shown to play essential role in the caspase 8 mediated cleavage of Bid (<u>B</u>H3-<u>i</u>nteracting domain <u>d</u>eath agonist) and requirement of Rb (<u>R</u>etino<u>b</u>lastoma) for Bid cleavage can be bypassed via inactivation of V-ATPase (HUANG *et al.*, 2007) in type 2 apoptosis in Rb deficient cells (Figure 44B). Bid (22 kDa) is a pro-apoptotic regulator of Bcl-2 family that is truncated to tBid (15 kDa) by caspase 8, which translocates to mitochondria to induce mitochondrial permeablization and release of apoptogenic factors (YIN, 2006). These findings point to a vital role that is being played by V-ATPase via directly interfering in apoptosis machinery by inhibiting a key component of apoptotic machinery. Also activation of V-ATPase have been reported to prevent apoptosis in various cell types, for example cardiomyocytes (GOTTLIEB *et al.*, 1996), to protect them against myocardial infarction and neutrophils, which were prevented from apoptosis in culture (GOTTLIEB *et al.*, 1995). Hence, activation of caspases, cleavage of V-ATPase subunits and subsequent inhibition thus can have great impact on the activation of apoptosis.

(A)
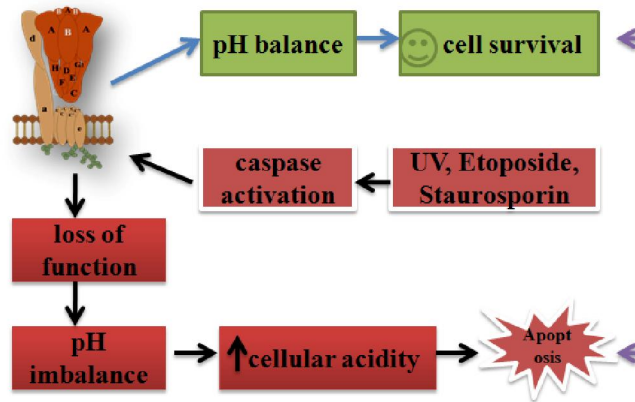
(B)
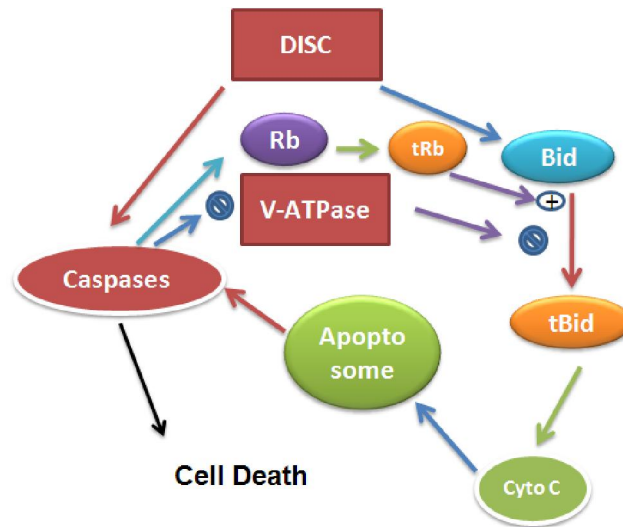
Figure 44. Possible role of V-ATPase in the process of apoptosis. (**A**) Vacuolar ATPase maintains a proper pH balance by constantly extruding protons from the cytosol and disruption of this activity by caspases during apoptosis may result in the elevation of cellular pH resulting in the execution of apoptosis (NANDA *et al.*, 1992) (**B**) The proposed role of V-ATPase in type 2 apoptosis. Inhibition of V-ATPase promotes Bid activation in Rb deficient cells, complimenting the requirement of Rb and thus promoting the cells to undergo apoptosis (HUANG *et al.*, 2007) demonstrating that V-ATPases have direct impact on the activation of key apoptotic components.

4.2   Structural and biochemical insights of subunit *d* of $V_1V_OATPase$

4.2.1 Low resolution structure of subunit *d* and formation of peripheral stalk

Subunit *d* is a non-integral protein with obvious absence of putative transmembrane regions, which remains firmly attached to the V_O membrane embedded domain unlike other peripheral subunits, which are either membrane embedded (for example, subunit *a*) or directly assembled to their soluble V_1 domain (for example, subunit A) (KANE *et al.*, 1989; ADACHI *et al.*, 1990; PUOPOLO *et al.*, 1992). This protein is an indispensable component of V-ATPase required for the assembly of Vo domain, and disruption of the subunit *d* gene results in the loss

of other membrane subunits like subunit *a,* as they fail to reach the membrane for assembly (BAUERLE *et al.*, 1993). Of the five eukaryotic V_O subunits, subunit *d* remains the least structurally and functionally characterized protein of V-ATPase.

Here, I report the successful attempt to purify and characterize this essential protein (Vma6p/subunit *d*) of *Saccharomyces cerevisiae* V-ATPase. Homogenous preparation of the protein was used to collect SAXS data from which a first low resolution structure could be solved. Subunit *d* in solution is a boxing glove-shaped molecule, consisting of two distinct domains (Figure 16, page 81), a major part with a width of about 6.5 nm and a protuberance of about 3.5 nm in length (THAKER *et al.*, 2007). A 3D electron microscopy reconstituted low resolution structure of V_O domain from negatively stained clathrin coated vesicles has been reported showing an asymmetric protein ring with two small opening on luminal side and a wide opening on cytoplasmic side overlaid with two uncharacterized masses (WILKENS and FORGAC, 2001). Of these two semi-circular fused masses (Figure 17, page 81), one of them is linked to the membrane, while the other mass is more exposed towards the cytoplasm but connected with the previous ring through a small bridge (WILKENS and FORGAC, 2001). According to 3D reconstituted model interpretations these additional densities were believed to be part of subunit *a* (N-terminal region) and subunit *d*, respectively (WILKENS and FORGAC, 2001). But due to the lack of structural data about these subunits, it remained elusive and an open question. Since we have now solved the first low resolution structure of subunit *d* (Figure 16, page 81), direct structural comparisons of the overall shape and domain organization of subunit *d* were made with the observed additional densities on the cytosolic face of V_O domain. Results indicated striking resemblance with overall shape of the membrane distal exposed mass in V_O structure with subunit *d* boxing glove shape as shown in figure 17 (THAKER *et al.*, 2007). Since subunit *a* is a *bona fide* membrane anchored protein, the location of subunit *d* became evident on the structural perspectives described here in figure 17, making a clear assignment of subunit *d* inside the V_O domain (THAKER *et al.*, 2007). Additional supporting data about the association of subunit *d* and *a* came from the observation that subunit *d* is unable to assemble with V_O in the cells lacking subunit *a* (GRAHAM *et al.*, 2000). Also, subunit *d* remains exposed on the cytosolic face, shown in the experiments, where mild proteolysis resulted in its cleavage in V_1V_O preparations (ADACHI *et al.*, 1990). In this direction, to understand the binding between two subunits, the initial results were obtained with fluorescence correlation and cross correlation spectroscopy (FCS, FCCS) experiments supporting that subunit *d* and the N-terminus of subunit *a*, a_{1-388} do associate with each other (Figure 29, page 97). Interaction was further confirmed by

an alternative approach of surface plasmon resonance (SPR) technique (Figure 30, page 99). The results of SPR revealed a strong affinity of interaction between subunit *d* and a_{1-388} with a dissociation constant (*kd/ka*) of $K_d = 6.0 (\pm1.8) \times 10^{-8}$ M (Figure 30) (THAKER *et al.*, 2009). These results showed the close proximity of subunit *d* and NH_2-domain of subunit *a* of yeast V_1V_O ATPase, and thus making a clear assignment of subunit *d* and subunit *a* inside the V_O complex.

To understand the binding partners of boxing glove shaped subunit *d* inside the V_1 and V_O domain, our laboratory has shown that subunit *d* does interact with subunit A thus linking the assembled *d* to V_1 domain (THAKER *et al.*, 2009). Taken together these data strongly support that subunit *d* is more extended in nature and do form a peripheral assembly with subunit *a* liking the V_O domain to the V_1 catalytic sector by directly associating with subunit A in the V_1. Previous findings have reported that the N-terminal region of subunit *a* is exposed on the cytoplasmic face of the vacuolar membrane (LENG *et al.*, 1999) and is also known to link directly with subunit A of the V_1 domain (LANDOLT-MARTICORENA *et al.*, 2000). Additionally, a peripheral orientation of subunit *a* and *d* in V_1V_O complex has been put forward in the previous works (FORGAC, 2000; CLARE *et al.*, 2006). All these existing data thereby strongly support that a peripheral stalk assembly formed by subunit *d* and *a* together with other subunits connecting V_1 with V_O in the fully assembled V-ATPase is a viable hypothesis put forward in previous studies (CLARE *et al.*, 2006; THAKER *et al.*, 2007). Such kind of peripheral structures has been shown in related F_1F_O ATP synthase where subunit *b* together with subunit links N-terminal part of the $_3$ $_3$ with membrane F_O subcomplex (SINGH *et al.*, 1996 ; WILKENS and CAPALDI, 1998). Taking into account the structural features of subunit *d*, we propose here that the small cavity of boxing glove shape structure forms a fit into the raised/exposed region of catalytic subunit A, which is typically formed by the non-homologous region (NHR) (Figure 45) (THAKER *et al.*, 2007). Both subunit *d* and the NHR of subunit A are characteristic features of eukaryotic V-ATPase which are absent from related F_1F_O ATP synthases (SHAO *et al.*, 2003). The NHR has been associated with the coupling of proton transport and ATP hydrolysis as well as reversible dissociation of V_1V_O *in vivo* (SHAO *et al.*, 2003). Furthermore, the NHR of subunit A has been shown to directly associate with a domain consisting of subunit *a* and subunit *d* of V_O subcomplex by the *in vivo* immunoprecipitation experiments (SHAO and FORGAC, 2004). Recently, besides the classical role of V-ATPase in the acidification of cellular compartments (GRÜBER, 2003), more refined features of these nano pumps have emerged (HURTADO-LORENZO *et al.*, 2006). V-ATPases has been reported to act

as a platform or scaffold for the interaction of small G-protein, Arf6 (ADP ribosylation factor 6) GTPases and corresponding guanine nucleotide exchange factors (GEF), ARNO (ADP-ribosylation factor nucleotide site opener), with the membrane ring subunit *c* and subunit *a*, respectively in a pH dependent manner, regulating the critical protein degradation pathways (HURTADO-LORENZO *et al.*, 2006). Proposed extended conformation of subunit *a* and *d* can make such interactions viable *in vivo* by providing a pH sensitive scaffold, regulating the networking of signaling pathways, which determines the fate of cell survival. In addition to this, the recent results also showed that C-terminal of subunit *d* is required for the retention of subunit E (OWEGI *et al.*, 2006), which imply that subunit *d* is directly influencing V_1 assembly and consequently all these data strongly support that subunit *d* is more extended *in vivo*, forming a peripheral stalk together with N-terminus of subunit *a* and subunit A (Figure 45) (THAKER *et al.*, 2009).
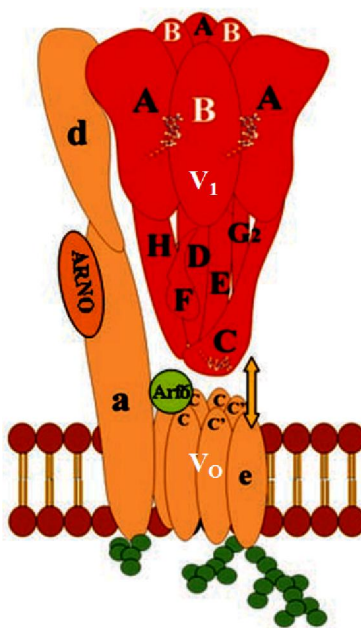
Figure 45. Proposed model of yeast V-ATPase showing an extended peripheral stalk, formed by the association of subunit *d* with subunits *a* and A, respectively, as per data obtained in the current study (GRÜBER and MARSHANSKY, 2008; THAKER *et al.*, 2009). N-terminal subunit a, a_{1-388} was shown to interact with subunit *d* using FCS and SPR techniques as well as with subunit A (THAKER *et al.*, 2009). Subunit *d* low resolution structure has been solved using SAXS measurements from homogenous recombinant protein preparations, which showed the protein consists of a two domain boxing glove shape structure in solution with a small cavity in the head domain, which we propose might be required for its association with the NHR-region of subunit A (THAKER *et al.*, 2007).

4.2.2 Structural aspects of subunit *d* of V-ATPase of *Saccharomyces cerevisiae*

Subunit *d* was isolated with a high degree of helicity in conformity with the predicted helical secondary structure as shown in figure 13 and analysis of $_{222}/_{208}$ ratio approached 1.0, which demonstrates the existence of helix-helix interaction, that might be relevant to the compact structure observed (Figure 16, page 81). Further, changes in the helix-helix interaction were

formed on the addition of cross-linking agent $CuCl_2$ demonstrating the close proximity of the cysteine residues (Figure 18, page 82). Initial results of cross-linking data were further studied by tryptic digestion and MALDI-TOF mapping of neighboring fragments using TMR or NEM labeled samples to follow the free cysteine residues which are on the surface or buried within, respectively. Peptide fingerprinting data (Table 3) revealed disulphide bond formation between Cys_{36} and Cys_{329}, bridging peptides $_{19}$GYRNGLLSNNQYIN LT QCDTLELK$_{43}$ and $_{322}$NITWIAECIAQNQR$_{335}$, demonstrating the near neighborhood of both termini and an example of helix-helix interaction inside the protein as discussed above (THAKER *et al.*, 2007). However, in DTT reduced samples smaller fragments from both termini were observed without any cross-linking. Sequence analysis of subunit *d* from all the eukaryotes described so far showed two and one conserved cysteine residues in the N- ($Cys_{36,127}$) and C-terminus (Cys_{329}), respectively (THAKER *et al.*, 2007). Close neighborhood of N- and C-termini is in line with the importance of these termini in proper folding and synthesis of this protein *in vivo* whereby subunit *d* constructs carrying deletions in the N- or C- termini (d_{1-328}, d_{1-298} and d_{38-345}) or at both termini in d_{11-189}, d_{38-189} and $d_{190-328}$ lead to less and/or unstable proteins, indicating major structural perturbations (Figure 23, page 89). Interestingly, a point mutation C329S also resulted in insoluble protein, demonstrating the essentiality of the cysteine bridge in the proper folding during its production (THAKER *et al.*, 2007). d_{11-345} was the only protein that could be purified in the amounts comparable to the wild type (Figure 24, page 91).

Moreover, changes in the structural conformations as monitored by tryptophan fluorescence could be observed when samples were either reduced, oxidized or left untreated as shown in figure 21 (Page 87), reflecting a change in the environment around the tryptophan residues. An increase in the quantum yield on reduction with DTT points to the enhanced polarity surrounding the tryptophan residues due to the possible conformational changes (THAKER *et al.*, 2007). However, minor variations were observed in CD data obtained in the presence of DTT but significant variations were seen when CD was measured in the presence of $CuCl_2$ (Figure 22, page 88), revealing a decrease in the -helical content in $CuCl_2$ cross-linked samples (THAKER *et al.*, 2007). These data reflect that the disulphide formation seems to be essential in the process of protein folding rather than stabilization of the produced subunit. It has been described that deletions of various lengths from N or C-termini destabilizes the subunit *d* and subverts the formation of a V_1V_O complex *in vivo* in yeast cells (OWEGI *et al.*, 2006). Further, various mutations in subunit strongly uncoupled proton translocation and ATP hydrolysis including a C329A mutation and 2-19 truncation prevented assembly of V_O and C-terminal truncations

resulted in the loss of subunit *d* at the membranes (OWEGI *et al.*, 2006). These results are in line with the biochemical data of subunit *d* (Vma6p) described here. Importance of disulphide during protein synthesis is further supported by the observation that a substantial increase in the levels of protein was observed in the expression *E. coli* host Rosetta-gami^{TM} 2 in comparison to BL21 (DE3) (Figure 10, page 76). Rosetta-gami^{TM} 2 (DE3) carries genetic modifications which facilitates enhanced disulphide formation compared to BL21 DE3 cells, but biochemically both proteins were alike (section 3.2.1). $CuCl_2$ addition created a disulphide bond between Cys_{127} and Cys_{165} as was made evident by tryptic digestion and MALDI-TOF analysis (Table 3, page 86). MALDI-TOF analysis of the non-reduced and $CuCl_2$ cross-linked *d* also revealed that Cys_{127} is accessible for NEM but not for the more bulky flurophore, TMR and therefore is not exposed in the protein, unlike the residues Cys_{165}, Cys_{207} and Cys_{296}. Biochemical modifications of protein with $CuCl_2$ and DTT altered secondary rather than tertiary structure as no overall changes in the measured SAXS data were observed (THAKER *et al.*, 2007).

Subunit C from A_1A_O ATP synthase has been proposed to be homologous to subunit *d* of V_1V_O ATPase in structure and function but at the same time a rather low (18%) sequence similarity could be found (IWATA *et al.*, 2004; YOKOYAMA and IMAMURA, 2005; OWEGI *et al.*, 2006; GRÜBER and MARSHANSKY, 2008) (THAKER *et al.*, 2007). A_1A_O ATP synthases are of archeal origin transferred by horizontal gene transfer (OLENDZENSKI *et al.*, 1998; BERNAL and STOCK, 2004) and they do synthesize ATP unlike that of V-ATPases, which hydrolyze ATP to drive the proton transport across the membrane (GRÜBER *et al.*, 2001; GRÜBER and MARSHANSKY, 2008). The high resolution structure of C subunit from *T. thermophilus* A_1A_O ATP synthase (IWATA *et al.*, 2004) showed that the protein is more compact and funnel shaped (Figure 46). The distance distribution function computed from the scattering pattern of the atomic model of the *T. thermophilus* C subunit (IWATA *et al.*, 2004) displayed that the structure differs significantly as compared with the subunit *d* (Figure 15B, page 80) (THAKER *et al.*, 2007). The symmetric profile of the distance distribution function characterizes the more compact structure of subunit C with a funnel shape (Figure 15B, page 80) (IWATA *et al.*, 2004). The major differences in the tertiary structure of subunit C of the bacterial A_1A_O synthase (IWATA *et al.*, 2004) and subunit *d* of the eukaryotic V_1V_O ATPase are that *d* is not only larger but also more anisometric, reflected by its boxing glove-shape and a two domain orientation (Figure 46). Superposition of the crystal structure of subunit C (IWATA *et al.*, 2004) and the low resolution structure of *d* presented in the figure 46, also indicates the differences in the additional volume of the upper domain and the protuberance of the lower part present in subunit *d*. Whereas

subunit *d* of V-ATPases is strongly attached to the V_O section during the physiological process of reversible disassembly of V_1V_O ATPase (KANE, 1995; SUMNER *et al.*, 1995; DAMES *et al.*, 2006) , subunit C of A_1A_O synthases are linked to the A_1 domain (CHABAN *et al.*, 2002; COSKUN *et al.*, 2004), thereby forming the bottom of the central stalk, and functionally linking the catalytic site events in the A_3B_3 hexamer with ion-conduction in the membrane section and vice-versa (CHABAN *et al.*, 2002). These structural, biochemical and topological diversities of both proteins are in line with the fact that subunit C of the *T. thermophilus* A_1A_O synthase does not functionally substitute for subunit *d* and does not complement the phenotype of *vma6* cells as shown most recently (OWEGI *et al.*, 2006).
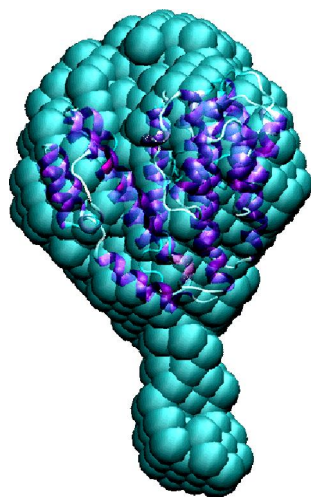
Figure 46. Superimposition of the A_1A_O ATP synthase subunit C (blue) structure (pdb 1r5z) on V-ATPase subunit *d* (green) (THAKER *et al.*, 2007). Subunit *d* showed a two domain boxing glove shape, whereas it's proposed homolog in the A_1A_O ATP synthase, subunit C, displayed more symmetrical funnel shaped structure. Besides the divergence in the topology and shape, both structures revealed difference in their overall volume as well (THAKER *et al.*, 2007).

4.2.3 Assembly subunit *d* with subunit G of yeast V-ATPase

From the SAXS results, subunit *d* was found to be an elongated molecule as shown in figure 16 (Page 81) and its association with V_O domain subunit *a* became evident when the structure was superimposed over the electron micrograph of V_O from bovine brain clathrin coated vesicle (THAKER *et al.*, 2007). The possible elongated assembly of *a/d* became more clear with the finding that subunit *d* interacts with subunit *a* and A (THAKER *et al.*, 2009). Subunit G is an elongated molecule in solution (ARMBRÜSTER *et al.*, 2003) and has been shown to interact with subunit *d* by immunoprecipitation pull downs (JONES *et al.*, 2005). However, no further studies have been reported to either map the domains or residues involved in the binding. We made the titration experiment with purified and ^{15}N labelled subunit G (^{15}N-G_{1-59}) in the presence of unlabeled subunit *d*, results as shown in figure 25 (Page 92),

demonstrating that these two proteins do interact in solution (RISHIKESAN *et al.*, 2009). The NMR studies in our lab have led to the complete amino acid assignment of HSQC spectrum of subunit G_{1-58} which was used to solve the 3D solution structure recently (RISHIKESAN *et al.*, 2009). Taking this advantage, subunit G $^{1}H^{15}N$ HSQC titration experiments in presence of subunit *d* showed the interaction between the two, and the already assigned HSQC spectrum was used to map the binding domain on G_{1-58} subunit. Analysis of the HSQC spectrum peaks revealed that the N-terminal region (Gly7-Lys34) of G_{1-58} is involved in association with subunit *d* (RISHIKESAN *et al.*, 2009). An intensity map of the residues involved in the binding to subunit *d* is shown in figure 25B (Page 92), indicating the assembly of subunit *d* with subunit G_{1-58} of the yeast V-ATPase occurs via the very N-terminus. The largest intensity changes were detected for the backbone amides of residues Ala9, Leu11, Glu15, Lys16, Ala18, His19, Val22 and Ala25 (B) (RISHIKESAN *et al.*, 2009). Recently, from our laboratory, a high resolution NMR structure of subunit G_{1-58} has been obtained which showed an extended -helix of about 68 Å (RISHIKESAN *et al.*, 2009). The entire subunit G is predicted to be a straight helix (ARMBRÜSTER *et al.*, 2003), and might be enable to bridge the V_1 and V_O domains of V-ATPase complex. The solution structure of subunit *d* described here showed that it consist of a 11 nm boxing glove shape, forming a two domain elongated structure (THAKER *et al.*, 2007). Such described structure of subunit *d* will make its association with elongated helical G subunit quite feasible, bringing the N-terminus of G close to V_O domain and allowing the remainder of its C-terminus to interact with V_1 domain subunit A and B, as reported previously (JONES *et al.*, 2005). These data further support the extended peripheral stalk formed by subunit *d* with subunits from the V_1 domain.

In conclusion, the data presented here demonstrate that subunit *d* (Vma6p) of the yeast vacuolar ATPase exists in solution as an elongated molecule, organized in two well-defined domains, as determined by two *ab initio* shape restoration procedures, reporting any kind of structural information for the first time (THAKER *et al.*, 2007). The similarity in shape with the mass of the recently determined low resolution structure of the V_O domain (WILKENS and FORGAC, 2001) allowed a clear assignment of subunit *d* inside the membrane domain, V_O (THAKER *et al.*, 2007). By using biochemical and molecular biology approaches, we establish that N- and C-termini of the protein are critical for proper folding, production, and stability of protein, which is in conformity and supported by the *in vivo* studies done in *Saccharomyces cerevisiae* (OWEGI *et al.*, 2006). More interestingly, a direct assembly of G/*d* is shown by NMR spectroscopy and binding region has been mapped to the N-terminus of G subunit (Gly7 - Lys34) (RISHIKESAN

et al., 2009). Moreover, a strong interaction between subunits *d* and *a* (THAKER *et al.*, 2009) as well as binding between subunit *d* and A support the hypothesis that subunit *d* along with the N-terminus of subunit *a* and components of V_1 form an extended peripheral stalk in V_1Vo ATPase.

4.3 Structural and biochemical characterization of subunit *a* of the vacuolar ATPase

Subunit *a* is a 100 kDa protein that is partially exposed on the cytosolic face via its NH_2-terminus and its COOH-domain comprises of putative transmembrane helices. Despite the fact that subunit *a* has been well studied in recent years yet no structural breakthrough has been obtained and a complete understanding on its associated partners in V_1V_O is lacking. However, studies have suggested that subunit *a* is indispensable for the assembly and coupling of ATP hydrolysis to proton transport in V_1V_O ATPase (KAWASAKI-NISHI *et al.*, 2001; QI and FORGAC, 2008). Most recently, subunit *a* has been recognized as a crucial element in the signal pathways involving ARNO (GDP/GTP exchanger) and GTPase, Arf6 in the cellular trafficking and degradation pathways (HURTADO-LORENZO *et al.*, 2006; MARSHANSKY, 2007).

Here the N-terminal subunit a_{1-388} fragment of *VPH1* gene of *Saccharomyces cerevisiae* was cloned and the protein was expressed and produced in *E. coli*, and the analysis of purified protein by CD spectroscopy reflects the proper secondary structure (Figure 27,28; page 95,96). Fluorescence correlation spectroscopy (FCS) and fluorescence cross correlation spectroscopy (FCCS) was used to determine the interaction between subunit *d* and *a* (Figure 29A, page 97) indicating the association between the two proteins. Interaction has been analyzed in the perspective of our previously proposed peripherally stalk assembly of subunit *d* (THAKER *et al.*, 2007), as described above in section 4.2.1 (Figure 45). To get insights into the 3D structure of subunit *a*/Vph1p, crystallization trials were done with subunit a_{1-388}. Promising results were observed with the formation of needle clusters in a condition containing 0.1 M Hepes sodium, pH 7.5, 2%, PEG 400 and 2 M ammonium sulfate during initial setup. However, several optimization rounds with different grid screen compositions as well as with other Hampton screens such as Salt Rx, Index Rx etc. could not yield any improvements in the needle clusters, to make them feasible for the diffraction yet to overcome this problem, as well as to map the binding domain of subunit *a* involved in the interaction with subunit *d*, several shorter constructs of NH_2-domian of subunit *a* were cloned (section 3.3.6), but none of these truncated proteins were soluble and could be poorly expressed in *E. coli* (Figure 32, page 101). These results showed that some minimum length might be required to attain the proper folding of subunit *a*. These data are consistent with the fact that subunit *a* is very unstable and extremely sensitive to

proteolytic cleavage, as was observed in the initial vacuolar preparations from the yeast when it was assumed that subunit *a* is not part of V-ATPase in lower eukaryotes (FORGAC, 1989; PERIN *et al.*, 1991). Due to the difficulties with the expression of yeast vacuolar ATPase subunit *a* proteins in *E. coli* heterologous system, several constructs were made from the mouse V_1V_O ATPase (section 3.3.8). Subunit *a* from different sources was chosen to study the conservation of its subunit function in various organisms. However, the problem of solubility persisted even with the shorter constructs from mouse *a2* NH_2-domain. Because of the problems encountered with the expression and solubility of subunit *a* constructs from several sources, further studies were focused with peptides from essential regions of the subunit *a2* of mouse V-ATPase. Subunit *a2* is one of the four isoforms found in V-ATPase of mouse, which is mainly expressed in kidney and liver cells (NISHI and FORGAC, 2000). Subunit *a2* has been recently associated with its novel function, acting as pH sensor element in a complex with ARNO and Arf proteins (HURTADO-LORENZO *et al.*, 2006; MARSHANSKY, 2007), playing an instrumental role in the degradation pathways. Various regions of the subunit *a2* have been modeled to be involved in the association of ARNO (Figure 47) (GRÜBER and MARSHANSKY, 2008). To get further insights into these essential regions of the subunit *a2*, I have solved the 3D NMR structure of subunit *a2* peptide $a2_{386-400}$ (Figure 38). This peptide of subunit *a2* is shown as region 22 in subunit *a2* model (Figure 47). Moreover, $a2_{386-400}$ has also been recently found to interact with ARNO (Arf-GEF) (MERKULOVA *et al.*, 2009).
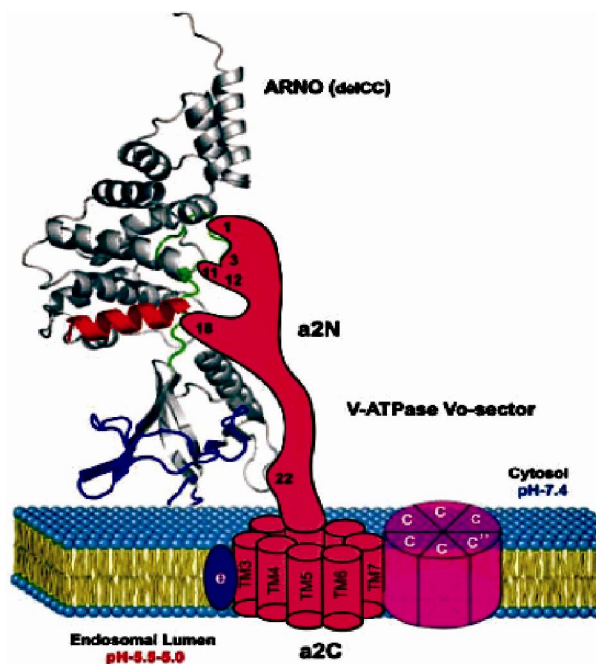

Figure 47. Modeled structure of ARNO (- coiled-coil region) and subunit a2 of mouse V-ATPase showing the probable regions of N-terminal part of subunit a2 that might be involved in interaction with ARNO. Poly-basic (PB) of ARNO is shown in red, pleckstrin homology (PH) domain in blue and linker-region of Sec7-PH region in green (GRÜBER and MARSHANSKY, 2008).

The solution structure of $a2_{386-400}$ peptide (Figure 38, page 106) showed an -helical C-terminus and a flexible N-terminal domain in line with the predicted structure based on the primary sequence using PSI-PRED program (Figure 35, page 104) (MCGUFFIN *et al.*, 2000). The structure of $a2_{386-40}$ can have important implications, whereby a flexible loop between two helices might be essential for the interaction with other proteins such as ARNO. Analysis of this structure by PDBSum (LASKOWSKI *et al.*, 2005) showed that a possible cleft is formed between N- and C-terminal domains.

As discussed above that V-ATPase has been recently reported to assemble with the signaling proteins such as ARNO (GTP/GDP exchanger) and Arf (small GTPase) via subunit *a* and *c* (HURTADO-LORENZO *et al.*, 2006), respectively, we intended to get more structural information about the regions of ARNO that are involved in its direct association with subunit *a*. The domain of ARNO protein that is required for association with subunit *a2* has been recently mapped to the poly-basic (PB) region of ARNO (379 – 400 aa) and more interestingly only the non-phosphorylated ARNO-PB form was found to interact with *a2* and phosphorylation at S392 inhibited ARNO binding with subunit *a2* (MERKULOVA *et al.*, 2009). Thus, it was presumed that the ARNO-PB domain undergoes remarkable structural and conformational changes upon phosphorylation at residue S392. In this context, I have solved the 3D NMR solution structure of ARNO-PB domain in its non-phosphorylated and phosphorylated states (Figure 40, page 111) from residues 375 – 400 (26 aa), which contains four residues of PH/PB linker at the N-terminus. Both structures exhibited helix-loop-helix configuration (Figure 40, page 111). Structural comparisons between $ARNO_{375-400}$ and $ARNO_{375-400(phos)}$ are described in the figure 41. $ARNO_{375-400(phos)}$ adopted a very stable geometry, whereas the $ARNO_{375-400}$ has a stable N-terminus -helix but a flexible backbone structure with short -helices at C-terminus (Figure 40C, page 111). A superimposition of the two structures over the N-terminus 1 – 10 residues showed a nice overlap with an RMSD of 0.68 Å but with differences in the C-terminus. An alignment resulted in a distance deviation of 105º at the loop region of $ARNO_{375-400}$ and $ARNO_{375-400(phos)}$, respectively. The phosphorylated and the unphosphorylated forms of the peptide influenced the structural changes in the C-termini, resulting in the disruption of the -helix at the S392 residue in the non-phosphorylated $ARNO_{375-400}$. In contrast, $ARNO_{375-400(phos)}$ displayed an extended helix through S392 and adopted a maximum stable structure in solution. In conclusion, the structure of $ARNO_{375-400}$ in the non-phosphorylated form can be conditionally related to its binding partner, subunit *a2* where the observed flexibility in the COOH-terminus can be partly explained due to the absence of binding partner (subunit *a2*) in solution. On contrary, $_{375-400(phos)}$ stable helix-loop-

helix structure shows inactive conformation that blocks the ARNO binding to subunit *a2*. Such kind of phosphoregulatory switches are known in bHLH (basic helix-loop-helix) proteins, where the binding affinity of proteins are modulated by phosphorylation and ability to interact with different binding partners is achieved (ANTHONY and SIMON, 2008). More recently, PB and Sec-7-PH linker regions have been found to be involved in the auto-inhibition of ARNO (DINITTO *et al.*, 2007). Earlier reports have shown that ARNO phosphorylation at S392 did not cause its activation (FRANK *et al.*, 1998) rather in a later report it was found that phosphorylation S392 negatively regulates exchange activity through a 'PH-domain electrostatic switch'. Introduction of negative charge in poly-basic (PB) reduced ARNO interaction with membranes *in vitro* and *in vivo* (SANTY *et al.*, 1999). Thus, structural information presented here can be used for further characterization and understanding the mechanism between ARNO/Arf6/V-ATPase with respect to the regulation of processes such as protein trafficking and actin cytoskeleton organization, in which they are involved.

5. Conclusion

This study was initiated to understand the mechanism of ARTS-promoted apoptosis, role of Livin and V-ATPase in the process of cell death. Initial findings showed subunit *d* of V_1V_O ATPase is a novel caspase 3 target, which was subsequently characterized by biochemical and structural techniques. Additional studies with V-ATPase focused on subunit *a* and signaling Arf-GEF protein, ARNO. Subunits *d* and *a* are indispensable for native proton pumping function as well as recruitment and scaffolding of ARNO/Arf6 which is involved in protein trafficking pathways. In summary work done in this dissertation led to the following conclusions:

i) During apoptosis, pro-apoptotic ARTS protein was prevented from degradation *in vivo*. Over expression of an E3 ligase anti-apoptotic Livin did not target ARTS ubiquitination and subsequent degradation by proteosome pathway, in cells that were induced to undergo apoptosis by staurosporine. Thus, Livin did not appear to act as an E3 ligase to ARTS. In contrast, Livin was found to undergo cleavage in ARTS-promoted apoptosis in response to staurosporine apoptotic stimuli. Further examination indicated a possible role of caspases in Livin degradation. Additionally, to screen for novel caspase cleavage sites in V-ATPase, subunit *d* of V_O domain of V_1V_O ATPase was found to be a target of caspase 3. To get further insights, studies in this direction are underway to detail function of observed cleavage and possible mechanism within the cell.

ii) Owing to the importance of subunit *d* in V-ATPase function and caspase 3 substrate, recombinantly produced and purified protein was studied, which resulted in first low resolution structure of subunit *d* showing a two domain-boxing glove low resolution structure. Further characterization of subunit *d* recombinant protein led to the identification of a disulphide bond between N- and C-termini (Cys36-Cys329) as well as importance of termini in the protein production and folding. On further investigations, a peripheral stalk formed by subunit *d* became evident, where binding experiments done with V_O domain subunit *a* and V_1 peripheral domain subunits G and A showed their association with subunit *d*.

iii) Subunit *a,* is a partially membrane anchored protein of V_O domain of V_1V_O ATPase. Studies with soluble N-terminal domain of subunit *a* (a_{1-388}) led to the identification subunit *d* as its binding partner. Initial crystallization with a_{1-388} resulted in the clustered needle forms of crystals, which will be further optimized in future to make them of diffractable quality, to get a high resolution structure of a_{1-388}. A region of mouse subunit *a2* involved in binding to ARNO has been characterized by solution nuclear magnetic resonance spectroscopy. The solution structures of ARNO PB-domain have been also solved in their active non-phosphorylated (which binds to subunit *a2*) and inactive phosphorylated (non-binding) forms, providing insights into the

essential conformations of both proteins. Future direction will include the structure determination of additional regions of subunit *a2* involved in the binding to ARNO as well as study of Arf6 and its binding partners in V-ATPase.

6. References

Adachi, I., H. Arai, R. Pimental and M. Forgac (1990). *Proteolysis and orientation on reconstitution of the coated vesicle proton pump*. J. Biol. Chem. **265**(2): 960-966.

Adachi, I., K. Puopolo, N. Marquez-Sterling, H. Arai and M. Forgac (1990). *Dissociation, cross-linking, and glycosylation of the coated vesicle proton pump*. J. Biol. Chem. **265**(2): 967-973.

Adams, D. S., K. R. Robinson, T. Fukumoto, S. Yuan, R. C. Albertson, P. Yelick, L. Kuo, M. McSweeney and M. Levin (2006). *Early, H+-V-ATPase-dependent proton flux is necessary for consistent left-right patterning of non-mammalian vertebrates*. Development **133**(9): 1657-1671.

Affar, E. B., M. Germain, E. Winstall, M. Vodenicharov, R. G. Shah, G. S. Salvesen and G. G. Poirier (2001). *Caspase-3-mediated Processing of Poly(ADP-ribose) Glycohydrolase during Apoptosis*. J. Biol. Chem. **276**(4): 2935-2942.

Andersen, J. L., E. Le Rouzic and V. Planelles (2008). *HIV-1 Vpr: Mechanisms of G2 arrest and apoptosis*. Experimental and Molecular Pathology **85**(1): 2-10.

Andersen, M. H., S. Reker, J. C. Becker and P. T. Straten (2004). *The Melanoma Inhibitor of Apoptosis Protein: A target for spontaneous cytotoxic T cell responses*. Journal of Investigative Dermatology **122**(2): 392-399.

Anderson, C. L. and G. T. Williams (2003). *Apoptosis gene hunting using retroviral expression cloning: identification of vacuolar ATPase subunit E*. TheScientificWorldJournal [electronic resource] **3**: 51-58.

Andrade, M. A., P. Chacón, J. J. Merelo and F. Morán (1993). *Evaluation of secondary structure of proteins from UV circular dichroism using an unsupervised learning neural network*. Prot. Eng. **6**: 383-390.

Anthony, F. B. and C. J. Simon (2008). *Phosphoregulation of Twist1 provides a mechanism of cell fate control* Curr Med Chem **15** (25): 2641-2647.

Apps, D. K., J. M. Percy and J. R. Perez-Castineira (1989). *Topography of a vacuolar-type H+-translocating ATPase: chromaffin-granule membrane ATPase I.* **263**: 81-88.

Armbrüster, A., S. M. Bailer, M. H. J. Koch, J. Godovac-Zimmermann and G. Grüber (2003). *Dimer formation of subunit G of the yeast V-ATPase*. FEBS Letters **546**(2-3): 395-400.

Armbrüster, A., H. Christina, H. Anne, S. Karin, B. r. Michael and G. Gerhard (2005). *Evidence for major structural changes in subunit C of the vacuolar ATPase due to nucleotide binding.* FEBS Letters **579**(9): 1961-1967.

Armbrüster, A., I. S. Dmitri, C. Ãœnal, J. Sandra, M. B. Susanne and G. b. Gerhard (2004). *Structural analysis of the stalk subunit Vma5p of the yeast V-ATPase in solution*. FEBS Letters **570**(1): 119-125.

Ashery, U., H. Koch, V. Scheuss, N. Brose and J. Rettig (1999). *A presynaptic role for the ADP ribosylation factor (ARF)-specific GDP/GTP exchange factor msec7-1*. Proceedings of the National Academy of Sciences of the United States of America **96**(3): 1094-1099.

Ashhab, Y., A. Alian, A. Polliack, A. Panet and D. B. Yehuda (2001). *Two splicing variants of a new inhibitor of apoptosis gene with different biological properties and tissue distribution pattern*. FEBS Letters **495**(1-2): 56-60.

Ashhab, Y., A. Alian, A. Polliack, O. Zelig, A. Panet and D. B. Yehuda (2001). *Livin, a new inhibitor of apoptosis protein, is expressed at high levels in some chronic lymphatic leukemia (CLL) patients, and may contribute to the apoptotic defect in low grade hematological malignancies*. Blood **98**(11 PART I).

Ashkenazi, A. and V. M. Dixit (1998). *Death receptors: signaling and modulation*. Science **281**(5381): 1305-1308.

Aviezer-Hagai, K., V. Padler-Karavani and N. Nelson (2003). *Biochemical support for the V-ATPase rotary mechanism: antibody against HA-tagged Vma7p or Vma16p but not Vma10p inhibits activity*. J Exp Biol **206**(18): 3227-3237.

Basu, A., D. Lu, B. Sun, A. N. Moor, G. R. Akkaraju and J. Huang (2002). *Proteolytic activation of protein kinase C-epsilon by caspase-mediated processing and transduction of antiapoptotic signals*. J. Biol. Chem. **277**(44): 41850-41856.

Bauerle, C., M. N. Ho, M. A. Lindorfer and T. H. Stevens (1993). *The Saccharomyces cerevisiae VMA6 gene encodes the 36-kDa subunit of the vacuolar H(+)-ATPase membrane sector*. J. Biol. Chem. **268**(17): 12749-12757.

Bergamaschi, D., Y. Samuels, N. J. O'Neil, G. Trigiante, T. Crook, J.-K. Hsieh, D. J. O'Connor, S. Zhong, I. Campargue, M. L. Tomlinson, P. E. Kuwabara and X. Lu (2003). *iASPP oncoprotein is a key inhibitor of p53 conserved from worm to human*. Nat Genet **33**(2): 162-167.

Bernal, R. A. and D. Stock (2004). *Three-dimensional ttructure of the intact Thermus thermophilus H+-ATPase/synthase by electron microscopy*. Structure **12**(10): 1789-1798.

Bernstein, F. C., T. F. Koetzle, G. J. B. Williams, E. G. Meyer, B. Jr., M. D., J. R. Rodgers, O. Kennard, T. Shimanouchi and M. Tasumi (1977). *The Protein Data Bank: a computer-based archival file for macromolecular structures*. J. Mol. Biol **112**: 535-542.

Beyenbach, K. W. and H. Wieczorek (2006). *The V-type H+ ATPase: Molecular structure and function, physiological roles and regulation*. Journal of Experimental Biology **209**(4): 577-589.

Blomgren, K., C. Zhu, X. Wang, J.-O. Karlsson, A.-L. Leverin, B. A. Bahr, C. Mallard and H. Hagberg (2001). *Synergistic activation of caspase-3 by m-calpain after neonatal hypoxia-ischemia. a mechanism of "pathological apoptosis"*. J. Biol. Chem. **276**(13): 10191-10198.

Blomgren K., e. a. (2001). *Synergistic activation of caspase-3 by m-calpain after neonatal hypoxia-ischemia: a mechanism of "pathological apoptosis*. J. Biol. Chem. **276**: 10191-10198.

Boulin, C. J., R. Kempf, A. Gabriel and M. H. J. Koch (1988). Nucl. Instrum. Meth. A **269**: 312-320.

Boulin, C. J., R. Kempf, M. H. J. Koch and S. M. McLaughlin (1986). Nucl. Instrum. Meth. A **249**: 399-407.

Bourne, H. R., D. A. Sanders and F. McCormick (1991). *The GTPase superfamily: conserved structure and molecular mechanism*. Nature **349**(6305): 117-127.

Bowman, E. J. and B. J. Bowman (2005). *V-ATPases as drug targets*. Journal of Bioenergetics and Biomembranes **37**(6): 431-435.

Breton, S. and D. Brown (2007). *New insights into the regulation of V-ATPase-dependent proton secretion*. American Journal of Physiology - Renal Physiology **292**(1).

Brown, D. and S. Breton (2000). *H+V-ATPase-dependent luminal acidification in the kidney collecting duct and the epididymis/vas deferens: Vesicle recycling and transcytotic pathways*. Journal of Experimental Biology **203**(1): 137-145.

Butt, T. R., S. C. Edavettal, J. P. Hall and M. R. Mattern (2005). *SUMO fusion technology for difficult-to-express proteins*. Protein Expression and Purification **43**(1): 1-9.

Cai, M., G. Wang, K. Tao and C. Cai (2008). *The apoptosis induction effect of siRNA recombinant expression vector targeting Livin gene in human colon cancer cells*. Chinese-German Journal of Clinical Oncology **7**(6): 344-347.

Chaban, Y., T. Ubbink-Kok, W. Keegstra, J. S. Lolkema and E. J. Boekema (2002). *Composition of the central stalk of the Na+-pumping V-ATPase from Caloramator fervidus*. EMBO Reports **3**(10): 982-987.

Chaiken, I., S. Rose and R. Karlsson (1992). *Analysis of macromolecular interactions using immobilized ligands*. Analytical Biochemistry **201**(2): 197-210.

Chang, H. and A. D. Schimmer (2007). *Livin/melanoma inhibitor of apoptosis protein as a potential therapeutic target for the treatment of malignancy*. Molecular Cancer Therapeutics **6**(1): 24-30.

Chardin, P., S. Paris, B. Antonny, S. Robineau, S. Beraud-Dufour, C. L. Jackson and M. Chabre (1996). *A human exchange factor for ARF contains Sec7- and pleckstrin-homology domains*. Nature **384**(6608): 481-484.

Charsky, C. M. H., N. J. Schumann and P. M. Kane (2000). *Mutational analysis of subunit G (Vma10p) of the yeast vacuolar H+-ATPase*. J. Biol. Chem. **275**(47): 37232-37239.

Chen, S.-H., M. R. Bubb, E. G. Yarmola, J. Zuo, J. Jiang, B. S. Lee, M. Lu, S. L. Gluck, I. R. Hurst and L. S. Holliday (2004). *Vacuolar H+-ATPase binding to microfilaments: regulation in response to phosphatidylinositol 3-kinase activity and detailed characterization of the actin-binding site in subunit b*
J. Biol. Chem. **279**(9): 7988-7998.

Clare, D. K., E. V. Orlova, M. A. Finbow, M. A. Harrison, J. B. C. Findlay and H. R. Saibil (2006). *An expanded and flexible form of the vacuolar ATPase membrane sector*. Structure **14**(7): 1149-1156.

Compton, M. A., L. A. Graham and T. H. Stevens (2006). *Vma9p (Subunit e) is an integral membrane V0 subunit of the yeast V-ATPase*. J. Biol. Chem. **281**(22): 15312-15319.

Cornilescu, G., F. Delaglio and A. Bax (1999). *Protein backbone angle restraints from searching a database for chemical shift and sequence homology*. Journal of Biomolecular NMR **13**(3): 289-302.

Coskun, U., G. Grüber, M. H. J. Koch, J. Godovac-Zimmermann, T. Lemker and V. Muller (2002). *Cross-talk in the A1-ATPase from Methanosarcina mazei Go1 due to nucleotide binding*. J. Biol. Chem. **277**(19): 17327-17333.

Coskun, Ü., V. F. Rizzo, M. H. J. Koch and G. Grüber (2004). *Ligand-dependent structural changes in the V₁ ATPase from Manduca sexta*. Journal of Bioenergetics and Biomembranes **36**(3): 249-256.

Creagh, E. M., H. Conroy and S. J. Martin (2003). *Caspase-activation pathways in apoptosis and immunity*. Immunological Reviews **193**: 10-21.

Crnkovic-Mertens, I., F. Hoppe-Seyler and K. Butz (2003). *Induction of apoptosis in tumor cells by siRNA-mediated silencing of the livin/ML-IAP/KIAP gene*. Oncogene **22**(51): 8330-8336.

Crnkovi -Mertens, I., J. Semzow, F. Hoppe-Seyler and K. Butz (2006). *Isoform-specific silencing of the Livin gene by RNA interference defines Livin   as key mediator of apoptosis inhibition in HeLa cells*. Journal of Molecular Medicine **84**(3): 232-240.

Crnkovi -Mertens, I., N. Wagener, J. Semzow, E. Gröne, A. Haferkamp, M. Hohenfellner, K. Butz and F. Hoppe-Seyler (2007). *Targeted inhibition of Livin resensitizes renal cancer cells towards apoptosis*. Cellular and Molecular Life Sciences (CMLS) **64**(9): 1137-1144.

Crook, N. E., R. J. Clem and L. K. Miller (1993). *An apoptosis-inhibiting baculovirus gene with a zinc finger-like motif*. J. Virol. **67**(4): 2168-2174.

Curtis, K. K., S. A. Francis, Y. Oluwatosin and P. M. Kane (2002). *Mutational Analysis of the Subunit C (Vma5p) of the Yeast Vacuolar H+-ATPase*. J. Biol. Chem. **277**(11): 8979-8988.

Dai, Z., W.-G. Zhu, C. D. Morrison, R. M. Brena, D. J. Smiraglia, A. Raval, Y.-Z. Wu, L. J. Rush, P. Ross, J. R. Molina, G. A. Otterson and C. Plass (2003). *A comprehensive search for DNA amplification in lung cancer identifies inhibitors of apoptosis cIAP1 and cIAP2 as candidate oncogenes*. Hum. Mol. Genet. **12**(7): 791-801.

Dames, P., B. Zimmermann, R. Schmidt, J. Rein, M. Voss, B. Schewe, B. Walz and O. Baumann (2006). *cAMP regulates plasma membrane vacuolar-type H+-ATPase assembly and activity in blowfly salivary glands*. Proceedings of the National Academy of Sciences of the United States of America **103**(10): 3926-3931.

de Graaf, A. O., T. de Witte and J. H. Jansen (2004). *Inhibitor of apoptosis proteins: New therapeutic targets in hematological cancer?* Leukemia **18**(11): 1751-1759.

DeLano, W. (2001). *The pyMol Molecular Graphics SystemSan Carlos, CA:*
. DeLano Scientific.

Demirci, F. Y. K., N. J. White, B. W. Rigatti, K. F. Lewis and M. B. Gorin (2001). *Identification, genomic structure, and screening of the vacuolar proton-ATPase membrane sector-associated protein M8-9 gene within the COD1 critical region (Xp11.4)*. Molecular Vision **7**: 234-239.

Deveraux, Q. L., E. Leo, H. R. Stennicke, K. Welsh, G. S. Salvesen and J. C. Reed (1999). *Cleavage of human inhibitor of apoptosis protein XIAP results in fragments with distinct specificities for caspases*. EMBO Journal **18**(19): 5242-5251.

Deveraux, Q. L. and J. C. Reed (1999). *IAP family proteins suppressors of apoptosis*. Genes & Development **13**(3): 239-252.

Deveraux, Q. L., N. Roy, H. R. Stennicke, T. Van Arsdale, Q. Zhou, S. M. Srinivasula, E. S. Alnemri, G. S. Salvesen and J. C. Reed (1998). *IAPs block apoptotic events induced by caspase-8 and cytochrome c by direct inhibition of distinct caspases*. EMBO Journal **17**(8): 2215-2223.

Deveraux, Q. L., H. R. Stennicke, G. S. Salvesen and J. C. Reed (1999). *Endogenous inhibitors of caspases*. Journal of Clinical Immunology **19**(6): 388-398.

Deveraux, Q. L., R. Takahashi, G. S. Salvesen and J. C. Reed (1997). *X-linked IAP is a direct inhibitor of cell-death proteases*. Nature **388**(6639): 300-304.

DiNitto, J. P., A. Delprato, M. T. Gabe Lee, T. C. Cronin, S. Huang, A. Guilherme, M. P. Czech and D. G. Lambright (2007). *Structural basis and mechanism of autoregulation in 3-phosphoinositide-dependent Grp1 family Arf GTPase exchange factors*. Molecular Cell **28**(4): 569-583.

Du, C., M. Fang, Y. Li, L. Li and X. Wang (2000). *Smac, a mitochondrial protein that promotes cytochrome c-dependent caspase activation by eliminating IAP inhibition*. Cell **102**(1): 33-42.

Duarte, A. M. S., E. R. de Jong, R. Wechselberger, C. P. M. van Mierlo and M. A. Hemminga (2007). *Segment TM7 from the cytoplasmic hemi-channel from VO-H+-V-ATPase includes a flexible region that has a potential role in proton translocation*. Biochimica et Biophysica Acta (BBA) - Biomembranes **1768**(9): 2263-2270.

Earnshaw, W. C., L. M. Martins and S. H. Kaufmann (1999). *Mammalian caspases: structure, activation, substrates, and functions during apoptosis*. Annual Review of Biochemistry **68**(1): 383-424.

Elhasid, R., D. Sahar, A. Merling, Y. Zivony, A. Rotem, M. Ben-Arush, S. Izraeli, D. Bercovich and S. Larisch (2004). *Mitochondrial pro-apoptotic ARTS protein is lost in the majority of acute lymphoblastic leukemia patients*. Oncogene **23**(32): 5468-5475.

Ellis, H. M. and H. R. Horvitz (1986). *Genetic control of programmed cell death in the nematode C. elegans*. Cell **44**(6): 817-829.

Errington, N. and A. J. Doig (2005). *A phosphoserine-lysine salt bridge within an alpha-helical peptide, the strongest alpha-helix side-chain interaction measured to date*. Biochemistry **44**(20): 7553-7558.

F. Delaglio, S., G. W. Grzesiek, G. Vuister, J. Zhu, P. and and A. Bax (1995). *NMRPipe: a multidimensional spectral processing system based on UNIX pipes*. J. Biomol. NMR **6**: 277-293.

Faty, M., M. Fink and Y. Barral (2002). *Septins: a ring to part mother and daughter*. Current Genetics **41**(3): 123-131.

Ferri, K. F. and G. Kroemer (2001). *Organelle-specific initiation of cell death pathways*. Nat Cell Biol **3**(11): E255-E263.

Field, C. M. and D. Kellogg (1999). *Septins: cytoskeletal polymers or signalling GTPases?* Trends in Cell Biology **9**(10): 387-394.

Forgac, M. (1989). *Structure and function of vacuolar class of ATP-driven proton pumps*. Physiol. Rev. **69**(3): 765-796.

Forgac, M. (2000). *Structure, mechanism and regulation of the clathrin-coated vesicle and yeast vacuolar H(+)-ATPases*. J Exp Biol **203**(1): 71-80.

Forgac, M. (2007). *Vacuolar ATPases: Rotary proton pumps in physiology and pathophysiology*. Nature Reviews Molecular Cell Biology **8**(11): 917-929.

Forgac, M., L. Cantley, B. Wiedenmann, L. Altstiel and D. Branton (1983). *Clathrin-coated vesicles contain an ATP-dependent proton pump*. Proceedings of the National Academy of Sciences **80**(5): 1300-1303.

Franco, M., J. Boretto, S. Robineau, S. Monier, B. Goud, P. Chardin and P. Chavrier (1998). *ARNO3, a Sec7-domain guanine nucleotide exchange factor for ADP ribosylation factor 1, is involved in the control of Golgi structure and function*. Proceedings of the National Academy of Sciences of the United States of America **95**(17): 9926-9931.

Franco, M., P. J. Peters, J. Boretto, E. Van Donselaar, A. Neri, C. D'Souza-Schorey and P. Chavrier (1999). *EFA6, a sec7 domain-containing exchange factor for ARF6, coordinates membrane recycling and actin cytoskeleton organization*. EMBO Journal **18**(6): 1480-1491.

Frank, S., S. Upender, S. H. Hansen and J. E. Casanova (1998). *ARNO is a guanine nucleotide exchange factor for ADP-ribosylation factor 6*. Journal of Biological Chemistry **273**(1): 23-27.

Frank, S. R., J. C. Hatfield and J. E. Casanova (1998). *Remodeling of the actin cytoskeleton is coordinately regulated by protein kinase C and the ADP-ribosylation factor nucleotide exchange factor ARNO*. Molecular Biology of the Cell **9**(11): 3133-3146.

Frattini, A., P. J. Orchard, C. Sobacchi, S. Giliani, M. Abinun, J. P. Mattsson, D. J. Keeling, A.-K. Andersson, P. Wallbrandt, L. Zecca, L. D. Notarangelo, P. Vezzoni and A. Villa (2000). *Defects in TCIRG1 subunit of the vacuolar proton pump are responsible for a subset of human autosomal recessive osteopetrosis*. Nat Genet **25**(3): 343-346.

Fröhlich, K.-U. and F. Madeo (2001). *Apoptosis in yeast: a new model for aging research*. Experimental Gerontology **37**(1): 27-31.

Gogarten, J. P., T. Starke, H. Kibak, J. Fishman and L. Taiz (1992). *Evolution and isoforms of V-ATPase subunits*. J Exp Biol **172**(1): 137-147.

Goll, D. E., V. F. Thompson, H. Li, W. E. I. Wei and J. Cong (2003). *The calpain system*. Physiol. Rev. **83**(3): 731-801.

Gottlieb, R. A., H. A. Giesing, J. Y. Zhu, R. L. Engler and B. M. Babior (1995). *Cell acidification in apoptosis: granulocyte colony-stimulating factor delays programmed cell death in neutrophils by up-regulating the vacuolar H(+)-ATPase*. Proceedings of the National Academy of Sciences of the United States of America **92**(13): 5965-5968.

Gottlieb, R. A., D. L. Gruol, J. Y. Zhu and R. L. Engler (1996). *Preconditioning rabbit cardiomyocytes: role of pH, vacuolar proton ATPase, and apoptosis*. J Clin Invest **97**: 2391-2396.

Graham, L. A., K. J. Hill and T. H. Stevens (1994). *VMA7 encodes a novel 14-kDa subunit of the Saccharomyces cerevisiae vacuolar H(+)-ATPase complex*. J. Biol. Chem. **269**(42): 25974-25977.

Graham, L. A., K. J. Hill and T. H. Stevens (1995). *VMA8 encodes a 32-kDa VO subunit of the Saccharomyces cerevisiae vacuolar H+-ATPase required for function and assembly of the enzyme complex*. J. Biol. Chem. **270**(25): 15037-15044.

Graham, L. A., B. Powell and T. H. Stevens (2000). *Composition and assembly of the yeast vacuolar H(+)-ATPase complex*. J Exp Biol **203**(1): 61-70.

Green, C. John, nbsp and D. R. Reed (1998). *Mitochondria and apoptosis*. Science **281**(5381): 1309-1312.

Grüber, G. (2003). *Introduction: a close look at the vacuolar ATPase*. Journal of Bioenergetics and Biomembranes **35**(4): 277-280.

Grüber, G., J. Godovac-Zimmermann, T. A. Link, U. Coskun, V. F. Rizzo, C. Betz and S. M. Bailer (2002). *Expression, purification, and characterization of subunit E, an essential subunit of the vacuolar ATPase*. Biochemical and Biophysical Research Communications **298**(3): 383-391.

Grüber, G. and V. Marshansky (2008). *New insights into structure-function relationships between archeal ATP synthase (A1AO) and vacuolar type ATPase (V1VO)*. BioEssays **30**: 1-14

Grüber, G., M. Radermacher, T. Ruiz, J. Godovac-Zimmermann, B. Canas, D. Kleine-Kohlbrecher, M. Huss, W. R. Harvey and H. Wieczorek (2000). *Three-dimensional structure and subunit topology of the V1 ATPase from Manduca sexta midgut*. Biochemistry **39**(29): 8609-8616.

Grüber, G., H. Wieczorek, W. R. Harvey and V. Muller (2001). *Structure-function relationships of A-, F- and V-ATPases*. J Exp Biol **204**(15): 2597-2605.

Gruss, H. J. and S. K. Dower (1995). *Tumor necrosis factor ligand superfamily: involvement in the pathology of malignant lymphomas*. Blood **85**(12): 3378-3404.

Guinier, A. and G. Fournet (1955). *Small-angle Scattering of X-rays*. Wiley, New York.

Gunyuzlu, P., W. White, G. Davis, G. Hollis and J. Toyn (2000). *A yeast genetic assay for caspase cleavage of the amyloid- precursor protein*. Molecular Biotechnology **15**(1): 29-37.

HaÌcki, J., L. Egger, L. Monney, S. Conus, T. RosseÌ, I. Fellay and C. Borner (2000). *Apoptotic crosstalk between the endoplasmic reticulum and mitochondria controlled by Bcl-2*. Oncogene **19**(19): 2286-2295.

Hangerton, M. (2000). *The biochemistry of apoptosis*. Nature **407**: 770-776.

Harju, S., H. Fedosyuk and K. Peterson (2004). *Rapid isolation of yeast genomic DNA: Bust n' Grab*. BMC Biotechnol **21**: 4-8.

Hawkins, C. J., S. L. Wang and B. A. Hay (1999). *A cloning method to identify caspases and their regulators in yeast: Identification of Drosophila IAP1 as an inhibitor of the Drosophila caspase DCP-1*. Proceedings of the National Academy of Sciences of the United States of America **96**(6): 2885-2890.

Hengartner, M. O. (2000). *The biochemistry of apoptosis*. Nature **407**(6805): 770-776.

Hengartner, M. O., R. Ellis and R. Horvitz (1992). *Caenorhabditis elegans gene ced-9 protects cells from programmed cell death*. Nature **356**(6369): 494-499.

Herrmann, T., P. Guntert and K. Wu¨thrich (2002). *Protein NMR structure determination with automated NOE assignment using the new software CANDID and the torsion angle dynamics algorithm DYANA* J. Mol. Biol.. **319**: 209-227.

Hiroto, I., T. Takayuki, I. Hiroshi, U. Hidetaka, Y. Yoichiro, T. Mizuho, I. Tomoko, M. Tadashi, Y. Takeshi, N. Minoru and K. Kimitoshi (2003). *Cellular pH regulators: potentially promising molecular targets for cancer chemotherapy*. Cancer treatment reviews **29**(6): 541-549.

Holley, C. L., M. R. Olson, D. A. Colón-Ramos and S. Kornbluth (2002). *Reaper eliminates IAP proteins through stimulated IAP degradation and generalized translational inhibition*. Nat Cell Biol **40**: 439 - 444

Holliday, L., M. Bubb, J. Jiang, I. Hurst and J. Zuo (2005). *Interactions Between Vacuolar H+-ATPases and Microfilaments in Osteoclasts*. Journal of Bioenergetics and Biomembranes **37**(6): 419-423.

Hong-Hermesdorf, A., A. Brux, A. Grüber, G. Grüber and K. Schumacher (2006). *A WNK kinase binds and phosphorylates V-ATPase subunit C*. FEBS Letters **580**(3): 932-939.

Hu, Y., L. Ding, D. M. Spencer and G. Nunez (1998). *WD-40 repeat region regulates Apaf-1 self-association and procaspase-9 activation*. J. Biol. Chem. **273**(50): 33489-33494.

Huang, X., A. Masselli, S. M. Frisch, I. C. Hunton, Y. Jiang and J. Y. J. Wang (2007). *Blockade of tumor necrosis factor-induced Bid cleavage by caspase-resistant Rb*. J. Biol. Chem. **282**(40): 29401-29413.

Hurtado-Lorenzo, A., M. Skinner, J. E. Annan, M. Futai, G.-H. Sun-Wada, S. Bourgoin, J. Casanova, A. Wildeman, S. Bechoua, D. A. Ausiello, D. Brown and V. Marshansky (2006). *V-ATPase interacts with ARNO and Arf6 in early endosomes and regulates the protein degradative pathway*. Nat Cell Biol **8**(2): 124-136.

Imoto, I., Z.-Q. Yang, A. Pimkhaokham, H. Tsuda, Y. Shimada, M. Imamura, M. Ohki and J. Inazawa (2001). *Identification of cIAP1 as a candidate target gene within an amplicon at 11q22 in esophageal squamous cell carcinomas*. Cancer Res **61**(18): 6629-6634.

Iwata, M., H. Imamura, E. Stambouli, C. Ikeda, M. Tamakoshi, K. Nagata, H. Makyio, B. Hankamer, J. Barber, M. Yoshida, K. Yokoyama and S. Iwata (2004). *Crystal structure of a*

central stalk subunit C and reversible association/dissociation of vacuole-type ATPase. PNAS **101**(1): 59-64.

Jansen, E. J. R., J. C. M. Holthuis, C. McGrouther, J. P. H. Burbach and G. J. M. Martens (1998). *Intracellular trafficking of the vacuolar H+-ATPase accessory subunit Ac45*. Journal of Cell Science **111**(20): 2999-3006.

Jefferies, K. C. and M. Forgac (2008). *Subunit H of the vacuolar (H+) ATPase inhibits ATP hydrolysis by the free V1 domain by interaction with the rotary subunit F*. J. Biol. Chem. **283**(8): 4512-4519.

Ji Yoo, S., J. R. Huh, I. Muro, H. Yu, L. Wang, S. L. Wang, R. M. R. Feldman, R. J. Clem, H. A. J. Mu?ller and B. A. Hay (2002). *Hid, Rpr and Grim negatively regulate DIAP1 levels through distinct mechanisms*. Nature Cell Biology **4**(6): 416-424.

Jiake Xu, H. T. F. C. W. K. H. M. Y. N. P. J. M. P. D. W. M. H. Z. (2003). *Effects of Bafilomycin A1: An inhibitor of vacuolar H (+)-ATPases on endocytosis and apoptosis in RAW cells and RAW cell-derived osteoclasts*. Journal of Cellular Biochemistry **88**(6): 1256-1264.

Jiang, X. and X. Wang (2004). *Cytochrome c-mediated apoptosis*. Annual Review of Biochemistry **73**(1): 87.

Jones, R. P. O., L. J. Durose, J. B. C. Findlay and M. A. Harrison (2005). *Defined sites of interaction between subunits E (Vma4p), C (Vma5p), and G (Vma10p) within the stator structure of the Vacuolar H(+)-ATPase*. Biochemistry **44**(10): 3933-3941.

Jonsson, U., L. Fagerstam, B. Ivarsson, B. Johnsson, R. Karlsson, K. Lundh, S. Lofas, B. Persson, H. Roos, I. Ronnberg, S. Sjolander, E. Stenberg, R. Stahlberg, C. Urbaniczky, H. Ostlin and M. Malmqvist (1991). *Real-time biospecific interaction analysis using surface plasmon resonance and a sensor chip technology*. BioTechniques **11**(5).

Kakinuma, Y., Y. Ohsumi and Y. Anraku (1981). *Properties of H+-translocating adenosine triphosphatase in vacuolar membranes of Saccharomyces cerevisiae*. J. Biol. Chem. **256**(21): 10859-10863.

Kane, P. M. (1995). *Disassembly and reassembly of the yeast vacuolar H+-ATPase in vivo*. Journal of Biological Chemistry **270**(28): 17025-17032.

Kane, P. M. (2000). *Regulation of V-ATPases by reversible disassembly*. FEBS Letters **469**(2-3): 137-141.

Kane, P. M. (2007). *The long physiological reach of the yeast vacuolar H+-ATPase*. Journal of Bioenergetics and Biomembranes **39**(5-6): 415-421.

Kane, P. M., C. T. Yamashiro and T. H. Stevens (1989). *Biochemical characterization of the yeast vacuolar H(+)-ATPase*. J. Biol. Chem. **264**(32): 19236-19244.

Karet, F. (2005). *Physiological and metabolic implications of V-ATPase isoforms in the Kidney*. Journal of Bioenergetics and Biomembranes **37**(6): 425-429.

Karlsson, J., I. Ora, I. Porn-Ares and S. Pahlman (2004). *Arsenic trioxide-induced death of neuroblastoma cells involves activation of Bax and does not require p53*. Clin Cancer Res **10**(9): 3179-3188.

Karlsson J., e. a. (2004). *Arsenic Trioxide-Induced Death of Neuroblastoma Cells Involves Activation of Bax and Does Not Require p53*. Clin. Can. Res. **10**: 3179-3188.

Karlsson, R., H. Roos, L. Fa?gerstam and B. Persson (1994). *Kinetic and concentration analysis using BIA technology*. Methods **6**(2): 99-110.

Kasof, G. M. and B. C. Gomes (2001). *Livin, a novel inhibitor of apoptosis protein family member*. Journal of Biological Chemistry **276**(5): 3238-3246.

Kaur, S., F. Wang, M. Venkatraman and M. Arsura (2005). *X-linked Inhibitor of Apoptosis (XIAP) Inhibits c-Jun N-terminal Kinase 1 (JNK1) activation by transforming growth factor {beta}1 (TGF-{beta}1) through ubiquitin-mediated proteosomal degradation of the TGF-{beta}1-activated Kinase 1 (TAK1)*. J. Biol. Chem. **280**(46): 38599-38608.

Kawasaki-Nishi, S., K. Bowers, T. Nishi, M. Forgac and T. H. Stevens (2001). *The amino-terminal domain of the vacuolar proton-translocating ATPase a subunit controls targeting and in vivo dissociation, and the carboxyl-terminal domain affects coupling of proton transport and ATP hydrolysis*. J. Biol. Chem. **276**(50): 47411-47420.

Kawasaki-Nishi, S., T. Nishi and M. Forgac (2001). *Arg-735 of the 100-kDa subunit a of the yeast V-ATPase is essential for proton translocation*. Proceedings of the National Academy of Sciences of the United States of America **98**(22): 12397-12402.

Kawasaki-Nishi, S., T. Nishi and M. Forgac (2001). *Yeast V-ATPase complexes containing different isoforms of the 100-kDa a-subunit differ in coupling efficiency and in vivo dissociation*. Journal of Biological Chemistry **276**(21): 17941-17948.

Kay, L. E., D. R. Muhandiram, N. A. Farrow, Y. Aubin and J. D. Forman-Kay (1996). *Correlation between dynamics and high affinity binding in an SH2 domain Interaction*. Biochemistry **35**(2): 361-368.

Kerr, J. F., A. H. Wyllie and A. R. Currie (1972). *Apoptosis: a basic biological phenomenon with wide-ranging implications in tissue kinetics*. Br J Cancer **26**: 239–257.

Kipp, M., B. L. Schwab, M. Przybylski, P. Nicotera and F. O. Fackelmayer (2000). *Apoptotic cleavage of scaffold attachment factor a (SAF-A) by caspase-3 occurs at a noncanonical cleavage site*. J. Biol. Chem. **275**(7): 5031-5036.

Kissel, H., M.-M. Georgescu, S. Larisch, K. Manova, G. R. Hunnicutt and H. T. Steller (2005). *The Sept4 locus is the required for sperm termianl differentiation in Mice*. Developmental Cell **8**: 353-364.

Kitagawa, N., H. Mazon, A. J. R. Heck and S. Wilkens (2008). *Stoichiometry of the peripheral stalk subunits E and G of yeast V1-ATPase determined by mass spectrometry*. J. Biol. Chem. **283**(6): 3329-3337.

Klarlund, J. K., A. Guilherme, J. J. Holik, J. V. Virbasius, A. Chawla and M. P. Czech (1997). *Signaling by phosphoinositide-3,4,5-trisphosphate through proteins containing pleckstrin and Sec7 homology domains*. Science **275**(5308): 1927-1930.

Kneller, D. and T. Goddard (1997). *SPARKY 3.105 edit.* San Francisco, CA, University of California.

Konarev, P. V., V. V. Volkov, A. V. Sokolova, M. H. J. Koch and D. I. Svergun (2003). *PRIMUS: a Windows PC-based system for small-angle scattering data analysis*. Journal of Applied Crystallography **36**(5): 1277-1282.

Koradi, R., M. Billeter and K. Wüthrich (1996). *MOLMOL: a program for display and analysis of macromolecular structures,*. J. Mol. Graphics **14**: 51-55.

Kornak, U., E. Reynders, A. Dimopoulou, J. van Reeuwijk, B. Fischer, A. Rajab, B. Budde, P. Nurnberg, F. Foulquier, D. Lefeber, Z. Urban, S. Gruenewald, W. Annaert, H. G. Brunner, H. van Bokhoven, R. Wevers, E. Morava, G. Matthijs, L. Van Maldergem and S. Mundlos (2008). *Impaired glycosylation and cutis laxa caused by mutations in the vesicular H+-ATPase subunit ATP6V0A2*. Nat Genet **40**(1): 32-34.

Kornak, U., A. Schulz, W. Friedrich, S. Uhlhaas, B. Kremens, T. Voit, C. Hasan, U. Bode, T. J. Jentsch and C. Kubisch (2000). *Mutations in the a3 subunit of the vacuolar H+-ATPase cause infantile malignant osteopetrosis*. Human Molecular Genetics **9**(13): 2059-2063.

Lagadic-Gossmann, D., L. Huc and V. Lecureur (2004). *Alterations of intracellular pH homeostasis in apoptosis: origins and roles*. Cell Death Differ **11**(9): 953-961.

Landolt-Marticorena, C., W. H. Kahr, P. Zawarinski, J. Correa and M. F. Manolson (1999). *Substrate- and inhibitor-induced conformational changes in the yeast V- ATPase provide evidence for communication between the catalytic and proton- translocating sectors*. Journal of Biological Chemistry **274**(37): 26057-26064.

Landolt-Marticorena, C., K. M. Williams, J. Correa, W. Chen and M. F. Manolson (2000). *Evidence that the NH2 terminus of Vph1p, an integral subunit of the V0 sector of the yeast V-ATPase, interacts directly with the Vma1p and Vma13p subunits of the V1 Sector*. J. Biol. Chem. **275**(20): 15449-15457.

Larisch, S. (2004). *The ARTS connection: role of ARTS in apoptosis and cancer*. Cell Cycle **3**(8): 1021-1023.

Larisch, S., Y. Yi, R. Lotan, H. Kerner, S. Eimerl, W. Tony Parks, Y. Gottfried, S. Birkey Reffey, M. P. de Caestecker, D. Danielpour, N. Book-Melamed, R. Timberg, C. S. Duckett, R. J. Lechleider, H. Steller, J. Orly, S.-J. Kim and A. B. Roberts (2000). *A novel mitochonrial septin like protein, ARTS, mediates apoptosis dependent on its P-loop motif*. Nat. Cell Bio. **2**: 915-921.

Laskowski, R. A., V. V. Chistyakov and J. M. Thornton (2005). *PDBsum more: new summaries and analyses of the known 3D structures of proteins and nucleic acids*. Nucl. Acids Res. **33**(suppl_1): D266-268.

Laskowski, R. A., N. M. Luscombe, M. B. Swindells and J. M. Thornton (1996). *Protein clefts in molecular recognition and function*. Protein Sci **5**(12): 2438-2452.

Lee, S.-H., J. Rho, D. Jeong, J.-Y. Sul, T. Kim, N. Kim, J.-S. Kang, T. Miyamoto, T. Suda, S.-K. Lee, R. J. Pignolo, B. Koczon-Jaremko, J. Lorenzo and Y. Choi (2007). *v-ATPase V0 subunit d2-deficient mice exhibit impaired osteoclast fusion and increased bone formation*. Nat Med **12**(12): 1403-1409.

Leng, X.-H., T. Nishi and M. Forgac (1999). *Transmembrane topography of the 100-kDa a subunit (Vph1p) of the yeast vacuolar proton-translocating ATPase*. J. Biol. Chem. **274**(21): 14655-14661.

Leng, X. H., M. F. Manolson and M. Forgac (1998). *Function of the COOH-terminal domain of Vph1p in activity and assembly of the yeast V-ATPase*. Journal of Biological Chemistry **273**(12): 6717-6723.

Leng, X. H., M. F. Manolson, Q. Liu and M. Forgac (1996). *Site-directed mutagenesis of the 100-kDA subunit (Vph1p) of the yeast vacuolar (H+)-ATPase*. Journal of Biological Chemistry **271**(37): 22487-22493.

Lepier, A., M. Azuma, W. R. Harvey and H. Wieczorek (1994). *K+/H+ antiport in the tobacco hornworm midgut: the K(+)-transporting component of the K+ pump*. J Exp Biol **196**(1): 361-373.

Li, G., Q. Yang, S. Krishnan, E. A. Alexander, S. C. Borkan and J. H. Schwartz (2006). *A novel cellular survival factor - the B2 subunit of vacuolar H+-ATPase inhibits apoptosis*. Cell Death Differ.

Li, H., H. Zhu, C.-j. Xu and J. Yuan (1998). *Cleavage of BID by caspase 8 mediates the mitochondrial damage in the Fas pathway of apoptosis*. Cell **94**(4): 491-501.

Li, J. and J. Yuan (2008). *Caspases in apoptosis and beyond*. Oncogene **27**(48): 6194-6206.

Lin, J.-H., G. Deng, Q. Huang and J. Morser (2000). *KIAP, a novel member of the Inhibitor of Apoptosis protein family*. Biochemical and Biophysical Research Communications **279**(3): 820-831.

Lipmann, F. (1941). Adv. Enzymol. **1**: 99–162.

Liston, P., W. G. Fong and R. G. Korneluk (2003). *The inhibitors of apoptosis: there is more to life than Bcl2*. Oncogene **22**(53): 8568-8580.

Liu, B., M. Han, J. K. Wen and L. Wang (2007). *Livin/ML-IAP as a new target for cancer treatment*. Cancer Letters **250**(2): 168-176.

Long, X., M. T. Crow, S. J. Sollott, L. O'Neill, D. S. Menees, M. Hipolito, d. Lourdes, M. O. Boluyt, T. Asai and L. E. G (1998). *Enhanced expression of p53 and apoptosis induced by blockade of the vacuolar proton ATPase in cardiomyocytes*. J Clin Invest **101**: 1453-1461.

Lotan, R., A. Rotem, H. Gonen, J. P. M. Finberg, S. Kemeny, H. Steller, A. Ciechanover and S. Larisch (2005). *Regulation of the Proapoptotic ARTS Protein by Ubiquitin-mediated Degradation*. J. Biol. Chem. **280**(27): 25802-25810.

Lu, M., Y. Y. Sautin, L. S. Holliday and S. L. Gluck (2003). *The glycolytic enzyme aldolase mediates assembly, expression and activity of V-ATPase*. J. Biol. Chem.: M303871200.

Ludovico, P., M. J. Sousa, M. T. Silva, C. Leao and M. Corte-Real (2001). *Saccharomyces cerevisiae commits to a programmed cell death process in response to acetic acid*. Microbiology **147**(9): 2409-2415.

Ludwig, J., S. Kerscher, U. Brandt, K. Pfeiffer, F. Getlawi, D. K. Apps and H. Schagger (1998). *Identification and characterization of a novel 9.2-kDa membrane sector-associated protein of vacuolar proton-ATPase from chromaffin granules*. J. Biol. Chem. **273**(18): 10939-10947.

Ma, L., Y. Huang, Z. Song, S. Feng, X. Tian, W. Du, X. Qiu, K. Heese and M. Wu (2006). *Livin promotes Smac/DIABLO degradation by ubiquitin-proteasome pathway*. Cell Death and Differentiation **13**(12): 2079-2088.

Madeo, F., E. Herker, C. Maldener, S. Wissing, S. Lächelt, M. Herlan, M. Fehr, K. Lauber, S. J. Sigrist, S. Wesselborg and K.-U. Fröhlich (2002). *A Caspase-related protease regulates apoptosis in yeast*. Molecular Cell **9**(4): 911-917.

Manolson, M. F., D. Proteau and E. W. Jones (1992). *Evidence for a conserved 95-120 kDa subunit associated with and essential for activity of V-ATPases*. J Exp Biol **172**(1): 105-112.

Manolson, M. F., D. Proteau and E. W. Jones (1992). *Evidence for a conserved 95-120 kDa subunit associated with and essential for activity of V-ATPases*. Journal of Experimental Biology **172**: 105-112.

Manolson, M. F., D. Proteau, R. A. Preston, A. Stenbit, B. T. Roberts, M. A. Hoyt, D. Preuss, J. Mulholland, D. Botstein and E. W. Jones (1992). *The VPH1 gene encodes a 95-kDa integral membrane polypeptide required for in vivo assembly and activity of the yeast vacuolar H(+)-ATPase*. J. Biol. Chem. **267**(20): 14294-14303.

Manolson, M. F., B. Wu, D. Proteau, B. E. Taillon, B. T. Roberts, M. A. Hoyt and E. W. Jones (1994). *STV1 gene encodes functional homologue of 95-kDa yeast vacuolar H(+)- ATPase subunit Vph1p*. J. Biol. Chem. **269**(19): 14064-14074.

Maranda, B., D. Brown, S. Bourgoin, J. E. Casanova, P. Vinay, D. A. Ausiello and V. Marshansky (2001). *Intra-endosomal pH-sensitive recruitment of the Arf-nucleotide exchange factor ARNO and Arf6 from cytoplasm to proximal tubule endosomes*. J. Biol. Chem. **276**(21): 18540-18550.

Marc R. Wilkins, I. L. E. G. A. B. J.-C. S. D. F. H. R. D. A. (1997). *Detailed peptide characterization using PEPTIDEMASS - a World-Wide-Web-accessible tool*. Electrophoresis **18**(3-4): 403-408.

Marshansky, V. (2007). *The V-ATPase a2-subunit as a putative endosomal pH-sensor*. Biochemical Society Transactions **35**(5): 1092-1099.

Marshansky, V. and M. Futai (2008). *The V-type H+-ATPase in vesicular trafficking: targeting, regulation and function*. Current Opinion in Cell Biology **20**(4): 415-426.

Martin, D. A. and K. B. Elkon (2004). *Mechanisms of apoptosis*. Rheumatic Disease Clinics of North America **30**(3): 441-454.

Martin, S. J. (2002). *Destabilizing influences in apoptosis: sowing the seeds of IAP destruction*. Cell **109**(7): 793-796.

Massenburg, D., J. S. Han, M. Liyanage, W. A. Patton, S. G. Rhee, J. Moss and M. Vaughan (1994). *Activation of rat brain phospholipase D by ADP-ribosylation factors 1,5, and 6: separation of ADP-ribosylation factor-dependent and oleate-dependent enzymes*. Proceedings of the National Academy of Sciences of the United States of America **91**(24): 11718-11722.

Mattson, M. (2000). *Apoptosis in neurodegenerative disorders*. Nat.Rev. Mol. Cell Biol. **1**: 120-129.

Mattsson, J. P., X. Li, S. B. Peng, F. Nilsson, P. Andersen, L. G. Lundberg, D. K. Stone and D. J. Keeling (2000). *Properties of three isoforms of the 116-kDa subunit of vacuolar H+- ATPase from a single vertebrate species: Cloning, gene expression and protein characterization of functionally distinct isoforms in Gallus gallus*. European Journal of Biochemistry **267**(13): 4115-4126.

McGuffin, L., K. Bryson and D. Jones (2000). *The PSIPRED protein structure prediction server*. Bioinformatics **16**: 404-405.

Meacci, E., S.-C. Tsai, R. Adamik, J. Moss and M. Vaughan (1997). *Cytohesin-1, a cytosolic guanine nucleotide-exchange protein for ADP-ribosylationâ€‰factor*. PNAS **94**: 1745-1748.

Merkulova, M., A. Bakulina, Y. R. Thaker, G. Grüber and V. Marshansky (2009). *Specific domains on the V-ATPase a2-isoform interact with regulatory elements of ARNO*. BBA Bioenerg.

Merzendorfer, H., M. Huss, R. Schmid, W. R. Harvey and H. Wieczorek (1999). *A Novel Insect V-ATPase Subunit M9.7 Is Glycosylated Extensively*. J. Biol. Chem. **274**(24): 17372-17378.

Mezghrani, A., A. Fassio, A. Benham, T. Simmen, I. Braakman and R. Sitia (2001). *Manipulation of oxidative protein folding and PDI redox state in mammalian cells*. EMBO Journal **20**(22): 6288-6296.

Morel, N. (2003). *Neurotransmitter disease: The dark side of the vacuolar-H+ATPase*. Biology of the Cell **95**(7): 453-457.

Morizane, Y., R. Honda, K. Fukami and H. Yasuda (2005). *X-Linked Inhibitor of Apoptosis functions as ubiquitin ligase toward mature caspase-9 and cytosolic Smac/DIABLO*. J Biochem **137**(2): 125-132.

Moss, J. and M. Vaughan (1998). *Molecules in the ARF Orbit*. J. Biol. Chem. **273**(34): 21431-21434.

Murata, Y., G.-H. Sun-Wada, T. Yoshimizu, A. Yamamoto, Y. Wada and M. Futai (2002). *Differential localization of the vacuolar H+ pump with G subunit isoforms (G1 and G2) in mouse neurons*. J. Biol. Chem. **277**(39): 36296-36303.

Nachmias, B., Y. Ashhab, V. Bucholtz, O. Drize, L. Kadouri, M. Lotem, T. Peretz, O. Mandelboim and D. Ben-Yehuda (2003). *Caspase-mediated cleavage converts Livin from an antiapoptotic to a proapoptotic factor: implications for drug-resistant melanoma*. Cancer Res **63**(19): 6340-6349.

Nachmias, B., I. Lazar, M. Elmalech, I. Abed-El-Rahaman, Y. Asshab, O. Mandelboim, R. Perlman and D. Ben-Yehuda (2007). *Subcellular localization determines the delicate balance between the anti- and pro-apoptotic activity of Livin*. Apoptosis **12**(7): 1129-1142.

Nagata, S. (1997). *Apoptosis by death factor*. Cell **88**(3): 355-365.

Nagel, W., P. Schilcher, L. Zeitlmann and W. Kolanus (1998). *The PH domain and the polybasic c domain of cytohesin-1 cooperate specifically in plasma membrane association and cellular function*. Mol. Biol. Cell **9**(8): 1981-1994.

Nakagawa, T., H. Zhu, N. Morishima, E. Li, J. Xu, B. A. Yankner and J. Yuan (2000). *Caspase-12 mediates endoplasmic-reticulum-specific apoptosis and cytotoxicity by amyloid-[beta]*. Nature **403**(6765): 98-103.

Nanda, A., A. Gukovskaya, J. Tseng and S. Grinstein (1992). *Activation of vacuolar-type proton pumps by protein kinase C. Role in neutrophil pH regulation*. J. Biol. Chem. **267**(32): 22740-22746.

Narula, J., N. Haider, E. Arbustini and Y. Chandrashekhar (2006). *Mechanisms of disease: apoptosis in heart failure - seeing hope in death*. Nature Clinical Practice Cardiovascular Medicine **3**(12): 681-688.

Nelson, H., S. Mandiyan and N. Nelson (1994). *The Saccharomyces cerevisiae VMA7 gene encodes a 14-kDa subunit of the vacuolar H(+)-ATPase catalytic sector*. J. Biol. Chem. **269**(39): 24150-24155.

Nelson, N. and W. R. Harvey (1999). *Vacuolar and plasma membrane proton-adenosinetriphosphatases*. Physiol. Rev. **79**(2): 361-385.

Nishi, T. (2005). *Subunit isoforms controlling the functions of the V-ATPase*. Seikagaku. The Journal of Japanese Biochemical Society **77**(4): 354-358.

Nishi, T. and M. Forgac (2000). *Molecular cloning and expression of three isoforms of the 100-kDa a subunit of the mouse vacuolar proton-translocating ATPase*. Journal of Biological Chemistry **275**(10): 6824-6830.

Nishi, T. and M. Forgac (2002). *The vacuolar (H+)-ATPases - Nature's most versatile proton pumps*. Nature Reviews Molecular Cell Biology **3**(2): 94-103.

Nishi, T., S. Kawasaki-Nishi and M. Forgac (2003). *Expression and function of the mouse V-ATPase d subunit isoforms*. J. Biol. Chem. **278**(47): 46396-46402.

Nishihara, T., S. Akifusa, T. Koseki, S. Kato, M. Muro and N. Hanada (1995). *Specific inhibitors of vacuolar type H+-ATPases induce apoptotic cell ceath*. Biochemical and Biophysical Research Communications **212**(1): 255-262.

Norgett, E. E., K. J. Borthwick, R. S. Al-Lamki, Y. Su, A. N. Smith and F. E. Karet (2007). *V1 and V0 domains of the human H+-ATPase are linked by an interaction between the G and a subunits*. J. Biol. Chem.: M701226200.

O'Brien, M. A. and R. Kirby (2008). *Apoptosis: A review of pro-apoptotic and anti-apoptotic pathways and dysregulation in disease*. Journal of Veterinary Emergency and Critical Care **18**(6): 572-585.

Ogilvie, I., R. Aggeler and R. A. Capaldi (1997). *Cross-linking of the delta subunit to one of the three alpha subunits has no effect on functioning, as expected if delta Is a part of the stator that links the F1 and F0 parts of the Escherichia coli ATP synthase*. J. Biol. Chem. **272**(26): 16652-16656.

Ohira, M., A. M. Smardon, C. M. H. Charsky, J. Liu, M. Tarsio and P. M. Kane (2006). *The E and G subunits of the yeast V-ATPase interact tightly and are both present at more than one copy per V1 complex*. J. Biol. Chem. **281**(32): 22752-22760.

Oka, T., Y. Murata, M. Namba, T. Yoshimizu, T. Toyomura, A. Yamamoto, G. H. Sun-Wada, N. Hamasaki, Y. Wada and M. Futai (2001). *a4, a unique kidney-specific isoform of mouse vacuolar H +-ATPase subunit a*. Journal of Biological Chemistry **276**(43): 40050-40054.

Olendzenski, L., E. Hilario and J. P. Gogarten (1998). *In: Syvanen K, Kado CI (eds) Horizontal gene transfer*. Chapman & Hall, New York: 349-362.

Owegi, M. A., A. L. Carenbauer, N. M. Wick, J. F. Brown, K. L. Terhune, S. A. Bilbo, R. S. Weaver, R. Shircliff, N. Newcomb and K. J. Parra-Belky (2005). *Mutational analysis of the stator subunit E of the yeast V-ATPase*. J. Biol. Chem. **280**(18): 18393-18402.

Owegi, M. A., D. L. Pappas, M. W. Finch, Jr., S. A. Bilbo, C. A. Resendiz, L. J. Jacquemin, A. Warrier, J. D. Trombley, K. M. McCulloch, K. L. M. Margalef, M. J. Mertz, J. M. Storms, C. A. Damin and K. J. Parra (2006). *Identification of a Domain in the Vo Subunit d That Is Critical for Coupling of the Yeast Vacuolar Proton-translocating ATPase*. J. Biol. Chem. **281**(40): 30001-30014.

Owegi, M. A., D. L. Pappas, Jr., M. W. Finch, S. A. Bilbo, C. A. Resendiz, L. J. Jacquemin, A. Warrier, J. D. Trombley, K. M. McCulloch, K. L. M. Margalef, M. J. Mertz, J. M. Storms, C. A. Damin and K. J. Parra (2006). *Identification of a domain in the Vo subunit d that is critical for coupling of the yeast V-ATPase*. J. Biol. Chem.: M605006200.

Page, R., W. Peti, I. A. Wilson, R. C. Stevens and K. Wüthrich (2005). *NMR screening and crystal quality of bacterially expressed prokaryotic and eukaryotic proteins in a structural genomics pipeline*. Proceedings of the National Academy of Sciences of the United States of America **102**(6): 1901-1905.

Pan, F., R. Malmberg and M. Momany (2007). *Analysis of septins across kingdoms reveals orthology and new motifs*. BMC Evolutionary Biology **7**(1): 103.

Park, H. J. *Effects of intracellular pH on apoptosis in HL-60 human leukemia cells*. Yonsei Med J **36**: 473-479.

Parra, K. J. and P. M. Kane (1998). *Reversible association between the V1 and V0 domains of yeast vacuolar H+-ATPase is an unconventional glucose-induced effect*. Molecular and Cellular Biology **18**(12): 7064-7074.

Parra, K. J., K. L. Keenan and P. M. Kane (2000). *The H subunit (Vma13p) of the yeast V-ATPase inhibits the ATPase activity of cytosolic V1 complexes*. J. Biol. Chem. **275**: 21761-67.

Per, U., J. M. Juan, C. Pablo and M. Federico (2001). *SOMCD: Method for evaluating protein secondary structure from UV circular dichroism spectra*. Proteins: Structure, Function, and Genetics **42**: 460-70

Perfettini, J. L., M. Castedo, T. Roumier, K. Andreau, R. Nardacci, M. Piacentini and G. Kroemer (2005). *Mechanisms of apoptosis induction by the HIV-1 envelope*. Cell Death and Differentiation **12**(SUPPL. 1): 916-923.

Peri, F. and C. Nüsslein-Volhard (2008). *Live imaging of neuronal degradation by microglia reveals a role for v0-ATPase a1 in phagosomal fusion in vivo*. Cell **133**(5): 916-927.

Perin, M. S., V. A. Fried, D. K. Stone, X. S. Xie and T. C. Sudhof (1991). *Structure of the 116-kDa polypeptide of the clathrin-coated vesicle/synaptic vesicle proton pump*. J. Biol. Chem. **266**(6): 3877-3881.

Peters, C., M. J. Bayer, S. Buhler, J. S. Andersen, M. Mann and A. Mayer (2001). *Trans-complex formation by proteolipid channels in the terminal phase of membrane fusion*. Nature **409**(6820): 581-588.

Preston, R. A., R. F. Murphy and E. W. Jones (1989). *Assay of vacuolar pH in yeast and identification of acidification-defective mutants*. Proceedings of the National Academy of Sciences of the United States of America **86**(18): 7027-7031.

Provencher, S. and J. Glöckner (1981). *Estimation of globular protein secondary structure from circular dichroism*. Biochemistry **20**(1): 33-7.

Puopolo, K., M. Sczekan, R. Magner and M. Forgac (1992). *The 40-kDa subunit enhances but is not required for activity of the coated vesicle proton pump*. J. Biol. Chem. **267**(8): 5171-5176.

Qi, J. and M. Forgac (2008). *Function and subunit interactions of the N-terminal domain of subunit a (Vph1p) of the yeast V-ATPase*. J. Biol. Chem.: M802442200.

Radermacher, M., T. Ruiz, H. Wieczorek and G. Grüber (2001). *The structure of the V1-ATPase determined by three-dimensional electron microscopy of single particles*. Journal of Structural Biology **135**(1): 26-37.

Reed, J. C. (2000). *Mechanisms of apoptosis.* Am J Pathol **157**(5): 1415-1430.

Ricci, J. E., C. Mun?oz-Pinedo, P. Fitzgerald, B. Bailly-Maitre, G. A. Perkins, N. Yadava, I. E. Scheffler, M. H. Ellisman and D. R. Green (2004). *Disruption of mitochondrial function during apoptosis is mediated by caspase cleavage of the p75 subunit of complex I of the electron transport chain.* Cell **117**(6): 773-786.

Riedl, S. J. and Y. Shi (2004). *Molecular mechanisms of caspase regulation during apoptosis.* Nature Reviews Molecular Cell Biology **5**(11): 897-907.

Rishikesan, S., S. Gayen, Y. R. Thaker, S. Vivekanandan, M. S. S. Manimekalai, Y. H. Yau, S. G. Shochat and G. Gerhard (2009). *Assembly of subunit d (Vma6p) and G (Vma10p) and the NMR solution structure of subunit G (G1-59) of the Saccharomyces cerevisiae V1VO ATPase.* BBA Bioenerg **(in press)**.

Rishikesan, S., Y. R. Thaker, R. Priya, S. Gayen, M. S. S. Manimekalai, C. Hunke and G. GrÃ¼ber (2008). *Spectroscopical identification of residues of subunit G of the yeast V-ATPase in its connection with subunit E.* Molecular Membrane Biology **25**(5): 400 - 410.

Rizzo, V. F., U. Coskun, M. Radermacher, T. Ruiz, A. Armbrüster and G. Grüber (2003). *Resolution of the V1 ATPase from Manduca sexta into subcomplexes and visualization of an ATPase-active A3B3EG complex by electron microscopy.* J. Biol. Chem. **278**(1): 270-275.

Roos, M., V. Soskic, S. Poznanovic and J. Godovac-Zimmermann (1998). *Post-translational modifications of endothelin receptor B from bovine lungs analyzed by mass spectrometry.* J Biol Chem **273**: 924-931.

Roukos, V., M. S. Iliou, H. Nishitani, M. Gentzel, M. Wilm, S. Taraviras and Z. Lygerou (2007). *Geminin cleavage during apoptosis by caspase-3 alters Its binding ability to the SWI/SNF subunit brahma.* J. Biol. Chem. **282**(13): 9346-9357.

Roy, N., Q. L. Deveraux, R. Takahashi, G. S. Salvesen and J. C. Reed (1997). *The c-IAP-1 and c-IAP-2 proteins are direct inhibitors of specific caspases*. EMBO Journal **16**(23): 6914-6925.

Sagermann, M., T. H. Stevens and B. W. Matthews (2001). *Crystal structure of the regulatory subunit H of the V-type ATPase of Saccharomyces cerevisiae*. Proceedings of the National Academy of Sciences **98**(13): 7134-7139.

Salvesen, G. S. and M. V. Dixit (1997). *Caspases: Intracellular signaling by proteolysis*. Cell **91**: 443-446.

Salvesen, G. S. and C. S. Duckett (2002). *IAP proteins: blocking the road to death's door*. Nat Rev Mol Cell Biol **3**(6): 401-410.

Sambade, M. and P. M. Kane (2004). *The yeast vacuolar proton-translocating ATPase contains a subunit homologous to the Manduca sexta and bovine e subunits that Is essential for function*. J. Biol. Chem. **279**(17): 17361-17365.

Samejima, K., P. A. Svingen, G. S. Basi, T. Kottke, P. W. Mesner, Jr., L. Stewart, F. Durrieu, G. G. Poirier, E. S. Alnemri, J. J. Champoux, S. H. Kaufmann and W. C. Earnshaw (1999). *Caspase-mediated cleavage of DNA topoisomerase I at unconventional sites during apoptosis*. J. Biol. Chem. **274**(7): 4335-4340.

Santy, L. C. and J. E. Casanova (2001). *Activation of ARF6 by ARNO stimulates epithelial cell migration through downstream activation of both Rac1 and phospholipase D*. J. Cell Biol. **154**(3): 599-610.

Santy, L. C. and J. E. Casanova (2001). *Activation of ARF6 by ARNO stimulates epithelial cell migration through downstream activation of both Rac1 and phospholipase D*. Journal of Cell Biology **154**(3): 599-610.

Santy, L. C., S. R. Frank, J. C. Hatfield and J. E. Casanova (1999). *Regulation of ARNO nucleotide exchange by a PH domain electrostatic switch*. Current Biology **9**(20): 1173-1176.

Saraste, M., P. R. Sibbald and A. Wittinghofer (1990). *The P-loop - A common motif in ATP-and GTP-binding proteins*. Trends in Biochemical Sciences **15**(11): 430-434.

Sato, K., S. Shikano, G. Xia, J. Takao, J.-S. Chung, J. P. D. Cruz, X.-S. Xie and K. Ariizumi (2006). *Selective expression of vacuolar H+-ATPase subunit d2 by particular subsets of dendritic cells among leukocytes*. Molecular Immunology **43**(9): 1443-1453.

Schulenberg, B. and R. A. Capaldi (1999). *The epsilon subunit of the F1F0 complex of Escherichia coli. cross-linking studies show the same structure in situ as when isolated*. J. Biol. Chem. **274**(40): 28351-28355.

Sennoune, S. R., K. Bakunts, G. M. Martinez, J. L. Chua-Tuan, Y. Kebir, M. N. Attaya and R. Martinez-Zaguilan (2004). *Vacuolar H+-ATPase in human breast cancer cells with distinct metastatic potential: distribution and functional activity*. Am J Physiol Cell Physiol **286**(6): C1443-1452.

Sennoune, S. R., D. Luo and R. Marti?nez-Zaguila?n (2004). *Plasmalemmal vacuolar-type H+-ATPase in cancer biology*. Cell Biochemistry and Biophysics **40**(2): 185-206.

Sennoune, S. R. and R. Martinez-Zaguilan (2007). *Plasmalemmal vacuolar H+-ATPases in angiogenesis, diabetes and cancer*. Journal of Bioenergetics and Biomembranes **39**(5-6): 427-433.

Shao, E. and M. Forgac (2004). *Involvement of the nonhomologous region of subunit A of the yeast V-ATPase in coupling and in vivo dissociation*. J. Biol. Chem. **279**(47): 48663-48670.

Shao, E., T. Nishi, S. Kawasaki-Nishi and M. Forgac (2003). *Mutational analysis of the non-homologous region of subunit A of the yeast V-ATPase*. J. Biol. Chem. **278**(15): 12985-12991.

Singh, S., P. Turina, C. J. Bustamante, D. J. a. Keller and R. A. Capaldi (1996). *Topographical structure of membrane-bound Escherichia coli F1FO ATP synthase in aqueous buffer*. FEBS Lett. **397**: 30-34.

Smith, A. N., F. Jouret, S. Bord, K. J. Borthwick, R. S. Al-Lamki, C. A. Wagner, D. C. Ireland, V. Cormier-Daire, A. Frattini, A. Villa, U. Kornak, O. Devuyst and F. E. Karet (2005). *Vacuolar H+-ATPase d2 subunit: molecular characterization, developmental regulation, and localization to specialized proton pumps in kidney and bone*. J Am Soc Nephrol **16**(5): 1245-1256.

Smith, A. N., R. C. Lovering, M. Futai, J. Takeda, D. Brown and F. E. Karet (2003). *Revised nomenclature for mammalian vacuolar-Type H+-ATPase subunit genes*. Molecular Cell **12**(4): 801-803.

Sreerama, N. and R. Woody (2000). *Estimation of protein secondary structure from circular dichroism spectra: comparison of CONTIN, SELCON, and CDSSTR methods with an expanded reference set.* Anal Biochem **287**: 252-260.

Stehberger, P. A., N. Schulz, K. E. Finberg, F. E. Karet, G. Giebisch, R. P. Lifton, J. P. Geibel and C. A. Wagner (2003). *Localization and regulation of the ATP6V0A4 (a4) vacuolar H+-ATPase subunit defective in an inherited form of distal renal tubular acidosis*. J Am Soc Nephrol **14**(12): 3027-3038.

Strompen, G., J. Dettmer, Y. D. Stierhof, K. Schumacher, G. Ju?rgens and U. Mayer (2005). *Arabidopsis vacuolar H+-ATPase subunit E isoform 1 is required for Golgi organization and vacuole function in embryogenesis*. Plant Journal **41**(1): 125-132.

Sulston, J. E. and H. R. Horvitz (1977). *Post-embryonic cell lineages of the nematode, Caenorhabditis elegans*. Developmental Biology **56**(1): 110-156.

Sulston, J. E., E. Schierenberg, J. G. White and J. N. Thomson (1983). *The embryonic cell lineage of the nematode Caenorhabditis elegans*. Developmental Biology **100**(1): 64-119.

Sumner, J.-P., J. A. T. Dow, F. G. P. Earley, U. Klein, D. Jäger and H. Wieczorek (1995). *Regulation of plasma membrane V-ATPase activity by dissociation of peripheral subunits*. J. Biol. Chem. **270**(10): 5649-5653.

Sun-Wada, G.-H., Y. Murata, M. Namba, A. Yamamoto, Y. Wada and M. Futai (2003). *Mouse proton pump ATPase C subunit isoforms (C2-a and C2-b) specifically expressed in kidney and lung*. J. Biol. Chem. **278**(45): 44843-44851.

Sun-Wada, G.-H., T. Toyomura, Y. Murata, A. Yamamoto, M. Futai and Y. Wada (2006). *The a3 isoform of V-ATPase regulates insulin secretion from pancreatic {beta}-cells*. J Cell Sci **119**(21): 4531-4540.

Sun-Wada, G.-H., T. Yoshimizu, Y. Imai-Senga, Y. Wada and M. Futai (2003). *Diversity of mouse proton-translocating ATPase: presence of multiple isoforms of the C, d and G subunits*. Gene **302**(1-2): 147-153.

Sun, J. G., R. X. Liao, Z. T. Chen, Z. X. Wang, Q. Zhang, Y. D. Hu and D. L. Wang (2005). *Gene transfection of Livin isoforms into A549 cell line and its effect on cell growth and sensitivity to chemotherapy and radiotherapy*. Zhonghua Jiehe he Huxi Zazhi **28**(12): 836-840.

Sun, X.-M., M. Butterworth, M. MacFarlane, W. Dubiel, A. Ciechanover and G. M. Cohen (2004). *Caspase activation inhibits proteasome function during apoptosis*. Molecular Cell **14**(1): 81-93.

Supek, F., L. Supekova, S. Mandiyan, Y. C. E. Pan, H. Nelson and N. Nelson (1994). *A novel accessory subunit for vacuolar H+-ATPase from chromaffin granules*. Journal of Biological Chemistry **269**(39): 24102-24106.

Sutton, V. R., M. E. Wowk, M. Cancilla and J. A. Trapani (2003). *Caspase activation by granzyme B is indirect, and caspase autoprocessing requires the release of proapoptotic mitochondrial factors*. Immunity **18**(3): 319-329.

Svergun, D. (1992). *Determination of the regularization parameter in indirect-transform methods using perceptual criteria*. Journal of Applied Crystallography **25**(4): 495-503.

Svergun, D. (1994). *Solution scattering from biopolymers: advanced contrast-variation data analysis*. Acta Crystallographica Section A **50**(3): 391-402.

Svergun, D., C. Barberato and M. H. J. Koch (1995). *CRYSOL - a program to evaluate X-ray solution scattering of biological macromolecules from atomic coordinates*. Journal of Applied Crystallography **28**(6): 768-773.

Svergun, D., A. Be irevi , H. Schrempf, M. Koch and G. Grüber (2000). *Solution structure and conformational changes of the Streptomyces chitin-binding protein (CHB1)*. Biochemistry **39**: 10677-83.

Svergun, D. I. (1999). *Restoring Low Resolution Structure of Biological Macromolecules from Solution Scattering Using Simulated Annealing*. Biophysical Journal **76**(6): 2879-2886.

Svergun, D. I., M. V. Petoukhov and M. H. J. Koch (2001). *Determination of domain structure of proteins from X-Ray solution scattering*. Biophys. J. **80**(6): 2946-2953.

Thaker, Y., M. Roessle and G. Grüber (2007). *The boxing glove shape of subunit d of the yeast V-ATPase in solution and the importance of disulfide formation for folding of this protein*. Journal of Bioenergetics and Biomembranes **39**(4): 275-289.

Thaker, Y. R., C. Hunke, Y. H. Yau, S. G. Shochat, Y. Li and G. Grüber (2009). *Association of the eukaryotic V1VO ATPase subunits a with d and d with A*. FEBS Lett.

Thaker, Y. R., M. Roessle and G. Grüber (2007). *The boxing glove shape of subunit d of the yeast V-ATPase in solution and the importance of disulfide formation for folding of this protein*. Journal of Bioenergetics and Biomembranes **39**(4): 275-289.

Toyomura, T., T. Oka, C. Yamaguchi, Y. Wada and M. Futai (2000). *Three subunit a isoforms of mouse vacuolar H+-ATPase. Preferential expression of the ?3 isoform during osteoclast differentiation*. Journal of Biological Chemistry **275**(12): 8760-8765.

Turner, C. E. and M. C. Brown (2001). *Cell motility: ARNO and ARF6 at the cutting edge.* Current Biology **11**(21).

Uren, A. G., E. J. Coulson and D. L. Vaux (1998). *Conservation of baculovirus inhibitor of apoptosis repeat proteins (BIRPs) in viruses, nematodes, vertebrates and yeasts.* Trends in Biochemical Sciences **23**(5): 159-162.

Uren, A. G., K. O'Rourke, L. Aravind, M. T. Pisabarro, S. Seshagiri, E. V. Koonin and V. M. Dixit (2000). *Identification of paracaspases and metacaspases: two ancient families of caspase-like proteins, one of which plays a key role in MALT lymphoma.* Molecular Cell **6**(4): 961-967.

Vaux, D. L. and J. Silke (2005). *IAPs, RINGs and ubiquitylation.* Nat Rev Mol Cell Biol **6**(4): 287-297.

Verhagen, A. M., P. G. Ekert, M. Pakusch, J. Silke, L. M. Connolly, G. E. Reid, R. L. Moritz, R. J. Simpson and D. L. Vaux (2000). *Identification of DIABLO, a mammalian protein that promotes apoptosis by binding to and antagonizing IAP proteins.* Cell **102**(1): 43-53.

Vitavska, O., H. Merzendorfer and H. Wieczorek (2005). *The V-ATPase subunit C binds to polymeric F-actin as well as to monomeric G-actin and induces cross-linking of actin filaments.* Journal of Biological Chemistry **280**(2): 1070-1076.

Vitavska, O., H. Wieczorek and H. Merzendorfer (2003). *A novel role for subunit C in mediating binding of the H+-V-ATPase to the actin cytoskeleton.* J. Biol. Chem. **278**(20): 18499-18505.

Vucic, D., H. R. Stennicke, M. T. Pisabarro, G. S. Salvesen and V. M. Dixit (2000). *ML-IAP, a novel inhibitor of apoptosis that is preferentially expressed in human melanomas.* Current Biology **10**(21): 1359-1366.

Wagner, C. A., K. E. Finberg, S. Breton, V. Marshansky, D. Brown and J. P. Geibel (2004). *Renal vacuolar H+-ATPase.* Physiol. Rev. **84**(4): 1263-1314.

Wang, S. Y., Y. Moriyama, M. Mandel, J. D. Hulmes, Y. C. Pan, W. Danho, H. Nelson and N. Nelson (1988). *Cloning of cDNA encoding a 32-kDa protein. An accessory polypeptide of the H+-ATPase from chromaffin granules*. J. Biol. Chem. **263**(33): 17638-17642.

Wang, X. W. and L. W. Fu (2004). *Inhibitor of apoptosis proteins (IAP): Novel anticancer targets*. Chinese Pharmacological Bulletin **20**(2): 129-133.

Wang, Y., T. Inoue and M. Forgac (2004). *TM2 but not TM4 of subunit c'' interacts with TM7 of subunit a of the yeast V-ATPase as defined by disulfide-mediated cross-linking*. Journal of Biological Chemistry **279**(43): 44628-44638.

Wang, Z. B., Y. Q. Liu and Y. F. Cui (2005). *Pathways to caspase activation*. Cell Biology International **29**(7): 489-496.

Wassmer, T., R. Kissmehl, J. Cohen and H. Plattner (2006). *Seventeen a-subunit isoforms of Paramecium V-ATPase provide high specialization in localization and function*. Molecular Biology of the Cell **17**(2): 917-930.

Waterhouse, N. J., D. M. Finucane, D. R. Green, J. S. Elce, S. Kumar, E. S. Alnemri, G. Litwack, K. KumKum, M. F. Lavin and D. J. Watters (1998). *Calpain activation is upstream of caspases in radiation-induced apoptosis*. Cell Death Diff. **5**: 1051-1061.

Weirich, C. S., J. P. Erzberger and Y. Barral (2008). *The septin family of GTPases: architecture and dynamics*. Nat Rev Mol Cell Biol **9**(6): 478-489.

Wieczorek, H., G. Gruber, W. R. Harvey, M. Huss and H. Merzendorfer (1999). *The plasma membrane H+-V-ATPase from tobacco hornworm midgut*. Journal of Bioenergetics and Biomembranes **31**(1): 67-74.

Wilkens, S. and M. Forgac (2001). *Three-dimensional structure of the vacuolar ATPase proton channel by electron microscopy*. J. Biol. Chem. **276**(47): 44064-44068.

Wilkens, S. a. and R. A. Capaldi (1998). *Electron microscopic evidence of two stalks linking the F1 and FO parts of the Escherichia coli ATP synthase*. Biochim. Biophys. Acta **1365**: 93-97.

Wishart, D. S., B. D. Sykes and F. M. Richards (1992). *The chemical shift index: a fast and simple method for the assignment of protein secondary structure through NMR spectroscopy* Biochemistry **31**: 1647-1651.

Wüthrich, K. (1986). *NMR of proteins and nuclei acids*. New York: Wiley, Interscience.

Wyllie, A. H., J. F. Kerr and A. R. Currie (1980). *Cell death: the significance of apoptosis*. Int Rev Cytol **68.** : 251-306.

Yan, H., B. Brouha, T. Liu, D. Raj, D. Biddle, R. Lee and D. Grossman (2006). *Proteolytic cleavage of Livin (ML-IAP) in apoptotic melanoma cells potentially mediated by a non-canonical caspase*. Journal of Dermatological Science **43**(3): 189-200.

Yang, L., T. Mashima, S. Sato, M. Mochizuki, H. Sakamoto, T. Yamori, T. Oh-hara and T. Tsuruo (2003). *Predominant suppression of apoptosome by inhibitor of apoptosis protein in non-small cell lung cancer H460 cells: therapeutic effect of a novel polyarginine-conjugated Smac peptide*. Cancer Res **63**(4): 831-837.

Yang, Q. H. and C. Du (2004). *Smac/DIABLO selectively reduces the levels of c-IAP1 and c-IAP2 but not that of XIAP and Livin in HeLa cells*. Journal of Biological Chemistry **279**(17): 16963-16970.

Yao, G., H. Feng, Y. Cai, W. Qi and K. Kong (2007). *Characterization of vacuolar-ATPase and selective inhibition of vacuolar-H(+)-ATPase in osteoclasts*. Biochemical and Biophysical Research Communications **357**(4): 821-827.

Yin, X.-M. (2006). *Bid, a BH3-only multi-functional molecule, is at the cross road of life and death*. Gene **369**: 7-19.

Yokoyama, K. and H. Imamura (2005). *Rotation, structure, and classification of prokaryotic V-ATPase*. Journal of Bioenergetics and Biomembranes **37**(6): 405-410.

Yoshimoto, Y. and M. Imoto (2002). *Induction of EGF-dependent apoptosis by vacuolar-type H+-ATPase inhibitors in A431 cells overexpressing the EGF receptor.* Experimental Cell Research **279**(1): 118-127.

Yossi, G., R. Asaf, L. Rona, S. Hermann and L. Sarit (2004). *The mitochondrial ARTS protein promotes apoptosis through targting XIAP*. EMBO **23**: 1627-1635.

Yuan, J. and H. R. Horvitz (1992). *The Caenorhabditis elegans cell death gene ced-4 encodes a novel protein and is expressed during the period of extensive programmed cell death.* Development **116**(2): 309-320.

Yuan, J., S. Shaham, S. Ledoux, H. M. Ellis and H. R. Horvitz (1993). *The C. elegans cell death gene ced-3 encodes a protein similar to mammalian interleukin-1[beta]-converting enzyme*. Cell **75**(4): 641-652.

Zhang, H. D., S. J. Yuan and H. P. Chen (2003). *Livin - Potential target for cancer treatment.* Chinese Pharmacological Bulletin **19**(8): 845-847.

Zhang, J., Y. Feng and M. Forgac (1994). *Proton conduction and bafilomycin binding by the V0 domain of the coated vesicle V-ATPase*. J. Biol. Chem. **269**(38): 23518-23523.

Zhang, J., M. Myers and M. Forgac (1992). *Characterization of the V0 domain of the coated vesicle (H+)-ATPase*. J. Biol. Chem. **267**(14): 9773-9778.

Zhaoyu, J. and W. S. El-Deiry (2005). *Overview of cell death signaling pathways*. Cancer Bio Thera **4**(2): 139-163.

Zhuang, Z., P. J. Linser and W. R. Harvey (1999). *Antibody to H(+) V-ATPase subunit E colocalizes with portasomes in alkaline larval midgut of a freshwater mosquito (Aedes aegypti).* J Exp Biol **202**(18): 2449-2460.

Author's publications related to this study

1. **Thaker, Y. R.**, Rössle, M. and Grüber, G. (2007) *The boxing glove shape of subunit d of the yeast V-ATPase in solution and the importance of disulfide formation for folding of this protein*. J. Bioenerg. Biomembr, 39, 275-89

2. **Thaker, Y. R.**, Rössle, M. and Grüber, G. (2007) *Low resolution structure of subunit d (Vma6p) of the Saccharomyces cerevisiae V-ATPase in solution*. 412, Annual Report of the German Electron Synchrotron (DESY) Germany

3. Rishikesan, S., **Thaker, Y. R.**, Priya, R., Gayen, S., Manimekalai, M. S. S., Hunke, C. and Grüber, G. (2008) *Spectroscopical identification of residues of subunit G of the yeast V-ATPase in its connection with subunit E*. Mol. Mem. Biol., 25: 400-410

4. **Thaker Y, R.,** Rishikesan, S., Grüber, G. (2008) *Solution structure of subunit d, E and G of the eukaryotic V-ATPase.* BBA-bioenerg., 1777, Supple.1, S18

5. Rishikesan, S., Gayen, S., **Thaker, Y. R.,** Vivekanandan, S., Manimekalai, M. S. S., Yau, H.N., Shochat G.S. and Grüber, G. (2008) *Assembly of subunit d (Vma6p) and G (Vma10p) and the NMR solution structure of subunit G (G_{1-59}) of the Saccharomyces cerevisiae V_1V_O ATPase.* BBA-bioenerg., (in press)

6. **Thaker, Y. R.,** Hunke, C., Yau, Y. H., Shochat, S. G., Li, Y. and Grüber, G. (2009) *Association of the eukaryotic V_1V_O ATPase subunits a with d and d with A.* FEBS letter., (submitted)

7. Merkulova, M., Bakulina, A., **Thaker, Y. R**., Grüber, G. and Marshansky, V. (2009) *Specific domains on the V-ATPase a2-isoform interact with regulatory elements of ARNO.* JBC., (submitted)

Conference presentation and poster

Oral presentation
1.   Fourth Biophysical Discussion Group Meeting, National University of Singapore, Singapore. 11th May 2007
Title**:** Structural traits of subunit *d* of the proton pump V_1V_O ATPase from yeast

Posters
1.   Joint Third AOHUPO and Fourth Structural Biology and Functional Genomics Conference, NUS, Singapore from 4-7th Dec 2006
Title: Low resolution structure of the subunit *d* of the *Saccharomyces cerevisiae* vacuolar ATPase in solution

2. 15th European Bioenergetics Conference (EBEC 2008) Dublin, Ireland from 19th – 24th July 2008

Title: Low resolution structure of subunit *d* and NMR titration experiments, studying the interaction of subunits E and G of V-ATPase from yeast

3. Joint 5th Structural Biology and Functional Genomics and 1st Biological Physics International Conference, NUS, Singapore from 9-11th Dec 2008

Title: NMR studies with subunit *E* of vacuolar ATPase from *Saccharomyces cerevisiae*